Heinrich Heine
Universität Düsseldorf

iGRAD*plant*
International
Graduate
Program
for Plant Science

The Role of Organellar Transporters in C_3/C_4-Metabolism

Inaugural-Dissertation

zur Erlangung des Doktorgrades

der Mathematisch-Naturwissenschaftlichen Fakultät

der Heinrich-Heine-Universität Düsseldorf

vorgelegt von

Franziska Kuhnert

aus Leipzig

Düsseldorf, März 2020

aus dem

Institut für Biochemie der Pflanzen

der Heinrich-Heine-Universität Düsseldorf

Gedruckt mit der Genehmigung der

Mathematisch-Naturwissenschaftlichen Fakultät

der Heinrich-Heine-Universität Düsseldorf

Referent: Prof. Dr. Andreas P. M. Weber

Korreferent: Prof. Dr. Peter Westhoff

Tag der mündlichen Prüfung:

Eidesstattliche Erklärung

Ich versichere an Eides Statt, dass die Dissertation von mir selbständig und ohne unzulässige fremde Hilfe unter Beachtung der „Grundsätze zur Sicherung guter wissenschaftlicher Praxis an der Heinrich-Heine-Universität Düsseldorf“ erstellt worden ist.

Die Dissertation habe ich in der vorgelegten oder in ähnlicher Form noch bei keiner anderen Institution eingereicht.

Ich habe bisher keine erfolglosen Promotionsversuche unternommen.

Düsseldorf, der 04.03.2020

Franziska Kuhnert

'The road goes ever on and on.'

J. R. R. Tolkien, The Lord of the Rings

Table of Contents

Summary 6

Zusammenfassung 7

Introduction 9

Photosynthesis 10

Photorespiration 10

Core pathway 11

Nitrogen re-assimilation 13

Glycine decarboxylase and serine hydroxymethyl transferase reaction 14

Auxiliary pathways 15

Transporters of the photorespiratory pathway 15

Strategies improving photosynthetic efficiency 16

C_4 photosynthesis 17

Biochemistry 18

References 21

Manuscript I 28

Rapid Single-Step Affinity Purification of HA-Tagged Plant Mitochondria 28

Manuscript II 49

The Mitochondrial Carrier À BOUT DE SOUFFLE is a Key Player in Photorespiratory Nitrogen Metabolism 49

Manuscript III 89

The Bile Acid Sodium Symporter 4 is Central to C_4 Metabolism in *Flaveria* Species 89

Acknowledgments 127

Summary

Subcellular compartmentalization enabled both pro- and eukaryotic organisms to target metabolic reactions into distinct organelles differing in their pH, redox state as well as metabolite- and protein content. Thus, spatial separation of entire pathways is enabled which in turn translates into new opportunities for regulatory finetuning of metabolic processes. To ensure metabolite flow within the metabolic network of the cell, organellar membranes contain pores, channels and transporters. *In vivo* analyses of transport proteins are challenging due to their low abundance and the frequent necessity to isolate intact organelles. To overcome these limitations, we adapted a rapid isolation technique for plant mitochondria (Manuscript I). We showed that respiratory active mitochondria from root, leaves or seedling tissues can be isolated within 25 minutes from as little as one gram of starting material with sufficient yields. Isolated mitochondria are pure and suitable for proteomics and enzymatic analyses. Optimization of our technique and application to other cell compartments will contribute to ongoing research about metabolite content, redox state and the role of transport proteins of different cellular compartments.

A prime example of a metabolically highly interconnected process is photorespiration. The photorespiratory pathway is a consequence of the oxygenase reaction of Rubisco and takes place in all organisms performing oxygenic photosynthesis. It relies on shuttling of intermediates between chloroplasts, peroxisomes, mitochondria and the cytosol. The photorespiratory pathway has been intensively studied during the last couple of decades, resulting in a comprehensive knowledge of its soluble enzymes. However, only few transport proteins have been identified so far. Recently, the mitochondrial carrier protein À BOUT DE SOUFFLE (BOU) has been described as a mitochondrial glutamate transporter. Knockout of *BOU* results in a strong photorespiratory phenotype, demonstrating its importance within the photorespiratory pathway. However, its physiological role remained enigmatic to date. Biochemical analyses of recombinant BOU and intact *bou-2* mitochondria revealed that BOU is a key regulator of nitrogen re-assimilation during photorespiration (Manuscript II).

To overcome the limitations caused by photorespiration some plants evolved a specialized mechanism to concentrate CO_2 at the site of Rubisco, known as C_4 photosynthesis. This adaptation reduces the rate of photorespiration and increases photosynthetic efficiency. However, the amount of transport steps per fixed molecule CO_2 increased from only one in C_3 to at least ten in C_4 species. We analyzed the role of the plastidic BILE ACID SODIUM SYMPORTER 4 (BASS4) from the C_4 species *Flaveria bidentis*. *BASS4* was previously identified in comparative transcriptomics analyses as a candidate transporter involved in C_4 photosynthesis. We found that BASS4 is a malate transporter with a clearly defined substrate spectrum that catalyzes sodium-driven malate symport *in vitro* (Manuscript III). Moreover, our results emphasize a crucial role of BASS4 within the C_4 pathway and suggest a novel malate transport system within the NADP-dependent malic enzyme subtype.

Zusammenfassung

Die Aufteilung der Zelle in verschiedene Kompartimente ermöglicht es sowohl pro- als auch eukaryotischen Organismen, einzelne Reaktionen oder ganze Stoffwechselwege auf verschiedene Organellen zu begrenzen, die sich unter anderem in ihrem pH-Wert, Redoxzustand sowie ihrer Metabolit- und Proteinzusammensetzung unterscheiden. Dadurch wird eine räumliche Trennung ganzer Stoffwechselwege ermöglicht, was die regulatorische Feinabstimmung verschiedener Prozesse erlaubt. Um den Fluss von Metaboliten innerhalb des metabolischen Netzwerks der Zelle sicherzustellen, enthalten die Membranen der Zellkompartimente verschiedene Poren, Kanäle und Transporter. *In vivo* Analysen von Transportproteinen gestalten sich meist als sehr schwierig, da die betreffenden Proteine nur in geringer Anzahl in der Zelle vorkommen. Außerdem ist es häufig notwendig, intakte Organellen zu isolieren. Um diese Einschränkungen zu überwinden, haben wir eine Methode für die schnelle Isolation von pflanzlichen Mitochondrien adaptiert (Manuskript I). Wir haben gezeigt, dass damit atmungsaktive Mitochondrien aus Blatt-, Wurzel- und Keimlingsgewebe innerhalb von 25 Minuten isoliert werden können. Dabei werden nur wenige Gramm Ausgangsmaterial benötigt und trotzdem können ausreichende Ausbeuten erzielt werden. Die isolierten Mitochondrien sind sehr rein und eignen sich für Proteom- und Enzymaktivitätsanalysen. Die Optimierung unserer Technik sowie deren Anwendung auf andere Zellorganellen wird zu fortlaufender Forschung über den Metabolitgehalt, Redoxzustand und die Rolle von Transportproteinen verschiedener Organellen beitragen.

Ein Paradebeispiel für einen metabolisch stark miteinander verbundenen Prozess ist die Photorespiration, welche als direkte Konsequenz der Oxygenierungsreaktion des Enzyms Rubisco in allen Organismen stattfindet, welche oxygene Photosynthese nutzen. Die Photorespiration ist vom Transport von Zwischenprodukten und Metaboliten zwischen Chloroplasten, Peroxisomen, Mitochondrien und dem Cytosol abhängig. Die Photorespiration wurde in den letzten Jahrzehnten eingehend studiert, was zu einem umfassenden Wissen über die löslichen Enzyme des Stoffwechselwegs führte. Allerdings wurden bisher nur wenige der notwendigen Transportproteine identifiziert. Vor kurzem wurde das Protein der mitochondrialen Carrier Familie À BOUT DE SOUFFLE (BOU) als mitochondrialer Glutamat-Transporter beschrieben. Knockout-Linien zeigen einen charakteristischen photorespiratorischen Phänotyp, was auf die Bedeutung des Proteins innerhalb der Photorespiration hinweist. Bisher konnte die physiologische Rolle des Proteins jedoch nicht eindeutig erklärt werden. Biochemische Untersuchungen mit rekombinantem BOU Protein und physiologische Analysen von intakten *bou-2* Mitochondrien weisen darauf hin, dass BOU eine Schlüsselrolle in der Ammoniumfixierung während der Photorespiration einnimmt (Manuskript II).

Um die Limitierung durch die Photorespiration zu reduzieren, haben einige Pflanzen einen speziellen Mechanismus entwickelt, bei dem CO_2 aktiv um Rubisco konzentriert wird. Dieser Photosynthesetyp ist als C_4 Photosynthese bekannt. Dabei wird die Rate der Photorespiration deutlich reduziert, wohingegen die Photosyntheseeffizienz erhöht wird. Allerdings benötigen C_4-

Pflanzen mindestens zehn Transportschritte pro Molekül fixiertem CO_2, während es in C_3-Pflanzen lediglich einer ist. Wir haben die Rolle des plastidären BILE ACID SODIUM SYMPORT proteins 4 (BASS4) aus der C_4-Pflanze *Flaveria bidentis* analysiert. *BASS4* wurde zuvor in vergleichenden Transkriptomanalysen als Kandidat für ein Transportprotein identifiziert, was an der C_4-Photosynthese beteiligt ist. Wir konnten BASS4 als einen Malat-Transporter mit einem klar definierten Substratspektrum identifizieren. BASS4 ist dazu in der Lage, Natrium-gesteuerten Malat-Symport *in vitro* zu katalysieren (Manuskript III). Darüber hinaus konnten wir zeigen, dass BASS4 eine entscheidende Rolle innerhalb der C_4-Photosynthese spielt. Außerdem deuten unsere Ergebnisse an, dass es sich dabei um ein neues Malat-Transportsystem innerhalb des NADP-Malatenzym-Typs handelt.

Introduction

Membrane proteins account for approximately 30% of the total protein content in most organisms (Paulsen et al., 1998; Krogh et al., 2001; Schwacke et al., 2003; Almén et al., 2009). They play a vital role in structure and dynamics of membrane systems, translocation of ions, metabolites, proteins and nucleotides, replication of organelles and whole cells, signal transduction, and immune response (Lodish, 2000; Heldt and Piechulla, 2011). In *Arabidopsis thaliana* (Arabidopsis), about 5% of all open reading frames encode for transport proteins mediating the active or passive shuttle of ions and metabolites across biological membranes (Elbourne et al., 2017). Transport proteins are key factors in connecting metabolic networks as many pro- and eukaryotic organisms are highly compartmentalized. Compartmentalization within cells presents an evolutionary advantage as (1) it accelerates chemical reactions (Fick, 1995), (2) it enables the generation of concentration gradients, and (3) it allows the creation and maintaining of different local environments (Diekmann and Pereira-Leal, 2013). However, many pathways are distributed over several compartments demonstrating the need of specialized transport proteins since biological membranes are impermeable for ions and metabolites. Enzymes, transporters and auxiliary proteins of metabolic networks have to be strictly regulated to maintain the flux through different pathways (Sweetlove and Fernie, 2013). To completely understand cellular processes and to be able to engineer them it is necessary to decipher the function and regulation of every reaction. The soluble proteins of many pathways have been well described in the last decades. However, due to their hydrophobic nature, analyses of membrane proteins are rather challenging. Functional characterization of transport proteins is often achieved by heterologous expression and transport studies with whole cells or purified proteins reconstituted into liposomes (Haferkamp and Linka, 2012). However, the choice of the expression system and detergent for purification and solubilization are major bottlenecks in the production of sufficient amounts of active transport proteins. Direct analyses of transport proteins *in vivo* are rarely achieved because of their low abundance in whole tissues and the frequent necessity of the isolation of intact organelles (Haferkamp and Linka, 2012).

This thesis focusses on the physiological and biochemical characterization of the mitochondrial carrier protein À BOUT DE SOUFFLE (BOU) from Arabidopsis (Manuscript II) and the plastidial BILE ACID SODIUM SYMPORTER 4 (BASS4) from *Flaveria bidentis* (*F. bidentis*; Manuscript III) within the cellular C_3/C_4-metabolism. Moreover, we successfully adapted a rapid isolation technique for Arabidopsis mitochondria (Manuscript I).

Photosynthesis

Photosynthesis is the basis for almost all life on earth. It is the process in which light energy provided by the sun is transformed into chemical energy in form of NADPH and ATP in the so-called light reactions. The produced energy and reducing equivalents are consumed in a second, so-called dark reaction to synthesize organic carbon compounds from CO_2. In plants and algae, the light reaction takes place in the thylakoids, a membrane system within the chloroplast stroma. Photons are captured by the light harvesting complexes of PSII and PSI and transferred as exciton to their reaction centers (Heldt and Piechulla, 2011) In the reaction center of PSII the transferred light energy is utilized to oxidize water creating molecular oxygen and releasing protons and electrons. The protons are released into the thylakoid lumen thereby generating a proton gradient. The electrons are transferred via pheophytin, plastoquinone and the cytochrome b_6f complex onto PSI releasing additional protons into the thylakoid lumen. In the reaction center of PSI the transferred light energy is utilized to transfer electrons via phylloquinone and ferredoxin to the final electron acceptor $NADP^+$ yielding NADPH (Heldt and Piechulla, 2011). The generated proton gradient is utilized by the ATP-synthase to synthesize ATP. In total, the splitting of two molecules H_2O leads to production of two molecules NADPH and three molecules ATP (Heldt and Piechulla, 2011). In the dark reaction previously generated energy in form of ATP and reducing equivalents in form of NADPH are consumed to assimilate CO_2 in the Calvin-Bassham-Benson cycle (CBBC; Calvin, 1962). In the first part of this cycle, CO_2 is fixed to ribulose 1,5-bisphosphate (RuBP) by the enzyme ribulose 1,5-bisphosphate carboxylase/oxygenase (Rubisco) yielding two molecules 3-phosphoglycerate (3-PGA) which are subsequently reduced to two molecules triose phosphate (TP) in the second part, before the carbon acceptor RuBP can be regenerated in the third part. In total, the assimilation of three molecules atmospheric CO_2 leads to the production of six molecules 3-PGA and subsequently six molecules TP from which five are required for the regeneration of three molecules RuBP. The residual one molecule TP represents the net product of the CBBC. It will be utilized by the chloroplast to synthesize starch or is exported by the triose phosphate-phosphate translocator (Calvin, 1962; Heldt and Piechulla, 2011).

Photorespiration

Rubisco which catalyzes the assimilation of CO_2 to RuBP is the first enzyme of the CBBC. Due to its low catalytic efficiency it is by far the most abundant protein on earth. Rubisco catalyzes merely three to ten reactions per second. To make up for its low catalytic efficiency plants contain high amounts of Rubisco, which can account for up to 50% of the soluble protein content in leaves (Makino and Osmond, 1991; Hartman and Harpel, 1994; Galmés et al., 2014). Besides its carboxylation activity Rubisco can fix molecular oxygen, producing one

molecule 3-PGA and one molecule 2-phosphoglycolate (2-PG). The latter is a dead-end metabolite and a toxic compound that inhibits the stromal enzymes triose phosphate isomerase, phosphofructokinase and sedoheptulose-1,7-bisphosphatase (Anderson, 1971; Bowes et al., 1971; Ogren and Bowes, 1971; Kelly and Latzko, 1976; Ogren, 1984; Flügel et al., 2017). Thus, it has to be rapidly converted in the photorespiratory pathway, which recovers one molecule 3-PGA from two molecules 2-PG (Somerville and Ogren, 1979; Ogren, 1984; Eisenhut et al., 2019). With the photorespiratory pathway 75% of previously fixed carbon that would have been lost as 2-PG is recovered as 3-PGA (South et al., 2017; Fig. 1). However, this comes at the cost of ATP and reducing equivalents, and decreases the photosynthetic efficiency up to 50% (Ogren, 1984; Peterhansel et al., 2010; Walker et al., 2016; South et al., 2017). Modelling analyses revealed that at a given temperature of 25°C and a carbon dioxide concentration of 350 ppm the ratio of Rubisco carboxylation to oxygenation is approximately 5:2 (Sharkey, 1988; Walker et al., 2016). On that basis, out of seven Rubisco reactions five are carboxylations requiring a total of 15 ATP and 10 NADPH and two are oxygenations requiring 7 ATP and 4 NADPH suggesting that photorespiration consumes 32% of total ATP and 28% of total NADPH levels in illuminated leaves at 25°C (Walker et al., 2016). However, photorespiration is strongly dependent on temperature by changing Rubisco kinetics, stomatal conductance, mesophyll conductance and the solubility of CO_2 in water (von Caemmerer, 2000; Walker et al., 2016).

Photorespiration is often considered a wasteful process. However, it is the second most abundant process in oxygenic photosynthesis performing organisms and highly interconnected with amino acid, nitrogen and C_1 metabolism (Sharkey, 1988; Eisenhut et al., 2019; Busch, 2020). Mutants of the photorespiratory pathway often show a conditional chlorotic or lethal phenotype at ambient CO_2. Mutants with this so-called photorespiratory phenotype can be rescued with elevated concentrations of CO_2 (Somerville, 2001; Peterhansel et al., 2010; Timm and Bauwe, 2013).

Core pathway

2-PG deriving from the oxygenation reaction of Rubisco is dephosphorylated in the chloroplast stroma by 2-phosphoglycolate phosphatase (PGLP) yielding glycolate (Fig. 1). Arabidopsis contains two genes encoding PGLP, *PGLP1* and *PGLP2*. However, only PGLP1 is localized to the chloroplast. *Atpglp1* knockout plants are characterized by reduced growth and a conditional lethal phenotype at ambient CO_2 conditions (Somerville and Ogren, 1979; Schwarte and Bauwe, 2007). Glycolate is exported from the chloroplasts by the plastidic glycolate/glycerate translocator (PLGG1; Pick et al., 2013) and the bile acid sodium symporter 6 (BASS6; South et al., 2017). Loss of *PLGG1* and *BASS6* results in accumulation of glycolate and a photorespiratory phenotype of the plants (Pick et al., 2013; South et al.,

2017). Glycolate enters the peroxisomes by a so far unknown transport system and is subsequently oxidized to glyoxylate by glycolate oxidase (GOX) using oxygen as electron acceptor (Volokita and Somerville, 1987). The resulting hydrogen peroxide is detoxified by catalase. Arabidopsis contains five genes encoding for GOX of which two could be identified as the major isoforms in leaf peroxisomes. They display functional redundancy, thus only a double knockout causes a photorespiratory phenotype (Reumann et al., 2007; Engqvist et al., 2015; Dellero et al., 2016). Glyoxylate is subsequently transaminated by glutamate:glyoxylate aminotransferase (GGAT) yielding glycine which is shuttled towards the mitochondria (Igarashi et al., 2003). Neither the peroxisomal nor a mitochondrial glycine transporter have been identified so far (Eisenhut et al., 2019). Transamination of glyoxylate requires glutamate and produces 2-oxoglutarate (2-OG). Arabidopsis contains two genes encoding for GGAT, *GGAT1* and *GGAT2*. Knockout of *GGAT1* shows only a mild photo-respiratory phenotype because both *GGAT1* and *GGAT2* contribute to GGAT activity in leaf peroxisomes (Igarashi et al., 2003; Liepman and Olsen, 2003; Igarashi et al., 2006). In the mitochondria two molecules of glycine are converted into one molecule of serine in the concerted reaction of glycine decarboxylase (GDC) and serine hydroxymethyl transferase (SHMT) releasing previously fixed ammonia and CO_2 (Voll et al., 2006; Engel et al., 2007). Serine enters the peroxisomes by a so far not identified transport system. In the peroxisomes, serine is deaminated to hydroxypyruvate catalyzed by serine:glyoxylate aminotransferase (SGAT). Deamination requires glyoxylate and produces glycine (Somerville and Ogren, 1980). Arabidopsis contains one gene encoding for SGAT whose knockout leads to a conditional lethal phenotype under ambient CO_2 (Liepman and Olsen, 2001; Timm and Bauwe, 2013). Hydroxypyruvate is subsequently reduced to glycerate by hydroxypyruvate reductase (HPR). Arabidopsis contains three genes encoding for HPR, peroxisomal *HPR1*, cytosolic *HPR2* and plastidic *HPR3*. Physiological analyses on single, double and triple mutants suggest that the majority of hydroxypyruvate is converted by the peroxisomal HPR1 (Timm et al., 2008; Timm et al., 2011). Glycerate leaves the peroxisomes and is imported into chloroplasts by PLGG1 where it is converted in the final step of the photorespiratory pathway into 3-PGA (Boldt et al., 2005; Pick et al., 2013). The produced 3-PGA enters the CBBC. Phosphorylation of glycerate is catalyzed by glycerate kinase (GLYK). In Arabidopsis GLYK is encoded by a single copy gene. Loss of *GLYK* results in a conditional lethal phenotype under ambient CO_2 (Boldt et al., 2005).

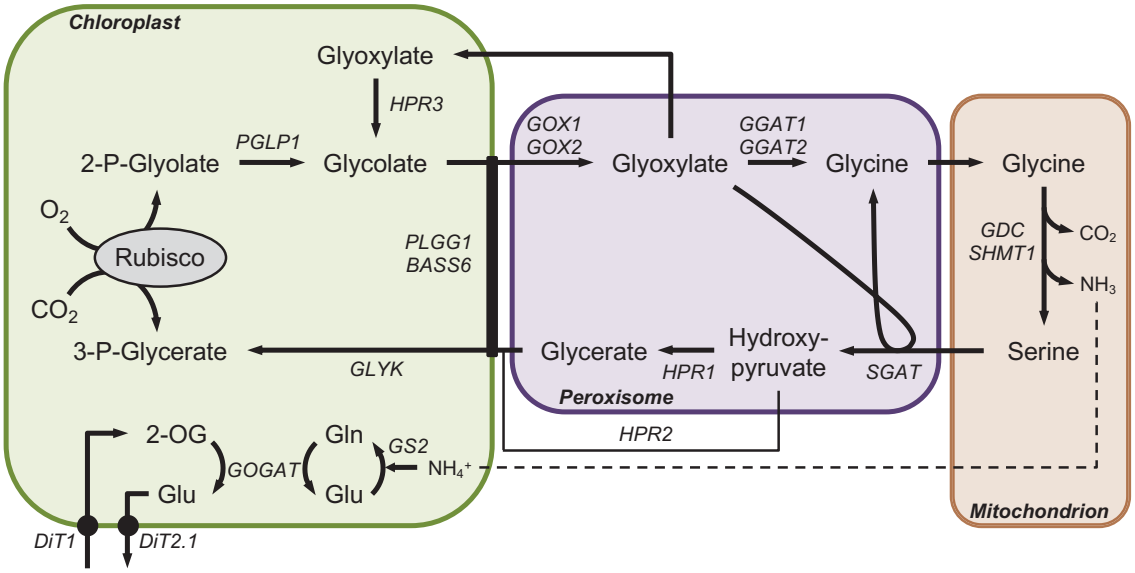

Figure 1: Schematic depiction of the photorespiratory pathway in Arabidopsis. Enzymes and transporters of the pathway are depicted in italics. Abbreviations: BASS6, bile acid sodium symporter 6; DiT, dicarboxylate transporter; GDC, glycine decarboxylase; GGAT, glutamate:glyoxylate aminotransferase; GLYK, glycerate kinase; GOX, glycolate oxidase; GOGAT; glutamine:2-oxoglutarate aminotransferase; GS, glutamine synthetase; HPR, hydroxypyruvate reductase; NH_3, ammonia; 2-OG, 2-oxoglutarate; PGLP, 2-phosphoglycolate phosphatase; PLGG1, plastidic glycolate/ glycerate translocator; SGAT, serine:glyoxylate aminotransferase; SHMT, serine hydroxymethyl transferase.

Nitrogen re-assimilation

Ammonia released by the GDC reaction in the mitochondria is re-assimilated by the plastidial glutamine synthetase (GS)/ferredoxin-dependent glutamine:oxoglutarate aminotransferase (FdGOGAT) system (Fig. 1; Miflin and Lea, 1980; Keys, 2006). It is widely assumed that ammonia diffuses towards the plastids where it is first re-assimilated to glutamate by GS yielding glutamine. Glutamine is utilized in a second reaction by FdGOGAT to transaminate 2-OG yielding two molecules of glutamate. One molecule is needed to re-assimilate another molecule of ammonia, whereas the second is likely shuttled towards the peroxisomes where glutamate is required for the GGAT reaction (Miflin and Lea, 1980; Somerville and Ogren, 1980; Coschigano et al., 1998). 2-OG carbon skeletons for the FdGOGAT reaction are provided by the dicarboxylate carrier DiT1 in counter-exchange with malate. The produced glutamate is exported from chloroplasts by the dicarboxylate carrier DiT2.1 in counter-exchange with malate. The two proteins form an efficient two-translocator system for 2-OG and glutamate without net uptake of malate (Weber et al., 1995; Renné et al., 2003; Schneidereit et al., 2006; Kinoshita et al., 2011). Ammonia re-assimilation is essential for the plant but comes with the cost of one molecule ATP consumed in the GS reaction and one molecule NADPH to reduce oxidized ferredoxin.

Glycine decarboxylase and serine hydroxymethyl transferase reaction

Oxidation of glycine and formation of serine in the mitochondria is catalyzed by GDC in concert with the SHMT. GDC is a multienzyme system composed of the P-(GLDP), H-(GLDH), T-(GLDT) and L-(GLDL) protein (Douce et al., 2001). The actual decarboxylation of glycine is facilitated by GLDP. Glycine enters the mitochondria and is coordinated by GLDP through the formation of a Schiff base with its cofactor pyridoxal 5'-phosphate. CO_2 is released and the remaining methylamine moiety is subsequently transferred onto the distal sulfur atom of the lipoamide cofactor of GLDH. The methylamine moiety is tightly coordinated by hydrogen bonds and Van der Waals contacts which lock the ammonia residue and prevent non-enzymatic cleavage of ammonia (Pares et al., 1994). The coordination of the methylamine group with GLDH is ruptured by GLDT. GLDT modifies the stability of methylated GLDH thereby leading to a release of the methylamine group. Ammonia is subsequently released by a nucleophilic attack catalyzed by tetrahydrofolate (THF), cofactor of GLDT, and the residual methylene subunit is transferred onto THF, forming 5,10-methylene-THF (Guilhaudis et al., 2000; Douce et al., 2001). In the last step of the GDC cycle, GLDL catalyzes the electron transfer from the oxidized lipoamide cofactor of GLDH towards NAD^+ facilitated by its cofactor FAD (Douce et al., 2001). GDC and SHMT are connected through the mitochondrial THF pool. During photorespiration SHMT transfers the C_1 unit from THF onto another molecule of glycine, yielding serine. Under non-photorespiratory conditions SHMT favors the reverse reaction in which glycine and 5,10-methylene-THF are produced from serine indicating that SHMT is constantly pushed out of its equilibrium during photorespiration (Besson et al., 1993; Douce et al., 2001; Hanson and Roje, 2001). It could be demonstrated that the rates of CO_2 release by GDC exceed the rate of normal TCA activity by a factor of five due to enormous concentrations of GDC in the mitochondrial matrix. In mitochondria of illuminated leaves GDC can account for up to 50% of the soluble protein content (Oliver et al., 1990; Douce et al., 2001).

Arabidopsis contains two genes encoding of GLDP, three genes encoding for GLDH, one gene encoding for GLDT, two genes encoding for GLDL and one gene encoding for the mitochondrial photorespiratory SHMT1 (Lutziger and Oliver, 2001; Bauwe and Kolukisaoglu, 2003; Voll et al., 2006; Peterhansel et al., 2010; Timm et al., 2018; Eisenhut et al., 2019). Single knockout of *GLDP* shows no obvious phenotype due to redundancy. A double knockout however is lethal, even under non-photorespiratory conditions (Engel et al., 2007). Same holds true for a knockout of *GLDT* (Timm et al., 2018). Deletion of the mitochondrial photorespiratory *SHMT1* shows a conditional photorespiratory phenotype, whereas the deletion of both mitochondrial *SHMT* is lethal (Voll et al., 2006; Engel et al., 2011). Lethality of a knockout of *GLDP*, *GLDT* and both *SHMT*s underlines the importance of C_1 metabolism

in plant development (Hanson and Roje, 2001; Engel et al., 2007; Engel et al., 2011; Timm et al., 2018; Eisenhut et al., 2019).

Auxiliary pathways

Photorespiration is a non-autonomous process as (1) it is dependent on auxiliary pathways that provide redox power, cofactors and substrates for enzymatic reactions, and (2) it is highly interconnected with the cellular metabolic network (Eisenhut et al., 2019; Busch, 2020). Peroxisomes for instance require a glutamate/2-OG shuttle system for the GGAT reaction and reductive power in form of NADH for the catalytic activity of HPR1. Reductive power is likely provided through a malate/oxaloacetate (OAA) shuttle system and peroxisomal malate dehydrogenase (pMDH; Cousins et al., 2008). Additionally, import of reducing equivalents might be facilitated by the peroxisomal NAD^+ carrier (PXN) which plays an important role in the fatty acid degradation during storage oil mobilization (Bernhardt et al., 2012). Recently, it was shown that PXN is involved in photorespiration and might play a role in modulating peroxisomal NAD^+/NADH pool (Li et al., 2018).

Photorespiration strongly interacts with mitochondrial metabolism as (1) NADH produced by the GDC reaction is oxidized by the respiratory chain, (2) the cofactor of SHMT and GLDT, THF, is a central component of one-carbon metabolism, (3) redox state of the mitochondria during photorespiration is regulated by the uncoupling proteins UCP1 and UCP2 which transport aspartate, glutamate and dicarboxylates, and (4) synthesis of cysteine by mitochondrial O-acetylserine lyase draws serine from the mitochondrial photorespiratory pool (Gardeström and Wigge, 1988; Hanson and Roje, 2001; Sweetlove et al., 2006; Heeg et al., 2008; Monné et al., 2018; Eisenhut et al., 2019; Busch, 2020).

Transporters of the photorespiratory pathway

The soluble enzymes of the photorespiratory pathway have been well described in the last decades. However, only few transporters have been identified to date (Eisenhut et al., 2019). At least nine transport steps are required to shuttle the core metabolites of the pathway (Eisenhut et al., 2013a). To date only the plastidial carriers for glycerate and glycolate PLGG1 and BASS6 were identified and characterized (Pick et al., 2013; South et al., 2017). Additional transport steps are required to shuttle substrates, cofactors and metabolites of auxiliary pathways (Eisenhut et al., 2013a). So far the dicarboxylate carriers DiT1 and DiT2.1 have been identified in the plastidial envelope. They modulate import of 2-OG in exchange for glutamate and are necessary for ammonia re-assimilation during photorespiration (Renné et al., 2003; Schneidereit et al., 2006; Kinoshita et al., 2011). Recently, it was shown that PXN is involved in photorespiration by modulating the peroxisomal NAD^+/NADH pool under fluctuating light conditions (Li et al., 2018). Mitochondrial transporters involved in photo-

respiration are the uncoupling proteins UCP1 and UCP2 and the mitochondrial carrier protein BOU (Sweetlove et al., 2006; Eisenhut et al., 2013b; Monné et al., 2018). UCP1 and UCP2 regulated mitochondrial redox state during photorespiration by transporting aspartate, glutamate and dicarboxylates (Sweetlove et al., 2006; Monné et al., 2018). BOU has recently been identified as mitochondrial glutamate carrier (Porcelli et al., 2018). Knockout of *BOU* leads to a strong conditional lethal photorespiratory phenotype. Moreover, *bou-2* lines show strongly reduced GDC activity in isolated mitochondria (Eisenhut et al., 2013b). However, the exact physiological function of BOU in relation to photorespiration could not be identified to date (Eisenhut et al., 2013b; Kuhnert et al., 2020).

Strategies improving photosynthetic efficiency

World population is estimated to increase by 2 billion people from 2019 to 2050, reaching a total of 9.7 billion people on earth (United Nations, 2019). With an increasing world population, the demand for food rises. To meet the demand in food production global agricultural production needs to double by 2050 (Ray et al., 2013). However, arable land is limited and constantly decreasing (Foley et al., 2005; Maurino and Weber, 2013; Roell and Zurbriggen, 2020). At the same time climate is drastically changing. Plants will have to cope with more extreme weather conditions such as heat, drought or flooding. Many strategies have been described in the last decades to improve crop productivity by increasing photosynthetic efficiency. Those strategies are of synthetic origin and involve the improvement of photosynthesis, the implementation of synthetic CO_2 fixation pathways, and bypasses of highly energy consuming or CO_2 releasing pathways such as photorespiration (Zhu et al., 2010; Parry et al., 2011; Raines, 2011; Evans, 2013; Amthor et al., 2019; Éva et al., 2019; Kubis and Bar-Even, 2019; Weber and Bar-Even, 2019; Roell and Zurbriggen, 2020). Strategies improving photosynthesis have been described for both, the light and the carbon fixing or dark reactions. Improving the photosynthetic light reactions in plants involves studies on the electron transport speed and capacity, photoprotection, PS antenna size, the photosynthetic available spectrum, and brassinosteroid biosynthesis, amongst others (Zhu et al., 2004; Sakamoto et al., 2006; Chida et al., 2007; Melis, 2009; von Caemmerer and Evans, 2010; Chen and Blankenship, 2011; Ort et al., 2011; Huo et al., 2016; Kromdijk et al., 2016). Many studies improving the dark reactions involve the CO_2 assimilating enzyme Rubisco or fructose-1,6-bisphosphatase and seduheptulose-1,7-bisphosphatase, which are rate limiting steps of the CBBC (Woodrow and Mott, 1993; Salvucci and Crafts-Brandner, 2004; Parry et al., 2011; Raines, 2011; Whitney et al., 2011; Yamori et al., 2012; Parry et al., 2013; Lin et al., 2014; Orr et al., 2016; Simkin et al., 2017). Recently, strategies have been described that not only improve Rubisco but also substitute it by alternative carboxylation reactions or replace the CBBC by other pathways such as the malonyl-CoA-oxaloacetate-glyoxylate cycle or the CETCH cycle (Bar-Even et al., 2010; Schwander et al., 2016; Bar-Even, 2018).

However, it is of ongoing research to analyze their compatibility *in planta*. A major target of synthetic biology is the photorespiratory pathway as it releases ammonia, previously fixed CO_2, and consumes ATP and NAD(P)H. Three main bypasses have been described that utilize glycolate and release CO_2 in the chloroplast, thereby avoiding the release of ammonia and circumvent the shuttle of metabolites through peroxisomes and mitochondria (Peterhansel et al., 2008; Peterhansel et al., 2013; South et al., 2019). Implementation of a synthetic glycolate pathway with a simultaneous reduction of PLGG1 lead to improved growth and productivity under field conditions (South et al., 2019). Additional shunts have been described that are CO_2 neutral and directly assimilated 2-PG into the CBBC in chloroplasts. However, their suitability *in planta* has yet to be analyzed (Trudeau et al., 2018).

Plants, algae and cyanobacteria themselves have evolved pathways to improve photosynthetic efficiency by concentrating CO_2 at the site of Rubisco. Such carbon concentrating mechanisms (CCM) can be grouped into biophysical and biochemical mechanisms. Some algae and cyanobacteria use biophysical CCMs. They actively transport CO_2 or bicarbonate into specialized microcompartments called pyrenoids (algae) and carboxysomes (cyanobacteria) leading to an increase of CO_2 at the site of Rubisco of up to 1000-fold (Shively et al., 1973; Badger et al., 1980; Wang et al., 2015; Kerfeld et al., 2018). Biochemical CCMs such as C_4 photosynthesis and crassulacean acid metabolism (CAM) have spatial (C_4) or temporal (CAM) distribution of CO_2 uptake and prefixation into a dicarboxylic acid, and decarboxylation of the formed acid and CO_2 assimilation by Rubisco (Hatch and Slack, 1966; Osmond, 1978). Plants of the genera *Chenopodiaceae* and *Hydrocharitaceae* perform a special version of C_4 photosynthesis. In this type, enzyme activities are not spatially distributed across two cells but within one single chlorenchyma cell (Freitag and Stichler, 2000; Edwards et al., 2004; von Caemmerer et al., 2014). Implementation of such CCMs into higher plants is of ongoing research (Leegood, 2013; von Caemmerer et al., 2017; Rae et al., 2017; Lim et al., 2019). To date a major challenge is the implementation of several genes into plants as well as suitable transformation techniques (Schuler et al., 2016). Additionally, many regulatory factors, anatomical genes, transporters, assembly factors and structural components of the biochemical and biophysical CCMs have not been identified so far.

C_4 photosynthesis

C_4 photosynthesis is characterized by the spatial distribution of CO_2 uptake by the mesophyll cells (MC) and CO_2 assimilation by Rubisco in the adjacent bundle sheath cells (BSC). C_4 photosynthesis was described more than 50 years ago by Hal Hatch and Roger Slack. With $^{14}CO_2$ labelling experiments they demonstrated that atmospheric CO_2 is first assimilated into

OAA, a C_4 acid. Thus, it was termed the 'C_4 decarboxylic acid pathway of photosynthesis', later abbreviated as C_4 pathway or C_4 photosynthesis (Hatch and Slack, 1966; von Caemmerer et al., 2017). C_4 photosynthesis is not only characterized by its distinct biochemistry but also by a specialized anatomical adaptation in the leaf, called Kranz anatomy (Dengler and Nelson, 1999). The vasculature in C_4 plants is surrounded by a layer of BSC, which in turn are encircled by MC. CO_2 is exclusively taken up by the MC and shuttled towards the BSC where the C_4 acid is decarboxylated. The BSC are of a gas-tight nature. They are separated from the adjacent MC by a cell wall that often contains an additional suberin layer or similar structures, which prevents CO_2 leakage and facilitates the concentration of CO_2 at the site of Rubisco (Hatch, 1987; Jenkins et al., 1989; von Caemmerer and Furbank, 2003). This CCM comes at the cost of more energy per fixed molecule of CO_2. However, it enhances water and nitrogen use efficiency. Moreover, C_4 plants have a strongly reduced CO_2 compensation point compared to C_3 plants (Sage, 2004; Ghannoum et al., 2010)

C_4 photosynthesis evolved within the past 40 million years which coincides with predictions about a reduction in CO_2 levels in the atmosphere. C_4 photosynthesis evolved independently in at least 60 lineages of different monocots and eudicots making it a prime example for evolutionary convergence in plant biology (Sage et al., 2011; Sage et al., 2012; Zhang et al., 2013; Sage, 2016). One of the key steps of this evolution was the neofunctionalization of enzymes and transporters from the C_3 ancestors often following gene duplication in these lineages (Monson, 2003). Since the discovery of C_4 photosynthesis in the late 1960s evolution of this trait has been a major research topic. An excellent model to study evolution of C_4 photosynthesis is the genus *Flaveria* as it contains C_3, C_3-C_4 intermediate, C_4-like and C_4 species within one closely related group (Ku et al., 1983; McKown et al., 2005; Gowik et al., 2011). Moreover, the C_4 species *F. bidentis* is transformable and a valuable tool for reverse genetic approaches (Chitty et al., 1994; Furbank et al., 1997; Pengelly et al., 2012).

Biochemistry

C_4 photosynthesis is generally classified into three distinct biochemical subtypes, depending on the decarboxylation enzyme in BSC: (1) NAD-dependent malic enzyme (NAD-ME), (2) NADP-dependent malic enzyme (NADP-ME), and (3) phosphoenolpyruvate carboxykinase (PEP-CK) type (Hatch et al., 1975). However, in many species two or more of these subtypes coexist (Chapman and Hatch, 1981; Furbank, 2011; Pick et al., 2011; Wang et al., 2014b). In all biochemical subtypes atmospheric CO_2 is taken up by the MC and converted into bicarbonate by cytosolic carbonic anhydrase. Bicarbonate is subsequently integrated into phosphoenolpyruvate by the primary carbon fixation enzyme phosphoenolpyruvate carboxylase, yielding OAA. In the case of NADP-ME types, OAA is imported into MC

chloroplasts where it is converted to malate by NADP-dependent malate dehydrogenase (MDH). Malate is subsequently exported from MC chloroplasts, diffuses towards BSC where it is imported into BSC chloroplasts and decarboxylated by NADP-ME. OAA is converted into aspartate by cytosolic aspartate aminotransferase (AspAT) and shuttled towards the BSC in case of NAD-ME and PEP-CK types. In NAD-ME types, aspartate enters the mitochondria where it is first converted into OAA by AspAT and finally into malate by NAD-dependent MDH. The latter is subsequently decarboxylated by mitochondrial NAD-ME. In the PEP-CK type aspartate is converted into OAA by cytosolic aspartate aminotransferase. The majority of OAA is decarboxylated by cytosolic PEP-CK. Additionally, mitochondrial NAD-ME is utilized to provided ATP for the decarboxylation reaction of PEP-CK thereby releasing additional CO_2 (Hatch, 1987; Furbank, 2011). The product of the decarboxylation reactions of NADP-ME and NAD-ME pyruvate diffuses towards the MC where it is imported into chloroplasts in a sodium or proton-coupled manner (Ohnishi and Kanai, 1987; Ohnishi and Kanai, 1990; Furumoto et al., 2011). In the MC chloroplasts PEP is regenerated by the enzyme pyruvate-phosphate dikinase and exported to the cytosol for the primary fixation reaction (Hatch, 1987; Furbank, 2011). In the NADP-ME type the majority of CO_2 is transported in form of malate. However, studies on *Flaveria* and *Zea mays* (*Z. mays*) demonstrated that a substantially amount of carbon is shuttled in form of aspartate (Meister et al., 1996; Pick et al., 2011; Weissmann et al., 2016). In *F. bidentis* aspartate accounts for 35–40% of the total carbon being assimilated in BSC chloroplasts (Meister et al., 1996). Interestingly, the majority of C_4 crop species (maize, sorghum, sugarcrane) belong to the NADP-ME type group providing evidence that this pathway is somewhat superior over the others (Sage, 2004; Furbank, 2011).

In total, NADP-ME type C_4 species require at least ten transport steps per fixed molecule CO_2 and at least 30 to produce one molecule of triose phosphate (Weber and von Caemmerer, 2010). To date, only few of those transporters have been identified or even characterized in detail. Transport proteins are often characterized by relatively low turnover numbers indicating that plants need to compensate for that by synthesizing high amounts of those proteins to maintain the flux through a certain pathway (Weber and von Caemmerer, 2010). This hypothesis was supported by comparative proteomic analyses on plastid envelopes of C_3 and C_4 species. Transporters with importance in the C_4 pathway are expected to be more abundant in the envelopes from C_4 species than C_3 (Bräutigam et al., 2008). Additionally, they are expected to be differentially abundant between MC and BSC within a C_4 species (Majeran et al., 2005; Majeran et al., 2008; Majeran et al., 2010). The same holds true for their transcript abundance in comparative transcriptomic studies (Bräutigam et al., 2011; Wang et al., 2014a; Denton et al., 2017; Billakurthi et al., 2018). In the NADP-ME type species *Z. mays* import of OAA in chloroplasts of MC in counter-

exchange with malate is likely facilitated by the OAA/malate translocator (Taniguchi et al., 2004). The protein has been analyzed biochemically. However, so far there are no mutant studies available. Malate import into chloroplasts of BSC in *Z. mays* is likely catalyzed in counter-exchange with aspartate by the dicarboxylate carrier DCT2. The protein has been investigated biochemically (Taniguchi et al., 2004). Additionally, mutant studies in *Z. mays* support the importance of DCT2 for C_4 metabolism (Weissmann et al., 2016). Recent studies on dicarboxylate carriers in *Sorghum bicolor* revealed a potential role for the malate transporter DCT4 in the C_4 pathway. However, the exact physiological function of the protein is a topic of ongoing research (Weissmann et al., 2019). In the NADP-ME type species *F. bidentis* pyruvate import into MC chloroplasts is likely facilitated by a two translocator system of the bile acid sodium symporter 2 together with the sodium/proton antiporter NHD1 (Furumoto et al., 2011). However, detailed physiological analyses including mutant studies are still lacking. Candidate for the export of PEP from the MC chloroplasts in all NADP-ME and NAD-ME type species is the PEP/phosphate translocator (Bräutigam et al., 2008; Majeran et al., 2008; Bräutigam et al., 2011). However, there haven't been any studies on the physiological role of the protein in C_4 photosynthesis. Especially the physiological roles of many transporters and transport candidates remains enigmatic due to a reduced availability of suitable transformation techniques for several C_4 species (Schuler et al., 2016).

References

Almén M, Nordström KJ, Fredriksson R, Schiöth HB (2009) Mapping the human membrane proteome: a majority of the human membrane proteins can be classified according to function and evolutionary origin. BMC Biol **7**: 50

Amthor JS, Bar-Even A, Hanson AD, Millar AH, Stitt M, Sweetlove LJ, Tyerman SD (2019) Engineering Strategies to Boost Crop Productivity by Cutting Respiratory Carbon Loss. Plant Cell **31**: 297–314

Anderson LE (1971) Chloroplast and cytoplasmic enzymes II. Pea leaf triose phosphate isomerases. Biochim Biophys Acta - Enzymol **235**: 237–244

Badger MR, Kaplan A, Berry JA (1980) Internal Inorganic Carbon Pool of Chlamydomonas reinhardtii. Evidence for a Carbon Dioxide-Concentrating Mechanism. Plant Physiol **66**: 407–413

Bar-Even A (2018) Daring metabolic designs for enhanced plant carbon fixation. Plant Sci **273**: 71–83

Bar-Even A, Noor E, Lewis NE, Milo R (2010) Design and analysis of synthetic carbon fixation pathways. Proc Natl Acad Sci U S A **107**: 8889–8894

Bauwe H, Kolukisaoglu Ü (2003) Genetic manipulation of glycine decarboxylation. J Exp Bot **54**: 1523–1535

Bernhardt K, Wilkinson S, Weber APM, Linka N (2012) A peroxisomal carrier delivers NAD+ and contributes to optimal fatty acid degradation during storage oil mobilization. Plant J **69**: 1–13

Besson V, Rebeille F, Neuburger M, Douce R, Cossins EA (1993) Effects of tetrahydrofolate polyglutamates on the kinetic parameters of serine hydroxymethyltransferase and glycine decarboxylase from pea leaf mitochondria. Biochem J **292**: 425–430

Billakurthi K, Wrobel TJ, Bräutigam A, Weber APM, Westhoff P, Gowik U (2018) Transcriptome dynamics in developing leaves from C3 and C4 Flaveria species reveal determinants of Kranz anatomy. bioRxiv. doi: 10.1101/473181

Boldt R, Edner C, Kolukisaoglu Ü, Hagemann M, Weckwerth W, Wienkoop S, Morgenthal K, Bauwe H (2005) d-GLYCERATE 3-KINASE, the Last Unknown Enzyme in the Photorespiratory Cycle in Arabidopsis, Belongs to a Novel Kinase Family. Plant Cell **17**: 2413–2420

Bowes G, Ogren WL, Hageman RH (1971) Phosphoglycolate production catalyzed by ribulose diphosphate carboxylase. Biochem Biophys Res Commun **45**: 716–722

Bräutigam A, Hoffmann-Benning S, Weber APM (2008) Comparative Proteomics of Chloroplast Envelopes from C3 and C4 Plants Reveals Specific Adaptations of the Plastid Envelope to C4 Photosynthesis and Candidate Proteins Required for Maintaining C4 Metabolite Fluxes. Plant Physiol **148**: 568–579

Bräutigam A, Kajala K, Wullenweber J, Sommer M, Gagneul D, Weber KL, Carr KM, Gowik U, Maß J, Lercher MJ, et al (2011) An mRNA Blueprint for C4 Photosynthesis Derived from Comparative Transcriptomics of Closely Related C3 and C4 Species. Plant Physiol **155**: 142–156

Busch FA (2020) Photorespiration in the context of Rubisco biochemistry, CO2 diffusion and metabolism. Plant J **101**: 919–939

von Caemmerer S (2000) Biochemical Models of Leaf Photosynthesis. doi: 10.1071/9780643103405

von Caemmerer S, Edwards GE, Koteyeva N, Cousins AB (2014) Single cell C4 photosynthesis in aquatic and terrestrial plants: A gas exchange perspective. Aquat Bot **118**: 71–80

von Caemmerer S, Evans JR (2010) Enhancing C3 Photosynthesis. Plant Physiol **154**: 589–592

von Caemmerer S, Furbank RT (2003) The C(4) pathway: an efficient CO(2) pump. Photosynth Res **77**: 191–207

von Caemmerer S, Ghannoum O, Furbank RT (2017) C4 photosynthesis: 50 years of discovery and innovation. J Exp Bot **68**: 97–102

Calvin M (1962) The Path of Carbon in Photosynthesis. Angew Chemie Int Ed English **1**: 65–75

Chapman KSR, Hatch MD (1981) Regulation of C4 photosynthesis: Mechanism of activation and inactivation of extracted pyruvate, inorganic phosphate dikinase in relation to dark/light regulation. Arch Biochem Biophys **210**: 82–89

Chen M, Blankenship RE (2011) Expanding the solar spectrum used by photosynthesis. Trends Plant Sci **16**: 427–431

Chida H, Nakazawa A, Akazaki H, Hirano T, Suruga K, Ogawa M, Satoh T, Kadokura K, Yamada S, Hakamata W, et al (2007) Expression of the Algal Cytochrome c6 Gene in Arabidopsis Enhances Photosynthesis and Growth. Plant Cell Physiol **48**: 948–957

Chitty JA, Furbank RT, Marshall JS, Chen Z, Taylor WC (1994) Genetic transformation of the C4 plant, Flaveria bidentis. Plant J **6**: 949–956

Coschigano KT, Melo-Oliveira R, Lim J, Coruzzi GM (1998) Arabidopsis gls Mutants and Distinct Fd-GOGAT Genes: Implications for Photorespiration and Primary Nitrogen Assimilation. Plant Cell **10**: 741–752

Cousins AB, Pracharoenwattana I, Zhou W, Smith SM, Badger MR (2008) Peroxisomal Malate Dehydrogenase Is Not Essential for Photorespiration in Arabidopsis But Its Absence Causes an Increase in the Stoichiometry of Photorespiratory CO 2 Release. Plant Physiol **148**: 786–795

Dellero Y, Jossier M, Glab N, Oury C, Tcherkez G, Hodges M (2016) Decreased glycolate oxidase activity leads to altered carbon allocation and leaf senescence after a transfer from high CO2 to ambient air in Arabidopsis thaliana. J Exp Bot **67**: 3149–3163

Dengler NG, Nelson T (1999) Leaf Structure and Development in C4 Plants. C4 Plant Biol. Elsevier, pp 133–172

Denton AK, Maß J, Külahoglu C, Lercher MJ, Bräutigam A, Weber APM (2017) Freeze-quenched maize mesophyll and bundle sheath separation uncovers bias in previous tissue-specific RNA-Seq data. J Exp Bot **68**: 147–160

Diekmann Y, Pereira-Leal JB (2013) Evolution of intracellular compartmentalization. Biochem J **449**: 319–31

Douce R, Bourguignon J, Neuburger M, Rébeillé F (2001) The glycine decarboxylase system: a fascinating complex. Trends Plant Sci **6**: 167–176

Edwards GE, Franceschi VR, Voznesenskaya E V. (2004) Single-Cell C4 Photosynthesis Versus The Dual-Cell (Kranz) Paradigm. Annu Rev Plant Biol **55**: 173–196

Eisenhut M, Pick TR, Bordych C, Weber APM (2013a) Towards closing the remaining gaps in photorespiration - the essential but unexplored role of transport proteins. Plant Biol **15**: 676–685

Eisenhut M, Planchais S, Cabassa C, Guivarc'h A, Justin A-M, Taconnat L, Renou J-P, Linka M, Gagneul D, Timm S, et al (2013b) Arabidopsis A BOUT DE SOUFFLE is a putative mitochondrial transporter involved in photorespiratory metabolism and is required for meristem growth at ambient CO2 levels. Plant J **73**: 836–849

Eisenhut M, Roell M, Weber APM (2019) Mechanistic understanding of photorespiration paves the way to a new green revolution. New Phytol **223**: 1762–1769

Elbourne LDH, Tetu SG, Hassan KA, Paulsen IT (2017) TransportDB 2.0: a database for exploring membrane transporters in sequenced genomes from all domains of life. Nucleic Acids Res **45**: D320–D324

Engel N, van den Daele K, Kolukisaoglu Ü, Morgenthal K, Weckwerth W, Pärnik T, Keerberg O, Bauwe H (2007) Deletion of Glycine Decarboxylase in Arabidopsis Is Lethal under Nonphotorespiratory Conditions. Plant Physiol **144**: 1328–1335

Engel N, Ewald R, Gupta KJ, Zrenner R, Hagemann M, Bauwe H (2011) The Presequence of Arabidopsis Serine Hydroxymethyltransferase SHM2 Selectively Prevents Import into Mesophyll Mitochondria. Plant Physiol **157**: 1711–1720

Engqvist MKM, Schmitz J, Gertzmann A, Florian A, Jaspert N, Arif M, Balazadeh S, Mueller-Roeber B, Fernie AR, Maurino VG (2015) GLYCOLATE OXIDASE3, a Glycolate Oxidase Homolog of Yeast l-Lactate Cytochrome c Oxidoreductase, Supports l-Lactate Oxidation in Roots of Arabidopsis. Plant Physiol **169**: 1042–1061

Éva C, Oszvald M, Tamás L (2019) Current and possible approaches for improving photosynthetic efficiency. Plant Sci **280**: 433–440

Evans JR (2013) Improving Photosynthesis. Plant Physiol **162**: 1780–1793

Fick A (1995) On liquid diffusion. J Memb Sci **100**: 33–38

Flügel F, Timm S, Arrivault S, Florian A, Stitt M, Fernie AR, Bauwe H (2017) The Photorespiratory Metabolite 2-Phosphoglycolate Regulates Photosynthesis and Starch Accumulation in Arabidopsis. Plant Cell **29**: 2537–2551

Foley JA, Defries R, Asner GP, Barford C, Bonan G, Carpenter SR, Chapin FS, Coe MT, Daily GC, Gibbs HK, et al (2005) Global consequences of land use. Science **309**: 570–574

Freitag H, Stichler W (2000) A remarkable new leaf type with unusual photosynthetic tissue in a central asiatic genus of chenopodiaceae. Plant Biol **2**: 154–160

Furbank RT (2011) Evolution of the C4 photosynthetic mechanism: are there really three C4 acid decarboxylation types? J Exp Bot **62**: 3103–3108

Furbank RT, Chitty JA, Jenkins CLD, Taylor WC, Trevanion SJ, Caemmerer S von, Ashton AR (1997) Genetic Manipulation of Key Photosynthetic Enzymes in the C4 Plant Flaveria bidentis. Funct Plant Biol **24**:

477

Furumoto T, Yamaguchi T, Ohshima-Ichie Y, Nakamura M, Tsuchida-Iwata Y, Shimamura M, Ohnishi J, Hata S, Gowik U, Westhoff P, et al (2011) A plastidial sodium-dependent pyruvate transporter. Nature **476**: 472–475

Galmés J, Kapralov M V., Andralojc PJ, Conesa MÀ, Keys AJ, Parry MAJ, Flexas J (2014) Expanding knowledge of the Rubisco kinetics variability in plant species: environmental and evolutionary trends. Plant Cell Environ **37**: 1989–2001

Gardeström P, Wigge B (1988) Influence of Photorespiration on ATP/ADP Ratios in the Chloroplasts, Mitochondria, and Cytosol, Studied by Rapid Fractionation of Barley (Hordeum vulgare) Protoplasts. Plant Physiol **88**: 69–76

Ghannoum O, Evans JR, von Caemmerer S (2010) Chapter 8 Nitrogen and Water Use Efficiency of C4 Plants. *In* AS Raghavendra, RF Sage, eds, C4 Photosynth. Relat. CO2 Conc. Mech. Springer Netherlands, Dordrecht, pp 129–146

Gowik U, Bräutigam A, Weber KL, Weber APM, Westhoff P (2011) Evolution of C4 Photosynthesis in the Genus Flaveria : How Many and Which Genes Does It Take to Make C4? Plant Cell **23**: 2087–2105

Guilhaudis L, Simorre J-P, Blackledge M, Marion D, Gans P, Neuburger M, Douce R (2000) Combined Structural and Biochemical Analysis of the H−T Complex in the Glycine Decarboxylase Cycle: Evidence for a Destabilization Mechanism of the H-Protein †. Biochemistry **39**: 4259–4266

Haferkamp I, Linka N (2012) Functional expression and characterisation of membrane transport proteins. Plant Biol **14**: 675–690

Hanson AD, Roje S (2001) One-Carbon Metabolism in Higher Plants. Annu Rev Plant Physiol Plant Mol Biol **52**: 119–137

Hartman FC, Harpel MR (1994) Structure, Function, Regulation, and Assembly of D-Ribulose-1,5-Bisphosphate Carboxylase/Oxygenase. Annu Rev Biochem **63**: 197–232

Hatch MD (1987) C4 photosynthesis: a unique blend of modified biochemistry, anatomy and ultrastructure. Biochim Biophys Acta - Rev Bioenerg **895**: 81–106

Hatch MD, Kagawa T, Craig S (1975) Subdivision of C_4-Pathway Species Based on Differing C_4 Acid Decarboxylating Systems and Ultrastructural Features. Funct Plant Biol **2**: 111–128

Hatch MD, Slack C (1966) Photosynthesis by sugar-cane leaves. A new carboxylation reaction and the pathway of sugar formation. Biochem J **101**: 103–111

Heeg C, Kruse C, Jost R, Gutensohn M, Ruppert T, Wirtz M, Hell R (2008) Analysis of the Arabidopsis O -Acetylserine(thiol)lyase Gene Family Demonstrates Compartment-Specific Differences in the Regulation of Cysteine Synthesis. Plant Cell **20**: 168–185

Heldt H-W, Piechulla B (2011) Plant Biochemistry. Plant Biochem. doi: 10.1016/B978-0-12-384986-1.00003-X

Huo Y, Wang M, Wei Y, Xia Z (2016) Overexpression of the Maize psbA Gene enhances drought tolerance through regulating antioxidant system, photosynthetic capability, and stress defense Gene expression in tobacco. Front Plant Sci **6**: 1–10

Igarashi D, Miwa T, Seki M, Kobayashi M, Kato T, Tabata S, Shinozaki K, Ohsumi C (2003) Identification of photorespiratory glutamate:glyoxylate aminotransferase (GGAT) gene in Arabidopsis. Plant J **33**: 975–987

Igarashi D, Tsuchida H, Miyao M, Ohsumi C (2006) Glutamate:Glyoxylate aminotransferase modulates amino acid content during photorespiration. Plant Physiol **142**: 901–910

Jenkins CLD, Furbank RT, Hatch MD (1989) Inorganic Carbon Diffusion between C4 Mesophyll and Bundle Sheath Cells. Plant Physiol **91**: 1356–1363

Kelly GJ, Latzko E (1976) Inhibition of spinach-leaf phosphofructokinase by 2-phosphoglycollate. FEBS Lett **68**: 55–58

Kerfeld CA, Aussignargues C, Zarzycki J, Cai F, Sutter M, Heinhorst S, Cannon GC (2018) Bacterial microcompartments. Nat Rev Microbiol **16**: 277–290

Keys AJ (2006) The re-assimilation of ammonia produced by photorespiration and the nitrogen economy of C3 higher plants. Photosynth Res **87**: 165–175

Kinoshita H, Nagasaki J, Yoshikawa N, Yamamoto A, Takito S, Kawasaki M, Sugiyama T, Miyake H, Weber APM, Taniguchi M (2011) The chloroplastic 2-oxoglutarate/malate transporter has dual function as the malate valve and in carbon/nitrogen metabolism. Plant J **65**: 15–26

Krogh A, Larsson B, von Heijne G, Sonnhammer EL (2001) Predicting transmembrane protein topology with a hidden markov model: application to complete genomes. J Mol Biol **305**: 567–580

Kromdijk J, Głowacka K, Leonelli L, Gabilly ST, Iwai M, Niyogi KK, Long SP (2016) Improving photosynthesis and crop productivity by accelerating recovery from photoprotection. Science **354**: 857–861

Ku MSB, Monson RK, Littlejohn RO, Nakamoto H, Fisher DB, Edwards GE (1983) Photosynthetic Characteristics of C3 -C4 Intermediate Flaveria Species. Plant Physiol **71**: 944–948

Kubis A, Bar-Even A (2019) Synthetic biology approaches for improving photosynthesis. J Exp Bot **70**: 1425–1433

Kuhnert F, Stefanski A, Overbeck N, Drews L, Reichert AS, Stühler K, Weber APM (2020) Rapid Single-Step Affinity Purification of HA-Tagged Plant Mitochondria. Plant Physiol **182**: 692–706

Leegood RC (2013) Strategies for engineering C4 photosynthesis. J Plant Physiol **170**: 378–388

Li J, Tietz S, Cruz JA, Strand DD, Xu Y, Chen J, Kramer DM, Hu J (2018) Photometric screens identified Arabidopsis peroxisome proteins that impact photosynthesis under dynamic light conditions. Plant J **97**: 460–474

Liepman AH, Olsen LJ (2003) Alanine Aminotransferase Homologs Catalyze the Glutamate:Glyoxylate Aminotransferase Reaction in Peroxisomes of Arabidopsis. Plant Physiol **131**: 215–227

Liepman AH, Olsen LJ (2001) Peroxisomal alanine : glyoxylate aminotransferase (AGT1) is a photorespiratory enzyme with multiple substrates in Arabidopsis thaliana. Plant J **25**: 487–498

Lim SD, Lee S, Choi W-G, Yim WC, Cushman JC (2019) Laying the Foundation for Crassulacean Acid Metabolism (CAM) Biodesign: Expression of the C4 Metabolism Cycle Genes of CAM in Arabidopsis. Front Plant Sci **10**: 1–20

Lin MT, Occhialini A, Andralojc PJ, Parry MAJ, Hanson MR (2014) A faster Rubisco with potential to increase photosynthesis in crops. Nature **513**: 547–550

Lodish HF (2000) Molecular Cell Biology, 4th ed. W.H. Freeman, New York

Lutziger I, Oliver DJ (2001) Characterization of Two cDNAs Encoding Mitochondrial Lipoamide Dehydrogenase from Arabidopsis. Plant Physiol **127**: 615–623

Majeran W, Cai Y, Sun Q, van Wijk KJ (2005) Functional Differentiation of Bundle Sheath and Mesophyll Maize Chloroplasts Determined by Comparative Proteomics. Plant Cell **17**: 3111–3140

Majeran W, Friso G, Ponnala L, Connolly B, Huang M, Reidel E, Zhang C, Asakura Y, Bhuiyan NH, Sun Q, et al (2010) Structural and Metabolic Transitions of C4 Leaf Development and Differentiation Defined by Microscopy and Quantitative Proteomics in Maize. Plant Cell **22**: 3509–3542

Majeran W, Zybailov B, Ytterberg AJ, Dunsmore J, Sun Q, van Wijk KJ (2008) Consequences of C4 Differentiation for Chloroplast Membrane Proteomes in Maize Mesophyll and Bundle Sheath Cells. Mol Cell Proteomics **7**: 1609–1638

Makino A, Osmond B (1991) Effects of nitrogen nutrition on nitrogen partitioning between chloroplasts and mitochondria in pea and wheat. Plant Physiol **96**: 355–362

Maurino VG, Weber APM (2013) Engineering photosynthesis in plants and synthetic microorganisms. J Exp Bot **64**: 743–751

McKown AD, Moncalvo J-M, Dengler NG (2005) Phylogeny of Flaveria (Asteraceae) and inference of C4 photosynthesis evolution. Am J Bot **92**: 1911–1928

Meister M, Agostino A, Hatch M (1996) The roles of malate and aspartate in C4 photosynthetic metabolism of Flaveria bidentis (L.). Planta **199**: 262–269

Melis A (2009) Solar energy conversion efficiencies in photosynthesis: Minimizing the chlorophyll antennae to maximize efficiency. Plant Sci **177**: 272–280

Miflin BJ, Lea PJ (1980) Ammonia Assimilation. *In* BJBT-AA and D Miflin, ed, Amin. Acids Deriv. Elsevier, pp 169–202

Monné M, Daddabbo L, Gagneul D, Obata T, Hielscher B, Palmieri L, Miniero DV, Fernie AR, Weber APMM, Palmieri F (2018) Uncoupling proteins 1 and 2 (UCP1 and UCP2) from Arabidopsis thaliana are mitochondrial transporters of aspartate, glutamate, and dicarboxylates. J Biol Chem **293**: 4213–4227

Monson RK (2003) Gene Duplication, Neofunctionalization, and the Evolution of C4 Photosynthesis. Int J Plant Sci **164**: S43–S54

Ogren WL (1984) Photorespiration: Pathways, Regulation, and Modification. Annu Rev Plant Physiol **35**: 415–442

Ogren WL, Bowes G (1971) Ribulose Diphosphate Carboxylase regulates Soybean Photorespiration. Nat New Biol **230**: 159–160

Ohnishi J, Kanai R (1987) Na + -induced uptake of pyruvate into mesophyll chloroplasts of a C4 plant, Panicum miliaceum. FEBS Lett **219**: 347–350

Ohnishi J, Kanai R (1990) Pyruvate uptake induced by a pH jump in mesophyll chloroplasts of maize and sorghum, NADP-malic enzyme type C4 species. FEBS Lett **269**: 122–124

Oliver DJ, Neuburger M, Bourguignon J, Douce R (1990) Interaction between the Component Enzymes of the Glycine Decarboxylase Multienzyme Complex. Plant Physiol **94**: 833–9

Orr D, Alcântara A, Kapralov M V., Andralojc J, Carmo-Silva E, Parry MAJ (2016) Surveying Rubisco diversity and temperature response to improve crop photosynthetic efficiency. Plant Physiol **172**: pp.00750.2016

Ort DR, Zhu X, Melis A (2011) Optimizing Antenna Size to Maximize Photosynthetic Efficiency. Plant Physiol **155**: 79–85

Osmond CB (1978) Crassulacean Acid Metabolism: A Curiosity in Context. Annu Rev Plant Physiol **29**: 379–414

Pares S, Cohen-Addad C, Sieker L, Neuburger M, Douce R (1994) X-ray structure determination at 2.6-A resolution of a lipoate-containing protein: the H-protein of the glycine decarboxylase complex from pea leaves. Proc Natl Acad Sci **91**: 4850–4853

Parry MAJ, Andralojc PJ, Scales JC, Salvucci ME, Carmo-Silva AE, Alonso H, Whitney SM (2013) Rubisco activity and regulation as targets for crop improvement. J Exp Bot **64**: 717–730

Parry MAJ, Reynolds M, Salvucci ME, Raines C, Andralojc PJ, Zhu X-G, Price GD, Condon AG, Furbank RT (2011) Raising yield potential of wheat. II. Increasing photosynthetic capacity and efficiency. J Exp Bot **62**: 453–467

Paulsen IT, Sliwinski MK, Nelissen B, Goffeau A, Saier MH (1998) Unified inventory of established and putative transporters encoded within the complete genome of Saccharomyces cerevisiae. FEBS Lett **430**: 116–125

Pengelly JJL, Tan J, Furbank RT, von Caemmerer S (2012) Antisense Reduction of NADP-Malic Enzyme in Flaveria bidentis Reduces Flow of CO2 through the C4 Cycle. Plant Physiol **160**: 1070–1080

Peterhansel C, Blume C, Offermann S (2013) Photorespiratory bypasses: how can they work? J Exp Bot **64**: 709–715

Peterhansel C, Horst I, Niessen M, Blume C, Kebeish R, Kürkcüoglu S, Kreuzaler F (2010) Photorespiration. Arab B **8**: e0130

Peterhansel C, Niessen M, Kebeish RM (2008) Metabolic engineering towards the enhancement of photosynthesis. Photochem Photobiol **84**: 1317–1323

Pick TR, Bräutigam A, Schlüter U, Denton AK, Colmsee C, Scholz U, Fahnenstich H, Pieruschka R, Rascher U, Sonnewald U, et al (2011) Systems Analysis of a Maize Leaf Developmental Gradient Redefines the Current C4 Model and Provides Candidates for Regulation. Plant Cell **23**: 4208–4220

Pick TR, Brautigam A, Schulz MA, Obata T, Fernie AR, Weber APM (2013) PLGG1, a plastidic glycolate glycerate transporter, is required for photorespiration and defines a unique class of metabolite transporters. Proc Natl Acad Sci **110**: 3185–3190

Porcelli V, Vozza A, Calcagnile V, Gorgoglione R, Arrigoni R, Fontanesi F, Marobbio CMT, Castegna A, Palmieri F, Palmieri L (2018) Molecular identification and functional characterization of a novel glutamate transporter in yeast and plant mitochondria. Biochim Biophys Acta - Bioenerg **1859**: 1249–1258

Rae BD, Long BM, Förster B, Nguyen ND, Velanis CN, Atkinson N, Hee WY, Mukherjee B, Price GD, McCormick AJ (2017) Progress and challenges of engineering a biophysical CO2-concentrating mechanism into higher plants. J Exp Bot **68**: 3717–3737

Raines CA (2011) Increasing Photosynthetic Carbon Assimilation in C 3 Plants to Improve Crop Yield: Current and Future Strategies. Plant Physiol **155**: 36–42

Ray DK, Mueller ND, West PC, Foley JA (2013) Yield Trends Are Insufficient to Double Global Crop Production by 2050. PLoS One **8**: e66428

Renné P, Dreßen U, Hebbeker U, Hille D, Flügge U-I, Westhoff P, Weber APM (2003) The Arabidopsis mutant dct is deficient in the plastidic glutamate/malate translocator DiT2. Plant J **35**: 316–331

Reumann S, Babujee L, Ma C, Wienkoop S, Siemsen T, Antonicelli GE, Rasche N, Lüder F, Weckwerth W, Jahn O (2007) Proteome Analysis of Arabidopsis Leaf Peroxisomes Reveals Novel Targeting Peptides, Metabolic Pathways, and Defense Mechanisms. Plant Cell **19**: 3170–3193

Roell M-S, Zurbriggen MD (2020) The impact of synthetic biology for future agriculture and nutrition. Curr Opin Biotechnol **61**: 102–109

Sage RF (2016) A portrait of the C4 photosynthetic family on the 50th anniversary of its discovery: species number, evolutionary lineages, and Hall of Fame. J Exp Bot **67**: 4039–4056

Sage RF (2004) The evolution of C_4 photosynthesis. New Phytol **161**: 341–370

Sage RF, Christin P-A, Edwards EJ (2011) The C4 plant lineages of planet Earth. J Exp Bot **62**: 3155–3169

Sage RF, Sage TL, Kocacinar F (2012) Photorespiration and the Evolution of C $_4$ Photosynthesis. Annu Rev Plant Biol **63**: 19–47

Sakamoto T, Morinaka Y, Ohnishi T, Sunohara H, Fujioka S, Ueguchi-Tanaka M, Mizutani M, Sakata K, Takatsuto S, Yoshida S, et al (2006) Erect leaves caused by brassinosteroid deficiency increase biomass production and grain yield in rice. Nat Biotechnol **24**: 105–109

Salvucci ME, Crafts-Brandner SJ (2004) Mechanism for deactivation of Rubisco under moderate heat stress. Physiol Plant **122**: 513–519

Schneidereit J, Häusler RE, Fiene G, Kaiser WM, Weber APM (2006) Antisense repression reveals a crucial role of the plastidic 2-oxoglutarate/malate translocator DiT1 at the interface between carbon and nitrogen metabolism. Plant J **45**: 206–224

Schuler ML, Mantegazza O, Weber APM (2016) Engineering C4 photosynthesis into C3 chassis in the synthetic biology age. Plant J **87**: 51–65

Schwacke R, Schneider A, van der Graaff E, Fischer K, Catoni E, Desimone M, Frommer WB, Flügge U-I, Kunze R (2003) ARAMEMNON, a Novel Database for Arabidopsis Integral Membrane Proteins. Plant Physiol **131**: 16–26

Schwander T, Schada von Borzyskowski L, Burgener S, Cortina NS, Erb TJ (2016) A synthetic pathway for the fixation of carbon dioxide in vitro. Science **354**: 900–904

Schwarte S, Bauwe H (2007) Identification of the Photorespiratory 2-Phosphoglycolate Phosphatase, PGLP1, in Arabidopsis. Plant Physiol **144**: 1580–1586

Sharkey TD (1988) Estimating the rate of photorespiration in leaves. Physiol Plant **73**: 147–152

Shively JM, Ball F, Brown DH, Saunders RE (1973) Functional Organelles in Prokaryotes: Polyhedral Inclusions (Carboxysomes) of Thiobacillus neapolitanus. Science **182**: 584–586

Simkin AJ, Lopez-Calcagno PE, Davey PA, Headland LR, Lawson T, Timm S, Bauwe H, Raines CA (2017) Simultaneous stimulation of sedoheptulose 1,7-bisphosphatase, fructose 1,6-bisphophate aldolase and the photorespiratory glycine decarboxylase-H protein increases CO2 assimilation, vegetative biomass and seed yield in Arabidopsis. Plant Biotechnol J **15**: 805–816

Somerville CR (2001) An Early Arabidopsis Demonstration. Resolving a Few Issues Concerning Photorespiration: Fig. 1. Plant Physiol **125**: 20–24

Somerville CR, Ogren WL (1979) A phosphoglycolate phosphatase-deficient mutant of Arabidopsis. Nature **280**: 833–836

Somerville CR, Ogren WL (1980) Photorespiration mutants of Arabidopsis thaliana deficient in serine-glyoxylate aminotransferase activity. Proc Natl Acad Sci **77**: 2684–2687

South PF, Cavanagh AP, Liu HW, Ort DR (2019) Synthetic glycolate metabolism pathways stimulate crop growth and productivity in the field. Science **363**: 45

South PF, Walker BJ, Cavanagh AP, Rolland V, Badger M, Ort DR (2017) Bile Acid Sodium Symporter BASS6 Can Transport Glycolate and Is Involved in Photorespiratory Metabolism in Arabidopsis thaliana. Plant Cell **29**: 808–823

Sweetlove LJ, Fernie AR (2013) The Spatial Organization of Metabolism Within the Plant Cell. Annu Rev Plant Biol **64**: 723–746

Sweetlove LJ, Lytovchenko A, Morgan M, Nunes-Nesi A, Taylor NL, Baxter CJ, Eickmeier I, Fernie AR (2006) Mitochondrial uncoupling protein is required for efficient photosynthesis. Proc Natl Acad Sci **103**: 19587–19592

Taniguchi Y, Nagasaki J, Kawasaki M, Miyake H, Sugiyama T, Taniguchi M (2004) Differentiation of Dicarboxylate Transporters in Mesophyll and Bundle Sheath Chloroplasts of Maize. Plant Cell Physiol **45**: 187–200

Timm S, Bauwe H (2013) The variety of photorespiratory phenotypes - employing the current status for future research directions on photorespiration. Plant Biol **15**: 737–747

Timm S, Florian A, Jahnke K, Nunes-Nesi A, Fernie AR, Bauwe H (2011) The Hydroxypyruvate-Reducing System in Arabidopsis: Multiple Enzymes for the Same End. Plant Physiol **155**: 694–705

Timm S, Giese J, Engel N, Wittmiß M, Florian A, Fernie AR, Bauwe H (2018) T-protein is present in large

excess over the other proteins of the glycine cleavage system in leaves of Arabidopsis. Planta **247**: 41–51

Timm S, Nunes-Nesi A, Pärnik T, Morgenthal K, Wienkoop S, Keerberg O, Weckwerth W, Kleczkowski LA, Fernie AR, Bauwe H (2008) A Cytosolic Pathway for the Conversion of Hydroxypyruvate to Glycerate during Photorespiration in Arabidopsis. Plant Cell **20**: 2848–2859

Trudeau DL, Edlich-Muth C, Zarzycki J, Scheffen M, Goldsmith M, Khersonsky O, Avizemer Z, Fleishman SJ, Cotton CARR, Erb TJ, et al (2018) Design and in vitro realization of carbon-conserving photorespiration. Proc Natl Acad Sci **115**: E11455–E11464

United Nations (2019) World Population Prospects 2019.

Voll LM, Jamai A, Renné P, Voll H, McClung CR, Weber APM (2006) The Photorespiratory Arabidopsis shm1 Mutant Is Deficient in SHM1. Plant Physiol **140**: 59–66

Volokita M, Somerville CR (1987) The Primary Structure of Spinach Glycolate Oxidase Deduced from the DNA Sequence of a cDNA Clone. J Biol Chem **262**: 15825–15828

Walker BJ, VanLoocke A, Bernacchi CJ, Ort DR (2016) The Costs of Photorespiration to Food Production Now and in the Future. Annu Rev Plant Biol **67**: 107–129

Wang L, Czedik-Eysenberg A, Mertz RA, Si Y, Tohge T, Nunes-Nesi A, Arrivault S, Dedow LK, Bryant DW, Zhou W, et al (2014a) Comparative analyses of C4 and C3 photosynthesis in developing leaves of maize and rice. Nat Biotechnol **32**: 1158–1165

Wang Y, Bräutigam A, Weber APM, Zhu X-G (2014b) Three distinct biochemical subtypes of C4 photosynthesis? A modelling analysis. J Exp Bot **65**: 3567–3578

Wang Y, Stessman DJ, Spalding MH (2015) The CO2 concentrating mechanism and photosynthetic carbon assimilation in limiting CO2: How Chlamydomonas works against the gradient. Plant J **82**: 429–448

Weber AP, von Caemmerer S (2010) Plastid transport and metabolism of C3 and C4 plants—comparative analysis and possible biotechnological exploitation. Curr Opin Plant Biol **13**: 256–264

Weber APM, Bar-Even A (2019) Update: Improving the efficiency of photosynthetic carbon reactions. Plant Physiol **179**: 803–812

Weber APM, Menzlaff E, Arbinger B, Gutensohn M, Eckerskorn C, Fluegge U-I (1995) The 2-oxoglutarate/malate translocator of chloroplast envelope membranes: molecular cloning of a transporter containing a 12-helix motif and expression of the functional protein in yeast cells. Biochemistry **34**: 2621–2627

Weissmann S, Huang P, Furuyama K, Wiechert MA, Taniguchi M, Schnable JC, Brutnell TP, Mockler TC (2019) DCT4 - a new member of the dicarboxylate transporter family in C4 grasses. bioRxiv. doi: 10.1101/762724

Weissmann S, Ma F, Furuyama K, Gierse J, Berg H, Shao Y, Taniguchi M, Allen DK, Brutnell TP (2016) Interactions of C4 Subtype Metabolic Activities and Transport in Maize Are Revealed through the Characterization of DCT2 Mutants. Plant Cell **28**: 466–484

Whitney SM, Houtz RL, Alonso H (2011) Advancing our understanding and capacity to engineer nature's CO2-sequestering enzyme, Rubisco. Plant Physiol **155**: 27–35

Woodrow IE, Mott KA (1993) Modelling C3 photosynthesis: A sensitivity analysis of the photosynthetic carbon-reduction cycle. Planta **191**: 421–432

Yamori W, Masumoto C, Fukayama H, Makino A (2012) Rubisco activase is a key regulator of non-steady-state photosynthesis at any leaf temperature and, to a lesser extent, of steady-state photosynthesis at high temperature. Plant J **71**: 871–880

Zhang YG, Pagani M, Liu Z, Bohaty SM, DeConto R (2013) A 40-million-year history of atmospheric CO2. Philos Trans R Soc A Math Phys Eng Sci **371**: 20130096

Zhu X-G, Long SP, Ort DR (2010) Improving Photosynthetic Efficiency for Greater Yield. Annu Rev Plant Biol **61**: 235–261

Zhu XG, Ort DR, Whitmarsh J, Long SP (2004) The slow reversibility of photosystem II thermal energy dissipation on transfer from high to low light may cause large losses in carbon gain by crop canopies: A theoretical analysis. J Exp Bot **55**: 1167–1175

Manuscript I

Rapid Single-Step Affinity Purification of HA-Tagged Plant Mitochondria

Status: published

Author contribution: FK generated transgenic lines harboring affinity-tagged mitochondria, isolated mitochondria, analyzed the data, and drafted the manuscript; AS, NO, and KS performed the proteomics analysis and analyzed the data; LD and ASR assisted with the Seahorse Analyzer measurements; APMW conceived and supervised the experiments and contributed to the writing of the manuscript.

Breakthrough Technologies

Rapid Single-Step Affinity Purification of HA-Tagged Plant Mitochondria[1][OPEN]

Franziska Kuhnert,[a] Anja Stefanski,[b] Nina Overbeck,[b] Leonie Drews,[c] Andreas S. Reichert,[c] Kai Stühler,[b] and Andreas P.M. Weber[a,2,3]

[a]Institute of Plant Biochemistry, Cluster of Excellence on Plant Science (CEPLAS), Heinrich Heine University, Universitätsstrasse 1, 40225 Düsseldorf, Germany
[b]Molecular Proteomics Laboratory, Biomedical Research Center, Heinrich Heine University, Universitätsstrasse 1, 40225 Düsseldorf, Germany
[c]Institute of Biochemistry and Molecular Biology I, Medical Faculty, Heinrich-Heine University, Universitätsstrasse 1, 40225 Düsseldorf, Germany

ORCID IDs: 0000-0002-0374-6671 (F.K.); 0000-0003-0970-4672 (A.P.M.W.).

Photosynthesis in plant cells would not be possible without the supportive role of mitochondria. However, isolating mitochondria from plant cells for physiological and biochemical analyses is a lengthy and tedious process. Established isolation protocols require multiple centrifugation steps and substantial amounts of starting material. To overcome these limitations, we tagged mitochondria in Arabidopsis (*Arabidopsis thaliana*) with a triple hemagglutinin tag for rapid purification via a single affinity-purification step. This protocol yields a substantial quantity of highly pure mitochondria from 1 g of Arabidopsis seedlings. The purified mitochondria were suitable for enzyme activity analyses and yielded sufficient amounts of proteins for deep proteomic profiling. We applied this method for the proteomic analysis of the Arabidopsis *bou-2* mutant deficient in the mitochondrial Glu transporter À BOUT DE SOUFFLE (BOU) and identified 27 differentially expressed mitochondrial proteins compared with tagged Col-0 controls. Our work sets the stage for the development of advanced mitochondria isolation protocols for distinct cell types.

In all eukaryotic organisms, mitochondria are the major source of ATP, which is produced via the oxidative phosphorylation (OXPHOS) pathway, thus playing a vital role in cellular energy metabolism. Mitochondria also participate in amino acid metabolism as well as in photorespiration in photosynthetic eukaryotes. Analysis of the biochemical and physiological functions of mitochondria frequently requires the isolation of intact mitochondria. Mitochondria can be isolated from leaf tissue in less than 1 h by differential centrifugation. This method yields mitochondria with good integrity and appropriate enzyme activity; however, mitochondria are frequently contaminated with plastids and peroxisomes. Hence, in many cases, a combination of differential centrifugation and Percoll density gradient is used (Millar et al., 2001; Werhahn et al., 2001; Keech et al., 2005). Whereas this produces a pure fraction of respiratory active mitochondria with low plastid and peroxisome contamination, such procedures generally take several hours and require up to 50 g of starting material for producing sufficient yields (Keech et al., 2005). Moreover, traditional protocols are not practical for the isolation of mitochondria from mutants with severely impaired growth or from less-abundant tissue types such as flowers and for the analysis of mitochondrial metabolites. Furthermore, media used for the isolation of mitochondria typically contain high concentrations of sugars and other metabolites that can potentially interfere with mass spectrometry (MS)-based metabolite analyses.

Recently, Chen and coworkers reported a method for the rapid isolation of mitochondria from human HeLa cell cultures via coimmunopurification (co-IP; Chen et al., 2016). The authors generated transgenic HeLa cell lines expressing a triple hemagglutinin (HA)-tagged enhanced GFP (eGFP) fused to the outer mitochondrial membrane (OMM) localization sequence of OMP25 (3×HA-eGFP-OMP25). Because the epitope tag was displayed on the surface of mitochondria, these transfected cell lines could be used to rapidly enrich mitochondria after cell homogenization. The HA-tagged

[1]This work was supported by the Deutsche Forschungsgemeinschaft (CRC 1208; and funding under Germany's Excellence Strategy [EXC-2048/1 - project ID 390686111]).

[2]Author for contact: aweber@hhu.de.
[3]Senior author.
The author responsible for distribution of materials integral to the findings presented in this article in accordance with the policy described in the Instructions for Authors (www.plantphysiol.org) is: Andreas P.M. Weber (aweber@hhu.de).

F.K. generated transgenic lines harboring affinity-tagged mitochondria, isolated mitochondria, analyzed the data, and drafted the manuscript; A.S., N.O., and K.S. performed the proteomics analysis and analyzed the data; L.D. and A.S.R. assisted with the Seahorse Analyzer measurements; A.P.M.W. conceived and supervised the experiments and contributed to the writing of the manuscript.

[OPEN]Articles can be viewed without a subscription.
www.plantphysiol.org/cgi/doi/10.1104/pp.19.00732

mitochondria were captured and pulled down using magnetic beads coated with an anti-HA-tag antibody. Given the small size (1-μm diameter) and nonporous behavior of anti-HA-tag beads, these beads performed better than the porous agarose matrix for the enrichment of mitochondria. Thus, the authors established a method that ensures a high yield of pure mitochondria in approximately 12 min. The isolated mitochondria showed high purity, integrity, and functionality. Additionally, the authors developed a simple potassium-based buffer system that maintains mitochondrial intactness and is compatible with downstream analyses, such as metabolite analysis by liquid chromatography (LC)/MS (Chen et al., 2016).

Photorespiration plays a crucial role in photosynthesis by detoxifying 2-phosphoglycolate, which is produced by the oxygenation of Rubisco and acts as an inhibitor of several plastidial enzymes (Ogren and Bowes, 1971; Kelly and Latzko, 1976; Husic et al., 1987). Plants reclaim 2-phosphoglycolate in the complex pathway of photorespiration, yielding 3-phosphoglycerate, which is returned to the Calvin Benson cycle. The photorespiratory pathway includes several enzymatic steps that occur in four subcellular compartments: plastids, peroxisomes, mitochondria, and the cytosol (Eisenhut et al., 2019). Knockout mutants of genes encoding enzymes and transporters involved in photorespiration often show a photorespiratory phenotype, characterized by chlorotic leaves and growth inhibition under ambient carbon dioxide (CO_2) conditions, which can be rescued in a CO_2-enriched environment (Peterhansel et al., 2010). A key step in photorespiration is the conversion of two Gly molecules into one Ser residue in the mitochondrial matrix, accompanied by the release of CO_2 and ammonia. This step is catalyzed by the Gly decarboxylase (GDC) multienzyme system, comprising the P-protein (GLDP), H-protein (GDCH), L-protein (GDCL), and T-protein (GLDT), in combination with Ser hydroxymethyltransferase (SHM; Voll et al., 2006; Engel et al., 2007). In green tissues, these proteins constitute up to 50% of the total protein content of the mitochondrial matrix, indicating the importance of Gly oxidation in mitochondria (Oliver et al., 1990).

The Arabidopsis (*Arabidopsis thaliana*) *bou-2* mutant was previously identified as lacking the mitochondrial Glu transporter À BOUT DE SOUFFLE (BOU), which is involved in photorespiration (Eisenhut et al., 2013; Porcelli et al., 2018). Plants lacking the inner mitochondrial membrane (IMM) protein BOU show a pronounced photorespiratory phenotype under ambient CO_2 conditions, significantly elevated CO_2 compensation point, and highly reduced GDC activity in the isolated mitochondria (Eisenhut et al., 2013). Because *BOU* is coexpressed with genes encoding components of the GDC complex and the *bou-2* mutant shows a similar metabolic phenotype as the *shm1* mutant, it was hypothesized that BOU transports a metabolite necessary for the proper functioning of GDC (Voll et al., 2006; Eisenhut et al., 2013). Recently, it was demonstrated that heterologously expressed BOU functions as a Glu transporter (Porcelli et al., 2018). Glu is neither a substrate nor a product of the reaction catalyzed by GDC. Besides its role in amino acid and nitrogen metabolism, Glu is necessary for the glutamylation of tetrahydrofolate (THF), a cofactor of GLDT and SHM (Suh et al., 2001). Glutamylation of THF increases its stability. Moreover, THF-dependent enzymes generally prefer polyglutamylated folates over monoglutamylated folates as a substrate (Suh et al., 2001). However, because (1) BOU is not the only Glu transporter in mitochondria, and (2) glutamylation of folates is not restricted to mitochondria, the exact physiological function of BOU remains unclear (Hanson and Gregory, 2011; Monné et al., 2018). Notably, a Glu/Gln shuttle across the mitochondrial membrane was previously suggested to support the reclamation of ammonia released during photorespiration (Linka and Weber, 2005).

Building on the previous work of Chen et al. (2016), we developed an affinity-tagging strategy for the rapid isolation of mitochondria from Arabidopsis. We generated transgenic Arabidopsis lines carrying an HA-tagged TRANSLOCASE OF THE OMM5 (TOM5) and isolated highly pure and intact mitochondria from these lines in less than 25 min. The isolated mitochondria were successfully subjected to proteomics and enzyme activity analyses. Moreover, we applied the isolation strategy to the *bou-2* mutant, revealing differential protein abundance and enzyme activities.

RESULTS

Identification of TOM5 as a Suitable Anchor Peptide and Generation of Affinity-Tagged Arabidopsis Lines

Recently, Chen et al. (2016) reported a rapid protocol for the isolation of intact mitochondria from transgenic HeLa cells expressing the mitochondrial fusion protein 3×HA-eGFP-OMP25 using co-IP. The Arabidopsis genome does not encode an ortholog of OMP25. Therefore, we screened the available Arabidopsis mitochondrial proteome data, including the OMM proteins with known topology and function, and identified TOM5 as a potential candidate for our mitochondria affinity-tagging approach. Together with TOM6, TOM7, TOM20, TOM22/9, and TOM40, TOM5 forms the protein import apparatus of plant mitochondria (Werhahn et al., 2003). In yeast (*Saccharomyces cerevisiae*), TOM5 is an integral protein of the OMM. It has a negatively charged N-terminal domain, which faces toward the cytosol (Dietmeier et al., 1997) and can be fused to GFP without altering the subcellular localization of TOM5 (Horie et al., 2003). The protein import machinery is well conserved among eukaryotes. The predicted N-terminal cytosolic domain of Arabidopsis TOM5 is necessary for the recognition of cytosolically synthesized mitochondrial preproteins (Wiedemann et al., 2004). Therefore, we generated an N-terminal

translational fusion of the Arabidopsis *TOM5* gene with the triple HA-tagged *synthetic GFP* (*sGFP*) gene under the control of the Arabidopsis *UBIQUITIN10* promoter (*UB10p*; *UB10p-3×HA-sGFP-TOM5*; Supplemental Fig. S1). The construct was used to stably transform Arabidopsis ecotype Columbia (Col-0) and *bou-2* mutant. Expression and localization of the fusion protein was verified in root and leaf tissues of 10-d-old Arabidopsis seedlings via confocal laser scanning microscopy. Arabidopsis lines expressing the 3×HA-sGFP-TOM5 protein in leaf and root mitochondria of Col-0 (tagged Col-0) and *bou-2* (tagged *bou-2*) seedlings were identified based on the colocalization of the fluorescent signal of GFP signal with that of the mitochondrial marker CMXRos (Fig. 1). CMXRos is a lipophilic cationic dye that accumulates in the mitochondria because of the negative membrane potential; thus, it solely stains mitochondria with an intact respiratory chain (Pendergrass et al., 2004). Because the fluorescent signals of the 3×HA-sGFP-TOM5 protein (green) fully overlapped with those of the MitoTracker (red), we conclude that overexpression of the *UB10p-3×HA-sGFP-TOM5* construct in Col-0 and *bou-2* does not affect mitochondrial intactness. Notably, tagged Col-0 or *bou-2* lines showed no apparent phenotypic differences compared with nontagged Col-0 or *bou-2* plants (control), respectively, under our culture conditions (Supplemental Fig. S2).

Affinity-Based Purification of Intact Mitochondria

Tagged Col-0 and *bou-2* lines were used for the isolation of intact HA-tagged mitochondria via co-IP using magnetic anti-HA beads. We chose HA as the epitope tag for purification because it has a high affinity for its cognate antibody, and Chen and coworkers previously demonstrated that the size and nonporous behavior of the anti-HA beads yields a high amount of mitochondria (Chen et al., 2016). Additionally, we used the LC/MS-compatible buffer containing KCl and KH_2PO_4 (KPBS) developed by Chen et al. (2016). Our purification procedure included five steps: homogenization of plant material in KPBS (1 min), filtration of the homogenate (1 min), two centrifugation steps (5 and 9 min), and co-IP (7 min, including washing steps). All together, mitochondria were purified from plant material in less than 25 min (Fig. 2). If the first low-speed centrifugation step used to remove contaminating chloroplasts and cell debris is omitted, the isolation time can be reduced to 18 min. The purified mitochondria were verified by immunoblot analyses using

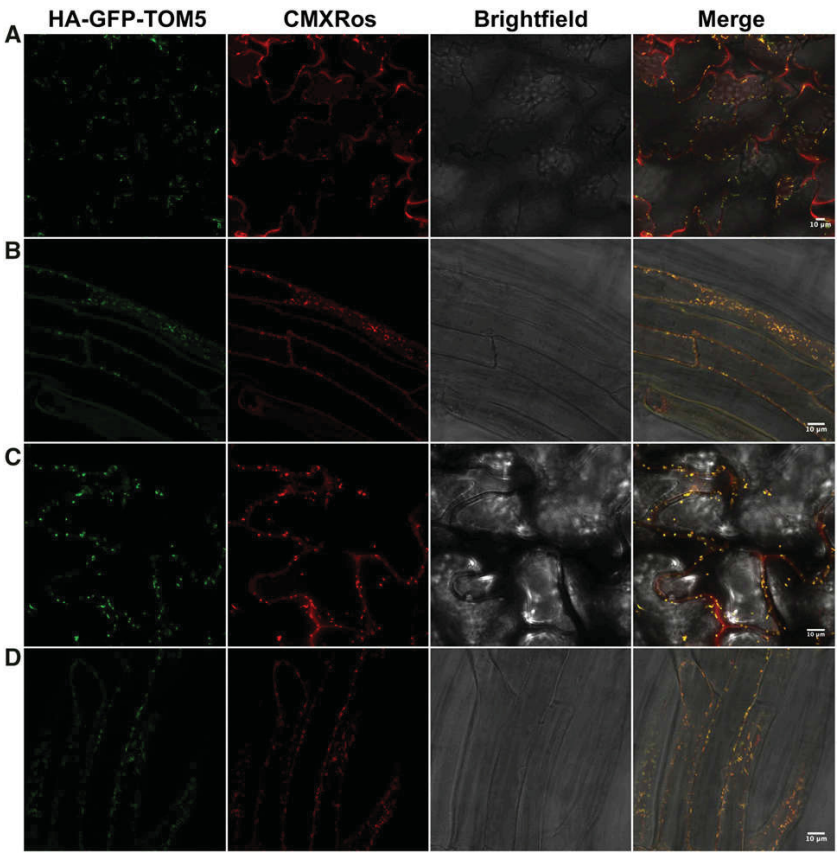

Figure 1. Confocal microscopy of epitope-tagged mitochondria in leaf and root tissues of 10-d-old Arabidopsis Col-0 and *bou-2* lines expressing the *UB10p-3×HA-sGFP-TOM5* construct. A to D, Images of tagged Col-0 leaf (A) and root (B) tissues and tagged *bou-2* leaf (C) and root (D) tissues expressing the 3×HA-sGFP-TOM5 protein. Pictures were taken of the epidermal layer of the first leaf pair (A and C) and the epidermal and cortex layer of the main root (B and D). Green color represents GFP signal, whereas red color represents the signal of mitochondrial marker MitoTracker red CMXRos. Bright field is shown in gray and merged images are shown in yellow. Scale bars = 10 μm.

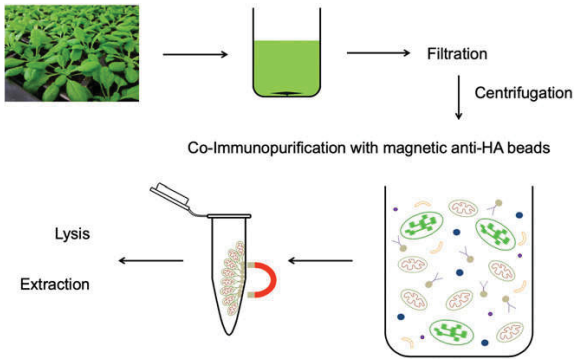

Figure 2. Workflow showing the rapid isolation of epitope-tagged mitochondria via co-IP from Arabidopsis. Tagged lines harboring the *UB10p-3×HA-sGFP-TOM5* construct were harvested and homogenized in a Warren blender. The extract was filtered and centrifuged to obtain a crude mitochondrial fraction. Epitope-tagged mitochondria were purified via co-IP using 50–250 μL magnetic anti-HA beads. The purified mitochondria were washed and either lysed for immunoblot analysis or extracted for proteomics. As a control, nontagged Col-0 was used.

known organelle-specific protein markers. Mitochondria were enriched via co-IP only from lines harboring the mitochondrial 3×HA-sGFP-TOM5 protein (tagged line), as demonstrated by immunoblot analyses with antibodies directed against different mitochondrial marker proteins including isocitrate dehydrogenase (IDH; mitochondrial matrix), alternative oxidase 1/2 (AOX1/2; IMM), and voltage-dependent anion channel1 (VDAC1; OMM). No enrichment of mitochondria was observed in control Col-0 lines, indicating that the beads bind specifically to the HA-tag on mitochondria in tagged lines (Fig. 3; Supplemental Fig. S3A). Comparison with classical mitochondria isolation protocols using differential centrifugation and density gradient purification revealed that the mitochondrial fraction enriched using our affinity-tagging method showed significantly less contamination with proteins from plastids, peroxisomes, the endoplasmic reticulum (ER), nuclei, and the cytosol (Fig. 3; Supplemental Fig. S3B). The following proteins were used as markers for different organelles: Rubisco large subunit (RbcL; plastid), catalase (Cat; peroxisome), lumenal-binding protein2 (BiP2; ER), histone H3 (nucleus), and heat shock cognate protein70 (HSC70; cytosol). Contamination with thylakoids, which are a major contaminant of leaf mitochondria, was assessed by determining the chlorophyll-to-protein ratio of isolated mitochondria. Rapidly enriched mitochondria show minor contamination by thylakoids (0.18 ± 0.08 μg Chl mg^{-1} protein). The here-presented chlorophyll-to-protein ratio is 2-fold lower compared to classical mitochondria isolations (0.34 ± 0.08 μg Chl mg^{-1} protein; Keech et al., 2005).

The intactness of mitochondria isolated from HA-tagged lines via co-IP was assessed based on respiratory measurements with the Seahorse Analyzer, the latency of malate dehydrogenase (MDH) activity, and mitochondrial staining with the mitochondrial marker CMXRos (Fig. 4). Mitochondria isolated with our affinity-tagging approach showed respiratory coupling with succinate as substrate. Respiration is inhibited by the respiratory chain inhibitor Antimycin A. Addition of the complex III inhibitor lead to a significant reduction of the oxygen consumption rate in the mitochondria but not the control samples (Fig. 4A). Intactness and activity was further verified by latency experiments with MDH. Activity of MDH was only present in detergent-treated samples containing enriched mitochondria but not the control or nontreated samples, indicating intactness of the OMM and IMM (Fig. 4B). Moreover, affinity-purified mitochondria retained the mitochondrial marker CMXRos that solely stains mitochondria with an active respiratory chain (Fig. 4C; Pendergrass et al., 2004).

Typically, we used 5–10 g of Arabidopsis seedlings grown on agar plates for the isolation of mitochondria, and this yielded 400–700 μg of total mitochondrial protein. However, mitochondria could also be isolated from 1 g of starting material, yielding 50–200 μg of total mitochondrial protein. This is advantageous for very young seedlings or mutants with severely impaired growth. Isolation from less than 1 g of starting material may also result in an appropriate yield of mitochondria, but this was not tested in this study. We found that recovery of mitochondria with our method was 7.1% ± 3.3%.

Taken together, our data indicate that mitochondria can be rapidly isolated via co-IP using a simple LC/MS-compatible buffer.

Enzyme Assays Using Mitochondria Affinity Purified from Tagged Col-0 and *bou-2* Mutant Lines

We used our rapid mitochondria isolation method to study the effect of the mitochondrial carrier protein BOU on mitochondrial metabolism in Arabidopsis.

To assess the effect of the *bou-2* mutant allele on mitochondrial metabolism, we rapidly isolated mitochondria from 10-d-old tagged Col-0 and *bou-2* seedlings grown under elevated CO_2 conditions (0.3%) and seedlings sampled 5 d after shift to ambient CO_2 conditions (0.038% CO_2), with three independent biological replicates included for each treatment. Mitochondria were lysed and used to measure the activity of MDH, Asp aminotransferase (AspAT), Glu dehydrogenase (GluDH), Ala aminotransferase (AlaAT), γ-aminobutyric acid transaminase (GABA-T), and formate dehydrogenase (FDH). Enzyme activities were calculated from the initial slopes. Enzyme activities in tagged *bou-2* mutant lines were compared with those in tagged Col-0 lines, which were set to 100% for both experimental conditions.

The activities of MDH and FDH were not affected in tagged *bou-2* mutant lines under any of the conditions tested (Fig. 5, A and B). The activities of AspAT and

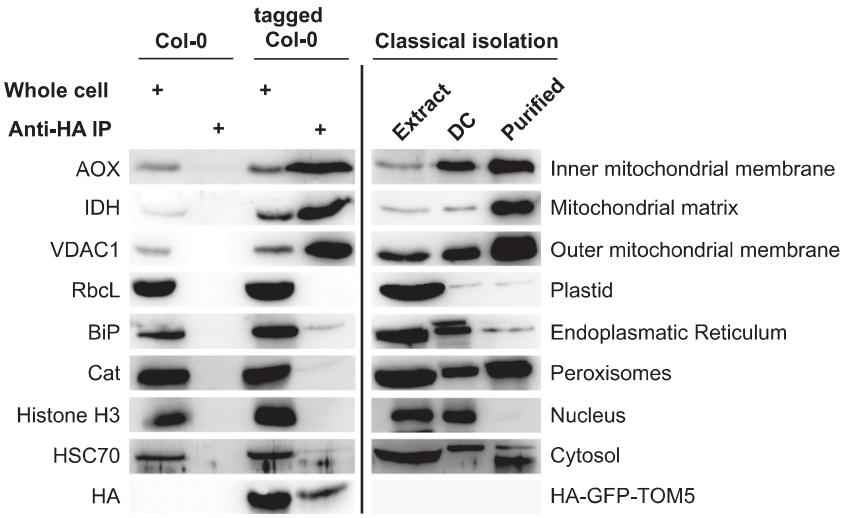

Figure 3. Assessment of the contamination of enriched mitochondria via co-IP or classical methods. Mitochondria isolations were performed on 10-d-old Col-0 and tagged Col-0 lines via co-IP using 150 μL magnetic anti-HA beads or on 10-d-old Col-0 via classical methods using differential centrifugation and gradient purification. Samples were taken after tissue homogenization (whole cell, extract), enrichment of mitochondria via co-IP (anti-HA-IP), differential centrifugation (DC), and density gradient purification (purified). Protein amounts were loaded as described in the "Materials and Methods." Names of organelle marker proteins are shown on the left side of the blots, and their subcellular localization is indicated on the right.

GABA-T in tagged mutant lines were similar to those in tagged Col-0 lines, when mitochondria were isolated from seedlings grown under elevated CO_2 conditions, but were significantly reduced in tagged mutant lines after the shift to ambient CO_2 conditions (Fig. 5, C and D). The activity of AlaAT was significantly reduced (Fig. 5E), whereas that of GluDH was significantly increased in tagged mutant lines under elevated CO_2 conditions; however, enzyme activity of the latter reverted back to the levels in tagged Col-0 when seedlings were shifted to ambient CO_2 conditions (Fig. 5F). Together, our results suggest a possible involvement of BOU in mitochondrial amino acid and nitrogen metabolism.

In addition, we found that the activity of MDH was strongly reduced in 4-week-old tagged *bou-2* mutant plants (Supplemental Fig. S4). However, no change was observed in MDH activity in 10-d-old tagged *bou-2* plants, suggesting pleiotropic effects in older leaf tissues due to accumulating photorespiratory intermediates.

Proteomic Analysis of Mitochondria Affinity Purified from Tagged Col-0 and *bou-2* Mutant Lines

Mitochondria were isolated from 10-d-old tagged Col-0 and *bou-2* seedlings grown under elevated CO_2 conditions, with four independent biological replicates included. Proteome analysis of the isolated mitochondria revealed 15,688 peptides belonging to 1240 proteins present in at least three of the four replicates (Supplemental Tables S1 and S2).

Subcellular localization of the quantified proteins was annotated using the SUBAcon database (Hooper et al., 2017). Summing up the label-free quantitation intensities of the spectra showed that 80% of the identified proteins in our study resulted from proteins localized or predicted to be localized to the mitochondria, 11.5% from plastid-localized proteins, and 5.7% from proteins with no clear subcellular localization (designated as ambiguous). If we apply the evaluation on all quantified peptides in this study, more than 90% of all identified peptides were assigned to mitochondria-localized proteins. Contamination of the mitochondrial proteins by proteins from peroxisomes, the ER, the Golgi, vacuoles, endomembranes, plasma membranes, nuclei, and the cytosol was less than 1% each (Supplemental Tables S1 and S2). These results indicate high purity of the rapidly isolated mitochondria, which was comparable with the purity of classically isolated mitochondria (Klodmann et al., 2011; Senkler et al., 2017).

Next, we compared our proteome data with previous proteomic analyses and quantified proteins and some of the subunits of known mitochondrial complexes (Supplemental Tables S1 and S2). The OXPHOS pathway of mitochondria consists of five protein complexes (I–V) located in the IMM. Complexes I to IV represent oxidoreductases, which comprise the respiratory chain that regenerates oxidized forms of cofactors involved in mitochondrial metabolism, thereby creating an electron flow. This leads to the simultaneous export of protons into the intermembrane space (IMS). The built-up proton gradient is used by complex V to generate ATP. Complex I is the largest complex involved in the OXPHOS pathway and comprises at least 47 protein subunits that form the so-called membrane and peripheral arms (Peters et al., 2013; Meyer et al., 2019). Except NDUA1, NDUB2, Nad4L, and Nad6 (At3g08610, At1g76200, AtMg00650, and AtMg00270, respectively), we could identify all complex I subunits in our proteomic data set, including eight previously proposed assembly factors (Meyer et al., 2019), five γ-carbonic anhydrases, and five additional proteins proposed to form a matrix-exposed domain attached to complex I (Sunderhaus et al., 2006). In addition to its function in the OXPHOS pathway, complex II also

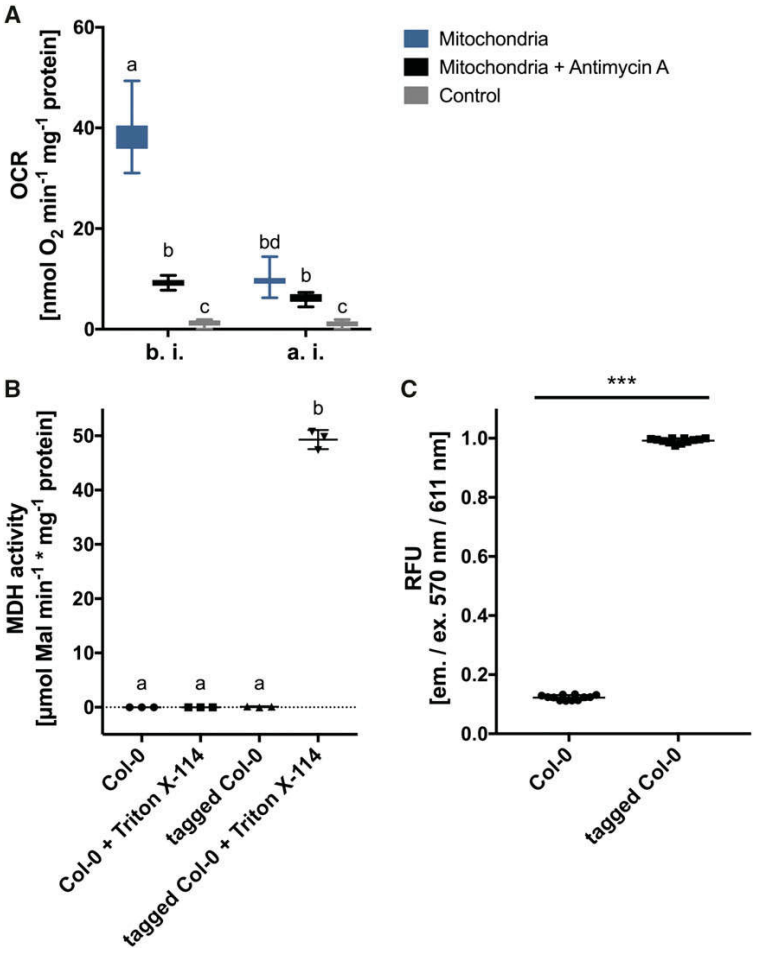

Figure 4. Intactness of rapidly enriched mitochondria isolated from 10-d-old tagged Col-0 lines via co-IP. Oxygen consumption rates (OCR) of purified mitochondria bound to magnetic anti-HA beads were measured using the Seahorse XFe96 Analyzer as described in the "Materials and Methods" (A). OCR were measured in the presence (black boxes) or absence (blue boxes) of the respiratory chain inhibitor antimycin A and before (b.i.) and after (a.i.) injection of antimycin A. Control (gray boxes) did not contain mitochondria. Data are shown in box and whiskers (min to max) of means of two (mitochondria + antimycin A, control) and three biological replicates (mitochondria). Different letters indicate statistically significant differences between means ($P < 0.05$; two-way ANOVA). Latency of malate dehydrogenase (MDH) activity was measured as described in the "Materials and Methods" (B). As control isolations were performed on Col-0 lines. Data represent mean ± SD of three biological replicates (each four technical replicates). Different letters indicate statistically significant differences between means ($P < 0.05$; one-way ANOVA). Purified mitochondria retain the mitochondrial marker MitoTracker red CMXRos that is able to stain mitochondria with an active membrane potential (C). Staining experiments were performed as described in the "Materials and Methods." As control isolations were performed on Col-0 lines. Data represent mean ± SD of three biological replicates (each four technical replicates). Asterisks indicate statistically significant differences (***$P < 0.001$; Student's *t* test).

participates in the tricarboxylic acid cycle (TCA). Six out of eight subunits of complex II (Millar et al., 2004) and the assembly factor SDHAF2 were identified in our data set. Additionally, peptides of all proteins and isoforms of complex III as well as eight of its assembly factors (Meyer et al., 2019) were identified in our data set. The cytochrome c oxidase complex (complex IV) consists of 16 proposed subunits in Arabidopsis (Mansilla et al., 2018). Of these, nine subunits and 11 assembly factors of complex IV were identified in our proteomic data set. Complex V consists of 15 subunits, of which 13 were identified in our proteomic data set; Atp6 (AtMg00410 and AtMg011701) and Atp9 (AtMg01080) were the only two subunits that could not be identified. In addition, we found three of the five proposed assembly factors (Meyer et al., 2019). Furthermore, we identified three proteins involved in the assembly of OXPHOS supercomplexes as well as alternative NADPH dehydrogenases and alternative oxidases that have previously been defined as alternative pathways (Meyer et al., 2019).

Except for the abovementioned subunits of the SDH complex, all proteins of the TCA cycle, including the pyruvate dehydrogenase complex, and the GDC multienzyme system were identified in the rapidly isolated mitochondria. Additionally, our proteomic data set contained a number of pentatricopeptide and tetratricopeptide repeat proteins involved in RNA metabolism as well as heat shock proteins and ribosomal proteins involved in protein control and turnover (Supplemental Table S1 and S2).

In Arabidopsis, the majority of mitochondrial proteins are encoded by nuclear genes, translated in the cytosol, and then imported into the mitochondria. The import and sorting of nuclear-encoded mitochondrial preproteins requires functional TOM and sorting and assembly machinery in the OMM, mitochondrial IMS import and assembly machinery in the IMS, and translocase of the IMM in the IMM (Murcha et al., 2014). In this study, we identified all proteins necessary for functional protein import into mitochondria in our proteome data set, except for the OMM protein TOM6, IMS protein ERV1, IMM protein PRAT5, and matrix

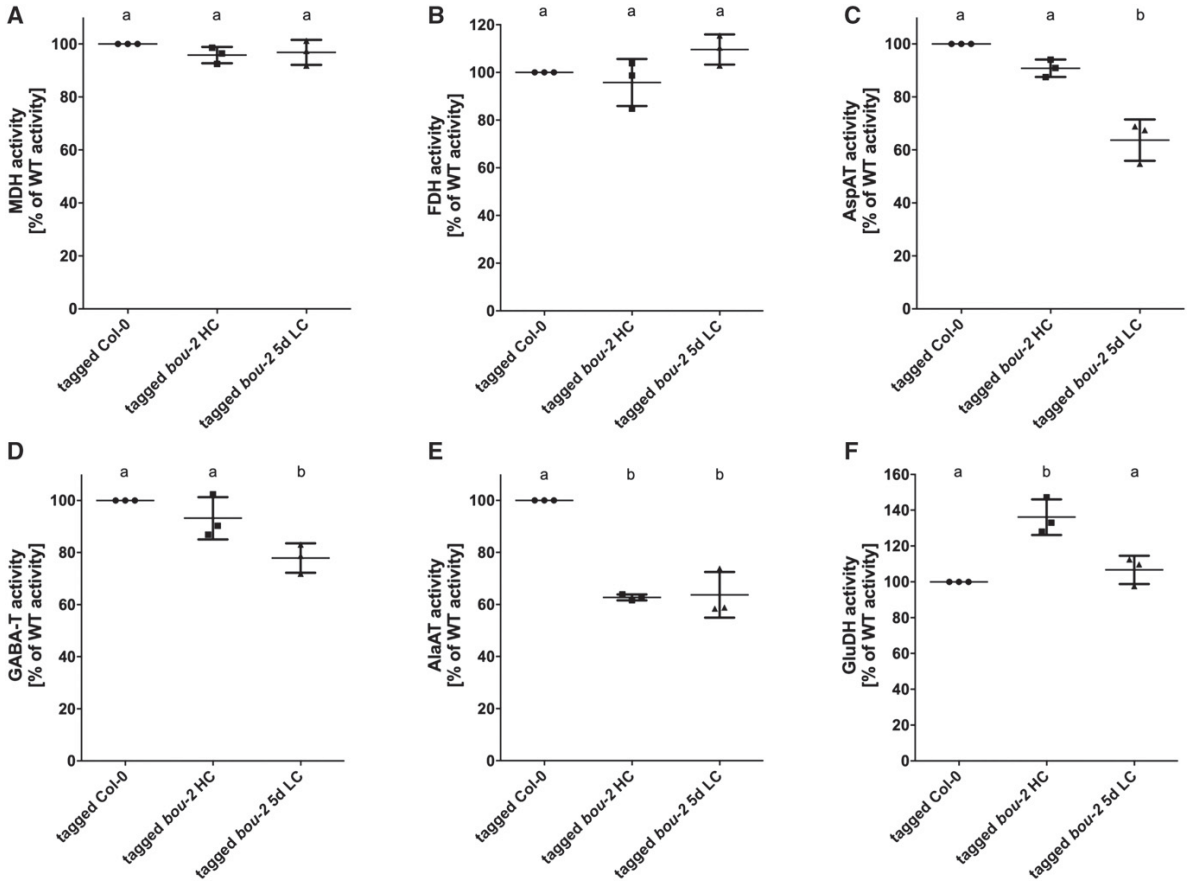

Figure 5. Characterization of enzyme activities in mitochondria isolated via co-IP from 10-d-old tagged Col-0 and *bou-2* lines. Plants were sampled following growth under 0.3% CO_2 (HC) and 5 d after shift to 0.038% CO_2 (5 d LC). A, Malate dehydrogenase (MDH) activity. Average tagged Col-0 activity: 38.2 ± 1.5 μmol min^{-1} mg^{-1} (HC), 49.4 ± 1.5. μmol min^{-1} mg^{-1} (5 d LC). B, Formate dehydrogenase (FDH) activity. Average tagged Col-0 activity: 17.8 ± 0.5 nmol min^{-1} mg^{-1} (HC), 33.6 ± 1.5 nmol min^{-1} mg^{-1} (5 d LC). C, Asp aminotransferase (AspAT) activity. Average tagged Col-0 activity: 4.31 ± 0.08 μmol min^{-1} mg^{-1} (HC), 3.74 ± 0.01 μmol min^{-1} mg^{-1} (5 d LC). D, γ-aminobutyric acid transaminase (GABA-T) activity. Average tagged Col-0 activity: 96.2 ± 4.3 nmol min^{-1} mg^{-1} (HC), 137.4 ± 1.0 nmol min^{-1} mg^{-1} (5 d LC). E, Ala aminotransferase (AlaAT) activity. Average tagged Col-0 activity: 0.92 ± 0.02 μmol min^{-1} mg^{-1} (HC), 0.75 ± 0.04 μmol min^{-1} mg^{-1} (5 d LC). F, Glu dehydrogenase (GluDH) activity. Average tagged Col-0 activity: 0.83 ± 0.05 μmol min^{-1} mg^{-1} (HC), 2.03 ± 0.04 μmol min^{-1} mg^{-1} (5 d LC). Activities were calculated from initial slopes. Enzyme activities in tagged Col-0 grown under elevated CO_2 conditions and 5 d after shift to ambient CO_2 conditions were each set to 100%. Data represent mean ± SD of three biological replicates (each four technical replicates). Different letters indicate statistically significant differences between means for each enzyme ($P < 0.05$; one-way ANOVA). WT, wild type.

proteins MGE1 and ZIM17. Additionally, we identified plant-specific import components, including OM64, PRAT3, and PRAT4 in the OMM (Murcha et al., 2015), and plant homologs to proteins of the mitochondrial contact site and cristae organizing system (MICOS), which connects the IMM to OMM (van der Laan et al., 2016). Other notable OMM proteins identified in our proteomic data set included GTPases MIRO1 and MIRO2, lipid biosynthesis protein PECT, and β-barrel proteins VDAC1to VDAC4 (Supplemental Table S1 and S2). Recently, it was shown that the cytosolic protein GAPC interacts with VDAC (Schneider et al., 2018); we also identified GAPC in our proteomic data set.

Overall, we conclude that mitochondria isolated using our rapid isolation method are suitable for proteomic analyses.

Differential Analysis of the Mitochondrial Proteome of Tagged Col-0 and *bou-2* Lines

To assess the effect of *bou-2* mutation on the mitochondrial proteome, we performed comparative proteomic

analysis of tagged Col-0 and *bou-2* lines. A total of 47 proteins showed significantly increased abundance in the mutant, of which five were localized to the mitochondria. Additionally, 44 proteins showed significantly decreased abundance in the tagged *bou-2* samples, of which 22 were predicted to be localized to the mitochondria (Table 1); among these proteins, BOU was the least abundant. The *bou-2* line is a GABI-Kat line that carries a T-DNA insertion in the second exon of the *BOU* gene (Kleinboelting et al., 2012; Eisenhut et al., 2013). We identified two peptides of BOU in at least three of the four replicates of tagged *bou-2* samples. Both peptides were translated from the first exon of the gene. Because the T-DNA was inserted in the second exon of the gene, it is possible that the first exon was translated. However, a functional protein is not synthesized in the knockout mutant (Eisenhut et al., 2013). Among the mitochondrial proteins showing significantly reduced abundance in tagged *bou-2* seedlings, we identified six proteins of the OXPHOS pathway (three complex I proteins and one protein each of complexes II, III, and V), two proteins involved in protein translocation, two proteins involved in metabolite transport, two proteins involved in lipid metabolism, three proteins involved in protein turnover/synthesis, one protein involved in the TCA cycle, and six proteins (including FDH) involved in other processes. Among the proteins with significantly increased abundance in tagged *bou-2* mutant, we identified two proteins involved in RNA/DNA metabolism, one protein involved in THF metabolism, one MIRO-related GTPase, and one LETM1-like protein (Table 1).

Previously, Eisenhut and colleagues showed that GDC activity is reduced in mitochondria isolated from 4-week-old *bou-2* mutant plants (Eisenhut et al., 2013). The authors showed that the *bou-2* mutant accumulated higher amounts of Gly than the wild type and exhibited differential amount and status of the P protein. Immunoblot analysis showed no differences in the levels of other GDC proteins in the *bou-2* mutant compared with the wild type (Eisenhut et al., 2013). In our proteomic data set, none of the proteins of the GDC complex or SHMT showed significant differences between tagged Col-0 and *bou-2* seedlings (Table 2). However, the amounts of GLDP1, GLDP2, GDCH1, GDCL1, GDCL2, and GLDT were slightly reduced, whereas those of SHM1, SHM2, and GDCH3 were increased in the tagged mutant compared with tagged Col-0. Among these proteins, the strongest reduction was detected in the amount of GDCH1. However, differences in protein levels between tagged Col-0 and *bou-2* seedlings were not statistically

Table 1. *List of signal changes for proteins showing significant differences in protein abundance between 10-d-old Col-0* UB10p-3×HA-sGFP-TOM5 *and* bou-2 UB10p-3×HA-sGFP-TOM5

Difference was calculated as change of $\log_2$ of normalized intensity. List includes only proteins that show mitochondrial localization. List ranges from most downregulated in *bou-2 UB10p-3×HA-sGFP-TOM5* (top) to most upregulated *bou-2 UB10p-3×HA-sGFP-TOM5* (bottom). Significance was calculated with Student's *t* test, $*P < 0.05$, $** P < 0.01$, $*** P < 0.001$.

AGI	Gene Symbol	Gene Description	Difference	Significance
AT5G46800	*BOU*	Mitochondrial substrate carrier family protein	−8.66407	***
AT2G42310	*AT2G42310*	ESSS subunit of NADH:ubiquinone oxidoreductase (complex I) protein	−2.0953	*
AT5G41685	*AT5G41685*	Mitochondrial outer membrane translocase complex, subunit Tom7	−1.90711	**
AT3G03100	*AT3G03100*	NADH:ubiquinone oxidoreductase, 17.2-kDa subunit	−1.33356	*
AT5G53650	*AT5G53650*	ABC transporter A family protein	−1.25252	*
AT5G67590	*FRO1*	NADH-ubiquinone oxidoreductase-like protein	−1.0968	*
AT5G40810	*AT5G40810*	Cytochrome C1 family	−1.06444	*
AT3G27280	*PHB4*	Prohibitin 4	−0.94888	*
AT3G27380	*SDH2-1*	Succinate dehydrogenase 2-1	−0.764682	*
AT4G37660	*AT4G37660*	Ribosomal protein L12/ATP-dependent Clp protease adaptor protein ClpS family protein	−0.732468	*
AT2G42210	*OEP16-3*	Mitochondrial import inner membrane translocase subunit Tim17/Tim22/Tim23 family protein	−0.710023	*
AT3G55400	*OVA1*	Methionyl-tRNA synthetase/Met-tRNA ligase/MetRS (cpMetRS)	−0.705525	*
AT5G14780	*FDH*	Formate dehydrogenase	−0.697987	**
AT2G38670	*PECT1*	Phosphorylethanolamine cytidylyltransferase 1	−0.606253	*
AT5G63400	*ADK1*	Adenylate kinase 1	−0.603703	*
AT1G79230	*MST1*	Mercaptopyruvate sulfurtransferase 1	−0.587758	*
AT4G30010	*AT4G30010*	ATP-dependent RNA helicase	−0.545131	*
AT3G03420	*AT3G03420*	Ku70-binding family protein	−0.531796	**
AT4G31810	*AT4G31810*	ATP-dependent caseinolytic (Clp) protease/crotonase family protein	−0.461768	*
AT1G19140	*AT1G19140*	Ubiquinone biosynthesis COQ9-like protein	−0.455841	*
AT4G31460	*AT4G31460*	Ribosomal L28 family	−0.430804	*
AT1G54220	*AT1G54220*	Dihydrolipoamide acetyltransferase, long form protein	−0.324755	*
AT3G59820	*LETM1*	LETM1-like protein	0.42657	*
AT5G27540	*MIRO1*	MIRO-related GTP-ase 1	0.447933	*
AT3G10160	*DFC*	DHFS-FPGS homolog C	0.507662	***
AT1G71260	*ATWHY2*	WHIRLY 2	0.51931	*
AT5G15980	*AT5G15980*	Pentatricopeptide repeat (PPR) superfamily protein	0.8335	*

Table 2. *List of changes in protein abundance of Gly decarboxylase proteins, SHM, and the enzymes MDH, FDH, ASP, γ-aminobutyric acid transaminase (POP2), AlaAT, and Glu dehydrogenase (GDH)*

Difference was calculated as change of $\log_2$ of normalized intensity. Significance was calculated with Student's *t* test, $P < 0.05$.

AGI	Gene Symbol	Gene Description	Difference	Significant
AT4G33010	*GLDP1*	Gly decarboxylase P-protein 1	−0.373902	no
AT2G26080	*GLDP2*	Gly decarboxylase P-protein 2	−0.155379	no
AT2G35370	*GDCH1*	Gly decarboxylase H-protein 1	−0.760396	no
AT1G32470	*GDCH3*	Gly decarboxylase H-protein 3	0.173202	no
AT1G11860	*GLDT*	Gly cleavage T-protein family	−0.164196	no
AT1G48030	*GDCL1*	Mitochondrial lipoamide dehydrogenase 1	−0.0284281	no
AT3G17240	*GDCL2*	Mitochondrial lipoamide dehydrogenase 2	−0.217162	no
AT4G37930	*SHM1*	Ser hydroxymethyltransferase 1	0.109162	no
AT5G26780	*SHM2*	Ser hydroxymethyltransferase 2	0.696879	no
AT5G14780	*FDH*	formate dehydrogenase	−0.697987	yes
AT5G18170	*GDH1*	Glu dehydrogenase 1	0.91113	no
AT5G07440	*GDH2*	Glu dehydrogenase 2	0.105005	no
AT3G22200	*POP2*	γ-aminobutyric acid transaminase	0.345683	no
AT1G17290	*AlaAT1*	Ala aminotransferase 1	0.640894	no
AT1G72330	*AlaAT2*	Ala aminotransferase 2	0.223008	no
AT2G30970	*ASP1*	Asp aminotransferase 1	0.399954	no
AT1G53240	*mMDH1*	Lactate/malate dehydrogenase family protein	0.564951	no
AT3G15020	*mMDH2*	Lactate/malate dehydrogenase family protein	0.0343099	no

significant. Only one peptide related to GDCH2 was detected in our data set; however, because it was detected in only one of the four replicates, it is not listed (Supplemental Table S1).

In this study, we showed that tagged mitochondria of the *bou-2* mutant displayed reduced AlaAT activity, increased GluDH activity, and no change in MDH, AspAT, GABA-T, and FDH activities under elevated CO_2 conditions compared with tagged Col-0 (Fig. 5). Except for FDH, none of the assayed enzymes showed significantly altered amounts in our proteomic data set (Table 2). The amount of FDH was significantly reduced in tagged *bou-2* samples; however, its activity was not altered in the tagged mutant under elevated CO_2 conditions compared to tagged Col-0, indicating posttranslational modification of FDH. The level of AlaAT was slightly increased in the tagged mutant but showed only 60% activity compared with tagged Col-0 under both elevated and ambient CO_2 conditions. The activities of MDH, AspAT, and GABA-T did not differ between tagged Col-0 and tagged *bou-2* mutant under elevated CO_2 conditions, although these proteins were more abundant in tagged mutant samples. The activity of GluDH was significantly increased in the tagged mutant compared with tagged Col-0 under elevated CO_2 conditions, which may be associated with the increased amount of protein detected in the tagged *bou-2* seedlings in our proteomic data set. However, this increase was not statistically significant.

Overall, we conclude that differences in the activities of MDH, AspAT, GluDH, AlaAT, GABA-T, and AlaAT measured in this study and that of GDC measured in a previous study most likely do not relate to changes in protein abundance in mitochondria of tagged Col-0 versus tagged *bou-2* mutant but instead might be caused by metabolic impairment or posttranslational modifications.

DISCUSSION

Recently, analyses of mitochondrial proteome content, complexome composition, posttranslational modifications, energy metabolism, OXPHOS complex formation and function, protein translocation, and metabolite shuttles have been conducted to further our understanding of mitochondrial metabolism in Arabidopsis (König et al., 2014; Fromm et al., 2016; De Col et al., 2017; Rao et al., 2017; Senkler et al., 2017; Porcelli et al., 2018; Hu et al., 2019; Kolli et al., 2019; Meyer et al., 2019; Nickel et al., 2019). Many of these analyses required the isolation of intact mitochondria. Here, we report a procedure for the rapid isolation of HA-tagged mitochondria from tagged Arabidopsis lines via co-IP. Mitochondria isolated using this method showed high enrichment of mitochondrial marker proteins with only minor contamination, as demonstrated by immunoblot and quantitative proteomic analyses (Fig. 3; Supplemental Tables S1 and S2).

The method reported here enables the isolation of intact mitochondria from Arabidopsis seedlings in less than 25 min (Figs. 2– 4). Moreover, by omitting the first low-speed centrifugation step, the method duration could be shortened to 18 min, although the resulting mitochondrial fraction contained a higher level of other contaminating cellular components. The mitochondrial fraction used for proteomic analyses in this study was obtained using the slightly longer protocol that results in lower contamination with nonmitochondrial proteins. Nevertheless, this isolation method is significantly faster than the standard isolation procedures that

generally take up to several hours. To date, we have been able to successfully isolate mitochondria from whole seedlings, leaves, and roots (data not shown). Moreover, this method could be used for the rapid isolation of mitochondria from other plant tissues, such as flowers and developing seeds, because (1) the expression of the affinity tag is driven by the ubiquitous *UB10p* promoter (Supplemental Fig. S1) and (2) only a small amount of starting material (as low as 1 g) is needed. Additionally, this method is advantageous for the isolation of mitochondria from very young tissues or mutants with growth defects or reduced biomass accumulation. The rapid isolation method is superior to the standard isolation protocols with respect to the yield of mitochondria; we were able to isolate 200 μg of total mitochondrial protein from 1 g of starting material and up to 700 μg total mitochondrial protein from 10 g of whole Arabidopsis seedlings. By contrast, the standard isolation protocols yield only 1.2 mg mitochondria from 50 g of leaves (Keech et al., 2005). Generally, a higher yield is expected using our isolation method, as the HA-tag has high affinity for its cognate antibody. However, yield strongly depends on the amount of beads per gram tissue and the extract-to-bead ratio. Further optimization of both may result in stable amounts of isolated mitochondria and even higher yields.

The purity of affinity-purified mitochondria was similar to that of mitochondria isolated using standard protocols including density gradients (Senkler et al., 2017). Immunoblot analysis revealed only minor contamination with proteins of the ER or peroxisomes in affinity-purified mitochondria (Fig. 3). These results were corroborated by quantitative proteomic analysis. Less than 3% of all quantified proteins were assigned to peroxisomes, the ER, the Golgi, vacuoles, endomembranes, plasma membranes, nuclei, and the cytosol. The highest contamination was due to plastid-localized proteins (Supplemental Tables S1 and S2). However, we cannot exclude the possibility that some of the contaminants bound nonspecifically to the beads, despite extensive washing. Approximately 80% of the identified proteins and 90% of the identified peptides showed mitochondrial localization (Supplemental Tables S1 and S2). Thus, we conclude that the purity of mitochondria isolated using the rapid affinity purification method is comparable with that of mitochondria isolated using traditional methods. Isolated mitochondria show respiratory coupling that is comparable with previous isolations using traditional methods (Keech et al., 2005). Consistent with this result, we could show that the mitochondrial marker CMXRos, a dye that solely stains mitochondria with an intact respiratory chain, was retained in the mitochondria after affinity purification. We could not efficiently elute the mitochondria from the magnetic beads with HA peptide. However, mitochondria could be efficiently eluted using SDS-PAGE or detergent lysis buffer. Elution of intact mitochondria might be achievable by integrating a protease cleavage site between the HA-tag and GFP; this will be explored in future studies.

In our data set, we were able to identify 96% and 99% of the proteins detected by Klodmann et al. (2011) and Senkler et al. (2017), respectively, in previous analyses of mitochondrial proteomes and their complexome composition (Supplemental Tables S1 and S2). On the basis of a recent review on the composition and function of OXPHOS in mitochondria (Meyer et al., 2019), we were able to identify 86% of all the predicted subunits and assembly factors. To date, all of the proteins reviewed in Meyer et al. (2019) have not been confirmed, and it might require an in-depth analysis or membrane enrichment to confirm their presence in mitochondria in proteomic studies. Previously, it was reported that the subunit ND4L is difficult to detect in proteomic studies because of its hydrophobic nature (Peters et al., 2013). Consistent with this observation, we also could not identify this protein in our proteome or in the list of quantified peptides (Supplemental Tables S1 and S2). However, we were able to detect all proteins of the TCA cycle (except two subunits of complex II), all GDC proteins, the majority of the proteins and subunits of the TIM/TOM protein import apparatus, metabolite transporters of amino acids, dicarboxylic acids, cofactors, ions and energy equivalents (e.g. BOU, BAC, UCP, DCT, SAMC, NDT, APC, AAC, and PHT), as well as many proteins involved in protein synthesis/turnover and DNA/RNA metabolism (Supplemental Tables S1 and S2). Thus, our rapidly isolated mitochondria showed good purity, integrity, and functionality.

Among all of the identified proteins, 20% could not be assigned to mitochondria. These proteins included components of PSI and PSII; these could be clearly categorized as contamination. However, we also identified proteins with unknown function and no clear prediction of localization. In addition, we detected proteins such as GAPC, which was previously shown to interact with the OMM protein VDAC (Schneider et al., 2018). Therefore, we predict that some of the proteins classified as contaminants might represent novel mitochondrial proteins, for example, as part of OMM protein complexes in the cytosol or as components of complexes at organellar contact sites. However, this needs to be evaluated in more detail in the future.

Application of the novel method to a mutant lacking the mitochondrial Glu transporter BOU resulted in the detection of surprisingly few changes in protein abundances compared with tagged Col-0. Only 22 mitochondrial proteins showed a significant reduction in abundance in the tagged *bou-2* mutant, whereas five proteins were significantly increased in abundance. However, only changes in a mitochondrial folylpoly-Glu synthetase (FGPS) and in FDH, which contributes to the production of CO_2 in the mitochondria by oxidizing formate, might be connected to photorespiration. Formate is released from 10-formyl-THF by 10-formyl deformylase, an enzyme

involved in the maintenance of the THF pool in mitochondrial matrix (Collakova et al., 2008). Reduced GDC activity in *bou-2* might result in a lower production of formate and finally a reduced abundance of FDH. FGPS is involved in vitamin B9 metabolism by catalyzing the glutamylation of THF, a cofactor of GLDT and SHM (Hanson and Gregory, 2011). No significant changes were detected in the abundance of any of the proteins of the GDC multienzyme system. SHM1, SHM2, and GDCH3 were slightly more abundant in the mutant than tagged Col-0, whereas the others seem to be slightly reduced; however, this trend did not meet the significance threshold (Table 2). The observed changes were not pronounced and did not explain why the GDC activity was reduced to approximately 15% of the Col-0 level in the *bou-2* mutant. A possible explanation could be that Eisenhut and coworkers used 4-week-old rosettes (Eisenhut et al., 2013), whereas we used 10-d-old seedlings in this study. This possibility is supported by the observation that no difference in MDH activity could be detected between 10-d-old mutant and tagged Col-0 seedlings (Fig. 5A). However, in 4-week-old leaves, the MDH activity was significantly reduced in the mutant compared with tagged Col-0 (Supplemental Fig. S2). In contrast to GDC, the abundance of FDH was significantly reduced in the mutant, whereas its activity was unaltered compared with tagged Col-0 (Table 1; Fig. 5B). Previously, FDH was identified in a Lys acetylome study of Arabidopsis mitochondria from 10-d-old Col-0 seedlings (König et al., 2014). This might indicate that FDH activity is more likely regulated by posttranslational modifications than by protein abundance.

The BOU protein was recently assigned the function of a Glu transporter (Porcelli et al., 2018). Glu is indirectly linked to photorespiration, as it is needed for the polyglutamylation of THF, which increases its stability and promotes the activity of THF-dependent enzymes (Hanson and Gregory, 2011). However, in addition to BOU, mitochondria-localized uncoupling proteins 1 and 2 show Glu uptake activity in Arabidopsis (Monné et al., 2018). This raises the question why knockout of the *BOU* gene leads to a photorespiratory phenotype in young tissues, if BOU is not the only Glu transporter of mitochondria. Additionally, polyglutamylation is not restricted to mitochondria, as Arabidopsis contains three isoforms of FGPS localized to mitochondria, plastids, and the cytosol (Hanson and Gregory, 2011). Folate transporters prefer monoglutamylated forms of THF, whereas enzymes generally prefer polyglutamylated forms (Suh et al., 2001). These data indicate that BOU performs other functions, in addition to Glu transport in vivo. We exclude its function as a mitochondrial Glu/Gln shuttle, as BOU shows no Gln uptake activity (Porcelli et al., 2018). However, it is possible that BOU is involved in folate metabolism, as folate biosynthesis occurs only in mitochondria (Hanson and Gregory, 2011). This possibility, however, needs to be investigated in future studies.

CONCLUSION

Our experiments show that, in addition to the analysis of protein-protein interactions, affinity tagging is a powerful tool for the isolation of functional organelles from Arabidopsis. The mitochondria isolated using this method showed high purity and integrity. Future studies will be required to efficiently elute mitochondria from magnetic beads and to determine the applicability of this method for metabolite analyses. To conduct metabolite analyses, it is encouraging that the LC/MS-compatible buffer system developed previously for mammalian mitochondria (Chen et al., 2016) can also be used for the isolation of mitochondria from plant tissues. Expressing the affinity tag under the control of cell-specific promoters will allow the isolation of mitochondria from specific cell types, such as meristems or guard cells (Yang et al., 2008; Schürholz et al., 2018). The use of cell-specific promoters in our construct will help unravel the complex role of mitochondria in various cell types. We expect that similar tagging strategies will be applicable to other plant cell organelles, such as plastids and peroxisomes. Moreover, simultaneous expression of several different affinity tags will facilitate the affinity purification of different organelles from a single extract.

MATERIALS AND METHODS

Plant Growth Conditions

Arabidopsis (*Arabidopsis thaliana*) ecotype Col-0 and *bou-2* mutant (GABI-Kat line number 079D12; http://www.gabi-kat.de/db/lineid.php; Kleinboelting et al., 2012; Eisenhut et al., 2013) were used in this study. Seeds were sterilized by washing with 70% (v/v) ethanol supplemented with 1% (v/v) Triton X-100 twice for 10 min each, followed by washing with 100% ethanol twice for 10 min each. Seeds were grown on half-strength Murashige and Skoog medium (pH 5.7) supplemented with 0.8% (w/v) agar. Seeds were subjected to cold stratification for 2 d at 4°C. After germination, seedlings were grown for 10 d under a 12-h light/12-h dark photoperiod under 100 μmol m^{-2} s^{-1} light intensity and a CO_2-enriched atmosphere (0.3% CO_2), unless otherwise stated.

Measurement of Dry Weight

Ten-day-old Arabidopsis Col-0, tagged Col-0, *bou-2*, and tagged *bou-2* were collected in 1.5-mL microcentrifuge tubes, dried for 3 d at 70°C, and then weighed.

Four-week-old Arabidopsis Col-0 and tagged Col-0 rosettes grown at ambient CO_2 conditions were collected in paper bags, dried for 5 d at 70°C, and then weighed.

Construction of Transgenic Lines

The HA epitope-tag was amplified with a start codon from the Gateway binary vector pGWB15 (GenBank accession AB289778). The coding sequence of sGFP, minus the start and stop codons but including a linker peptide (GGSG) at the 5′ and 3′ ends, was amplified from the Gateway binary vector pGWB4 (GenBank accession AB289767). The coding sequence of *TOM5* (At5g08040; minus the start codon) was amplified from Arabidopsis cDNA. Starting from the 5′ end to the 3′ end, the amplified 3×HA-tag, sGFP, and TOM5 were cloned into the pUTKan vector (Krebs et al., 2012) under the control of the Arabidopsis *UB10p* using restriction endonucleases. The construct was introduced into *Agrobacterium tumefaciens*, strain GV3101::pMP90 (Koncz and Schell, 1986), which was then introduced into Col-0 and *bou-2*

plants via *Agrobacterium*-mediated transformation using the floral-dip method, as described previously (Clough and Bent, 1998). Homozygotes of the T3 generation were used for analyses.

The generated vector pUTKan-*3×HA-sGFP-TOM5* has been deposited on Addgene (ID 130674).

Confocal Laser Scanning Microscopy

The expression of 3×HA-sGFP-TOM5 was verified via confocal laser scanning microscopy using the Zeiss LSM 78 Confocal Microscope and Zeiss ZEN software. The Col-0 and *bou-2* seedlings regenerated from independent transformation events were incubated with 200 nM MitoTracker red CMXRos (Molecular Probes) in half-strength Murashige and Skoog supplemented with 3% (w/v) Suc for 15 min. Images were captured using the following excitation/emission wavelengths: sGFP (488 nm/490–550 nm) and MitoTracker red CMXRos (561 nm/580–625 nm). Pictures were processed using the ImageJ software (https://imagej.nih.gov/ij/).

Rapid Isolation of Mitochondria Using co-IP

Epitope-tagged mitochondria were rapidly isolated using co-IP, as described previously (Chen et al., 2016). In brief, 1 to 10 g of Arabidopsis seedlings were harvested and homogenized in 40 mL KPBS (10 mM KH_2PO_4 [pH 7.25] and 136 mM KCl) twice for 5 s at low speed and 15 s at high speed in a Warren blender. The resulting homogenate was filtered through three layers of miracloth supported by a nylon mesh (pore size 40 μm) and centrifuged at 2500*g* for 5 min. The pellet containing cell debris and chloroplasts was discarded. The supernatant was subsequently centrifuged at 20,000*g* for 9 min. The pellet representing the crude mitochondrial fraction was resuspended in 1 mL KPBS using a fine paintbrush and homogenized with three strokes using a Potter-Elvehjem (B. Braun, Melsungen). Crude mitochondria were incubated with 50 to 250 μL prewashed magnetic anti-HA beads (Thermo Fisher Scientific) on an end-over-end rotator for 5 min in 1.5-mL microcentrifuge tubes. Magnetic beads were prewashed according to the manufacturer's instructions using phosphate-buffered saline supplemented with 0.5% (v/v) Triton X-114. Magnetic beads were separated using a magnetic stand (DYNAL, DynaMag-2 Magnet, Invitrogen) and washed at least three times with each 1 mL KPBS. The purified mitochondria were lysed using 50 to 250 μL mitochondria lysis buffer (50 mM TES/KOH [pH 7.5], 2 mM EDTA, 5 mM $MgCl_2$, 10% [v/v] glycerol, and 0.1% [v/v] Triton X-100) for enzyme activity assays and immunoblot analysis or directly frozen in liquid nitrogen for proteome analyses. All steps were carried out at 4°C. The amount of protein recovered after lysis was determined using the Quick Start Bradford Protein Assay Kit (Bio-Rad), with bovine serum albumin as the standard. Chlorophyll content of rapidly enriched mitochondria was measured as previously described (Porra, 2002).

Isolation of Mitochondria Using the Traditional Approach

Mitochondria were isolated from 10-d-old Col-0 seedlings via differential centrifugation and Percoll gradient purification, as described previously (Kühn et al., 2015).

Immunoblot Analysis

25 μg of total leaf extract and 6.45 μg of isolated mitochondria fractions were heated at 96°C in SDS-PAGE loading buffer for 10 min and separated on 12% SDS-polyacrylamide gels (Laemmli, 1970). Proteins were transferred to 0.2-μm polyvinylidene difluoride membranes (Bio-Rad) or 0.45-μm nitrocellulose membranes (Thermo Scientific) using standard protocols. Protein transfer was verified by staining the membranes with Ponceau S red (Sigma Aldrich). Membranes were blocked according to the manufacturer's instructions for 1 h, washed with Tris-buffered saline containing 0.1% (v/v) Tween 20 (TBST), and subsequently incubated with either a primary antibody or a single-step antibody overnight at 4°C. Antibodies against marker proteins were diluted as follows: anti-AOX (1:1000), anti-IDH (1:5000), anti-VDAC1 (1:5000), anti-HA-horseradish peroxidase (HRP; 1:5000; Miltenyi Biotec), anti-RbcL (1:7500), anti-Cat (1:1000), anti-BiP2 (1:2000), anti-Histone H3 (1:5000), and anti-HSC70 (1:3000). Membranes were washed with TBST twice for 10 min each and incubated with the secondary goat anti-rabbit-HRP antibody (1:5000; Merck Millipore) at room temperature for 1 h or at 4°C overnight. Subsequently, membranes were washed with TBST five times for 5 min each and visualized using a chemiluminescence detection system (Immobilon Western HRP Substrate, Merck Millipore). All steps were carried out with phosphate-buffered saline when using anti-Cat antibody. Antibodies were purchased from Agrisera if not stated otherwise.

Seahorse XFe96 Extracellular Flux Analyzer

Mitochondria were isolated from 10-d-old tagged Col-0 as described above. Purified mitochondria bound to magnetic anti-HA beads were resuspended in mitochondria assay buffer for Seahorse Analyzer measurement (70 mM Suc, 220 mM mannitol, 10 mM KH_2PO_4, 5 mM $MgCl_2$, 2 mM HEPES, 1 mM EGTA, 0.2% [w/v] fatty acid-free bovine serum albumin, pH 7.2 at 37°C) to a concentration of 0.2 μg/μL. Each 20-μL mitochondria suspension (4 μg total mitochondrial protein) per well was analyzed in a cell culture plate for Seahorse Analyzer using an Agilent Seahorse XFe96 Extracellular Flux Analyzer (Agilent Technologies). Mitochondria were attached to the bottom of the plate using a magnetic stand. Subsequently, mitochondria assay buffer for Seahorse Analyzer measurement including succinate as substrate (final concentration 10 mM) was carefully added. Assay protocol was adapted from the Agilent Seahorse XF Cell Mito Stress Test manual. First basal respiration with succinate as substrate was measured in the presence or absence of antimycin A (final concentration 4 μM; Sigma Aldrich), following injection of antimycin A (to a final concentration of 4 μM) to inhibit the respiratory chain. Cartridge hydration overnight was performed according to the manufacturer's instruction. Control isolations were performed on 10-d-old Col-0 seedlings.

Recovery

Mitochondrial recovery was determined based on cytochrome c oxidase activity in homogenized extract and isolated mitochondria via co-IP, as described previously (Lai et al., 2019). Cytochrome c oxidase activity was measured by following the oxidation of cytochrome c at 550 nm (Spinazzi et al., 2012). The assay mixture contained 50 mM potassium phosphate buffer (pH 7.0), 40 μM fully reduced cytochrome c, and 0.1 to 0.5 μg total mitochondrial protein or 5 to 10 μg total extract protein.

Staining of Intact Mitochondria

In mitochondria, staining experiments purified mitochondria bound to 100 μL magnetic anti-HA beads were incubated for 15 min in 1 mL KPBS supplemented with 200 nM MitoTracker red CMXRos in the dark on an end-over-end rotator. Magnetic beads were washed three times with KPBS. Mitochondria were lysed using 1 mL mitochondria lysis buffer. Released fluorescence was measured using a fluorescence spectrophotometer (SynergyH1, BioTek) with the following excitation/emission settings: 570 nm/600 to 650 nm.

Latency of MDH Activity

To assess latency of MDH activity, purified mitochondria bound to 100 μL magnetic anti-HA beads were first eluted in 100 μL KPBS followed by elution in 100 μL KPBS with 0.1% (v/v) Triton X-114. MDH activity in both elution fractions was measured as described previously (Tomaz et al., 2010).

Enzyme Assays

Activities of mitochondrial enzymes were measured using a plate-reader spectrophotometer (SynergyH1, BioTek) based on the A_{340}. Mitochondria were enriched using 150-μL magnetic anti-HA beads and lysed in 200 to 250 μL mitochondrial lysis buffer. The activity of MDH was measured based on the oxidation of NADH to NAD^+ at 340 nm, as described previously (Tomaz et al., 2010). The reaction mixture contained 50 mM KH_2PO_4 (pH 7.5), 0.2 mM NADH, 5 mM EDTA, 10 mM $MgCl_2$, 2 mM OAA (Tomaz et al., 2010), and 0.1 to 0.4 μg total mitochondrial protein. AspAT activity was measured in a reaction coupled with MDH, as described previously (Wilkie and Warren, 1998), with 0.3 to 1 μg total mitochondrial protein per assay. No external pyridoxal-5′-phosphate was added to the reaction mixture. GluDH activity was measured as described previously (Turano et al., 1996), based on the reduction of NAD^+ to NADH at 340 nm. To determine the amination activity, 0.5 to 2 μg total mitochondrial

protein was used per assay. GABA-T activity was measured in a reaction coupled with succinate-semialdehyde dehydrogenase (SSADH), as described previously (Clark et al., 2009). The assay buffer contained 50 mM 3-{[2-hydroxy-1,1-bis(hydroxymethyl)ethyl]amino}-1-propanesulfonic acid (pH 9), 0.2 mM NAD^+, 0.625 mM EDTA, 8 mM GABA, 2 mM pyruvate, 1 U/mL SSADH, and 2 to 5 μg total mitochondrial protein. The NAD^+-dependent SSADH was purified from *Escherichia coli*, as described previously (Clark et al., 2009). The recombinant purified protein catalyzed the production of NADH with a specific activity of 1.6 U/mg protein. AlaAT activity was measured in reaction coupled with lactate dehydrogenase, as described previously (Miyashita et al., 2007), with 1 to 5 μg total mitochondrial protein. FDH activity was measured based on the reduction of NAD^+ to NADH at 340 nm and 30°C, with 1 to 5 μg total mitochondrial protein. The assay buffer contained 100 mM potassium phosphate buffer (pH 7.5), 1 mM NAD^+, and 50 mM sodium formate.

Sample Preparation for LC/MS Analysis

To elute proteins from magnetic beads, 30 μL of Laemmli buffer was added to the reaction mixture, and samples were incubated at 95°C for 10 min. Subsequently, 20 μL of protein sample was loaded on an SDS-polyacrylamide gel for in-gel digestion. The isolated gel pieces were reduced using 50 μL of 10 mM dithiothreitol, then alkylated using 50 μL of 50 mM iodoacetamide, and finally digested using 6 μL of trypsin (200 ng) in 100 mM ammonium bicarbonate. The peptides were resolved in 15 μL of 0.1% (v/v) trifluoracetic acid and subjected to LC/MS analysis.

LC/MS Analysis

The LC/MS analysis was performed on a Q Exactive Plus mass spectrometer (Thermo Scientific) connected to an Ultimate 3000 Rapid Separation LC system (Dionex; Thermo Scientific) and equipped with an Acclaim PepMap 100 C18 column (75 μm inner diameter × 25 cm length × 2 mm particle size; Thermo Scientific). The length of the isocratic LC gradient was 120 min. The mass spectrometer was operated in positive mode and coupled with a nano electrospray ionization source. Capillary temperature was set at 250°C, and source voltage was set at 1.4 kV. The survey scans were conducted at a mass to charge (m/z) of 200 to 2000 and a resolution of 70,000. The automatic gain control was set at 3,000,000, and the maximum fill time was set at 50 ms. The 10 most intensive peptide ions were isolated and fragmented by high-energy collision dissociation.

Computational MS Data Analysis

Peptide and protein identification and quantification was performed using MaxQuant version 1.5.5.1 (MPI for Biochemistry) with default parameters. The identified Arabidopsis peptides and proteins were queried against a specific proteome database (UP0000006548, downloaded 12/11/17) from UniProt. The oxidation and acetylation of Met residues at the N termini of proteins were set as variable modifications, whereas carbamidomethylations at Cys residues were considered as fixed modification. Peptides and proteins were accepted with a false discovery rate of 1%. Unique and razor peptides were used for label-free quantification, and peptides with variable modifications were included in the quantification. The minimal ratio count was set to two, and the "matched between runs" option was enabled.

Normalized intensities, as provided by MaxQuant, were analyzed using the Perseus framework (version 1.5.0.15; MPI for Biochemistry; Tyanova et al., 2016). Only proteins containing at least two unique peptides and a minimum of three valid values in at least one group were quantified. Proteins that were identified only by site or marked as a contaminant (from the MaxQuant contaminant list) were excluded from the analysis. Differential enrichment of proteins in the two groups (Col-0; *bou-2*) was assessed using Student's t test. Significance analysis was applied on $\log_2$-transformed values using an S0 constant of 0 and a false discovery rate of 5% as threshold cutoffs (Benjamini and Hochberg, 1995).

The MS proteomics data has been deposited to the ProteomeXchange Consortium via the PRIDE partner repository with the data set identifier PXD014137.

Accession Numbers

Sequence data from this article can be found in the GenBank/EMBL data libraries under accession numbers AAF82782 (AlaAT1), AAF82781 (AlaAT2), AEC08469 (AspAT), OAO95225 (BOU), AED92076 (FDH), AEE76603 (GABA-T), AED92515 (GluDH1), AED91158 (GluDH2), AEE74011 (GluDH3), BAF44962 (sGFP), Q9ZP06 (mMDH1), Q9LKA3 (mMDH2), and OAO94076 (TOM5).

Supplemental Data

The following supplemental materials are available.

Supplemental Figure S1. Schematic representation of the vector used to label mitochondria with triple HA-tag.

Supplemental Figure S2. Phenotypic analysis of transgenic lines.

Supplemental Figure S3. Original images of all immunoblots related to Figure 3.

Supplemental Figure S4. Activity of MDH in mitochondria rapidly isolated from 4-week-old Col-0 and *bou-2* leaves expressing the *UBI10p-3×HA-sGFP-TOM5* construct.

Supplemental Table S1. List of proteins identified and quantified in 10-d-old Col-0 and *bou-2* plants expressing the 3×HA-sGFP-TOM5 protein.

Supplemental Table S2. List of raw intensities and reliability of all quantified peptides.

Received June 16, 2019; accepted November 22, 2019; published December 9, 2019.

LITERATURE CITED

Benjamini Y, Hochberg Y (1995) Controlling the false discovery rate: A practical and powerful approach to multiple testing. J R Stat Soc Series B Stat Methodol **57:** 289–300

Chen WW, Freinkman E, Wang T, Birsoy K, Sabatini DM (2016) Absolute quantification of matrix metabolites reveals the dynamics of mitochondrial metabolism. Cell **166:** 1324–1337.e11

Clark SM, Di Leo R, Dhanoa PK, Van Cauwenberghe OR, Mullen RT, Shelp BJ (2009) Biochemical characterization, mitochondrial localization, expression, and potential functions for an *Arabidopsis* gamma-aminobutyrate transaminase that utilizes both pyruvate and glyoxylate. J Exp Bot **60:** 1743–1757

Clough SJ, Bent AF (1998) Floral dip: A simplified method for *Agrobacterium*-mediated transformation of *Arabidopsis thaliana*. Plant J **16:** 735–743

De Col V, Fuchs P, Nietzel T, Elsässer M, Voon CP, Candeo A, Seeliger I, Fricker MD, Grefen C, Møller IM, et al (2017) ATP sensing in living plant cells reveals tissue gradients and stress dynamics of energy physiology. eLife **6:** 1–29

Collakova E, Goyer A, Naponelli V, Krassovskaya I, Gregory JF III, Hanson AD, Shachar-Hill Y (2008) Arabidopsis 10-formyl tetrahydrofolate deformylases are essential for photorespiration. Plant Cell **20:** 1818–1832

Dietmeier K, Hönlinger A, Bömer U, Dekker PJ, Eckerskorn C, Lottspeich F, Kübrich M, Pfanner N (1997) Tom5 functionally links mitochondrial preprotein receptors to the general import pore. Nature **388:** 195–200

Eisenhut M, Planchais S, Cabassa C, Guivarc'h A, Justin AM, Taconnat L, Renou JP, Linka M, Gagneul D, Timm S, et al (2013) *Arabidopsis* A BOUT DE SOUFFLE is a putative mitochondrial transporter involved in photorespiratory metabolism and is required for meristem growth at ambient CO_2 levels. Plant J **73:** 836–849

Eisenhut M, Roell MS, Weber APM (2019) Mechanistic understanding of photorespiration paves the way to a new green revolution. New Phytol **223:** 1762–1769

Engel N, van den Daele K, Kolukisaoglu U, Morgenthal K, Weckwerth W, Pärnik T, Keerberg O, Bauwe H (2007) Deletion of glycine decarboxylase in Arabidopsis is lethal under nonphotorespiratory conditions. Plant Physiol **144:** 1328–1335

Fromm S, Senkler J, Eubel H, Peterhänsel C, Braun H-P (2016) Life without complex I: Proteome analyses of an *Arabidopsis* mutant lacking the mitochondrial NADH dehydrogenase complex. J Exp Bot **67:** 3079–3093

Hanson AD, Gregory JF III (2011) Folate biosynthesis, turnover, and transport in plants. Annu Rev Plant Biol **62:** 105–125

Hooper CM, Castleden IR, Tanz SK, Aryamanesh N, Millar AH (2017) SUBA4: The interactive data analysis centre for *Arabidopsis* subcellular protein locations. Nucleic Acids Res **45**(D1): D1064–D1074

Horie C, Suzuki H, Sakaguchi M, Mihara K (2003) Targeting and assembly of mitochondrial tail-anchored protein Tom5 to the TOM complex depend on a signal distinct from that of tail-anchored proteins dispersed in the membrane. J Biol Chem **278:** 41462–41471

Hu Y, Zou W, Wang Z, Zhang Y, Hu Y, Qian J, Wu X, Ren Y, Zhao J (2019) Translocase of the outer mitochondrial membrane 40 is required for mitochondrial biogenesis and embryo development in *Arabidopsis*. Front Plant Sci **10:** 389

Husic DW, Husic HD, Tolbert NE, Black CC (1987) The oxidative photosynthetic carbon cycle or C2 cycle. CRC Crit Rev Plant Sci **5:** 45–100

Keech O, Dizengremel P, Gardeström P (2005) Preparation of leaf mitochondria from *Arabidopsis thaliana*. Physiol Plant **124:** 403–409

Kelly GJ, Latzko E (1976) Inhibition of spinach-leaf phosphofructokinase by 2-phosphoglycollate. FEBS Lett **68:** 55–58

Kleinboelting N, Huep G, Kloetgen A, Viehoever P, Weisshaar B (2012) GABI-Kat SimpleSearch: New features of the *Arabidopsis thaliana* T-DNA mutant database. Nucleic Acids Res **40:** D1211–D1215

Klodmann J, Senkler M, Rode C, Braun H-P (2011) Defining the protein complex proteome of plant mitochondria. Plant Physiol **157:** 587–598

Kolli R, Soll J, Carrie C (2019) OXA2b is crucial for proper membrane insertion of COX2 during biogenesis of complex IV in plant mitochondria. Plant Physiol **179:** 601–615

Koncz C, Schell J (1986) The promoter of TL-DNA gene 5 controls the tissue-specific expression of chimaeric genes carried by a novel type of *Agrobacterium* binary vector. Mol Gen Genet **204:** 383–396

König AC, Hartl M, Boersema PJ, Mann M, Finkemeier I (2014) The mitochondrial lysine acetylome of *Arabidopsis*. Mitochondrion **19**(Pt B): 252–260

Krebs M, Held K, Binder A, Hashimoto K, Den Herder G, Parniske M, Kudla J, Schumacher K (2012) FRET-based genetically encoded sensors allow high-resolution live cell imaging of Ca^{2+} dynamics. Plant J **69:** 181–192

Kühn K, Obata T, Feher K, Bock R, Fernie AR, Meyer EH (2015) Complete mitochondrial complex I deficiency induces an up-regulation of respiratory fluxes that is abolished by traces of functional complex I. Plant Physiol **168:** 1537–1549

van der Laan M, Horvath SE, Pfanner N (2016) Mitochondrial contact site and cristae organizing system. Curr Opin Cell Biol **41:** 33–42

Laemmli UK (1970) Cleavage of structural proteins during the assembly of the head of bacteriophage T4. Nature **227:** 680–685

Lai N, M Kummitha C, Rosca MG, Fujioka H, Tandler B, Hoppel CL (2019) Isolation of mitochondrial subpopulations from skeletal muscle: Optimizing recovery and preserving integrity. Acta Physiol (Oxf) **225:** e13182

Linka M, Weber APM (2005) Shuffling ammonia between mitochondria and plastids during photorespiration. Trends Plant Sci **10:** 461–465

Mansilla N, Racca S, Gras DE, Gonzalez DH, Welchen E (2018) The complexity of mitochondrial complex IV: An update of cytochrome c oxidase biogenesis in plants. Int J Mol Sci **19:** 1–34

Meyer EH, Welchen E, Carrie C (2019) Assembly of the complexes of the oxidative phosphorylation system in land plant mitochondria. Annu Rev Plant Biol **70:** 23–50

Millar AH, Eubel H, Jänsch L, Kruft V, Heazlewood JL, Braun H-P (2004) Mitochondrial cytochrome c oxidase and succinate dehydrogenase complexes contain plant specific subunits. Plant Mol Biol **56:** 77–90

Millar AH, Sweetlove LJ, Giegé P, Leaver CJ (2001) Analysis of the Arabidopsis mitochondrial proteome. Plant Physiol **127:** 1711–1727

Miyashita Y, Dolferus R, Ismond KP, Good AG (2007) Alanine aminotransferase catalyses the breakdown of alanine after hypoxia in *Arabidopsis thaliana*. Plant J **49:** 1108–1121

Monné M, Daddabbo L, Gagneul D, Obata T, Hielscher B, Palmieri L, Miniero DV, Fernie AR, Weber APM, Palmieri F (2018) Uncoupling proteins 1 and 2 (UCP1 and UCP2) from *Arabidopsis thaliana* are mitochondrial transporters of aspartate, glutamate, and dicarboxylates. J Biol Chem **293:** 4213–4227

Murcha MW, Kmiec B, Kubiszewski-Jakubiak S, Teixeira PF, Glaser E, Whelan J (2014) Protein import into plant mitochondria: Signals, machinery, processing, and regulation. J Exp Bot **65:** 6301–6335

Murcha MW, Narsai R, Devenish J, Kubiszewski-Jakubiak S, Whelan J (2015) MPIC: A mitochondrial protein import components database for plant and non-plant species. Plant Cell Physiol **56:** e10

Nickel C, Horneff R, Heermann R, Neumann B, Jung K, Soll J, Schwenkert S (2019) Phosphorylation of the outer membrane mitochondrial protein OM64 influences protein import into mitochondria. Mitochondrion **44:** 93–102

Ogren WL, Bowes G (1971) Ribulose diphosphate carboxylase regulates soybean photorespiration. Nat New Biol **230:** 159–160

Oliver DJ, Neuburger M, Bourguignon J, Douce R (1990) Interaction between the component enzymes of the glycine decarboxylase multienzyme complex. Plant Physiol **94:** 833–839

Pendergrass W, Wolf N, Poot M (2004) Efficacy of MitoTracker green and CMXrosamine to measure changes in mitochondrial membrane potentials in living cells and tissues. Cytometry A **61:** 162–169

Peterhansel C, Horst I, Niessen M, Blume C, Kebeish R, Kürkcüoglu S, Kreuzaler F (2010) Photorespiration. Arabidopsis Book **8:** e0130

Peters K, Belt K, Braun H-P (2013) 3D gel map of *Arabidopsis* complex I. Front Plant Sci **4:** 153

Porcelli V, Vozza A, Calcagnile V, Gorgoglione R, Arrigoni R, Fontanesi F, Marobbio CMT, Castegna A, Palmieri F, Palmieri L (2018) Molecular identification and functional characterization of a novel glutamate transporter in yeast and plant mitochondria. Biochim Biophys Acta Bioenerg **1859:** 1249–1258

Porra RJ (2002) The chequered history of the development and use of simultaneous equations for the accurate determination of chlorophylls a and b. Photosynth Res **73:** 149–156

Rao RSP, Salvato F, Thal B, Eubel H, Thelen JJ, Møller IM (2017) The proteome of higher plant mitochondria. Mitochondrion **33:** 22–37

Schneider M, Knuesting J, Birkholz O, Heinisch JJ, Scheibe R (2018) Cytosolic GAPDH as a redox-dependent regulator of energy metabolism. BMC Plant Biol **18:** 184

Schürholz A-K, López-Salmerón V, Li Z, Forner J, Wenzl C, Gaillochet C, Augustin S, Barro AV, Fuchs M, Gebert M, et al (2018) A comprehensive toolkit for inducible, cell type-specific gene expression in Arabidopsis. Plant Physiol **178:** 40–53

Senkler J, Senkler M, Eubel H, Hildebrandt T, Lengwenus C, Schertl P, Schwarzländer M, Wagner S, Wittig I, Braun HP (2017) The mitochondrial complexome of *Arabidopsis thaliana*. Plant J **89:** 1079–1092

Spinazzi M, Casarin A, Pertegato V, Salviati L, Angelini C (2012) Assessment of mitochondrial respiratory chain enzymatic activities on tissues and cultured cells. Nat Protoc **7:** 1235–1246

Suh JR, Herbig AK, Stover PJ (2001) New perspectives on folate catabolism. Annu Rev Nutr **21:** 255–282

Sunderhaus S, Dudkina NV, Jänsch L, Klodmann J, Heinemeyer J, Perales M, Zabaleta E, Boekema EJ, Braun HP (2006) Carbonic anhydrase subunits form a matrix-exposed domain attached to the membrane arm of mitochondrial complex I in plants. J Biol Chem **281:** 6482–6488

Tomaz T, Bagard M, Pracharoenwattana I, Lindén P, Lee CP, Carroll AJ, Ströher E, Smith SM, Gardeström P, Millar AH (2010) Mitochondrial malate dehydrogenase lowers leaf respiration and alters photorespiration and plant growth in Arabidopsis. Plant Physiol **154:** 1143–1157

Turano FJ, Dashner R, Upadhyaya A, Caldwell CR (1996) Purfication of mitochondrial glutamate dehydrogenase from dark-grown soybean seedlings. Plant Physiol **112:** 1357–1364

Tyanova S, Temu T, Sinitcyn P, Carlson A, Hein MY, Geiger T, Mann M, Cox J (2016) The Perseus computational platform for comprehensive analysis of (prote)omics data. Nat Methods **13:** 731–740

Voll LM, Jamai A, Renné P, Voll H, McClung CR, Weber APM (2006) The photorespiratory Arabidopsis shm1 mutant is deficient in SHM1. Plant Physiol **140:** 59–66

Werhahn W, Jänsch L, Braun HP (2003) Identification of novel subunits of the TOM complex from *Arabidopsis thaliana*. Plant Physiol Biochem **41:** 407–416

Werhahn W, Niemeyer A, Jänsch L, Kruft V, Schmitz UK, Braun H (2001) Purification and characterization of the preprotein translocase of the outer mitochondrial membrane from Arabidopsis. Identification of multiple forms of TOM20. Plant Physiol **125:** 943–954

Wiedemann N, Frazier AE, Pfanner N (2004) The protein import machinery of mitochondria. J Biol Chem **279:** 14473–14476

Wilkie SE, Warren MJ (1998) Recombinant expression, purification, and characterization of three isoenzymes of aspartate aminotransferase from *Arabidopsis thaliana*. Protein Expr Purif **12:** 381–389

Yang Y, Costa A, Leonhardt N, Siegel RS, Schroeder JI (2008) Isolation of a strong *Arabidopsis* guard cell promoter and its potential as a research tool. Plant Methods **4:** 6

Supplemental Figure S1

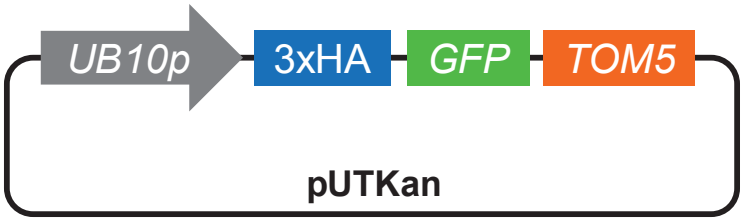

Supplemental Figure S1: Schematic representation of the vector used to label mitochondria with triple HA-tag. The N-terminal end of Arabidopsis gene encoding the outer mitochondrial membrane protein TOM5 (At5g08040) was fused to the *synthetic green fluorescent protein* (*sGFP*) gene labeled with a triple hemagglutinin (3×HA) tag for co-immunopurification. The cassette was cloned into the pUTKan vector under the control of the Arabidopsis *UBIQUITIN10* promoter (*UB10p*) and stably introduced into Arabidopsis via the floral dip method.

Supplemental Figure S2

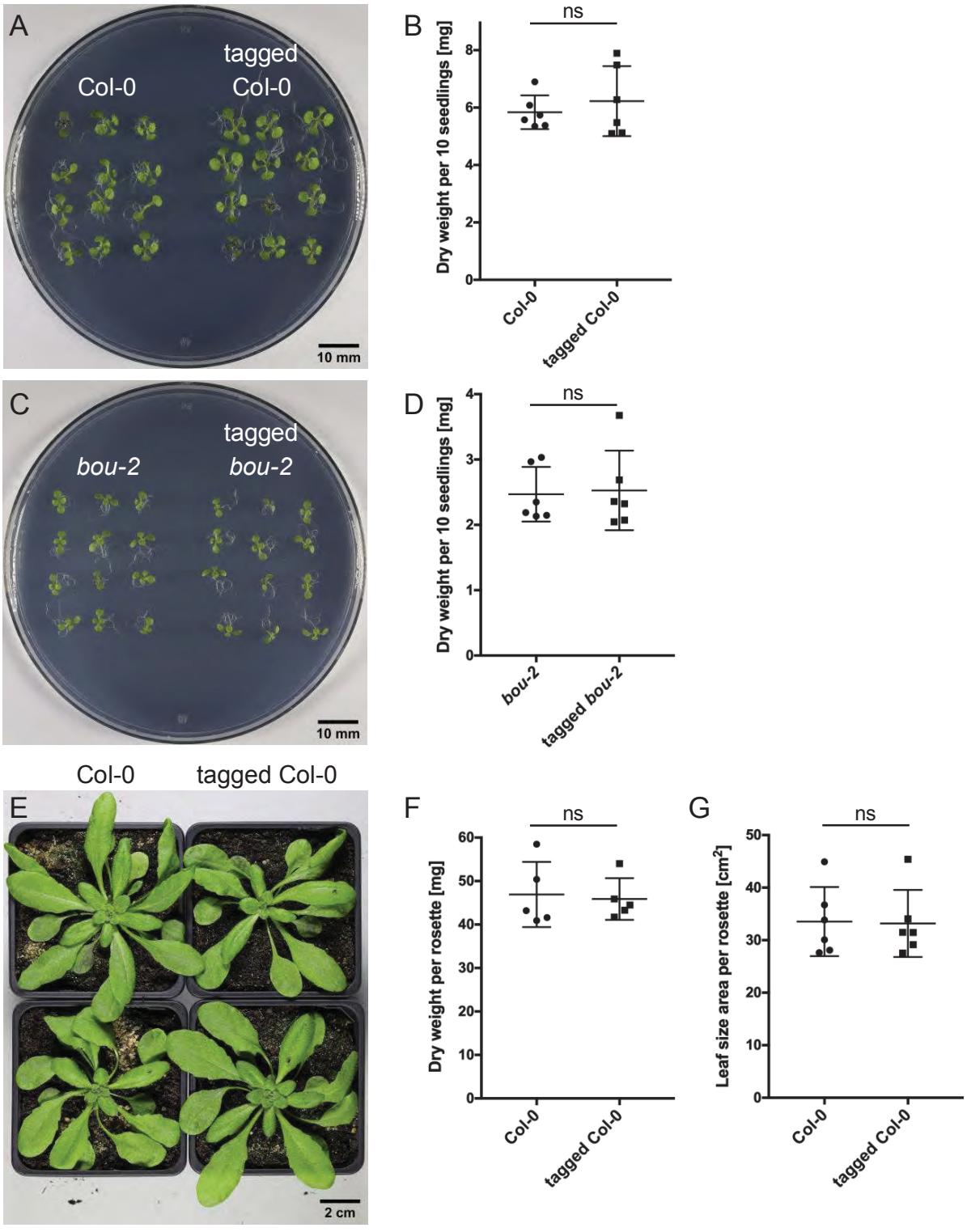

Supplemental Figure S2: Phenotypic analysis of transgenic lines. Photographs of Col-0 and tagged Col-0 (A) and *bou-2* and tagged *bou-2* (C) were taken after 10 days growth in a CO_2- enriched atmosphere. Scale bars = 10 mm. Dry weight of Col-0 and tagged Col-0 (B) and bou-2 and tagged bou-2 (D) was determined after 10 days growth in a CO_2-enriched atmosphere. Photographs of Col-0 and tagged Col-0 grown on soil were taken after 4 weeks growth at ambient CO_2 conditions (E). Scale bar = 2 cm. Dry weight of Col-0 and tagged Col-0 grown on soil (F) and leaf area size per rosette (G) were determined after 4 weeks growth at ambient CO_2 conditions. Data represent mean ± SD of five (F) and six (B, D, G) biological replicates. Significance was calculated with Student's *t*-test ($P < 0.05$).

Supplemental Figure S3

A

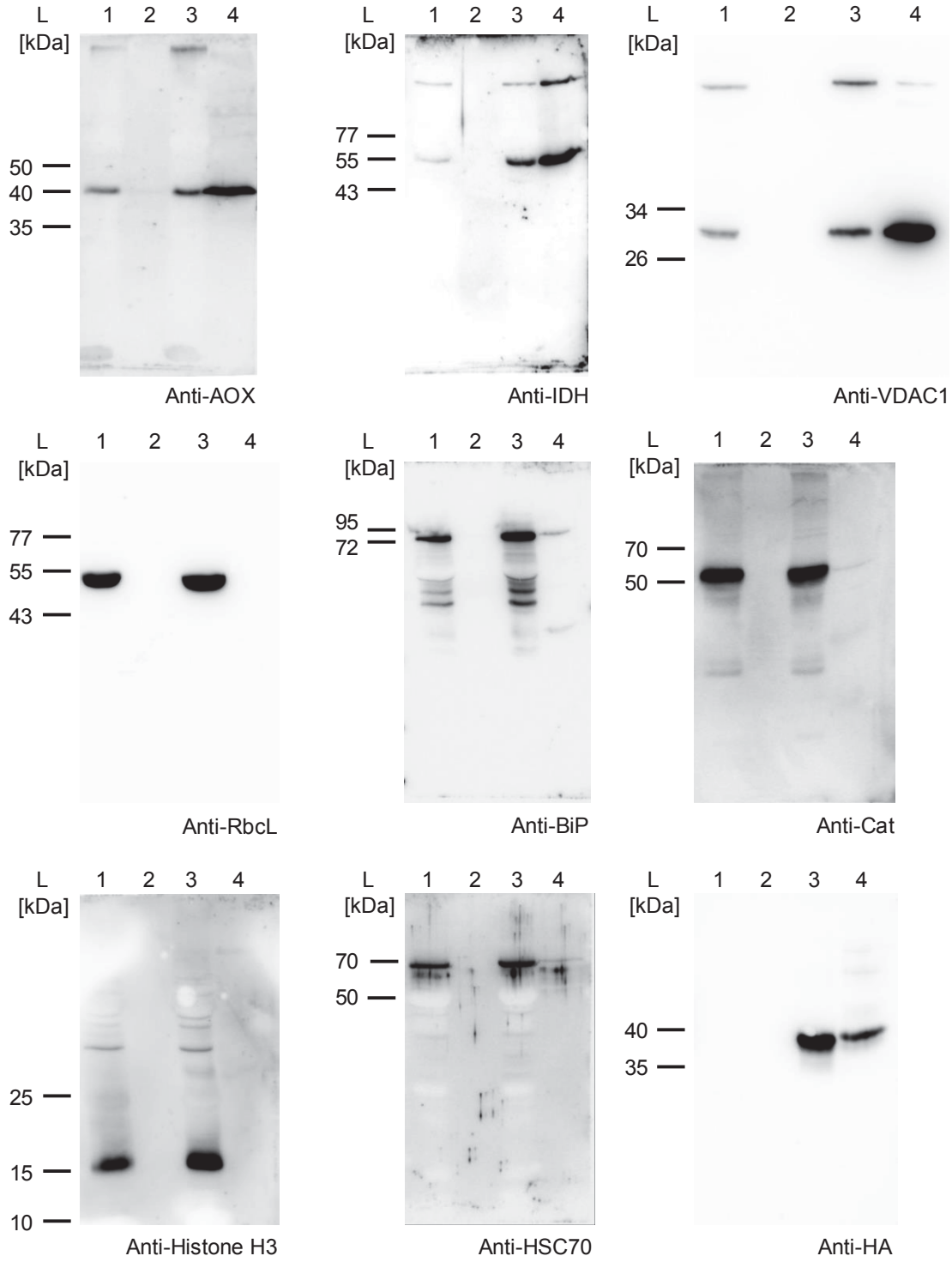

Supplemental Figure S3

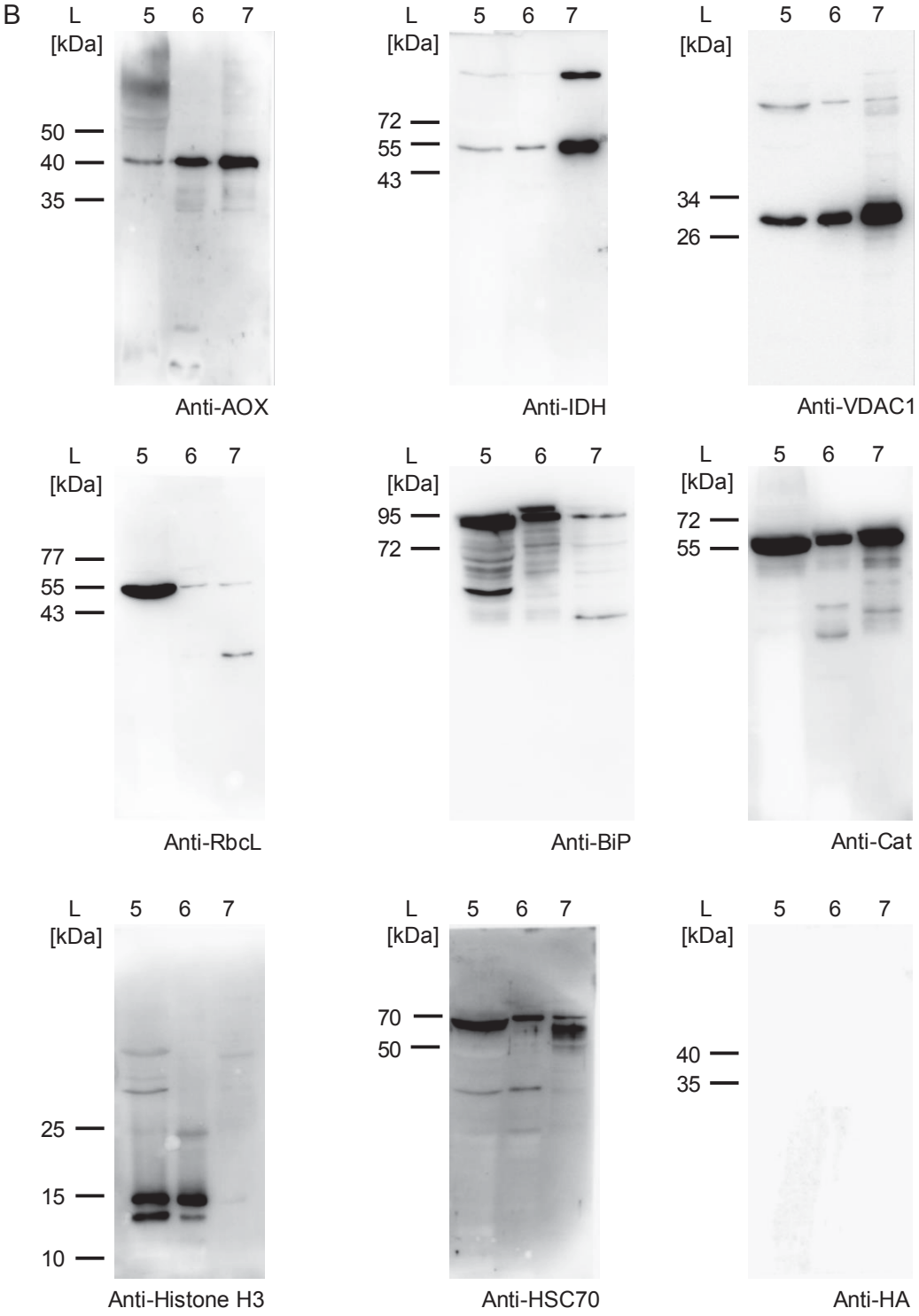

Supplemental Figure S3: Original images of all immunoblots related to Figure 3. Mitochondria were isolated via co-IP (A) from Col-0 (1, 2) and tagged Col-0 (3, 4) seedlings or via density gradient purification (B) from Col-0 seedlings (5–7) as stated in Materials and Methods. Samples after tissue homogenization (1, 3, 5), enriched mitochondria via co-IP (2, 4), crude mitochondria after differential centrifugation (6), and enriched mitochondria via density gradient purification (7) were processed for SDS-PAGE and immunoblot analysis as described in Materials and Methods.

Supplemental Figure S4

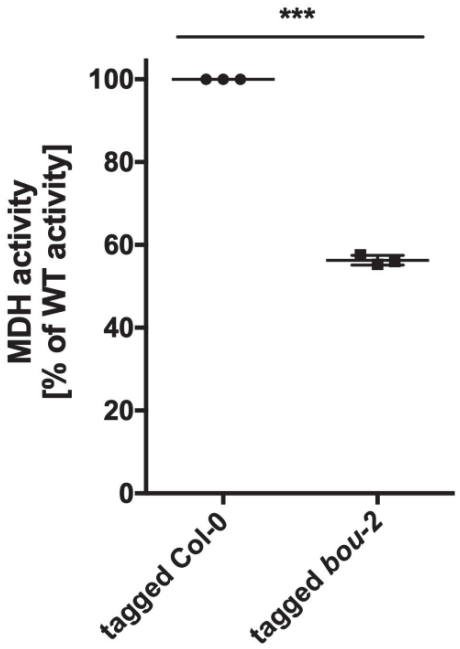

Supplemental Figure S4: Activity of malate dehydrogenase (MDH) in mitochondria rapidly isolated from 4-week-old Col-0 and *bou-2* leaves expressing the *UB10p-3×HA-sGFP-TOM5* construct. MDH activity was measured as described in Materials and Methods. Activities were calculated from initial slopes. Enzyme activity in tagged Col-0 was set to 100%. Average tagged Col-0 activity: 18.1. ± 2.2 µmol min^{-1} mg^{-1}. Data represent mean ± SD of three biological replicates (each four technical replicates). Asterisks indicate statistically significant differences (***, $P < 0.001$; Student's *t*-test).

Manuscript II

The Mitochondrial Carrier À BOUT DE SOUFFLE is a Key Player in Photorespiratory Nitrogen Metabolism

The Mitochondrial Carrier À BOUT DE SOUFFLE is a Key Player in Photorespiratory Nitrogen Metabolism

Franziska Kuhnert[1], Leonie Kraska[1], Simon Strobbe[2], Jana Verstraete[3], Maite Colinas[4], Michael Moulin[4], Philipp Westhoff[5], Marion Eisenhut[1], Teresa Fitzpatrick[4], Christophe Stove[3], Dominique Van Der Straeten[2], Andreas P.M. Weber[1]

[1]Institute of Plant Biochemistry, Cluster of Excellence on Plant Science (CEPLAS), Heinrich Heine University, Universitätsstrasse 1, 40225 Düsseldorf, Germany

[2]Laboratory of Functional Plant Biology, Department of Biology, Ghent University, K.L. Ledeganckstraat 35, 9000 Ghent, Belgium

[3]Laboratory of Toxicology, Department of Bioanalysis, Ghent University, Ottergemsesteenweg 460, 9000 Ghent, Belgium

[4]Department of Botany and Plant Biology, University of Geneva, Quai E. Ansermet 30, 1211 Geneva, Switzerland

[5]Plant Metabolism and Metabolomics Facility, Cluster of Excellence on Plant Science (CEPLAS), Heinrich Heine University, Universitätsstrasse 1, 40225 Düsseldorf, Germany

One-sentence summary: The mitochondrial carrier À BOUT DE SOUFFLE is a glutamate transporter with a clearly defined substrate spectrum that is of critical importance for photorespiratory nitrogen metabolism.

Author contribution: FK performed mitochondria isolations, enzyme assays, protein purification, uptake experiments, extracted metabolites, analyzed data, designed experiments, and wrote the manuscript; LK assisted with mitochondria isolation and uptake measurements; PW performed amino acid analyses on rapidly isolated mitochondria; SS, JV, CS, DVDS performed Vitamin B_9 analysis and analyzed data; MC, MM, TF performed Vitamin B_6 analysis and analyzed data; ME designed experiments; APMW designed research and supervised the experiments

ABSTRACT

Photorespiration is a complex pathway unique to all organisms performing oxygenic photosynthesis. It is essential to recycle the toxic product of the oxygenation reaction of Rubisco, 2-phosphoglycolate. The pathway is highly compartmentalized with reactions taking place in chloroplasts, peroxisomes, mitochondria, and the cytosol. The enzymatic reactions in the different organelles are connected by specialized transport proteins of which to date only very few have been identified. The *Arabidopsis thaliana* protein À BOUT DE SOUFFLE (BOU) was previously identified as a mitochondrial glutamate carrier involved in photorespiration. Deletion of *BOU* led to accumulation of photorespiratory intermediates and a strongly reduced glycine decarboxylase (GDC) activity. Here, we show that BOU has a clearly defined substrate spectrum. We analyzed vitamin B_6 and B_9 levels, cofactors of the GDC, in whole seedlings and isolated mitochondria demonstrating that the levels of active cofactors of the GDC are not limited in *bou-2*. The analysis of the vitamin B_9 content revealed a potential regulatory function of the metabolite 5-formyltetrahydrofolate in photorespiration and C_1 metabolism. Our data on enzyme activities suggest a function of BOU in photorespiratory nitrogen metabolism. We hypothesize that BOU mediates glutamate export under photorespiratory conditions to provide acceptor molecules of glutamate for re-assimilation of ammonia in chloroplasts.

INTRODUCTION

All organisms performing oxygenic photosynthesis assimilate atmospheric carbon dioxide (CO_2) into organic carbon compounds by the enzyme ribulose 1,5-bisphosphate carboxylase/oxygenase (Rubisco). The carboxylation reaction of Rubisco leads to the production of two molecules 3-phosphoglycerate (3-PGA) that are converted into triose phosphate through the Calvin-Bassham-Benson cycle (CBBC; Calvin, 1962). However, Rubisco shows additional affinity for molecular oxygen (O_2). The oxygenation reaction of Rubisco leads to the production of one molecule 3-PGA and one molecule 2-phosphoglycolate (2-PG). The latter is a toxic compound that cannot be metabolized in the CBBC but inhibits the two plastidial enzymes, triose phosphate isomerase and phosphofructokinase (Anderson, 1971; Bowes et al., 1971; Ogren and Bowes, 1971; Kelly and Latzko, 1976; Ogren, 1984). Thus, 2-PG has to be recycled in a pathway known as photorespiration. Photorespiration is a highly compartmentalized, complex process that recovers one molecule 3-PGA from two molecules 2-PG with the loss of one molecule CO_2 (Somerville and Ogren, 1979; Ogren, 1984; Eisenhut et al., 2019).

The pathway starts in the chloroplast stroma where 2-PG deriving from the oxygenation reaction of Rubisco is dephosphorylated by 2-phosphoglycolate phosphatase (PGLP) forming glycolate (Somerville and Ogren, 1979; Schwarte and Bauwe, 2007). Glycolate enters the peroxisome where it is converted into glycine in a series of two reactions catalyzed by (1) glycolate oxidase (Volokita and Somerville, 1987) and (2) glutamate:glyoxylate aminotransferase (GGAT; Igarashi et al., 2003). In the mitochondria two molecules of glycine are converted into one molecule of serine by a combined reaction of glycine decarboxylase (GDC) and serine hydroxymethyl transferase (SHMT) releasing one molecule of CO_2 and an equimolar amount of ammonia (NH_3; Voll et al., 2006; Engel et al., 2007). Serine subsequently enters the peroxisomes where it is first deaminated by serine:glyoxylate aminotransferase (Somerville and Ogren, 1980), the resulting hydroxypyruvate is then reduced by the peroxisomal hydroxypyruvate reductase (HPR) yielding glycerate (Givan and Kleczkowski, 1992). Alternatively, a cytosolic bypass exists (Timm et al., 2008). Glycerate is shuttled back to the chloroplast where it is phosphorylated in the final step by glycerate kinase yielding 3-PGA (Boldt et al., 2005). With the photorespiratory pathway 75% of previously fixed carbon that would have been lost as 2-PG is recovered as 3-PGA. However, this comes at the cost of ATP and reducing equivalents, and decreases the photosynthetic efficiency up to 50% (Ogren, 1984; Peterhansel et al., 2010; Walker et al., 2016; South et al., 2017). The remaining 25% of the carbon are released in the mitochondria in the concerted reaction of GDC and SHMT. In addition, an equimolar amount of NH_3 is released as well. It is widely assumed that NH_3 diffuses from the mitochondrial matrix to the chloroplast where it is first re-assimilated to glutamate by the

glutamine synthetase (GS) yielding glutamine. Glutamine is used in a second reaction by the ferredoxin-dependent glutamine:oxoglutarate aminotransferase (FdGOGAT) to transaminate 2-oxoglutarate (2-OG) yielding two molecules of glutamate. One molecule is needed to re-assimilate another molecule of NH_3, whereas the second is likely shuttled towards the peroxisomes where glutamate is required for the GGAT reaction (Miflin and Lea, 1980; Somerville and Ogren, 1980; Coschigano et al., 1998).

Mutants with reduced expression or full knockout of genes of the photorespiratory pathway typically show a so-called photorespiratory phenotype. It is characterized by reduced growth and chlorotic leaves under ambient CO_2 (0.038% [v/v] CO_2 in air) conditions, and can be rescued with elevated concentrations of CO_2 (at least 0.3% [v/v] CO_2 in air; Somerville, 2001; Peterhansel et al., 2010). However, the severity of this phenotype strongly varies (Timm and Bauwe, 2013). Deletion of the peroxisomal *GGAT1* for example shows a rather mild photorespiratory phenotype as the effect can likely be complemented by the activity of GGAT2 and other peroxisomal aminotransferases (Igarashi et al., 2003; Liepman and Olsen, 2003). Knockout of *PGLP* shows a strong photorespiratory phenotype with severely impaired growth under ambient CO_2 conditions (Schwarte and Bauwe, 2007). A double knockout of the P-protein (GDCP) or the T-protein of the GDC (GDCT), or both mitochondrial SHMTs is even lethal under elevated CO_2 conditions (Engel et al., 2007; Engel et al., 2011; Timm et al., 2018). Besides their function in photorespiration, GDC and SHMT play an important role in cellular C_1 metabolism linked by one of their cofactors tetrahydrofolate (THF). The lethality of a knockout of GDC and SHMT under elevated CO_2 conditions underlines the importance of C_1 metabolism in plant development (Hanson and Roje, 2001; Engel et al., 2007; Eisenhut et al., 2019). Under photorespiratory conditions, GDC decarboxylates glycine and transfers the residual C_1 unit to THF, forming 5,10-methylene-THF. From there it is transferred onto another molecule of glycine by the reaction of SHMT. Under non-photorespiratory conditions, SHMT favors the reverse reaction in which 5,10-methylene-THF and glycine are produced from serine (Douce et al., 2001; Hanson and Roje, 2001; Engel et al., 2011). The mitochondrial THF pool is maintained by a series of enzymatic reactions, which finally leads to the release of THF by 10-formyl-THF deformylase (FDF) from 10-formyl-THF. The photorespiratory phenotype of a double knockout mutant in *FDF1* and *FDF2* pinpoints the importance of FDF for photorespiratory metabolism (Collakova et al., 2008).

Despite the comprehensive knowledge about the soluble enzymes of the photorespiratory pathway only few transport proteins have been identified and characterized so far. There are at least 25 transport steps involved including the shuttle of core metabolites of the pathway, the nitrogen cycle, cofactors or their precursors, and metabolites of auxiliary pathways, such as malate and oxaloacetate (OAA; Eisenhut et al., 2013a). To date the plastidic glycolate/glycerate translocator (PLGG1), the bile acid sodium symporter 6 (BASS6), and the

plastidic dicarboxylate transporters DiT1 and DiT2.1 have been identified on the molecular level and analyzed in detail (Somerville and Somerville, 1985; Woo et al., 1987; Renné et al., 2003; Pick et al., 2013; South et al., 2017). All four proteins are localized to the inner envelope of chloroplasts. PLGG1 and BASS6 are transporters of the photorespiratory core metabolites glycerate (PLGG1) and glycolate (PLGG1, BASS6; Pick et al., 2013; South et al., 2017). DiT1 and DiT2.1 function as 2-OG/malate (DiT1) and glutamate/malate (DiT2.1) transporters that are essential for nitrogen re-assimilation in chloroplasts (Renné et al., 2003; Schneidereit et al., 2006). Transporters or channels in the peroxisomal membrane that are involved in the translocation of one or more photorespiratory intermediates have not been identified yet. Also genes encoding for transporters that shuttle the core metabolites glycine and/or serine across the inner mitochondrial membrane have not been isolated so far. However, the uncoupling proteins UCP1 and UCP2 that regulate mitochondrial redox state by transporting aspartate, glutamate and dicarboxylates, and the mitochondrial carrier family protein À BOUT DE SOUFFLE (BOU) were assigned as mitochondrial transporters involved in photorespiration (Sweetlove et al., 2006; Eisenhut et al., 2013b; Monné et al., 2018).

Due to its high homology to mammalian carnitine acyl carriers BOU was first described as plant carnitine-acylcarnitine carrier. It was hypothesized that plant mitochondrial metabolism relies on BOU transport function in the light as an alternative or complementation to the glyoxylate cycle (Lawand et al., 2002). Later, it was shown that BOU is involved in photo-respiration since the mutant displayed a photorespiratory phenotype, a significantly reduced CO_2 assimilation rate, a significantly increased CO_2 compensation point, strongly reduced GDC activity in isolated mitochondria, and accumulation of photorespiratory intermediates (Eisenhut et al., 2013b). The study also showed that the knock out mutant *bou-2* has a similar metabolic phenotype as *shm1*. Together with the strongly reduced GDC activity Eisenhut and coworkers concluded that BOU is important for proper function of GDC (Eisenhut et al., 2013b). In a very recent study with reconstituted BOU protein, glutamate was identified as a transport substrate of BOU (Porcelli et al., 2018). How a glutamate transport activity relates to the phenotypic and metabolic appearance of *bou-2* could not be fully explained to date. Using rapid isolation of plant mitochondria via co-Immunopurification (co-IP), we obtained results on a differential proteomic analysis and activities of mitochondrial enzymes, which indicated that BOU is likely involved in THF- and nitrogen metabolism (Kuhnert et al., 2020).

Here, we applied our rapid isolation protocol to get a more detailed insight into THF metabolism of *bou-2*. Furthermore, we could show that BOU shows transport activity for glutamate but not for other photorespiratory intermediates. Our data suggest that BOU functions as a mitochondrial glutamate exporter providing glutamate for re-assimilation of nitrogen in chloroplasts and is thus a central player in plant photorespiration.

RESULTS

BOU functions as glutamate transporter in *Arabidopsis thaliana*

Recently, it was shown that Arabidopsis BOU transports glutamate (Porcelli et al., 2018). Glutamate is neither a substrate nor a product of the concerted reaction of GDC and SHMT in the mitochondria. It is essential for polyglutamylation of THF, a cofactor of GDC and SHMT. However, polyglutamylation of THF is not restricted to the mitochondria and does not explain the strong photorespiratory phenotype of *bou-2* (Hanson and Roje, 2001; Mehrshahi et al., 2010; Hanson and Gregory, 2011); thus indicating an additional role of BOU in photo-respiratory metabolism. Therefore, we heterologously expressed BOU in *E. coli*, purified it from inclusion bodies and reconstituted it into liposomes (Supplemental Fig. S1A, B). BOU showed uptake activity for glutamate (Fig. 1A) as demonstrated previously (Porcelli et al., 2018).

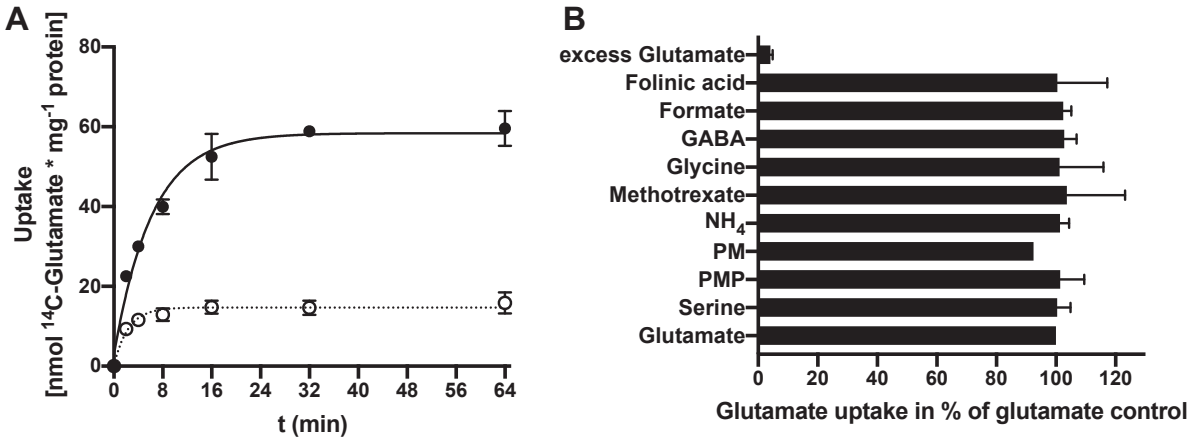

Figure 1: Biochemical characterization of BOU. Representative glutamate uptake using recombinant BOU protein (**A**). BOU protein was heterologously expressed in *E. coli*, purified from inclusion bodies, and reconstituted into liposomes via the detergent removal method with (filled symbols, solid line) or without (open symbols, dotted line) preloading of 20 mM glutamate. Transport was initiated by adding 0.2 mM glutamate/^{14}C-labeled glutamate to proteoliposomes. Samples were taken after 2, 4, 8, 16, 32 and 64 min and the radioactivity in the liposomes was measured by liquid scintillation counting. Values represent mean ± SD of technical triplicates. Effect of different metabolites on the glutamate transport activity of BOU (**B**). Proteoliposomes were preloaded with 20 mM glutamate. Transport experiments were performed as described above. Potential substrates or inhibitors were added at a final concentration of 2 mM together with the radioactive labeled glutamate. Transport rates were calculated from initial velocities. Glutamate transport rate was set to 100%. Values are given as mean ± SD of at least three independent experiments (excess glutamate, folinic acid, formate, GABA, glycine, PMP, serine, glutamate), two independent experiments (NH_4, Methotrexate), or one experiment (PM). Abbreviations: GABA, γ-aminobutyric acid; PM, pyridoxamine; PMP, pyridoxamine 5'-phosphate.

We used the confirmed glutamate transport activity of BOU to test its *in vitro* activity for additional substrates that are involved in mitochondrial photorespiratory, C_1, or nitrogen metabolism. Therefore, we preloaded liposomes with glutamate and added the respective

substrates externally in excess. If BOU shows affinity for an additional substrate besides glutamate, the substrate will compete with the radioactive labelled glutamate; thus leading to a reduction in the glutamate uptake activity of BOU. As control we performed experiments without any additions and with externally added glutamate in excess. We used this experimental setup to test possible affinities of BOU for the photorespiratory core metabolites glycine and serine, the B_6 vitamers pyridoxamine (PM) and pyridoxamine 5'-phosphate (PMP), the mitochondrial metabolites γ-aminobutyric acid (GABA), formate and NH_4, folinic acid, an inhibitor of SHMT activity, and methotrexate, a Vitamin B_9 (folate) analogue that inhibits dihydrofolate reductase (Werkheiser, 1961). Uptake activity of BOU was not affected by any of the tested metabolites (Fig. 1B). Only excess glutamate showed a reduction in the glutamate transport activity of BOU. Thus, we conclude that BOU has a clearly defined substrate spectrum, which is in line with previous studies (Porcelli et al., 2018).

Mitochondrial membranes show uptake activity for phosphate and malate

As demonstrated above activity of BOU seems to be restricted to glutamate. To assess the physiological role of BOU *in vivo*, we isolated mitochondria from 2-weeks old Arabidopsis wildtype (WT) and *bou-2* seedlings grown under elevated CO_2 conditions (HC) via differential centrifugation and Percoll density gradient purification. Mitochondria of both genotypes were successfully enriched and showed only minor contamination with chloroplasts as shown by immunoblot analyses with antibodies directed against the mitochondrial marker protein alternative oxidase (AOX) and the plastidic marker protein Rubisco (large subunit, RbcL; Supplemental Fig. S2). Enriched organelles were lysed with detergent and the membranes reconstituted into liposomes via the detergent removal method. Activity of reconstituted mitochondrial membranes was assessed by measuring phosphate and malate uptake. Isolated mitochondrial membranes of WT and *bou-2* seedlings showed uptake activity for phosphate and malate when liposomes were preloaded with phosphate or malate, respectively (Fig. 2A, B), indicating that the mitochondrial membrane proteins remained active during isolation of the organelles and subsequent detergent treatment. Only little uptake was observed without preloading indicating either uni- or symport activity of the reconstituted membranes or partially leakiness of the liposomes (Fig. 2A, B). Next, we assessed whether our system was suitable for measuring glutamate uptake of isolated mitochondrial membranes. Therefore, we prepared liposomes with reconstituted mitochondrial membranes of WT and *bou-2* with or without preloading of 20 mM glutamate and measured uptake activity of ^{14}C-glutamate/0.2 mM glutamate. At the given glutamate concentration, there was no difference in uptake activity between liposomes with and without preloading for reconstituted membranes from WT seedlings (Fig. 2C). Glutamate uptake activity of mitochondrial membranes isolated from *bou-2* seedlings was reduced compared to

WT indicating a reduced glutamate transport capacity of *bou-2* mitochondrial membranes (Fig. 2C).

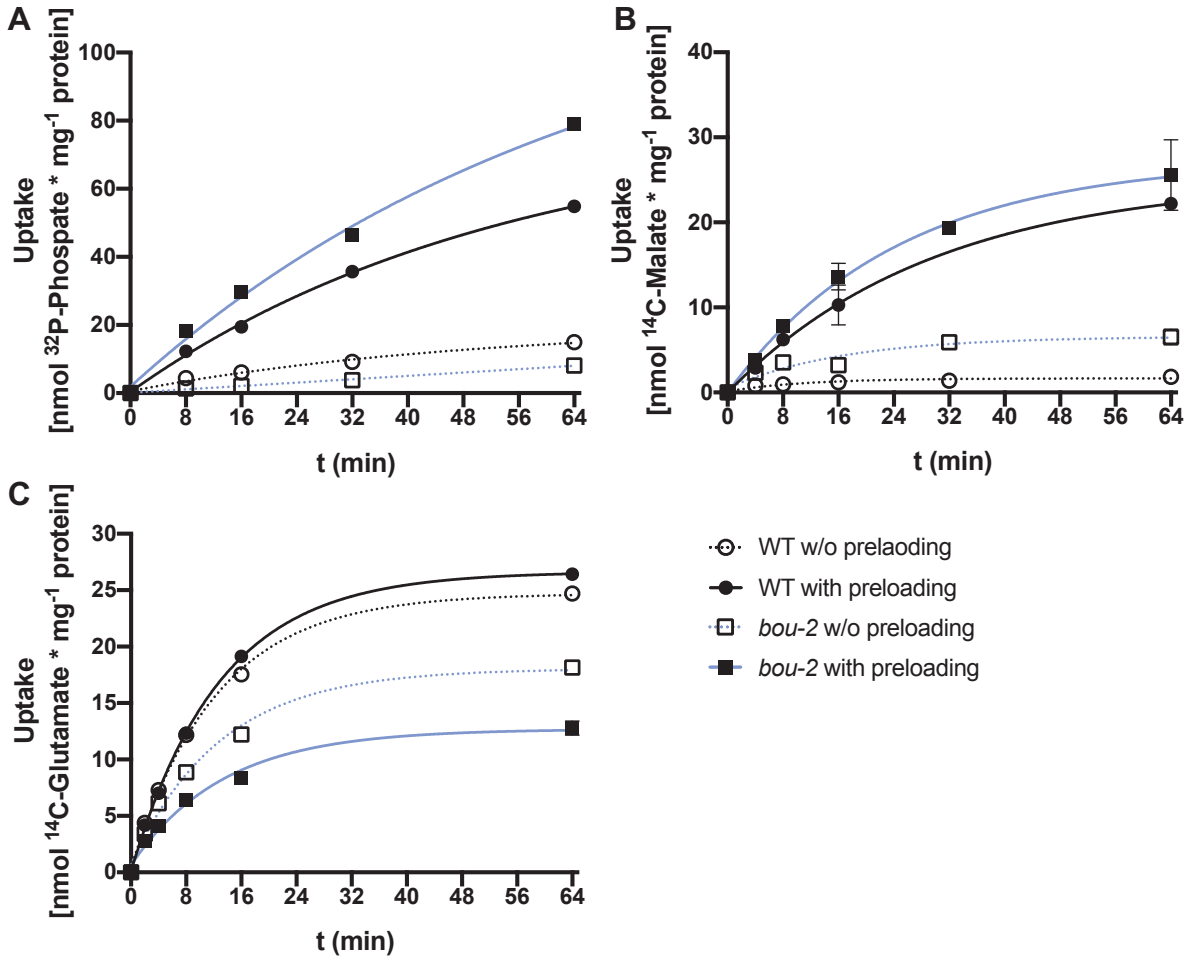

Figure 2: Uptake analyses of isolated mitochondrial membranes from Arabidopsis wildtype (WT) and *bou-2* seedlings. Mitochondria were purified from 2-weeks old Arabidopsis WT (circles) and *bou-2* (squares) seedlings grown at elevated CO_2 conditions (0.3% [v/v] CO_2) via differential centrifugation and density gradient purification as described in Materials and Methods. Mitochondrial membranes were solubilized from enriched mitochondria fractions and reconstituted into liposomes with (filled symbols, solid lines) or without (open symbols, dotted lines) preloading of substrate. Uptake of ^{32}P-phosphate (**A**), ^{14}C-malate (**B**) and ^{14}C-glutamate (**C**) was measured as described in Materials and Methods. Values represent mean ± SD of two biological replicates.

Glutamylation state of folates is not affected in *bou-2*

Previously, it was shown that BOU is involved in photorespiration as isolated mitochondria from *bou-2* rosettes showed strongly reduced GDC activity compared to WT. In the same study it was suggested that BOU transports a metabolite required for proper GDC activity, e.g., a cofactor or its precursor (Eisenhut et al., 2013b). Glutamate is essential for polyglutamylation of THF a cofactor of GDC and SHMT. Folate-dependent enzymes and transporters have generally higher affinity for polyglutamylated folates than their monoglutamylated forms (Suh et al., 2001; Hanson and Gregory, 2011). Therefore, we

analyzed total folate content as well as the ratio of poly- to monoglutamylated forms in 10-day old WT and *bou-2* seedlings grown at HC and five days after shift to ambient CO_2 (AC).

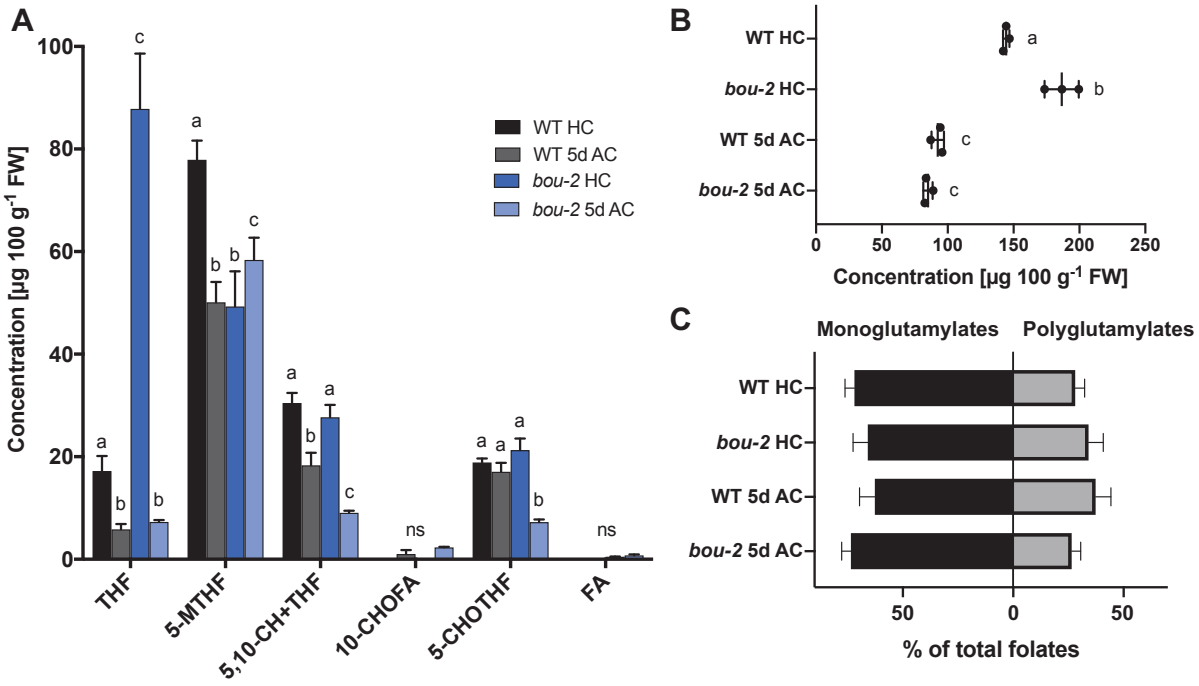

Figure 3: Quantification of folate levels in Arabidopsis WT and *bou-2* seedlings. Samples were harvested after 10-days growth in elevated CO_2 conditions (HC; 0.3% [v/v] CO_2) and five days after shift to ambient CO_2 (5d AC; 0.038% [v/v] CO_2), and folates quantified as described in Materials and Methods. Quantification of various folate types (mono- and polyglutamylated forms, **A**). Values are given as mean ± SD of three biological replicates. Letters indicate statistically significant differences between means ($P < 0.05$; two-way ANOVA; corrected by Tukey's multiple comparisons test). Total folate content (**B**). Values are given as mean ± SD of three biological replicates. Letters indicate statistically significant differences between means ($P < 0.05$; one-way ANOVA; corrected by Tukey's multiple comparisons test). Glutamylation state as percent of total folates (**C**). Values are given as mean ± SD of three biological replicates. Abbreviations: 5,10-CH+THF, 5,10-methenyltetrahydrofolate; 10-CHOFA, 10-formyl folic acid; 5-CHOTHF; 5-formyltetrahydrofolate; FA, folic acid; 5-MTHF, 5-methyltetrahydrofolate; THF, tetrahydrofolate; WT, wildtype.

We found that THF content was significantly enriched in the mutant grown at HC but reverted back to WT level after shift to AC (Fig. 3A). The most abundant folate in WT seedlings was 5-methyltetrahydrofolate (5-MTHF). 5-MTHF is the most reduced folate. It is generated from 5,10-methylene-THF by the NADH-dependent 5,10-methylene reductase, likely in the cytosol. 5-MTHF is used to catalyze the conversion of homocysteine to methionine, which can be further converted into S-adenosylmethionine or incorporated into proteins (Roje et al., 1999; Hanson and Roje, 2001). 5-MTHF levels were significantly reduced in the mutant under HC but significantly increased under AC (Fig. 3A). Decarboxylation of glycine and transfer of the residual C_1 unit to THF leads to the production of 5,10-methylene-THF. Under photorespiratory conditions the C_1 unit is transferred from there onto a second molecule of

glycine, yielding serine. Under non-photorespiratory conditions SHMT catalyzes the reverse reaction in which 5,10-methylene-THF and glycine are produced from serine (Douce et al., 2001; Hanson and Roje, 2001). 5,10-methylene-THF can be converted into 5,10-methenyl-THF (5,10-CH+THF) in the C_1 cycle in the mitochondria (Hanson and Roje, 2001; Collakova et al., 2008). Plants can interconvert 5,10-CH+THF and 5-formyl-THF (5-CHOTHF). 5-CHOTHF is produced by a second catalytic activity of SHMT and inhibits SHMT activity. Reconversion into 5,10-CH+THF occurs via 5-CHOTHF cycloligase (Goyer et al., 2005; Collakova et al., 2008). Levels of 5,10-CH+THF and 5-CHOTHF were not altered under HC but significantly reduced in AC (Fig. 3A), suggesting a functional C_1 cycle under non-photorespiratory conditions. 10-formyl folic acid (10-CHOFA) and folic acid (FA) are degradation products of 10-formyl-THF and dihydrofolate, respectively. They do not play any important role in C_1 metabolism, thus we could only detect traces of them (Fig. 3A). Total folate content was significantly increased in the mutant grown at HC, due to the significant increase in THF levels. It reverted back to WT level after shift to AC (Fig. 3B). Glutamylation state of the measured folate pool was not altered in the mutant under any of the applied conditions (Fig. 3C; Supplemental Fig. S3A-D).

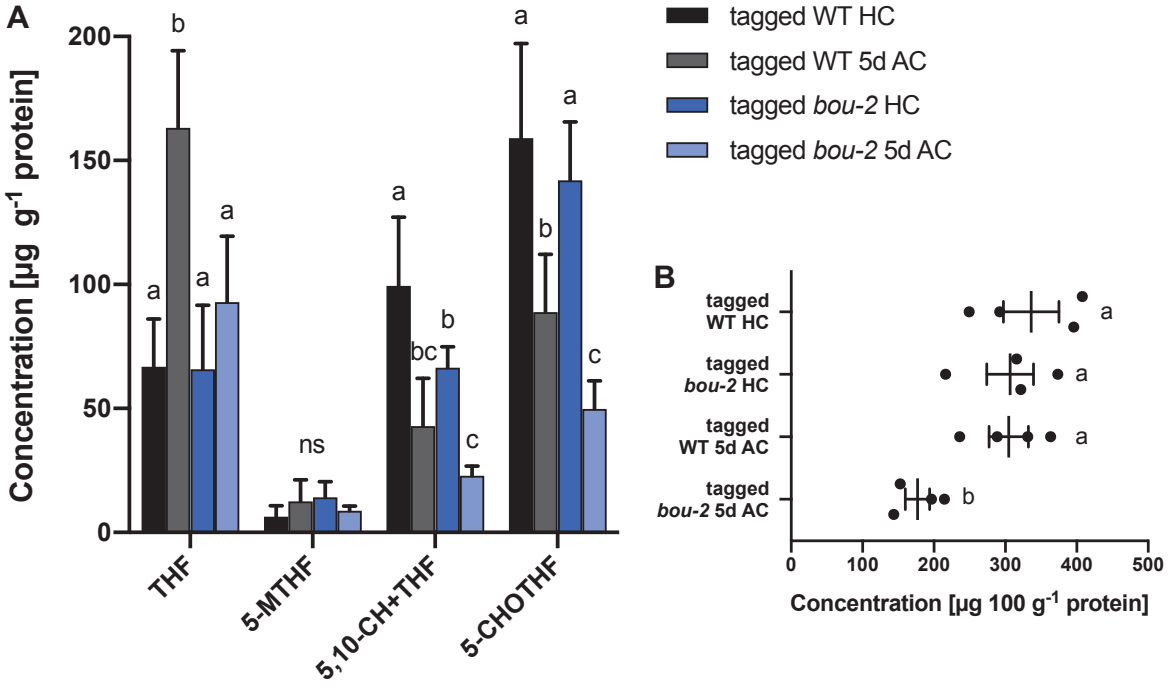

Figure 4: Quantification of folate levels in isolated mitochondria of tagged WT and tagged *bou-2*. Mitochondria were isolated from 10-day old tagged WT and tagged *bou-2* seedlings grown in elevated CO_2 conditions (HC; 0.3% [v/v] CO_2) and five days after shift to ambient CO_2 (5d AC; 0.038% [v/v] CO_2) via co-IP, and folates quantified as described in Materials and Methods. Quantification of various folate types (polyglutamylated forms, **A**). Total folate content (**B**). Values are given as mean ± SD of four biological replicates (**A**, **B**). Letters indicate statistically significant differences between means ($P < 0.05$; one-way ANOVA; corrected by Tukey's multiple comparisons test). Abbreviations: 5,10-CH+THF, 5,10-methenyltetrahydrofolate; 5-CHOTHF; 5-formyl-tetrahydrofolate; 5-MTHF, 5-methyltetrahydrofolate; THF, tetrahydrofolate; WT, wildtype.

The folate pool in total seedlings showed significant changes for specific folates in the *bou-2* mutant (Fig. 3A). However, the glutamylation state of the folate pool was not affected in *bou-2* (Fig. 3C). Folate, especially THF, is an essential cofactor for all organisms, which supplies C_1 units to synthesize proteins, nucleic acid, methylated molecules, and vitamins (Hanson and Roje, 2001). Thus, folates are distributed all over the cell. The mitochondrial folate pool accounts only for a fraction of the folates measured in total seedling tissue. Therefore, we analyzed the folate pool in isolated mitochondria by using our previously adapted rapid mitochondria isolation technique (Kuhnert et al., 2020). Mitochondria were isolated from 10-day old tagged WT and tagged *bou-2* seedlings grown at HC and five days after shift to AC via co-Immunopurification, and subsequently subjected to a total folate analysis (Fig. 4A, B). Interestingly, we only detected polyglutamylated folates but not any monoglutamylates in isolated mitochondria. Levels of THF and 5-CHOTHF were not altered in the mutant grown at HC, but were significantly reduced after shift to AC (Fig. 4A). 5,10-CH+THF was significantly reduced in *bou-2* mitochondria isolated from seedlings grown at HC. It changed back to WT level after shift to AC. We detected low amounts of 5-MTHF in our isolated mitochondria (Fig. 4A). 5-MTHF is likely only produced in the cytosol and might be a result of a contamination of our rapidly isolated mitochondria. Total folate levels were not changed in mitochondria of tagged WT and tagged *bou-2* grown at HC, but were significantly reduced in tagged *bou-2* mitochondria after shift to AC (Fig. 4B). Taken together our results indicate that folate metabolism is disturbed in the mutant under photorespiratory conditions. However, *bou-2* mitochondria do contain a sufficient pool of glutamylated folates to drive GDC and SHMT reaction.

Quantification of vitamin B_6 levels in *bou-2* and *shm1*

Analyses of folate contents in WT and *bou-2* revealed that the photorespiratory phenotype is not caused by a reduction in glutamylated folates, since *bou-2* mitochondria do contain sufficient amounts of glutamylated THF (Fig. 4). Previously, it was suggested that GDC activity is reduced in the mutant due to a lack in stability of the multienzyme system or one of its components. It could be shown that especially GLDP was degraded to a higher extent in the mutant compared to WT (Eisenhut et al., 2013b). GLDP is a pyridoxal 5'-phosphate (PLP) dependent enzyme and the component of the system that catalyzes the actual decarboxylation of glycine. PLP is the active form of vitamin B_6 an essential nutrient that acts as cofactor for many enzymes including aminotransferases and decarboxylases. The term vitamin B_6 refers to a group of the structural relatively similar compounds pyridoxal (PL), pyridoxine (PN), pyridoxine 5'-phosphate (PNP), PLP, PM and PMP. As the stability of GLDP was affected in the *bou-2* mutant and it is PLP-dependent we analyzed the vitamin B_6 content in 8-day old WT and *bou-2* seedlings grown at HC, and two (2d AC) and five days (5d AC) after shift to AC.

bou-2 seedlings grown at HC showed a significant reduction in PMP levels compared to WT, whereas levels of PM, PN, PNP, PL and PLP were not affected in the mutant. The PL and PLP content were significantly reduced when seedlings were shifted from HC to AC. However, this pattern was observed in both WT and *bou-2* seedlings (Fig. 5A). The overall vitamin B_6 content was significantly increased in the mutant at HC. It returned to WT levels after shift to AC (Supplemental Fig. S4A). Additionally, we performed the analysis with 5-weeks old rosette leaves since GDC activity was measured in older plants with the same result (Supplemental Fig. S4B). Furthermore, we performed the analysis with the *shm1* mutant deficient in the mitochondrial *SHMT* as it showed a similar metabolic phenotype compared to *bou-2* (Voll et al., 2006; Eisenhut et al., 2013b). The PM, PN, PL and PNP contents were not affected in the *shm1* mutant at HC. Levels of PMP were significantly reduced in the mutant compared to WT at HC, whereas the levels of PLP were significantly reduced under all conditions (Fig. 5B). Interestingly, *bou-2* and *shm1* seedlings showed a similar vitamin B_6 pattern, except for the changes in PLP (Fig. 5).

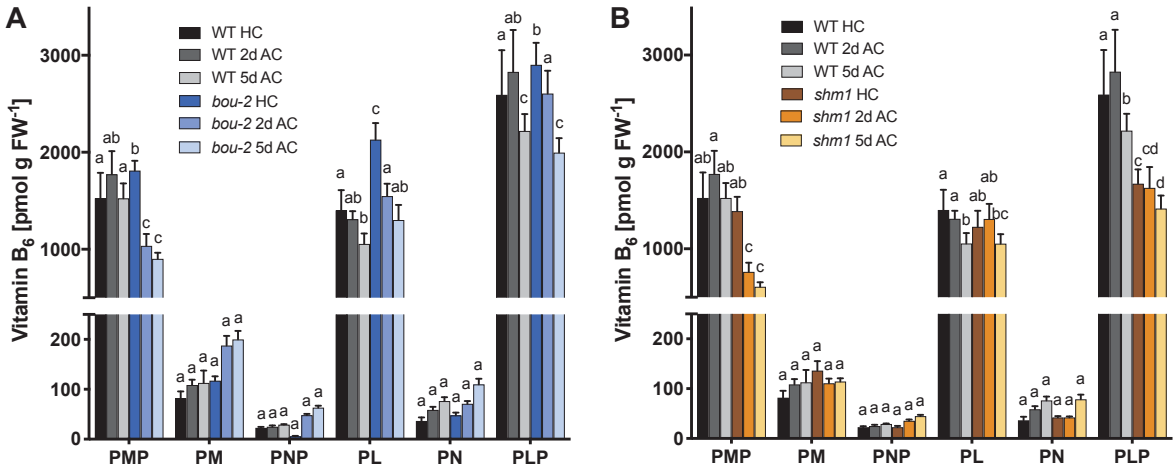

Figure 5: Quantification of vitamin B_6 levels in seedlings. Arabidopsis wildtype (WT), *bou-2* (**A**) and *shm1* (**B**) seedlings were harvested after 8-days growth in elevated CO_2 conditions (HC; 0.3% [v/v] CO_2), and two (2d AC) and five days (5d AC) after shift to ambient CO_2 (0.038% [v/v] CO_2), and vitamin B_6 levels were quantified as described in Materials and Methods. Values are given as mean ± SD of six biological replicates. Letters indicate statistically significant differences between means ($P < 0.05$; one-way ANOVA; corrected by Tukey's multiple comparisons test).

During the analysis of the vitamin B_6 content we found five additional peaks in the chromatogram of WT and *bou-2* samples. They did not correspond to any of the vitamin B_6 peaks in the standard. Thus, they were named Peak 1–5 after their appearance in the chromatogram (Supplemental Fig. S4C). The corresponding metabolites of Peak 1, 2 and 5 were not affected in *bou-2* seedlings (Supplemental Fig. S4D). The corresponding metabolites of Peak 3 and 4 were significantly increased in *bou-2* seedlings grown at HC. Additionally, the corresponding metabolite of Peak 4 was significantly accumulating in *bou-2* seedlings after

shift to AC (Supplemental Fig. S4D). So far we were not able to identify the corresponding metabolites.

To gain insight into the mitochondrial vitamin B_6 metabolism we applied our rapid isolation strategy on 10-day old tagged WT seedlings (Kuhnert et al., 2020). A preliminary experiment showed that we were able to detect B_6 vitamers in rapidly isolated mitochondria (Supplemental Fig. S4E). The chromatogram showed two clear peaks that correspond to the B_6 vitamers PMP and PLP. An additional peak at a retention time of approximately 8 min might correspond to the before mentioned Peak 4 (Supplemental Fig. S4E). Previously, it was demonstrated that mitochondria contain a PMP/PNP oxidase (PDX3) catalyzing the oxidation of PMP or PNP to PLP (Colinas et al., 2014; Niehaus et al., 2014; Colinas et al., 2016). Since we only detected PMP and PLP in isolated mitochondria, mitochondrial vitamin B_6 metabolism might be dependent on import of PMP from the cytosol.

Activities of mitochondrial enzymes indicate that mitochondrial metabolism is strongly impaired in *bou-2*

Previous results demonstrated that *bou-2* rosette leaves showed reduced GDC activity in isolated mitochondria and accumulated intermediates of the tricarboxylic acid (TCA) cycle (Eisenhut et al., 2013b). Our results revealed that BOU transport function is not directly linked to GDC activity (Figs. 3–5). However, a loss of *BOU* results in a dysfunctional photorespiratory pathway likely caused by a reduction in GDC activity. As BOU is a mitochondrial membrane protein of the inner mitochondrial membrane we analyzed the impact of a loss of *BOU* on mitochondrial signature enzyme activities. To this end, we isolated mitochondria from WT and *bou-2* rosette leaves grown at HC and five days after shift to AC by differential centrifugation and Percoll density gradient purification, and analyzed activities of mitochondrial aspartate aminotransferase (AspAT), γ-aminobutyric acid transaminase (GABA-T) and malate dehydrogenase (MDH). In addition, we performed isolations on WT and *bou-2* root tissue. Mitochondrial AspAT activity was significantly reduced to about 80% of WT activity in *bou-2* in 6-weeks old rosette leaves grown at HC and 4-weeks old rosette leaves grown at HC after shift to AC for five days. Mitochondria isolated from 2-weeks old *bou-2* root tissue showed a strong reduction in AspAT activity with only 20% of WT activity remaining (Fig. 6A). GABA-T activity was not changed in mitochondria isolated from 6-weeks old rosette leaves grown at HC. However, it was significantly reduced when mitochondria were isolated from 4-weeks old rosette leaves grown at HC after shift to AC for five days. GABA-T activity could not be detected in mitochondria isolated from root tissue (Fig. 6B). We additionally confirmed the reduction in AspAT activity by running native gels with samples of whole leaf extracts and isolated mitochondria. Native gels were used to perform AspAT activity staining. We detected two bands in the AspAT activity staining of

whole leaf samples, referring to the plastidial (lower band) and the mitochondrial isoform (upper band), respectively. The intensities of the bands did not differ between WT and *bou-2* samples. Isolated mitochondria showed only one band after the activity staining, referring to the mitochondrial isoform of AspAT. Its intensity was reduced in isolated mitochondria from *bou-2* compared to WT indicating a reduction in AspAT activity in the mutant (Fig. 6C). Both enzymes, AspAT and GABA-T, are dependent on PLP. Reduction in AspAT and GABA-T activity is possibly related to a disturbed vitamin B_6 content in *bou-2* (Fig. 5A, B; Supplemental Fig. S4).

Furthermore, we analyzed the activity of mitochondrial MDH. MDH activity was reduced to about 80% of WT activity in *bou-2* mitochondria isolated from 4-weeks old rosette leaves grown at HC after shift to AC for five days. Mitochondria isolated from *bou-2* root tissue showed a reduction in MDH activity to about 20% of WT activity (Fig. 6D). Reduction in MDH activity might be caused by reduced GDC activity in *bou-2* as photorespiration, TCA cycle and respiration in mitochondria are closely connected (Gardeström and Wigge, 1988; Obata et al., 2016). Thus, it might be a pleiotropic effect caused by a dysfunctional photorespiratory pathway and not a direct effect of a loss of *BOU*. Interestingly, AspAT activity and MDH activity reduction show the same pattern. AspAT activity is even reduced at HC (Fig. 6). Taken together, these results indicate that mitochondrial metabolism is strongly impaired in older leaf tissue, which leads to pleiotropic effects caused by a dysfunctional photorespiratory pathway.

Traditional mitochondria isolations that yield sufficient amounts of pure mitochondria generally require a few hours and substantial amounts of leaf material (Millar et al., 2001; Werhahn et al., 2001; Keech et al., 2005). To exclude that the differences in enzyme activities we observed are due to changes during the long time period needed for mitochondria isolation, we applied our rapid mitochondria isolation technique. Therefore, we rapidly isolated mitochondria from 5-weeks old Arabidopsis tagged WT and tagged *bou-2* leaves grown at HC after shift to AC. We found that both AspAT and MDH activities are reduced in the mutant to a greater extent than when mitochondria were isolated with the traditional approach (Supplemental Fig. S5A, B). However, both enzymatic activities showed the same amount of reduction, which is in line with our previous results. GABA-T activity was reduced to about 50% of WT activity in the mutant, which coincided with our previous results (Supplemental Fig. S5C). Further analyses will be necessary to determine the exact effect of BOU on mitochondrial metabolism. Because the mitochondrial metabolism in *bou-2* is highly impaired in older leaf tissue further analyses should be performed on young seedling tissue.

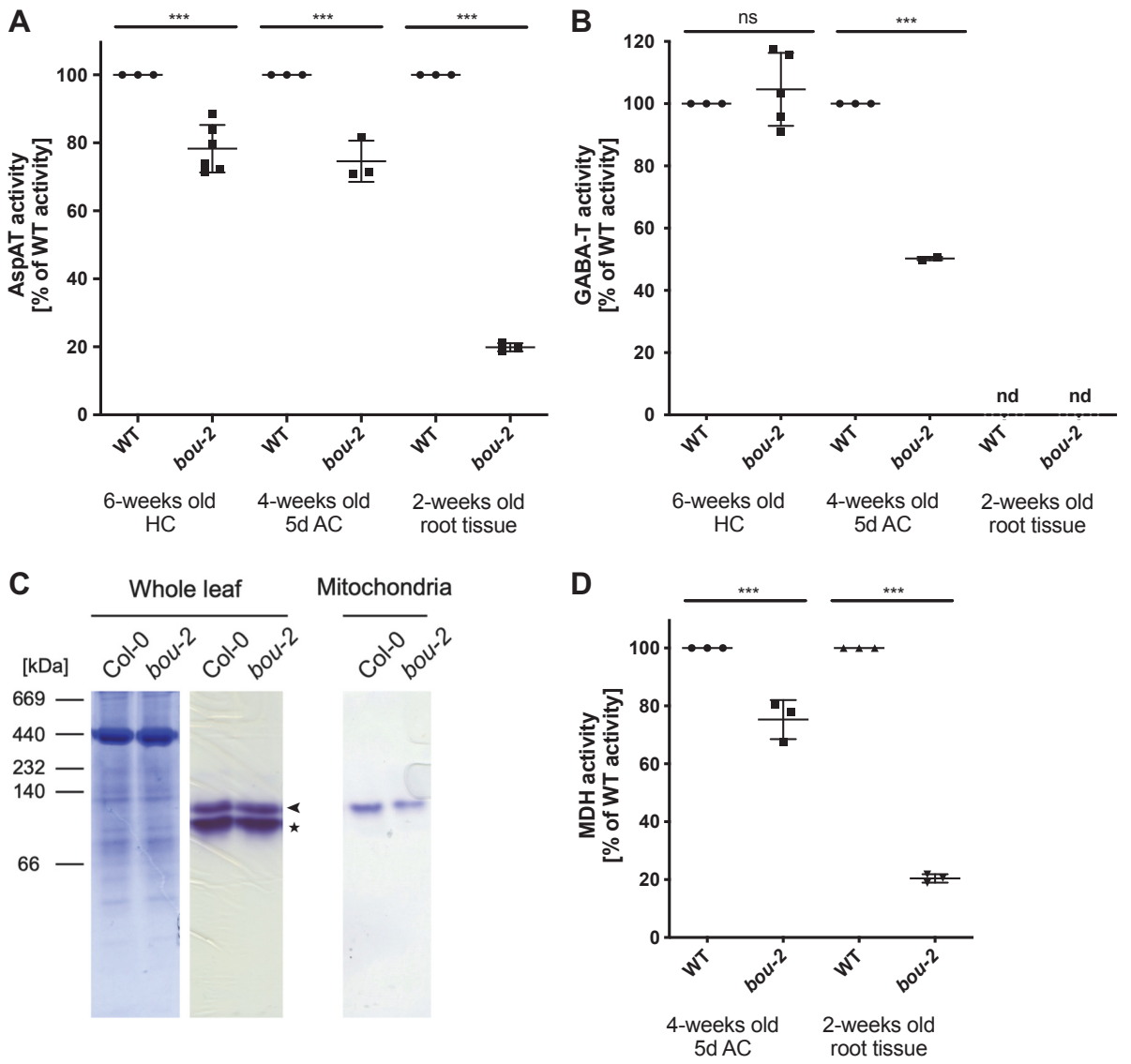

Figure 6: Effect of *BOU* deletion on mitochondrial metabolism. Mitochondria were isolated from 6-weeks old wildtype (WT) and *bou-2* plants grown at elevated CO_2 conditions (HC; 0.3% [v/v] CO_2), 4-weeks old WT and *bou-2* plants grown at elevated CO_2 conditions after shift to ambient CO_2 for five days (5d AC; 0.038% [v/v] CO_2), and 2-weeks old WT and *bou-2* root tissue as via differential centrifugation and Percoll density gradient purification as described in Materials and Methods. (**A**) Aspartate aminotransferase (AspAT) activity. Average WT activity: 0.89 ± 0.05 U mg^{-1} protein (HC), 1.1 ± 0.1 U mg^{-1} protein (5d AC), 0.58 ± 0.05 U mg^{-1} protein (root). (**B**) γ-Aminobutyric acid transaminase (GABA-T) activity. Average WT activity: 25.1 ± 2.5 mU mg^{-1} protein (HC), 33 ± 3 mU mg^{-1} protein (5d AC). (**D**) Malate dehydrogenase (MDH) activity. Average WT activity: 16.2 ± 3.1 U mg^{-1} protein (5d AC), 8.71 ± 0.46 U mg^{-1} protein (root). Values are given as mean ± SD of at least three biological replicates. Asterisks indicate statistically significant differences between means (***, $P < 0.001$; Student's *t*-test). Representative picture of AspAT activity staining of whole leaf extract and isolated mitochondria (**C**). Whole leaf extracts and isolated mitochondria from 6-weeks old leaf tissue were prepared as described in Materials and Methods. Protein samples were separated on native gradient gels and AspAT activity staining was performed as described in Materials and Methods. Plastidic isoform of AspAT is indicated by a star symbol, mitochondrial isoform by an arrow next to the bands. Abbreviations: nd, not detected; ns, not significant.

DISCUSSION

The Arabidopsis *bou-2* mutant was isolated in the early 2000s. It was first characterized as carnitine-acylcarnitine carrier due to its homology to yeast and mammalian carnitine-acylcarnitine transporters (Lawand et al., 2002). Later, it was reported that BOU is a transporter involved in photorespiration as the mutant showed a photorespiratory phenotype and strongly impaired GDC activity in isolated mitochondria (Eisenhut et al., 2013b). Recently, it was demonstrated that recombinant BOU transports glutamate *in vitro* (Porcelli et al., 2018). This finding was rather unexpected, since glutamate is neither a substrate nor a product of the reaction catalyzed by GDC and SHMT. Thus, the link of BOU transport activity to its functional significance in photorespiration remains enigmatic to date. Here, we report a biochemical and metabolite analysis of the *bou-2* mutant to gain detailed insight into a possible role of BOU in mitochondrial photorespiratory metabolism. The use of an artificial liposome system with reconstituted recombinant protein or isolated mitochondrial membranes permitted a careful substrate analysis of BOU and its role *in vivo*, whereas studies on the vitamin B_6 and folate content in total seedlings as well as isolated mitochondria enabled a detailed insight into the link between photorespiration and its cofactor metabolism and pointed out a possible regulatory function of 5-formyl-THF.

BOU transport function in *Arabidopsis thaliana*

Even though it is often considered a wasteful process, photorespiration is the second most abundant process in oxygenic photosynthesis-performing organisms (Sharkey, 1988). While the soluble enzymes of the photorespiratory pathway have been thoroughly characterized in the last decades only little is known about the transport proteins catalyzing the shuttle of metabolites between plastids, peroxisomes, mitochondria, and the cytosol (Eisenhut et al., 2019). The only identified and characterized core metabolite transporters to date are PLGG1 and BASS6 (Pick et al., 2013; South et al., 2017). Previously, it was hypothesized that the mitochondrial membrane protein BOU catalyzes the transport of glycine or serine or a metabolite needed for efficient GDC activity (Eisenhut et al., 2013b). However, recently it was demonstrated that BOU transports glutamate (Porcelli et al., 2018). We verified the glutamate uptake activity of BOU in our *in vitro* system (Fig. 1A). Thus, we exploited the system to test the activity of BOU for metabolites that are either directly or indirectly involved in photorespiration and have not been tested in previous studies (Porcelli et al., 2018). As a matter of fact, we did not test those substrates directly but added them besides glutamate externally in excess. If those metabolites are either substrates of BOU or inhibitors of the glutamate transport function of BOU, we should observe a reduction in the glutamate transport activity. However, the glutamate transport activity of BOU remained unchanged indicating that BOU has a clearly defined substrate spectrum (Fig. 1B). Neither our study nor

previous ones have tested 2-OG as substrate. During the decarboxylation of glycine in the mitochondria NH_3 is released. It is widely accepted that NH_3 diffuses towards the plastids where it is re-assimilated by the GS/FdGOGAT system (Miflin and Lea, 1980; Somerville and Ogren, 1980; Eisenhut et al., 2019). However, previously it was suggested that NH_3 released by GDC is shuttled in form of amino acids (Linka and Weber, 2005). NH_3 could be incorporated into 2-OG in the mitochondria by glutamate dehydrogenase (GluDH), yielding glutamate. The latter is exported to the cytosol in counter-exchange with 2-OG providing a new acceptor molecule for the GluDH reaction. Exported glutamate could be shuttled towards the plastids for NH_3 re-assimilation by the GS/FdGOGAT system or the peroxisomes as substrate for the GGAT reaction. Consistent with this hypothesis, the so far characterized mitochondrial dicarboxylate carriers (DIC) show only poor activity for 2-OG (Palmieri et al., 2008). However, the mitochondrial di- and tricarboxylate carrier (DTC), which is encoded by a single gene in Arabidopsis is able to transport 2-OG efficiently and is highly expressed in leaf tissue (Picault et al., 2002; Winter et al., 2007). Additionally, we cannot exclude that BOU shows activity for other folate species especially mono- and polyglutamylated B_9 vitamers as those could not be tested so far because they are commercially not available.

To further investigate the function of BOU *in vivo* we analyzed the uptake activity of isolated mitochondrial membranes from WT and *bou-2* seedlings. We were able to set up a system capable of measuring phosphate and malate uptake (Fig. 2A, B). However, measuring glutamate uptake has proven to be difficult (Fig. 2C) which is not obvious because BOU is a very abundant mitochondrial membrane protein (Fuchs et al., 2020). We found no difference in glutamate uptake activity of mitochondrial membranes isolated from WT (Fig. 1C). One possible explanation for our results could be the low K_m value of BOU (25.3 ± 3.2 µM; Porcelli et al., 2018). We preloaded our liposomes with 20 mM glutamate and measured the uptake of externally added 0.2 mM glutamate which is approximately ten times higher than the K_m of BOU. At the given concentration BOU is at its maximum velocity. Because BOU can catalyze glutamate uniport as well, we might see no difference between with and without preloading in our liposome system. Therefore, we should test different glutamate concentrations and use the isolated membranes to measure uniport activity by performing efflux studies. We expected the mutant to show a strongly reduced capability of transporting glutamate. However, BOU is not the only mitochondrial transporter capable of transporting glutamate. Recently, the mitochondrial membrane proteins UCP1 and UCP2 have been characterized. They show high activity for aspartate and glutamate in an antiport manner but can also catalyze glutamate and aspartate uniport (Monné et al., 2018). Their K_m values for glutamate are considerably higher than the K_m value of BOU (1.9 ± 0.2 mM, UCP1; 2.5 ± 0.2 mM, UCP2; Monné et al., 2018). However, their maximum velocities are approximately 40 to 70 times higher indicating that even at concentrations lower than their K_m value they might

contribute to the measured glutamate uptake activity in our *in vitro* system. *In vivo*, it was reported that they catalyze glutamate/aspartate antiport, whereas BOU likely catalyzes glutamate uniport. Moreover the K_m value of BOU for glutamate is approximately 100 times lower than that of UCP1 and UCP2 (Monné et al., 2018; Porcelli et al., 2018), indicating a crucial function of BOU at low glutamate concentrations that can not be complemented by UCP1 and UCP2.

Posttranslational modifications of proteins are essential factors regulating enzyme activities and affinities between enzymes and their substrates. Previously, it was shown that BOU can be acetylated at lysine 247 in the amino acid sequence of BOU (König et al., 2014). Acetylation of lysine residues can mask the positive charge of the ε-amino group and thereby change the affinity of the protein to its substrate. Thus, the acetylation site of BOU might be a potential regulation of its transport activity. However, this has to be tested in further studies.

Mitochondrial metabolism is strongly impaired in *bou-2*

In a previous study, it was reported that *bou-2* rosette leaves accumulate intermediates of the TCA cycle and branched chain amino acids under photorespiratory conditions, and show reduced GDC activity in isolated mitochondria. From the elevated levels of isocitrate, 2-OG, succinate, fumarate and malate it was suggested that *bou-2* showed increased respiration under photorespiratory conditions (Eisenhut et al., 2013b). However, our enzyme assay data indicated that the increased levels of TCA cycle intermediates in the mutant might be caused by a reduction in enzyme activities of the TCA cycle as we see a significant reduction in MDH activity in mitochondria from rosette leaves (Fig. 6D). Additionally, we found that AspAT and GABA-T activity are reduced in *bou-2* after shift to AC (Fig. 6A, B). Together, these data suggest that the mitochondrial metabolism is strongly impaired in older leaf tissue likely due to accumulating photorespiratory intermediates. Therefore, older leaf tissue might not be the ideal developmental stage to study the metabolic effects in *bou-2* as many of the effects that have been observed are likely secondary effects caused by a dysfunctional photorespiratory pathway.

MDH, AspAT, and GABA-T activity were not altered in isolated mitochondria from *bou-2* seedlings grown at HC. MDH activity was also not affected after shift to AC indicating that mitochondrial metabolism is not generally impaired in young seedling tissue (Kuhnert et al., 2020). Thus, seedlings are more suitable to study the metabolic effect of a loss of *BOU in vivo*. Previously, it was shown that glycine acts as an inhibitor of GABA-T activity (Shelp et al., 2012). Accumulating amounts of GABA in *bou-2* were taken as an indicator of reduced GABA-T activity caused by glycine accumulation in mitochondria (Eisenhut et al., 2013b). In line with previous metabolite analyses GABA-T activity is significantly reduced in *bou*-2 mitochondria from older leaf tissue after shift to AC (Fig. 6B). Interestingly, *bou-2*

mitochondria from 10-day old seedlings do not show reduced GABA-T activity after shift to AC indicating that there is either no or not sufficient accumulation of glycine under these conditions. Additionally, we were not able to detect a significant decrease in the protein abundance of any of the proteins of the GDC or the SHMT in mitochondria isolated from seedlings indicating that GDC stability might not be impaired at HC in the early seedling stage in *bou-2* (Kuhnert et al., 2020). Further studies will determine whether the GDC activity is already impaired in young seedling tissue of *bou-2*.

Analyses on rapidly isolated mitochondria give insight into cofactor metabolism

Analysis of the folate content in whole seedlings revealed only minor differences between WT and *bou-2* (Fig. 3). Glutamylation state of the folate pool was not affected in *bou-2* suggesting that the mutant has a sufficient amount of active folates to drive GDC and SHMT reaction in the mitochondria (Figs. 3C, 4A). Interestingly, the total folate content was significantly increased in *bou-2* grown at HC (Fig. 3B). Especially the THF content was approximately five times higher in the mutant compared to WT (Fig. 3A). We can exclude that THF accumulates in mitochondria in *bou-2* grown at HC (Fig. 4A). Further analyses will determine in which compartment THF accumulates in *bou-2* and how this affects C_1 metabolism. Interestingly, we detected only polyglutamylated folates in isolated mitochondria (Fig. 4A). This observation was not entirely unexpected as mitochondria contain the enzyme that catalyzes the polyglutamylation of folates but not those that catalyze the reverse reaction (Hanson and Gregory, 2011). In addition, it was reported that folate-dependent enzymes have higher affinity towards polyglutamylates compared to their monoglutamylated forms (Suh et al., 2001; Hanson and Gregory, 2011). In a previous study, monoglutamylated folates could be detected in isolated mitochondria (Mehrshahi et al., 2010). However, they isolated organelles traditionally via density gradient purification. As this isolation method requires a few hours it might affect the state and composition of the mitochondrial folate pool. To exclude that within our isolation procedure the glutamylation state of the mitochondrial folate pool was affected, analyses with the mutant deficient in the mitochondrial folylpolyglutamate synthetase should be considered.

The analysis of the mitochondrial folate pool revealed a possible regulatory function of 5-formyl-THF, which is an inhibitor of SHMT activity. 5-formyl-THF was increased in mitochondria isolated from seedlings grown at HC compared to those after shift to AC (Fig. 4A), indicating that SHMT activity is inhibited under non-photorespiratory conditions to direct flux of glycine into C_1 metabolism. Under photorespiratory conditions 5-formyl-THF is reduced as flux needs to be directed into serine biosynthesis to reclaim 3-PGA in the photorespiratory pathway. Our results demonstrate that rapidly isolated mitochondria can be used for metabolite analyses. We will exploit this newly adapted technique for plant

mitochondria to measure the vitamin B_6 content in isolated mitochondria as nothing has been reported about the content and distribution of B_6 vitamers in different organelles so far (Gerdes et al., 2012).

Our preliminary analysis suggested that mitochondria contain PMP and PLP, but likely none of the other vitamers of B_6 (Supplemental Fig. S4E). Those results are in accordance with the present knowledge about the mitochondrial localization of the salvage pathway enzyme PDX3 and suggest that mitochondria do not contain the phosphorylating or dephosphorylating salvage pathway enzymes (Colinas et al., 2014; Niehaus et al., 2014; Colinas et al., 2016). In addition, this indicates that Arabidopsis mitochondria are likely dependent on PMP import from the cytosol. We showed that BOU can not catalyze this transport function (Fig. 1B). Therefore, mitochondria likely contain a so far not identified PMP/PNP transport protein.

Furthermore, our rapid isolation method will be useful to determine whether the additional HPLC peaks we identified in whole seedling tissue correspond to metabolites that might accumulate in mitochondria. The corresponding metabolites could be modified versions of the known group of B_6 vitamers, e.g. generated by glycosylation, phosphorylation or other modifications. So far we could not identify them. Especially Peak 4 should be analyzed in more detail in ongoing research, as (1) the corresponding metabolite is more abundant in samples shifted from elevated to ambient CO_2 conditions and (2) it is accumulating in the *bou-2* mutant which is characterized by a dysfunctional photorespiratory metabolism (Supplemental Fig. S4D). Because we observed the peak in the chromatogram of the isolated mitochondria sample we hypothesize that it might be a so far unidentified intermediate of vitamin B_6 produced by the GDC and SHMT reaction. Alternatively, we hypothesize that the corresponding metabolite accumulates in mutants with a disturbed photorespiratory pathway. However, both hypotheses await further analyses. If the latter hypothesis holds true we might likely be able to identify this peak in chromatograms of the *shm1* samples.

The vitamin B_6 analysis of whole seedlings revealed, a similar pattern of the *bou-2* and *shm1* seedlings (Fig. 5). The *shm1* mutant is deficient in the mitochondrial *SHMT* and characterized by a strong reduction in mitochondrial SHMT activity (Voll et al., 2006). SHMT is neither involved in the *de novo* synthesis nor the salvage pathway of vitamin B_6. However, it is a PLP-dependent enzyme. Our results on the vitamin B_6 quantification indicate that the overall reduction of PLP levels might be a result of the reduction of SHMT activity and are likely a pleiotropic effect caused by a dysfunctional photorespiratory pathway. This suggests, that the disturbed vitamin B_6 profile in *bou-2* seedlings might be a result of a dysfunctional photorespiratory pathway and not a direct effect of a loss of BOU transport function. Further

analyses will reveal if the changes in vitamin B_6 content in whole seedlings reflect the changes in mitochondrial metabolism due to a loss of *BOU*. Additionally, we will use our rapid isolation strategy to gain more information about the distribution and accumulation of the corresponding metabolites of the so far unknown peaks.

BOU functions as mitochondrial glutamate exporter under photorespiratory conditions

Our results demonstrate that *bou-2* mitochondria contain a sufficient amount of glutamylated folates to drive GDC and SHMT reaction (Fig. 5). To date we cannot exclude, that BOU is a transporter for glutamylated folates or that they need to be imported into *bou-2* mitochondria due to reduced availability of glutamate. However, mitochondria are a hub for nitrogen metabolism and glutamate production (Fig. 7). Several catabolic pathways, such as the degradation of thylakoids via lysine and the mitochondrial 2-hydroxyglutarate metabolism, degradation of proteins via branched chain amino acids, and degradation of proline and ornithine lead to the production of glutamate in mitochondria (Araújo et al., 2010; Verslues and Sharma, 2010; Engqvist et al., 2014; Hildebrandt et al., 2015). Additionally glutamate is synthesized by mitochondrial GluDH and a product of several aminotransferase reactions (Fig. 7). Taken together this suggests that mitochondria do not necessarily depend on import of glutamate for example for polyglutamylation of THF. Mitochondria are rather a major source of glutamate as GluDH that synthesize glutamate from 2-OG are localized to the mitochondria. Detailed research about the physiological role of GluDH is still ongoing. To date it is widely accepted that the vast majority of NH_3 is re-assimilated by the GS/FdGOGAT system in chloroplasts (Miflin and Lea, 1980; Lea and Miflin, 2010). GluDH theoretically has the capability of fixing NH_3 but has been demonstrated to operate in the glutamate deaminating direction *in vivo* (Robinson et al., 1992; Dubois et al., 2003). However, under high NH_3 conditions caused by e.g., hypoxia, it could be shown that GluDH is able to catalyze NH_3 assimilation *in vivo* (Yamaya and Oaks, 1987; Dubois et al., 2003; Limami et al., 2008). During photorespiratory conditions high amounts of NH_3 are released in the mitochondria and could potentially shift the reaction equilibrium into NH_3 fixation by GluDH rather than deamination. Produced glutamate needs to be exported and shuttled into chloroplasts for NH_3 re-assimilation by GS/FdGOGAT system. We hypothesize that BOU acts as bidirectional mitochondrial glutamate transporter that connects carbon and nitrogen metabolism. Under carbon starvation conditions it may act as glutamate importer for deamination of glutamate by GluDH producing 2-OG that enters the TCA cycle. Under photorespiratory conditions it may export glutamate yielded by partially NH_3 fixation and other catabolic pathways from the mitochondria to provide an acceptor molecule for NH_3 re-assimilation in plastids (Fig. 7). Therefore, we hypothesize that the *bou-2* phenotype is mainly caused by a decreased availability of glutamate for re-assimilation of nitrogen by the GS/FdGOGAT system. In addition to that, there might be an accumulation of glutamate in the

mitochondria or a depletion of 2-OG from the TCA cycle due to NH_3 toxicity or partially NH_3 fixation which in turn would lead to a reduction in respiration and consequently a reduced GDC activity. Proving this hypothesis is a subject of our ongoing research. For human cell lines it has been reported that under hyperammonemic conditions mitochondrial respiration is inhibited because NH_3 is removed by mitochondrial GluDH which depletes 2-OG from the TCA cycle. Inhibiting GluDH activity could rescue the respiratory phenotype of the cells (Drews et al., 2019). To analyze the role of GluDH in the *bou-2* genotype this experiment might be taken into consideration. Our above-described hypothesis is supported by the fact that (1) *DTC* is co-expressed with *BOU* and both are highly abundant in leaf tissue indicating that DTC might deliver 2-OG as acceptor for GluDH reaction, (2) mutants deficient in *GS* or *FdGOGAT* show a photorespiratory phenotype similar to *bou-2*, and (3) transcripts of *GS*, *DiT1* and *DiT2.1* are reduced in *bou-2* indicating that the nitrogen re-assimilation pathway is disturbed in *bou-2* (Coschigano et al., 1998; Picault et al., 2002; Winter et al., 2007; Kissen et al., 2010; Samuilov et al., 2018). Further analyses will reveal if the reduction in GS transcript are reflected in reduced activity of the enzyme. A preliminary amino acid analysis of isolated mitochondria from tagged WT and tagged *bou-2* revealed a potential accumulation of glutamate in tagged *bou-2* mitochondria supporting a function of BOU as glutamate exporter (Supplemental Fig. 6). However, the analysis has to be optimized and repeated with more replicates.

BOU protein was biochemically characterized with its yeast homolog YMC2 (Porcelli et al., 2018). YMC2 like BOU is a mitochondrial transport protein with a high affinity for glutamate. Currently, we are adapting complementation studies of the *bou-2* mutant with the YMC2 protein to resolve remaining concerns about BOU transport function. Additionally, we will use our mitochondria tagging approach to study amino acid content and accumulation in *bou-2* mitochondria before and after complementation with YMC2.

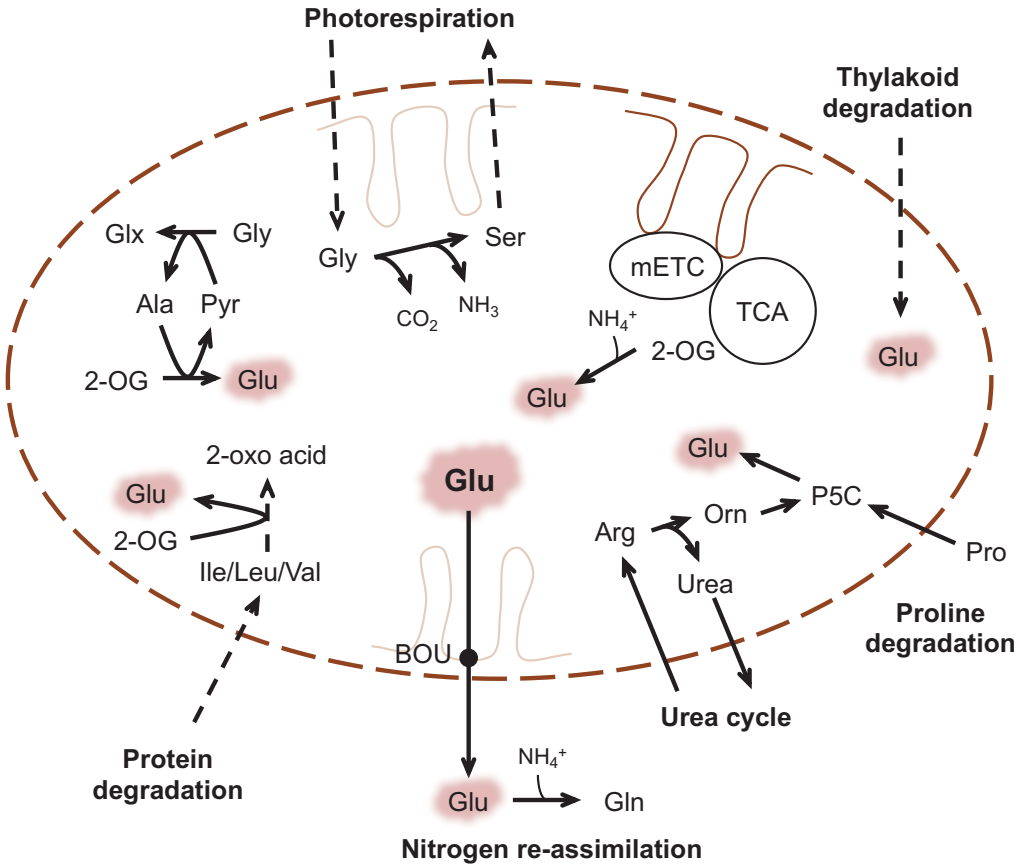

Figure 7: Role of BOU in mitochondrial glutamate metabolism. Abbreviations: Glx, glyoxylate; mETC, mitochondrial electron transport chain; 2-OG, 2-oxoglutarate; Orn, ornithine; P5C, pyrroline-5-carboxylate; Pyr, pyruvate; TCA, tricarboxylic acid cycle.

We conclude that BOU is a mitochondrial glutamate transporter with bidirectional transport activity that plays a crucial role in connecting photorespiratory nitrogen metabolism. Our results suggest that NH_3 released by GDC reaction might be partially assimilated by mitochondrial GluDH reaction providing glutamate as acceptor molecule for re-assimilation of nitrogen in plastids during photorespiration. We note that a *GluDH* triple knockout mutant shows no apparent photorespiratory phenotype indicating that under standard condition this pathway is not the sole source of glutamate necessary for NH_3 re-assimilation (Fontaine et al., 2012). However, the physiological role of GluDH in photorespiration has not been analyzed so far as many studies focused on its role during carbon starvation during prolonged dark conditions (Miyashita and Good, 2008; Fontaine et al., 2012). Especially, analyses of *GluDH* knockout mutants in the *bou-2* background might contribute to further our understanding of nitrogen metabolism during photorespiration.

MATERIALS AND METHODS

Plant growth conditions

Arabidopsis thaliana (Arabidopsis) *bou-2* mutant (GABI-Kat line number 079D12; http://www.gabi-kat.de/db/lineid.php) (Kleinboelting et al., 2012; Eisenhut et al., 2013b), *shm1* mutant (Voll et al., 2006), tagged Col-0 (tagged WT) and tagged *bou-2* (Kuhnert et al., 2020) were used as mutants in this study. Arabidopsis ecotype Columbia was used as wildtype (WT) in this study. Seeds were sterilized by washing with 70% (v/v) ethanol supplemented with 1% (v/v) Triton X-114, 100% ethanol, dried and grown on half-strength Murashige and Skoog medium (pH 5.7) supplemented with 0.8% (w/v) agar. After cold stratification for two days at 4ºC seedlings were grown under 12 h light/12 h dark photoperiod with a light intensity of 100 µmol photons m^{-2} s^{-1} in a CO_2-enriched atmosphere (0.3% [v/v] CO_2; HC).

After 10 days, seedlings were either harvested for isolation of mitochondria and metabolite analyses or transferred to soil and grown under the above-described growing conditions, unless otherwise stated.

Roots were grown in the dark in liquid half-strength Murashige and Skoog medium (pH 5.7) supplemented with 3% (w/v) sucrose at 28°C under constant shaking for two weeks.

Heterologous expression of BOU in *E. coli* and purification from inclusion bodies

The coding sequence of Arabidopsis *BOU* (At5g46800) was amplified by PCR from Arabidopsis cDNA using the primers 5' CAC ACT CTA GAA GCC GGA TCT CAG TG 3' and 5' CAC ACG AGA TAT ACC CAT GGC GGA TG 3' and introduced into the expression vector pET-16b (Merck Millipore) via restriction-based cloning.

E. coli Rosetta BL21(DE3) cells (Novagen) carrying the expression construct were grown in liquid lysogeny broth medium containing 200 µg/ml ampicillin and 25 µg/ml chloramphenicol at 37°C with 140 rpm to an OD_{600} of 0.6. Protein expression was induced with isopropyl β-d-1-thiogalactopyranoside (IPTG) to a final concentration of 0.5 mM and the cultures were incubated at 37°C with 140 rpm for 2 h. Cells were harvested by centrifugation at 4,000 x *g* for 15 min and stored at -20°C.

All following steps were performed at 4°C unless stated otherwise. Cells were resuspended in lysis buffer (50 mM Tris/HCl [pH 7.4], 1 mM EDTA, 0.5 M NaCl, 10% [v/v] Glycerol, 1 mM DTT, 1 mM PMSF, 0.1 mM AEBSF, 1 µg/ml Pepstatin, 2 µg/ml Leupeptin, 1 mg/ml Lysozyme) at a ratio of 4 ml per gram wet weight cells and incubated for 30 min with gentle shaking. 3-[(3-Cholamidopropyl)dimethylammonio]-1-propanesulfonate (CHAPS) was added to a final concentration of 6 mM and the suspension was incubated for 30 min with gentle shaking. Subsequently, 5 mM ATP, 10 mM $MgCl_2$ and a few DNase crystals were added and the suspension was incubated for 20 min at room temperature with gentle shaking. Cells

were pelleted by centrifugation (3,000 x *g*; 10 min). The pellet containing the inclusion bodies was resuspended in 1.5 ml lysis buffer using a paint brush and subsequently centrifuged for 10 min at 1,000 x *g*. The supernatant containing the inclusion bodies was transferred into a new tube and centrifuged for 15 min 12,000 x *g*. The pellet containing the inclusion bodies was washed with 1 ml washing buffer I (10 mM Tris/HCl [pH 7.0], 0.1 mM EDTA, 1 mM DTT, 3% [v/v] Triton X-114) followed by washing with 1 ml washing buffer II (10 mM Tris/HCl [pH 7.0], 0.1 mM EDTA, 1 mM DTT). The washed inclusion bodies were solubilized in 80 µl solubilization buffer I (10 mM Tris/HCl [pH 7.0], 0.1 mM EDTA, 1 mM DTT, 1.67% [w/v] N-lauroylsarcosine) supplemented with 24 µl of a 10% (w/v) cardiolipin solution and incubated for 5 min on ice. Subsequently 696 µl of solubilization buffer II (10 mM Tris/HCl [pH 7.0], 0.1 mM EDTA, 1 mM DTT) was added and the suspension was centrifuged for 5 min at 12,000 x *g* to pellet non-solubilized proteins. The supernatant was immediately used for reconstitution.

Reconstitution of recombinant BOU in liposomes

Heterologously expressed BOU was reconstituted into liposomes via the detergent removal method. In brief, 20 µg solubilized BOU in a total volume of 200 µl 20 mM PIPES (pH 7.0) were carefully mixed with 75 µl 10% (v/v) Triton X-114. Immediately, 100 µl of a sonified 10% (w/v) phospholipid solution (L-α-phosphatidylcholine from egg yolk; Sigma Aldrich) and 4 µl of a 10% (w/v) cardiolipin solution were added, and carefully mixed by pipetting up and down. The suspension was topped up to 700 µl with 20 mM PIPES (pH 7.0) with or without the addition of glutamate to a final concentration of 20 mM, and passed through an Amberlite XAD-2 (Sigma Aldrich) column for at least 13 times until tight proteoliposomes had been formed. Amberlite XAD-2 was previously activated with 100% methanol, washed with ddH2O and pre-equilibrated with 20 mM PIPES (pH 7.0) with or without 2 mM glutamate. The amount of Amberlite XAD-2 needed was calculated according to the manufacturer's instructions. One gram of dry resin can adsorb 0.37 g of Triton X-114. Proteoliposomes were either directly used for uptake experiments or stored for one day at 4°C.

Isolation of mitochondria

Mitochondria from 10-day old and 2-weeks old Arabidopsis WT and *bou-2* seedlings, 4–6-weeks old Arabidopsis WT and *bou-2* rosette leaves, and 2-weeks old Arabidopsis WT and *bou-2* root cultures were isolated as previously described via differential centrifugation and Percoll density gradient purification (Kühn et al., 2015). BSA was omitted from all solutions. Purified mitochondria were directly used for enzyme assays and native PAGE or pelleted for 30 min at 10,000 x *g*, frozen in liquid nitrogen and stored at -80°C.

Mitochondria from 10-day old and 4-week old WT, *bou-2*, tagged WT and tagged *bou-2* seedlings were rapidly isolated via co-IP, as previously described (Kuhnert et al., 2020). Purified mitochondria bound to beads were directly frozen in liquid nitrogen and extracted for metabolite analyses or lysed for enzyme assays.

Solubilization of mitochondrial membranes and reconstitution into liposomes

Pelleted mitochondria were resuspended in mitochondria resuspension buffer (10 mM PIPES [pH 7.0], 50 mM NaCl, 1 mM EDTA, 2% [v/v] Triton X-114), incubated on ice for 20 min, and subsequently centrifuged for 10 min at 138,000 x *g* at 4°C. The supernatant containing the solubilized mitochondrial membranes was used for reconstitution into liposomes via the detergent removal method as described above. Each, 50 µg total mitochondrial protein extract was used per reconstitution.

Uptake experiments with radioactive labeled substrates

Liposomes harboring heterologously expressed BOU or isolated mitochondrial membranes were reconstituted as described above. External substrate was removed by size exclusion chromatography using Sephadex G-75 columns (GE-Healthcare) pre-equilibrated with buffer A (20 mM Tricine-KOH, [pH 7.0], 50 mM NaCl). Transport was initiated by adding ^{14}C-labeled substrate and 0.2 mM non-labeled substrate to proteoliposomes with or without preloading of substrate. Uptake of external L-[14C]-glutamate or L-[14C]-malate or [32P]-phosphate (all from Hartmann Analytics) was measured at 30°C. Transport was stopped by adding 140 µl of the mixture to pre-equilibrated size-exclusion columns. Liposomes were separated from external radioactivity by passing through Sephadex G-75 medium (Sigma Aldrich) columns pre-equilibrated with buffer A. The radioactivity inside the liposomes was determined by liquid scintillation counting (LS 6000, Beckmann).
Affinity of heterologously expressed BOU for different substrates was determined using the inhibitor method. Substrates to be tested were added in excess (2 mM) to proteoliposomes together with the radioactive labeled substrate.

SDS PAGE and immunoblot

Samples of heterologously expressed protein, total leaf protein, and isolated mitochondria were analyzed by SDS-PAGE using standard protocols (Laemmli, 1970). Proteins were transferred onto nitrocellulose membranes using a semi-dry blotting system. Nitrocellulose membranes were probed with antibodies raised against the hexa histidine-tag (1:5000; Miltenyi Biotec), the large subunit of Rubisco (1:7500, Agrisera), and alternative oxidase 1/2 (1:1000, Agrisera) according to the manufacturer's instruction. After incubating with a secondary horseradish peroxidase-coupled antibody, immunodetected proteins were

visualized using a chemiluminescent detection system (Immobilon Western HRP Substrate, Merck Millipore).

Native PAGE and AspAT in-gel activity staining

Leaf material was harvested from the aerial part of the plants before isolation of mitochondria, immediately frozen in liquid nitrogen and ground to a fine powder. Aliquots of 50 mg ground and frozen leaf material was extracted in 500 µl ice-cold native extraction buffer (50 mM Tris/HCl [pH 6.8], 10% [v/v] glycerol, 0.01% [w/v] bromphenol blue), incubated for 10 min at 4°C on an end-over-end rotator (30 rpm) and subsequently centrifuged for 5 min at 13,000 x *g* at 4°C. The supernatant containing the extracted proteins was used for native PAGE. Mitochondria from 4–6-weeks old Arabidopsis were isolated via differential centrifugation an Percoll density purification as described above. Enriched mitochondria after Percoll density purification were used for native PAGE. Aliquots of 30 µg total leaf protein and 10 µg isolated mitochondrial protein were incubated in native loading buffer (50 mM Tris/HCl [pH 6.8] 20% [v/v] glycerol, 0.01% [w/v] bromphenol blue) and analyzed by native PAGE and AspAT in-gel activity staining. Gels consisted of a 4% stacking gel (~1 cm wide) and a 5–16% gradient running gel (~6 cm wide). Gradient gels for native PAGE were prepared in 375 mM Tris/HCl (pH 8.8) with a peristaltic pump. Stacking gels were prepared in 62.5 mM Tris/HCl (pH 6.8). Electrophoresis was carried out at 10 mA, 100 V at 4°C with native running buffer (25 mM Tris/HCl [pH 8.3], 192 mM glycine). Gels were either stained in coomassie or AspAT activity staining buffer (100 mM Tris/HCl [pH 7.5], 5 mM 2-OG, 10 mM L-cysteine sulfinic acid, 0.005% [w/v] phenazine methosulfate, 0.02% [w/v] MTT) as described previously (Stejskal, 1994).

Enzyme assays

Activities of AspAT, GABA-T, and MDH were assayed in a plate-reader spectrophotometer based on the absorbance at 340 nm as previously described (Wilkie and Warren, 1998; Clark et al., 2009; Tomaz et al., 2010; Kuhnert et al., 2020). Recombinant succinate-semialdehyde dehydrogenase was produced as described previously (Clark et al., 2009).

LC–MS/MS determination of mono- and polyglutamylated folates

Levels of mono- and polyglutamylated folates were determined in approximately 200 mg of Arabidopsis seedling material and approximately 100 µg total mitochondrial protein by liquid chromatography with tandem mass spectrometry detection as described in Blancquaert et al. (2013) and Navarrete et al. (2012). Seedling samples were taken after 10-days growth at HC and five days after shift to ambient CO_2 (0.03% [v/v] CO_2; AC) conditions. Mitochondria were rapidly isolated via co-IP from 10-day old WT, tagged WT and tagged *bou-2* seedlings grown in HC and five days after shift to AC as described above.

HPLC analysis of B_6 vitamers

Levels of B_6 vitamers were determined from Arabidopsis WT, *bou-2* and *shm1* seedling tissue and rapidly isolated mitochondria by HPLC as described previously (Szydlowski et al., 2013; Colinas et al., 2016). Seedling samples were taken in the middle of the light period after 8-days growth in HC, and two and five days after shift to AC. Mitochondria were rapidly isolated via co-IP from 10-day old WT and tagged WT as described above.

Reversed-phase liquid chromatography/ mass spectrometry analysis of amino acids

Amino acids in isolated mitochondria were quantified using an Agilent (Santa Clara, USA) 6530 Quadrupole-Time-of-Flight mass spectrometer coupled to an Agilent (Santa Clara, USA) 1290 HPLC system (Gu et al., 2007). For chromatographic separation a Waters Symmetry C18 column (2.1 × 100 mm, 3.5-µm particle size) was used with column oven temperature at 30°C. The injection volume was set to 10 µl, and the HPLC flow rate was 0.3 ml/min using the following mobile phases and gradient: Starting conditions were 98% mobile phase A (1 mM aqueous perfluoroheptanoic acid) and 2% mobile phase B (100% Acetonitrile). Within 0.1 min B increased to 20%, following a 40% increase after 2.3 min. This was hold until 4 min before dropping down to 2% until 4.1 min. Equilibration time with start conditions was 4 min. Mass spectra were acquired using electrospray ionization in positive ion mode. The source parameters were set as follows: capillary voltage 3500 V, gas temperature 250°C, drying gas flow of 5 l/min, nebulizer pressure 25 psig, sheath gas temperature 350°C, and a sheath gas flow of 10 l/min. The fragmentor was set to 100 V, the skimmer to 65 V and the Oct1 RF Vpp to 750 V. Data were acquired with MassHunter Workstation Data Aqusition (Version B.08.00; Agilent) and processed and analyzed for quantification with MassHunter Quantitative Analysis (Version B.08.00; Agilent). Retention times of target metabolites were verified with standard compounds as reference. The peak area of the target metabolites were normalized to the peak area of the internal Standard dimethylphenylalanine for relative quantification.

Determination of protein content

Protein concentrations of purified inclusion bodies, total leaf protein and isolated mitochondria were determined using the Quick Start™ Bradford Protein Assay Kit (Bio-Rad) according to the manufacturer's instruction.

SUPPLEMENTAL DATA

Supplemental Figure S1. Heterologous expression of BOU and reconstitution into liposomes.

Supplemental Figure S2. Immunoblot analysis of isolated mitochondria of wildtype (WT) and *bou-2* seedlings.

Supplemental Figure S3. Glutamylation state of quantified folates.

Supplemental Figure S4. Vitamin B_6 analysis.

Supplemental Figure S5. Enzyme activities in rapidly isolated mitochondria.

Supplemental Figure S6. Preliminary amino acid analyses in rapidly isolated mitochondria of tagged WT and tagged *bou-2*.

REFERENCES

Anderson LE (1971) Chloroplast and cytoplasmic enzymes II. Pea leaf triose phosphate isomerases. Biochim Biophys Acta - Enzymol **235**: 237–244

Araújo WL, Ishizaki K, Nunes-Nesi A, Larson TR, Tohge T, Krahnert I, Witt S, Obata T, Schauer N, Graham IA, et al (2010) Identification of the 2-Hydroxyglutarate and Isovaleryl-CoA Dehydrogenases as Alternative Electron Donors Linking Lysine Catabolism to the Electron Transport Chain of Arabidopsis Mitochondria. Plant Cell **22**: 1549–1563

Blancquaert D, Storozhenko S, Van Daele J, Stove C, Visser RGF, Lambert W, Van Der Straeten D (2013) Enhancing pterin and para-aminobenzoate content is not sufficient to successfully biofortify potato tubers and Arabidopsis thaliana plants with folate. J Exp Bot **64**: 3899–3909

Boldt R, Edner C, Kolukisaoglu Ü, Hagemann M, Weckwerth W, Wienkoop S, Morgenthal K, Bauwe H (2005) d-GLYCERATE 3-KINASE, the Last Unknown Enzyme in the Photorespiratory Cycle in Arabidopsis, Belongs to a Novel Kinase Family. Plant Cell **17**: 2413–2420

Bowes G, Ogren WL, Hageman RH (1971) Phosphoglycolate production catalyzed by ribulose diphosphate carboxylase. Biochem Biophys Res Commun **45**: 716–722

Calvin M (1962) The Path of Carbon in Photosynthesis. Angew Chemie Int Ed English **1**: 65–75

Clark SM, Di Leo R, Dhanoa PK, Van Cauwenberghe OR, Mullen RT, Shelp BJ (2009) Biochemical characterization, mitochondrial localization, expression, and potential functions for an Arabidopsis γ-aminobutyrate transaminase that utilizes both pyruvate and glyoxylate. J Exp Bot **60**: 1743–1757

Colinas M, Eisenhut M, Tohge T, Pesquera M, Fernie AR, Weber APM, Fitzpatrick TB (2016) Balancing of B6 Vitamers Is Essential for Plant Development and Metabolism in Arabidopsis. Plant Cell **28**: 439–453

Colinas M, Shaw H V., Loubéry S, Kaufmann M, Moulin M, Fitzpatrick TB (2014) A pathway for repair of NAD(P)H in plants. J Biol Chem **289**: 14692–14706

Collakova E, Goyer A, Naponelli V, Krassovskaya I, Gregory JF, Hanson AD, Shachar-Hill Y (2008) Arabidopsis 10-Formyl Tetrahydrofolate Deformylases Are Essential for Photorespiration. Plant Cell **20**: 1818–1832

Coschigano KT, Melo-Oliveira R, Lim J, Coruzzi GM (1998) Arabidopsis gls Mutants and Distinct Fd-GOGAT Genes: Implications for Photorespiration and Primary Nitrogen Assimilation. Plant Cell **10**: 741–752

Douce R, Bourguignon J, Neuburger M, Rébeillé F (2001) The glycine decarboxylase system: a fascinating complex. Trends Plant Sci **6**: 167–176

Drews L, Zimmermann M, Poss RE, Brilhaus D, Bergmann L, Wiek C, Piekorz RP, Weber APM, Mettler-Altmann T, Reichert AS (2019) Ammonia inhibits energy metabolism in astrocytes in a rapid and GDH2-dependent manner. bioRxiv 683763

Dubois F, Tercé-Laforgue T, Gonzalez-Moro M-B, Estavillo J-M, Sangwan R, Gallais A, Hirel B (2003) Glutamate dehydrogenase in plants: is there a new story for an old enzyme? Plant Physiol Biochem **41**: 565–576

Eisenhut M, Pick TR, Bordych C, Weber APM (2013a) Towards closing the remaining gaps in photorespiration - the essential but unexplored role of transport proteins. Plant Biol **15**: 676–685

Eisenhut M, Planchais S, Cabassa C, Guivarc'h A, Justin A-M, Taconnat L, Renou J-P, Linka M, Gagneul D, Timm S, et al (2013b) Arabidopsis A BOUT DE SOUFFLE is a putative mitochondrial transporter involved in photorespiratory metabolism and is required for meristem growth at ambient CO 2 levels. Plant J **73**: 836–849

Eisenhut M, Roell M, Weber APM (2019) Mechanistic understanding of photorespiration paves the way to a new green revolution. New Phytol **223**: 1762–1769

Engel N, van den Daele K, Kolukisaoglu Ü, Morgenthal K, Weckwerth W, Pärnik T, Keerberg O, Bauwe H (2007) Deletion of Glycine Decarboxylase in Arabidopsis Is Lethal under Nonphotorespiratory Conditions. Plant Physiol **144**: 1328–1335

Engel N, Ewald R, Gupta KJ, Zrenner R, Hagemann M, Bauwe H (2011) The Presequence of Arabidopsis Serine Hydroxymethyltransferase SHM2 Selectively Prevents Import into Mesophyll Mitochondria. Plant Physiol **157**: 1711–1720

Engqvist MKM, Eßer C, Maier A, Lercher MJ, Maurino VG (2014) Mitochondrial 2-hydroxyglutarate metabolism. Mitochondrion **19**: 275–281

Fontaine J-X, Tercé-Laforgue T, Armengaud P, Clément G, Renou J-P, Pelletier S, Catterou M, Azzopardi M, Gibon Y, Lea PJ, et al (2012) Characterization of a NADH-Dependent Glutamate Dehydrogenase

Mutant of *Arabidopsis* Demonstrates the Key Role of this Enzyme in Root Carbon and Nitrogen Metabolism. Plant Cell **24**: 4044–4065

Fuchs P, Rugen N, Carrie C, Elsässer M, Finkemeier I, Giese J, Hildebrandt TM, Kühn K, Maurino VG, Ruberti C, et al (2020) Single organelle function and organization as estimated from Arabidopsis mitochondrial proteomics. Plant J **101**: 420–441

Gardeström P, Wigge B (1988) Influence of Photorespiration on ATP/ADP Ratios in the Chloroplasts, Mitochondria, and Cytosol, Studied by Rapid Fractionation of Barley (Hordeum vulgare) Protoplasts. Plant Physiol **88**: 69–76

Gerdes S, Lerma-Ortiz C, Frelin O, Seaver SMD, Henry CS, de Crécy-Lagard V, Hanson AD (2012) Plant B Vitamin Pathways and their Compartmentation: a Guide for the Perplexed. J Exp Bot **63**: 5379–5395

Givan C V., Kleczkowski LA (1992) The Enzymic Reduction of Glyoxylate and Hydroxypyruvate in Leaves of Higher Plants. Plant Physiol **100**: 552–556

Goyer A, Collakova E, de la Garza RD, Quinlivan EP, Williamson J, Gregory JF, Shachar-Hill Y, Hanson AD (2005) 5-Formyltetrahydrofolate Is an Inhibitory but Well Tolerated Metabolite in Arabidopsis Leaves. J Biol Chem **280**: 26137–26142

Gu L, Jones AD, Last RL (2007) LC−MS/MS Assay for Protein Amino Acids and Metabolically Related Compounds for Large-Scale Screening of Metabolic Phenotypes. Anal Chem **79**: 8067–8075

Hanson AD, Gregory JF (2011) Folate Biosynthesis, Turnover, and Transport in Plants. Annu Rev Plant Biol **62**: 105–125

Hanson AD, Roje S (2001) One-Carbon Metabolism in Higher Plants. Annu Rev Plant Physiol Plant Mol Biol **52**: 119–137

Hildebrandt TM, Nunes Nesi A, Araújo WL, Braun H-P (2015) Amino Acid Catabolism in Plants. Mol Plant **8**: 1563–1579

Igarashi D, Miwa T, Seki M, Kobayashi M, Kato T, Tabata S, Shinozaki K, Ohsumi C (2003) Identification of photorespiratory glutamate:glyoxylate aminotransferase (GGAT) gene in Arabidopsis. Plant J **33**: 975–987

Keech O, Dizengremel P, Gardeström P (2005) Preparation of leaf mitochondria from Arabidopsis thaliana. Physiol Plant **124**: 403–409

Kelly GJ, Latzko E (1976) Inhibition of spinach-leaf phosphofructokinase by 2-phosphoglycollate. FEBS Lett **68**: 55–58

Kissen R, Winge P, Tran D, Jørstad TS, Størseth TR, Christensen T, Bones AM (2010) Transcriptional profiling of an Fd-GOGAT1/GLU1 mutant in Arabidopsis thaliana reveals a multiple stress response and extensive reprogramming of the transcriptome. BMC Genomics **11**: 190

Kleinboelting N, Huep G, Kloetgen A, Viehoever P, Weisshaar B (2012) GABI-Kat SimpleSearch: new features of the Arabidopsis thaliana T-DNA mutant database. Nucleic Acids Res **40**: D1211–D1215

König A-C, Hartl M, Boersema PJ, Mann M, Finkemeier I (2014) The mitochondrial lysine acetylome of Arabidopsis. Mitochondrion **19**: 252–260

Kühn K, Obata T, Feher K, Bock R, Fernie AR, Meyer EH (2015) Complete Mitochondrial Complex I Deficiency Induces an Up-Regulation of Respiratory Fluxes That Is Abolished by Traces of Functional Complex I. Plant Physiol **168**: 1537–1549

Kuhnert F, Stefanski A, Overbeck N, Drews L, Reichert AS, Stühler K, Weber APM (2020) Rapid Single-Step Affinity Purification of HA-Tagged Plant Mitochondria. Plant Physiol **182**: 692–706

Laemmli UK (1970) Cleavage of Structural Proteins during the Assembly of the Head of Bacteriophage T4. Nature **227**: 680–685

Lawand S, Dorne A-J, Long D, Coupland G, Mache R, Carol P (2002) Arabidopsis A BOUT DE SOUFFLE , Which Is Homologous with Mammalian Carnitine Acyl Carrier, Is Required for Postembryonic Growth in the Light. Plant Cell **14**: 2161–2173

Lea PJ, Miflin BJ (2010) Nitrogen Assimilation and its Relevance to Crop Improvement. Annu. Plant Rev. Vol. 42. Wiley-Blackwell, Oxford, UK, pp 1–40

Liepman AH, Olsen LJ (2003) Alanine Aminotransferase Homologs Catalyze the Glutamate:Glyoxylate Aminotransferase Reaction in Peroxisomes of Arabidopsis. Plant Physiol **131**: 215–227

Limami AM, Glévarec G, Ricoult C, Cliquet J-B, Planchet E (2008) Concerted modulation of alanine and glutamate metabolism in young Medicago truncatula seedlings under hypoxic stress. J Exp Bot **59**: 2325–2335

Linka M, Weber APM (2005) Shuffling ammonia between mitochondria and plastids during photorespiration.

Trends Plant Sci **10**: 461–465

Mehrshahi P, Gonzalez-Jorge S, Akhtar TA, Ward JL, Santoyo-Castelazo A, Marcus SE, Lara-Núñez A, Ravanel S, Hawkins ND, Beale MH, et al (2010) Functional analysis of folate polyglutamylation and its essential role in plant metabolism and development. Plant J **64**: 267–279

Miflin BJ, Lea PJ (1980) Ammonia Assimilation. *In* BJBT-AA and D Miflin, ed, Amin. Acids Deriv. Elsevier, pp 169–202

Millar AH, Sweetlove LJ, Giegé P, Leaver CJ (2001) Analysis of the Arabidopsis Mitochondrial Proteome. Plant Physiol **127**: 1711–1727

Miyashita Y, Good AG (2008) NAD(H)-dependent glutamate dehydrogenase is essential for the survival of Arabidopsis thaliana during dark-induced carbon starvation. J Exp Bot **59**: 667–680

Monné M, Daddabbo L, Gagneul D, Obata T, Hielscher B, Palmieri L, Miniero DV, Fernie AR, Weber APMM, Palmieri F (2018) Uncoupling proteins 1 and 2 (UCP1 and UCP2) from Arabidopsis thaliana are mitochondrial transporters of aspartate, glutamate, and dicarboxylates. J Biol Chem **293**: 4213–4227

Navarrete O, Van Daele J, Stove C, Lambert W, Van Der Straeten D, Storozhenko S (2012) A folate independent role for cytosolic HPPK/DHPS upon stress in Arabidopsis thaliana. Phytochemistry **73**: 23–33

Niehaus TD, Richardson LGL, Gidda SK, ElBadawi-Sidhu M, Meissen JK, Mullen RT, Fiehn O, Hanson AD (2014) Plants Utilize a Highly Conserved System for Repair of NADH and NADPH Hydrates. Plant Physiol **165**: 52–61

Obata T, Florian A, Timm S, Bauwe H, Fernie AR (2016) On the metabolic interactions of (photo)respiration. J Exp Bot **67**: 3003–3014

Ogren WL (1984) Photorespiration: Pathways, Regulation, and Modification. Annu Rev Plant Physiol **35**: 415–442

Ogren WL, Bowes G (1971) Ribulose Diphosphate Carboxylase regulates Soybean Photorespiration. Nat New Biol **230**: 159–160

Palmieri L, Picault N, Arrigoni R, Besin E, Palmieri F, Hodges M (2008) Molecular identification of three Arabidopsis thaliana mitochondrial dicarboxylate carrier isoforms: organ distribution, bacterial expression, reconstitution into liposomes and functional characterization. Biochem J **410**: 621–629

Peterhansel C, Horst I, Niessen M, Blume C, Kebeish R, Kürkcüoglu S, Kreuzaler F (2010) Photorespiration. Arab B **8**: e0130

Picault N, Palmieri L, Pisano I, Hodges M, Palmieri F (2002) Identification of a Novel Transporter for Dicarboxylates and Tricarboxylates in Plant Mitochondria. J Biol Chem **277**: 24204–24211

Pick TR, Brautigam A, Schulz MA, Obata T, Fernie AR, Weber APM (2013) PLGG1, a plastidic glycolate glycerate transporter, is required for photorespiration and defines a unique class of metabolite transporters. Proc Natl Acad Sci **110**: 3185–3190

Porcelli V, Vozza A, Calcagnile V, Gorgoglione R, Arrigoni R, Fontanesi F, Marobbio CMT, Castegna A, Palmieri F, Palmieri L (2018) Molecular identification and functional characterization of a novel glutamate transporter in yeast and plant mitochondria. Biochim Biophys Acta - Bioenerg **1859**: 1249–1258

Renné P, Dreßen U, Hebbeker U, Hille D, Flügge U-I, Westhoff P, Weber APM (2003) The Arabidopsis mutant dct is deficient in the plastidic glutamate/malate translocator DiT2. Plant J **35**: 316–331

Robinson SA, Stewart GR, Phillips R (1992) Regulation of Glutamate Dehydrogenase Activity in Relation to Carbon Limitation and Protein Catabolism in Carrot Cell Suspension Cultures. Plant Physiol **98**: 1190–1195

Roje S, Wang H, McNeil SD, Raymond RK, Appling DR, Shachar-Hill Y, Bohnert HJ, Hanson AD (1999) Isolation, Characterization, and Functional Expression of cDNAs Encoding NADH-dependent Methylenetetrahydrofolate Reductase from Higher Plants. J Biol Chem **274**: 36089–36096

Samuilov S, Brilhaus D, Rademacher N, Flachbart S, Arab L, Alfarraj S, Kuhnert F, Kopriva S, Weber APM, Mettler-Altmann T, et al (2018) The Photorespiratory BOU Gene Mutation Alters Sulfur Assimilation and Its Crosstalk With Carbon and Nitrogen Metabolism in Arabidopsis thaliana. Front Plant Sci **9**: 1–21

Schneidereit J, Häusler RE, Fiene G, Kaiser WM, Weber APM (2006) Antisense repression reveals a crucial role of the plastidic 2-oxoglutarate/malate translocator DiT1 at the interface between carbon and nitrogen metabolism. Plant J **45**: 206–224

Schwarte S, Bauwe H (2007) Identification of the Photorespiratory 2-Phosphoglycolate Phosphatase, PGLP1, in Arabidopsis. Plant Physiol **144**: 1580–1586

Sharkey TD (1988) Estimating the rate of photorespiration in leaves. Physiol Plant **73**: 147–152

Shelp BJ, Mullen RT, Waller JC (2012) Compartmentation of GABA metabolism raises intriguing questions.

Trends Plant Sci **17**: 57–59

Somerville CR (2001) An Early Arabidopsis Demonstration. Resolving a Few Issues Concerning Photorespiration: Fig. 1. Plant Physiol **125**: 20–24

Somerville CR, Ogren WL (1979) A phosphoglycolate phosphatase-deficient mutant of Arabidopsis. Nature **280**: 833–836

Somerville CR, Ogren WL (1980) Photorespiration mutants of Arabidopsis thaliana deficient in serine-glyoxylate aminotransferase activity. Proc Natl Acad Sci **77**: 2684–2687

Somerville SC, Somerville CR (1985) A mutant of Arabidopsis deficient in chloroplast dicarboxylate transport is missing an envelope protein. Plant Sci Lett **37**: 217–220

South PF, Walker BJ, Cavanagh AP, Rolland V, Badger M, Ort DR (2017) Bile Acid Sodium Symporter BASS6 Can Transport Glycolate and Is Involved in Photorespiratory Metabolism in Arabidopsis thaliana. Plant Cell **29**: 808–823

Stejskal J (1994) Aspartate aminotransferase isozymes in plants: Comparison of two staining methods in polyacrylamide gels. Biol Plant **36**: 359–364

Suh JR, Herbig AK, Stover PJ (2001) New Perspectives On Folate Catabolism. Annu Rev Nutr **21**: 255–282

Sweetlove LJ, Lytovchenko A, Morgan M, Nunes-Nesi A, Taylor NL, Baxter CJ, Eickmeier I, Fernie AR (2006) Mitochondrial uncoupling protein is required for efficient photosynthesis. Proc Natl Acad Sci **103**: 19587–19592

Szydlowski N, Bürkle L, Pourcel L, Moulin M, Stolz J, Fitzpatrick TB (2013) Recycling of pyridoxine (vitamin B6) by PUP1 in Arabidopsis. Plant J **75**: 40–52

Timm S, Bauwe H (2013) The variety of photorespiratory phenotypes - employing the current status for future research directions on photorespiration. Plant Biol **15**: 737–747

Timm S, Giese J, Engel N, Wittmiß M, Florian A, Fernie AR, Bauwe H (2018) T-protein is present in large excess over the other proteins of the glycine cleavage system in leaves of Arabidopsis. Planta **247**: 41–51

Timm S, Nunes-Nesi A, Pärnik T, Morgenthal K, Wienkoop S, Keerberg O, Weckwerth W, Kleczkowski LA, Fernie AR, Bauwe H (2008) A Cytosolic Pathway for the Conversion of Hydroxypyruvate to Glycerate during Photorespiration in Arabidopsis. Plant Cell **20**: 2848–2859

Tomaz T, Bagard M, Pracharoenwattana I, Lindén P, Lee CP, Carroll AJ, Ströher E, Smith SM, Gardeström P, Millar AH (2010) Mitochondrial Malate Dehydrogenase Lowers Leaf Respiration and Alters Photorespiration and Plant Growth in Arabidopsis. Plant Physiol **154**: 1143–1157

Verslues PE, Sharma S (2010) Proline Metabolism and Its Implications for Plant-Environment Interaction. Arab B **8**: e0140

Voll LM, Jamai A, Renné P, Voll H, McClung CR, Weber APM (2006) The Photorespiratory Arabidopsis shm1 Mutant Is Deficient in SHM1. Plant Physiol **140**: 59–66

Volokita M, Somerville CR (1987) The Primary Structure of Spinach Glycolate Oxidase Deduced from the DNA Sequence of a cDNA Clone. J Biol Chem **262**: 15825–15828

Walker BJ, VanLoocke A, Bernacchi CJ, Ort DR (2016) The Costs of Photorespiration to Food Production Now and in the Future. Annu Rev Plant Biol **67**: 107–129

Werhahn W, Niemeyer A, Jänsch L, Kruft V, Schmitz UK, Braun H-P (2001) Purification and Characterization of the Preprotein Translocase of the Outer Mitochondrial Membrane from Arabidopsis. Identification of Multiple Forms of TOM20. Plant Physiol **125**: 943–954

Werkheiser C (1961) Specific Binding of 4-Amino Folic Acid Analogues by Folic Acid Reductase. J Biol Chem **236**: 888–893

Wilkie SE, Warren MJ (1998) Recombinant Expression, Purification, and Characterization of Three Isoenzymes of Aspartate Aminotransferase from Arabidopsis thaliana. Protein Expr Purif **12**: 381–389

Winter D, Vinegar B, Nahal H, Ammar R, Wilson G V., Provart NJ (2007) An "Electronic Fluorescent Pictograph" Browser for Exploring and Analyzing Large-Scale Biological Data Sets. PLoS One **2**: e718

Woo KC, Flügge UI, Heldt HW (1987) A Two-Translocator Model for the Transport of 2-Oxoglutarate and Glutamate in Chloroplasts during Ammonia Assimilation in the Light. Plant Physiol **84**: 624–632

Yamaya T, Oaks A (1987) Synthesis of glutamate by mitochondria - An anaplerotic function for glutamate dehydrogenase. Physiol Plant **70**: 749–756

SUPPLEMENTS

Supplemental Figure S1

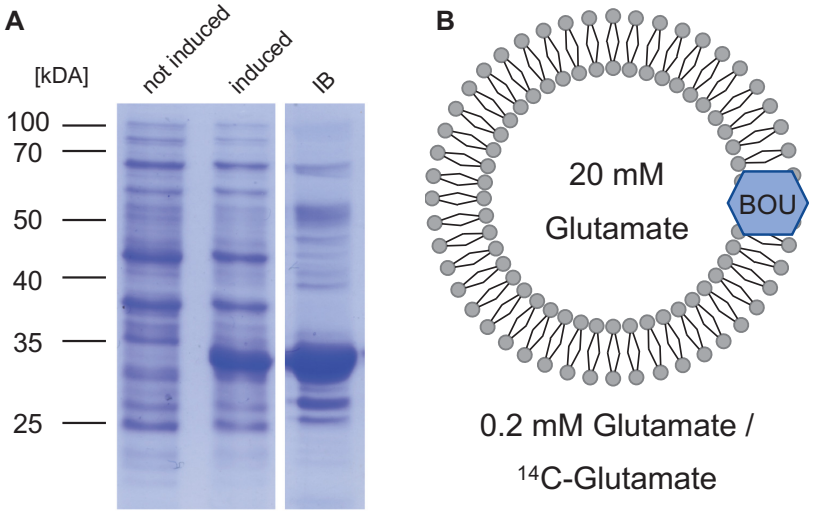

Supplemental Figure S1: Heterologous expression of BOU and reconstitution into liposomes. His-BOU was heterologously expressed in *E. coli* and purified from inclusion bodies as described in Materials and Methods (**A**). Samples of the expression cultures were taken before induction (not induced) and 2 h after induction (induced) with 0.5 mM IPTG. Sample of the purified inclusion bodies (IB) was taken before reconstitution. Samples were analyzed by SDS-PAGE as described in Materials and Methods. Schematic representation of proteoliposomes used for glutamate homo-exchange uptake experiments (**B**). Blue hexagon represents reconstituted BOU protein.

Supplemental Figure S2

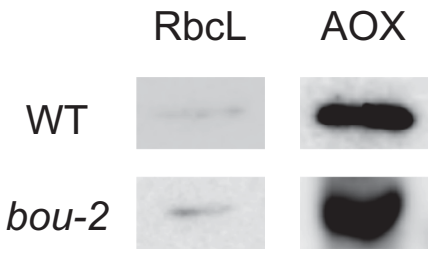

Supplemental Figure S2: Immunoblot analysis of isolated mitochondria of wildtype (WT) and *bou-2* seedlings. Mitochondria were isolated via differential centrifugation and Percoll density purification as described in Materials and Methods. 10 µg enriched mitochondrial protein was separated on 12% SDS-PAGE separating gels. Proteins were transferred onto nitrocellulose membranes using the semi-dry method. Membranes were probed with antibodies directed against the mitochondrial marker protein alternative oxidase (AOX) and the plastidic marker protein Rubisco, large subunit (RbcL) according to the manufacturer's instructions. Bands were visualized as described in Materials and Methods.

Supplemental Figure S3

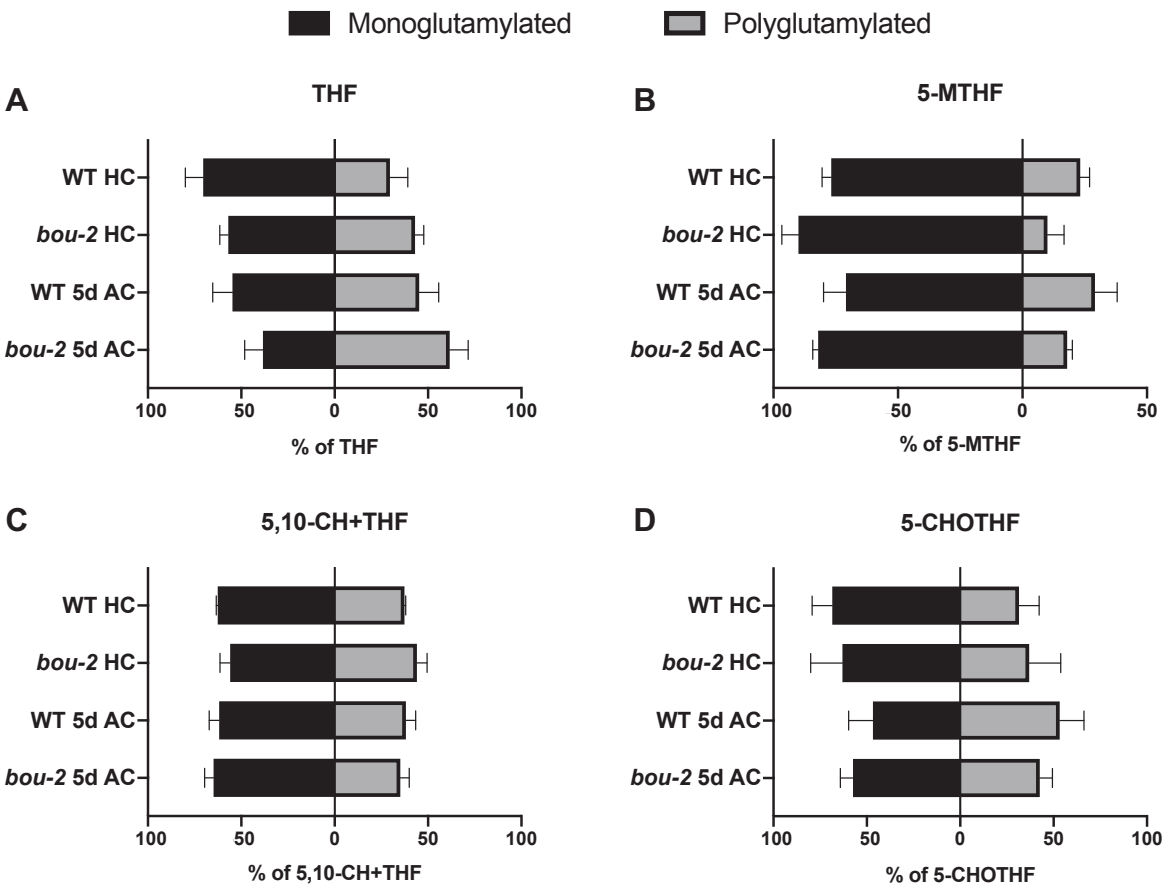

Supplemental Figure S3: Glutamylation state of quantified folates. Wildtype (WT) and *bou-2* seedlings were harvested after 10-days growth in elevated CO_2 conditions (HC; 0.3% [v/v] CO_2) and five days after shift to ambient CO_2 (5d AC; 0.038% [v/v] CO_2), and folates quantified as described in Materials and Methods. Glutamylation state of THF (**A**), 5-MTHF (**B**), 5,10-CH+THF (**C**), and 5-CHOTHF (**D**) is given as percent of the respective metabolite. Values are given as mean ± SD of three biological replicates. Abbreviations: 5,10-CH+THF, 5,10-methenyltetrahydrofolate; 5-CHOTHF; 5-formyltetrahydrofolate; 5-MTHF, 5-methyletrahydrofolate; THF, tetrahydrofolate.

Supplemental Figure S4

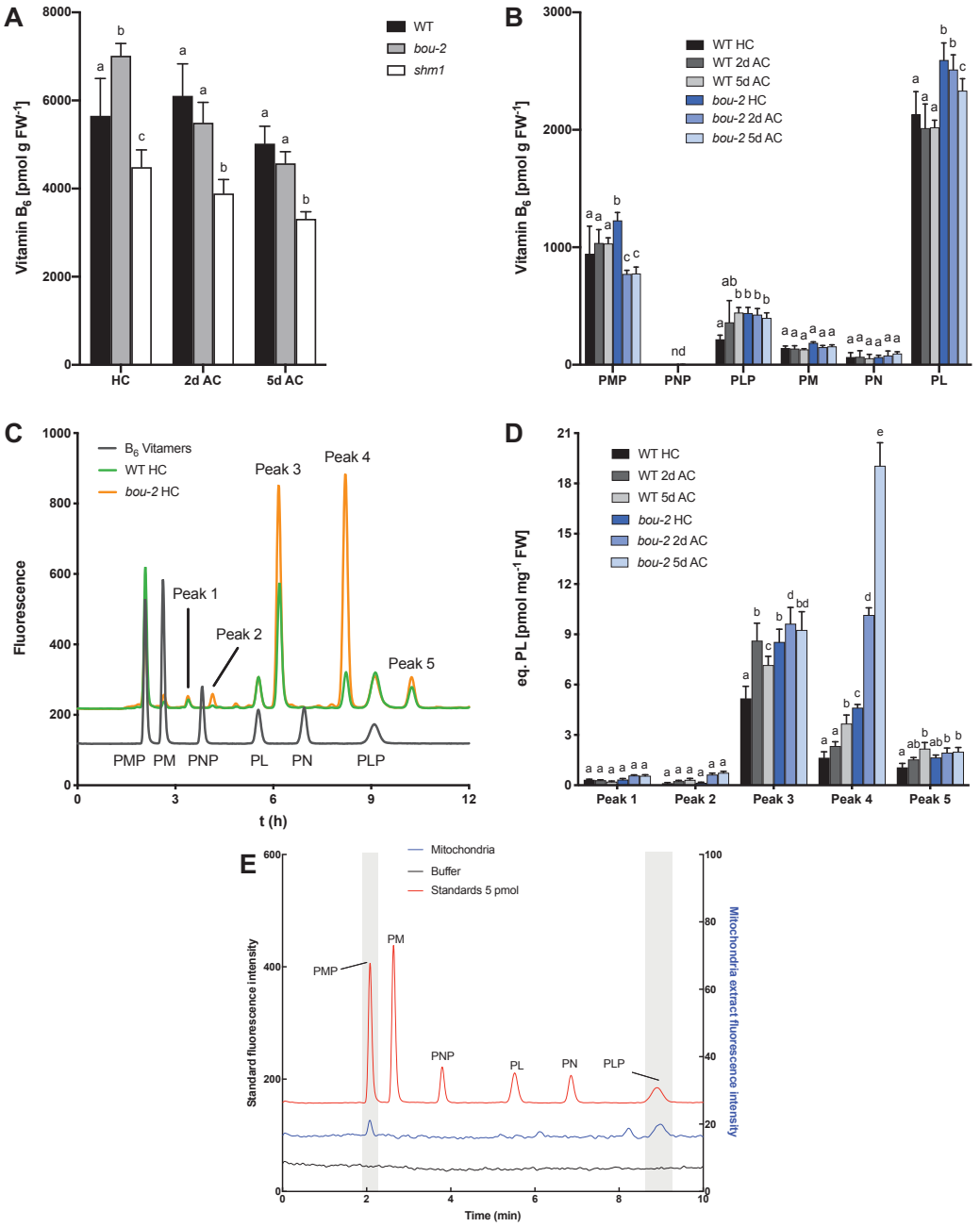

Supplemental Figure S4: Vitamin B_6 analysis. Total Vitamer B_6 content in 8-day old wildtype (WT, black bars), *bou-2* (grey bars) and *shm1* (white bars) seedlings grown under elevated CO_2 conditions (HC; 0.3% [v/v] CO_2) and two (2d AC) and five days (5d AC) after shift to ambient CO_2 (0.038% [v/v] CO_2; **A**). Vitamin B_6 analysis in 5-weeks old WT and *bou-2* rosettes grown under elevated CO_2 conditions (HC; 0.3% [v/v] CO_2) and two (2d AC) and five days (5d AC) after shift to ambient CO_2 (0.038% [v/v] CO_2; **B**). Chromatogram of vitamin B_6 standard (black line), WT HC (green line) and *bou-2* HC (orange line) showing the peaks of so far unknown metabolites (**C**). Quantification of the additional peaks (**D**). Chromatogram of vitamin B_6 standard (red line), isolated mitochondria sample (blue line) and isolation buffer (black line; **E**). Peaks that are present in the standard and the mitochondrial sample are highlighted in grey. Values are given as mean ± SD of six biological replicates (**A**, **B**, **D**). Letters indicate statistically significant differences between means ($P < 0.05$; two-way ANOVA; corrected by Tukey's multiple comparisons test). Abbreviations: PL, pyridoxal; PLP, pyridoxal 5'-phosphate; PM, pyridoxamine; PMP, pyridoxamine 5'-phosphate; PN, pyridoxine; PNP, pyridoxine 5'-phosphate.

Supplemental Figure S5

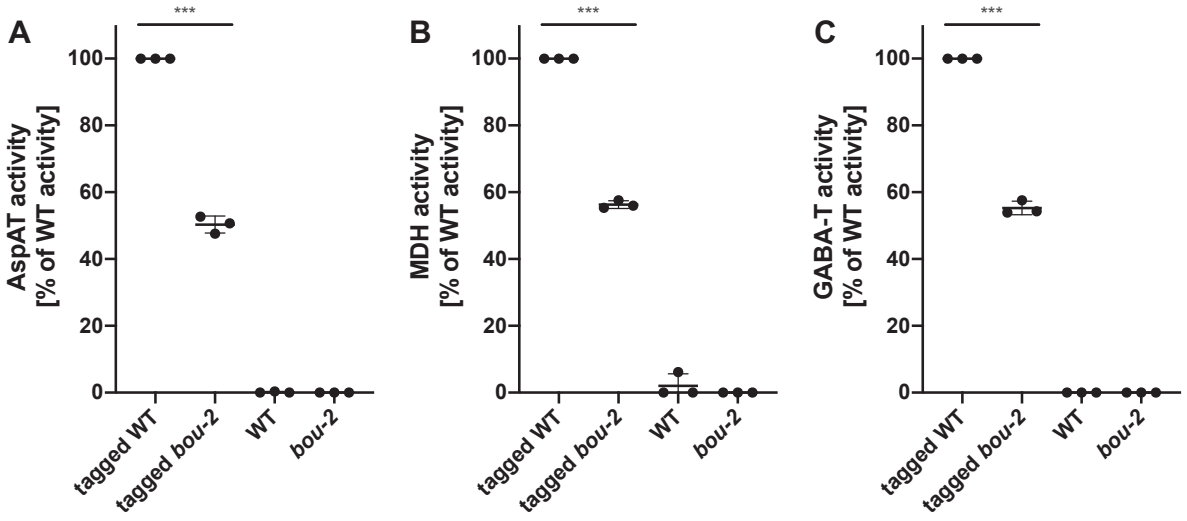

Supplemental Figure S5: Enzyme activities in rapidly isolated mitochondria. Mitochondria were rapidly isolated from 5-weeks old tagged WT, tagged *bou-2*, WT and *bou-2* leaf tissue grown under elevated CO_2 conditions (0.3% [v/v] CO_2) after shift to ambient CO_2 conditions (0.038% [v/v] CO_2) for five days as described in Materials and Methods. (**A**) Aspartate aminotransferase (AspAT) activity. Average tagged WT activity: 1.13 ± 0.25 U mg^{-1} protein. (**B**) Malate dehydrogenase (MDH) activity. Average tagged WT activity: 18.1 ± 2.2 U mg^{-1} protein. (**C**) γ-Aminobutyric acid transaminase (GABA-T) activity. Average tagged WT activity: 27.6 ± 1.8 mU mg^{-1} protein. Values are given as mean ± SD of three biological replicates. Asterisks indicate statistically significant differences between means (***, $P < 0.001$; Student's *t*-test). WT, wildtype.

Supplemental Figure S6

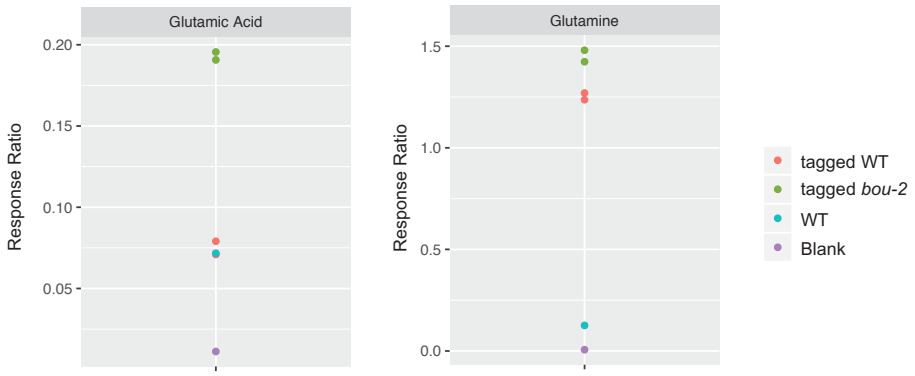

Supplemental Figure S6: Preliminary amino acid analyses in rapidly isolated mitochondria of tagged WT and tagged *bou-2*. Mitochondria of tagged WT (red circle), tagged *bou-2* (green circle) and WT (blue circle) were isolated as described in Materials and Methods. Amino acids were quantified by LC/MS as described in Materials and Methods. WT, wildtype.

Manuscript III

The Bile Acid Sodium Symporter 4 is Central to C_4 Metabolism in *Flaveria* Species

The Bile Acid Sodium Symporter 4 is Central to C_4 Metabolism in *Flaveria* Species

Franziska Kuhnert[1], Philipp Westhoff[2], Hiroaki Hanada[3], Yuri Munekage[3], Tsuyoshi Furumoto[4] and Andreas P. M. Weber[1]

[1]Institute of Plant Biochemistry, Cluster of Excellence on Plant Science (CEPLAS), Heinrich Heine University, Universitätsstrasse 1, 40225 Düsseldorf, Germany

[2]Plant Metabolism and Metabolomics Facility, Cluster of Excellence on Plant Science (CEPLAS), Heinrich Heine University, Universitätsstrasse 1, 40225 Düsseldorf, Germany

[3]Department of Bioscience, School of Science and Technology, Kwansei Gakuin University, 2-1 Gakuen, Sandan, Hyogo, 669-1337, Japan

[4]Institute of Department of Agriculture, Ryukoku University, 1-5, Yokotani, Oe-cho, Seta, Otsu, Shiga 520-2194, Japan

One-sentence summary: In *Flaveria bidentis* the plastidial bile acid sodium symport protein 4, catalyzing sodium driven malate symport *in vitro*, is of critical importance for the carbon concentrating mechanism during C_4 photosynthesis.

Author contribution: FK performed biochemical analyses, enzyme assays, extracted metabolites, analyzed data, designed experiments, and wrote the manuscript; PW performed metabolite analysis and analyzed the data; HH and YN generated and selected transgenic *Flaveria bidentis* plants; TF cloned constructs for *Flaveria bidentis* transformation and designed the research; APMW designed the researched and supervised the experiments.

ABSTRACT

The spatial distribution of CO_2 pre-fixation in mesophyll cells and decarboxylation in bundle sheath cells (BSC) enables C_4 plants to efficiently concentrate CO_2 around Rubisco. This minimizes the rate of photorespiration and increases water and nitrogen use efficiency. The evolution of two distinct cell types increased the transport steps per fixed molecule CO_2 from only one in C_3 to at least 10 in C_4 species, thus increasing the need of specialized transport proteins. However, only few of them have been characterized so far. Here, we characterized a protein of the bile acid sodium symport (BASS) family, BASS4. We show that BASS4 is a malate transport protein with a very defined substrate spectrum that is able to catalyze sodium-driven malate symport *in vitro*. Transcriptional repression of *BASS4* in *Flaveria bidentis* results in reduced growth and a carbon concentrating phenotype. Our results indicate that BASS4 functions as a BSC-specific malate translocator in C_4 *Flaveria* suggesting a novel malate transport system in the NADP-ME type clade.

INTRODUCTION

C_4 photosynthesis is characterized by the spatial separation of the photosynthetic carbon reactions in two distinct cell types. These cover the mesophyll cells (MC) and the bundle sheath cells (BSC). The separation of the biochemical reactions led to a concentration of atmospheric CO_2 at the site of Rubisco. This reduces the rate of photorespiration and increases photosynthetic efficiency. (Hatch and Slack, 1966; Hatch, 1987; von Caemmerer and Furbank, 2003). Key steps of this pathway are the primary fixation of CO_2 in the MC to a C_3 acid, shuttling of the formed C_4 acid towards the BSC, and its subsequent decarboxylation at the site of Rubisco (Hatch, 1987). Depending on the enzyme that catalyzes the decarboxylation reaction in the BSC, C_4 photosynthesis is generally classified into three biochemical subtypes: NAD-dependent malic enzyme (NAD-ME), NADP-dependent malic enzyme (NADP-ME), and phosphoenolpyruvate carboxykinase (PEP-CK) type (Hatch et al., 1975). However, in many species two or more of these subtypes coexist (Chapman and Hatch, 1981; Furbank, 2011; Pick et al., 2011; Wang et al., 2014b).

The transformable C_4 model species *Flaveria bidentis* (*F. bidentis*) belongs to the NADP-ME type group (Ku et al., 1983; Chitty et al., 1994; Meister et al., 1996). In all C_4 subtypes phosphoenolpyruvate (PEP) serves as substrate for PEPC-dependent carboxylation in MC. In the NADP-ME type, produced oxaloacetate (OAA) is imported into the MC chloroplast and converted into malate by NADP-dependent MDH. Malate is used as stable intermediate for intercellular transport from the MC to the BSC. Alternatively aspartate, produced from OAA via aspartate aminotransferase (AspAT) in MC chloroplasts, serves as C_4 carbon backbone for shuttling to the BSC (Hatch, 1987; Meister et al., 1996; Furbank, 2011). In *F. bidentis* aspartate accounts for 35–40% of the total carbon being assimilated in BSC chloroplasts (Meister et al., 1996). In BSC chloroplasts malate is decarboxylated via NADP-ME releasing CO_2 at the site of Rubisco. Produced pyruvate is transported to the MC for CO_2 acceptor regeneration (Hatch, 1987; Furbank, 2011).

In total, NADP-ME type C_4 species require at least ten transport steps per fixed molecule CO_2 and at least 30 to produce one molecule of triose phosphate (Weber and von Caemmerer, 2010). A key transport step is the import of malate into BSC chloroplasts. In the NADP-ME type C_4 species *Zea mays* (*Z. mays*) this step is catalyzed by the dicarboxylate transporter 2 (DCT2), likely in antiport with aspartate (Weissmann et al., 2016). In comparative transcriptomic analyses it could be shown that *DCT2* is significantly enriched in C_4 species compared to C_3. The transcript is enriched in BSC compared to MC, and its expression along a developmental leaf gradient coincides with the expression of known C_4 genes (e.g. *NADP-ME*, *PPDK*; Pick et al., 2011; Tausta et al., 2014; Wang et al., 2014a; Ding et al., 2015; Denton et al., 2017). The transcriptional observations are further confirmed

by proteomics studies (Taniguchi et al., 2004; Bräutigam et al., 2008; Majeran et al., 2008; Majeran et al., 2010). However, in *F. bidentis*, *DCT2* is not highly expressed, it shows no differential expression between MC and BSC or between C_3 and C_4 *Flaveria* species (Furumoto et al., 2011; Billakurthi et al., 2018). Previously it was shown that the protein has higher activity for succinate and fumarate than malate (Renné et al., 2003). Taken together this suggests that in *F. bidentis* the malate import into BSC chloroplasts is catalyzed by a so far unknown transport protein.

An excellent model to study not only C_4 photosynthesis but also the evolution from C_3 to C_4 is the genus *Flaveria* as it contains C_3, C_3-C_4 intermediate, C_4-like and C_4 species within one closely related group (Ku et al., 1983; McKown et al., 2005; Gowik et al., 2011). By analyzing transcript abundancies between the C_3 species *F. pringlei* and the closely related C_4 species *F. trinerva* and *F. bidentis* candidates for transport proteins of the core C_4 pathway could be identified. Candidates were chosen based on the assumptions that (1) the gene encoding the transport protein should be expressed to a higher degree in the C_4 species, (2) its expression should be regulated by light, and (3) it should contain a plastid transit peptide (Furumoto et al., 2011). Following these criteria a member of the bile acid sodium symport (BASS) family, BASS2, could be identified and characterized as pyruvate/sodium symporter in *Arabidopsis thaliana* and *Flaveria*. In *Flaveria BASS2* transcript is extremely abundant in C_4 compared to C_3 species. *BASS2* transcript accumulates in leaves during the light period and its abundance coincides with the abundance of *NADP-ME* and *PPDK* transcript. The protein is more abundant in MC compared to BSC chloroplasts, indicating an essential function within the C_4 pathway (Furumoto et al., 2011; Billakurthi et al., 2018).

Proteins of the BASS family were first identified in the mammalian liver (Alrefai and Gill, 2007), but were later found to be present in plants as well (Gigolashvili et al., 2009; Furumoto et al., 2011; South et al., 2017). Arabidopsis BASS1 was recently described as plastidial pantoate transporter (Huang et al., 2018). BASS5 has previously been identified as a component of the glucosinolate biosynthetic pathway in Arabidopsis (Gigolashvili et al., 2009), whereas Arabidopsis BASS6 is a glycolate transporter involved in photorespiration (South et al., 2017). As BASS4 in plants has not been characterized so far and shows a C_4-like expression pattern in comparative transcriptomic analyses (Furumoto et al., 2011; Billakurthi et al., 2018), we hypothesize that it functions as malate importer of BSC chloroplasts with special importance in C_4 photosynthesis.

RESULTS

BASS4-1 is a malate transporter in the C_4 species *F. bidentis*

The Bile Acid Sodium Symporter (BASS) family comprises of transport proteins that are well conserved among pro- and eukaryotes (Alrefai and Gill, 2007; Furumoto et al., 2011; Claro da Silva et al., 2013). In plants, they are localized to the inner envelope of plastids and defined by a broad substrate spectrum ranging from small solutes to vitamins (Gigolashvili et al., 2009; Furumoto et al., 2011; South et al., 2017; Huang et al., 2018). In *F. bidentis* two genes could be identified from transcriptomics data that encode for BASS4 (Furumoto et al., 2011), which were named *BASS4-1* and *BASS4-2*. The respective proteins share 69% sequence identity (Supplemental Fig. S1A; Madeira et al., 2019) and contain predicted plastid transit peptide of 66 amino acids (FbBASS4-1) and 39 amino acids (FbBASS4-2). Further six to ten transmembrane domains are predicted respectively (Supplemental Fig. S1B, Supplemental Fig. S1C; Sonnhammer et al., 1998; Krogh et al., 2001). FbBASS4 shows homology to proteins from *F. trinerva*, *F. pringlei*, *Sorghum bicolor* (*S. bicolor*; Sb09g237100), *Oryza sativa* (Os02g32930), and *Arabidopsis thaliana* (*A. thaliana*; At3g56160) that are predicted BASS4 proteins (Furumoto et al., 2011). However, none of the homologous proteins have been characterized to date.

To identify substrates of FbBASS4-1 and FbBASS4-2 both proteins were heterologously expressed in yeast (*Saccharomyces cerevisiae*) for following in vitro analysis by transport assays. Recombinant protein expression was improved by predicted plastidial transit peptide removal, previously shown to influence expression levels in non-plant hosts (Renné et al., 2003). Upon heterologous expression proteins had a calculated molecular mass of 42.1 kDa for FbBASS4-1 and 45.9 kDa for FbBASS4-2, and accumulated in yeast membranes (Supplemental Fig. S2A). Yeast membranes were isolated, reconstituted into a liposome system in which liposomes were either preloaded with or without malate, and the uptake of externally added radioactive labeled malate was measured (Supplemental Fig. S2B). Empty vector served as control to test for endogenous activity of the isolated yeast membranes which was subtracted from the samples with heterologously expressed protein. Liposomes reconstituted with FbBASS4-1 protein showed high rates of malate homo-exchange activity (Fig. 1A) whereas those reconstituted with FbBASS4-2 showed no uptake (Fig. 1B). Uptake experiments with FbBASS4-2 were repeated with different concentration of malate, aspartate and 2-oxoglutarate (2-OG) as substrates, and protein expressed in the Wheat germ cell-free expression system with the same result (data not shown).

In a detailed biochemical analysis heterologously expressed BASS4 shows no transport activity for different substrates of the core C_4 pathway (Fig. 1C; alanine, aspartate, pyruvate). Also no activity was detectable for known substrates of dicarboxylate transporters from

Arabidopsis, spinach and maize (Fig. 1C; glutamate, 2-OG, OAA; Weber et al., 1995; Taniguchi et al., 2002; Renné et al., 2003).

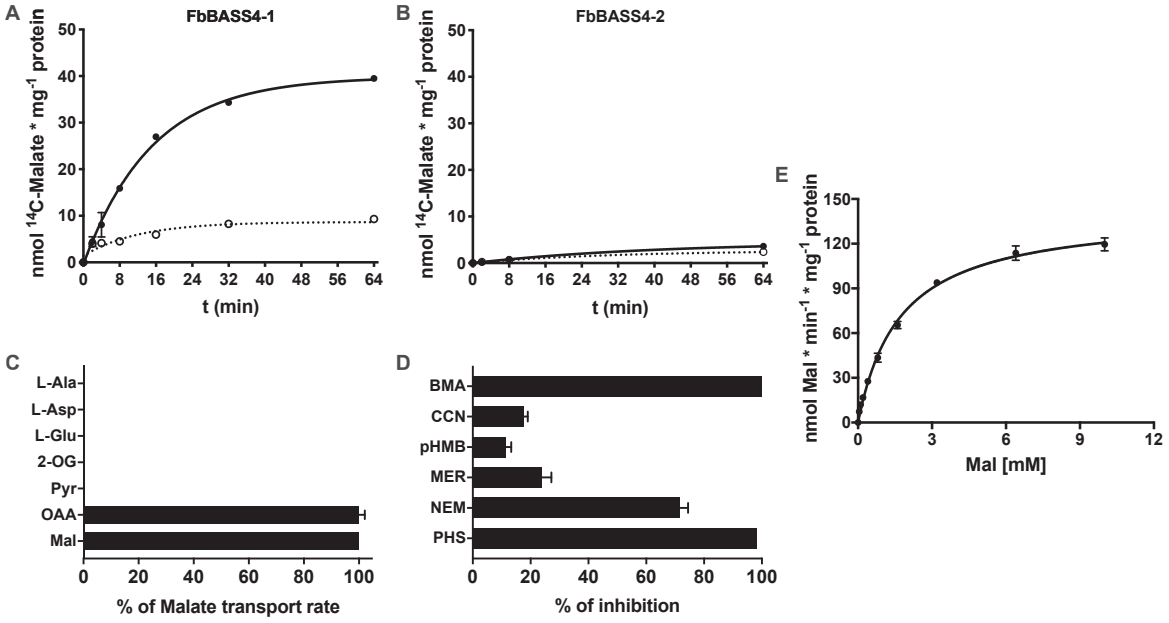

Figure 1: Biochemical characterization of FbBASS4. Representative malate uptake of FbBASS4-1 (**A**) and FbBASS4-2 (**B**). Proteins were heterologously expressed in yeast, reconstituted into liposomes with (filled symbols, solid line) or without (open symbols, dotted line) preloading of 20 mM malate, and transport was initiated by adding 0.2 mM malate/^{14}C-labeled malate to proteoliposomes. Samples were taken after 2, 4, 8, 16, 32 and 64 min and the radioactivity in the liposomes was measured by liquid scintillation counting. Values represent mean ± SD of technical triplicates. Substrate specificity of FbBASS4-1 (**C**). Proteoliposomes were preloaded with 20 mM alanine (L-Ala), aspartate (L-Asp), glutamate (L-Glu), 2-oxoglutarate (2-OG), pyruvate (Pyr), oxaloacetate (OAA) or malate (Mal). Transport was measured in homo-exchange (same substrate in and out; L-Ala, L-Asp, L-Glu, 2-OG, Mal) or hetero-exchange (different substrate in and out; Pyr, OAA; with Mal as external substrate) manner. Transport experiment was performed as described above. Transport rate was calculated from initial velocities. Malate transport rate was set to 100%. Values are given as mean ± SD of three independent experiments. Effect of different inhibitors on the malate transport rate of FbBASS4-1 (**D**). Proteoliposomes were preloaded with 20 mM malate. Transport experiment was performed as described above. Inhibitors were added 2 min before the ^{14}C-labeled malate in the following concentrations: butylmalonic acid (BMA) 5 mM, α-cyano-4-hydroxycinnamic acid (CCN) 1 mM, *p*-Hydroxymercuribenzoic (pHMB) 0.1 mM, mersalyl (MER) 0.1 mM, N-ethylmaleimide (NEM) 1 mM, and phenylsuccinic acid (PHS) 5 mM. Transport rate was calculated from initial velocities. Values are given as mean ± SD of three independent experiments. Michaelis-Menten-Plot of FbBASS4-1 (**E**). Liposomes were preloaded with 20 mM malate. Uptake of external malate (0–10 mM) was measured for 10 min, reactions were stopped with BMA, and the radioactivity in the liposomes was measured by liquid scintillation counting. Malate transport rate was calculated from initial velocities. K_m was calculated from Michaelis-Menten-Plot. Values represent mean ± SD of three replicates. R^2 = 0.995.

These results were confirmed with inhibitor studies. Malate transport rate of FbBASS4-1 was inhibited to almost 100% with butylmalonic acid (BMA) and phenylsuccinic acid (PHS) which are substrate analogs of malate (Fig. 1D). α-Cyano-4-hydroxycinnamic acid (CCN) has previously been used as a classic inhibitor of monocarboxylate transport systems that

catalyze uptake of lactate and pyruvate (Halestrap et al., 1980). In line with our result on the substrate specificity of FbBASS4-1 it inhibits the malate transport rate only to 17.5% (Fig. 1D). *p*-Hydroxymercuribenzoic acid (pHMB) and mersalyl (MER) have previously been reported as inhibitors of dicarboxylate and phosphate carriers that reversibly bind to SH-groups of cysteine residues (Palmieri et al., 1974). They lead to an inhibition of the malate transport rate of about 12% (pHMB) and 24% (MER), respectively (Fig. 1D). N-ethyl-maleimide (NEM) irreversibly binds to SH-groups of cysteine residues (Smyth et al., 1964). It results in a 72% inhibition of the malate transport rate (Fig.1D).

Table 1: $K_{m,\ app}$ of malate for recombinant dicarboxylate transporter from different C_3 (*S. oleracea*, *A. thaliana*) and C_4 (*Z. mays*, *S. bicolor*, *F. bidentis*) species. K_m values were taken from previous studies as indicated in the 'Reference' column. K_m of *F. bidentis* BASS4-1 was calculated from Michaelis-Menten plot. The value represents mean ± SE of three independent experiments.

Protein	Organism	$K_{m,\ app}$ [mM]	Reference
Dit1	*S oleracea*	0.35 ± 0.03	Renné et al., 2003
Dit2	*S. oleracea*	0.30 ± 0.10	Renné et al., 2003
Dit1	*A. thaliana*	0.70	Taniguchi et al., 2002
Dit2.1	*A. thaliana*	0.41	Taniguchi et al., 2002
OMT	*Z. mays*	0.61 ± 0.07	Taniguchi et al., 2004
DCT1	*Z. mays*	1.10 ± 0.10	Taniguchi et al., 2004
DCT2	*Z. mays*	0.85 ± 0.44	Taniguchi et al., 2004
DCT1	*S. bicolor*	1.24 ± 0.14	Weissmann et al., 2019
DCT2	*S. bicolor*	0.71 ± 0.10	Weissmann et al., 2019
DCT4	*S. bicolor*	1.13 ± 0.10	Weissmann et al., 2019
BASS4-1	*F. bidentis*	1.70 ± 0.09	Our study

Next, we analyzed the apparent K_m value of FbBASS4-1 to assess its physiological role *in vivo*. Therefore, we preloaded proteoliposomes with saturating concentrations of malate and measured the initial velocity of different externally applied malate concentrations (Fig. 1E). FbBASS4-1 is able to effectively transport malate. The protein has an apparent K_m of 1.7 ± 0.09 mM (Table 1). The given value is approximately threefold higher compared to the dicarboxylate carriers of the C_3 species *A. thaliana* and *Spinacia oleracea* (*S. oleracea*; Taniguchi et al., 2002; Renné et al., 2003). However, it is similar to reported K_m values for photosynthetic relevant dicarboxylate carriers in the C_4 species *Z. mays* and *S. bicolor* (Table 1; Taniguchi et al., 2004; Weissmann et al., 2016; Weissmann et al., 2019).

Our biochemical data indicate that FbBASS4-1 is a malate-specific transport protein with a very defined substrate spectrum that is efficiently able to transport malate in the C_4 species *F. bidentis* (Fig. 1).

FbBASS4-1 catalyzes sodium-driven malate symport *in vitro*

As shown above, FbBASS4-1 is a transport protein that shows uptake activity for OAA and is able to efficiently transport malate *in vitro* (Fig. 1). Previous studies on dicarboxylate transporters revealed that they are antiporters that mediated malate transport with a counter exchange substrate (e.g. aspartate, glutamate, 2-OG ,OAA; Weber et al., 1995; Taniguchi et al., 2002; Renné et al., 2003; Weissmann et al., 2016). However, FbBASS4-1 is not a classical dicarboxylate transporter as its substrate specificity is restricted to malate and OAA. It is a member of the BASS family of which many carriers have shown to catalyze sodium-driven symport of their respective substrates (Alrefai and Gill, 2007; Furumoto et al., 2011). Thus, we hypothesize that FbBASS4-1 catalyzes sodium-driven malate symport *in vitro*.

Within the C_4 cycle of the NADP-ME type species *Z. mays*, malate import into BSC chloroplasts is catalyzed by the dicarboxylate transporter 2 (ZmDCT2), likely in antiport with aspartate (Weissmann et al., 2016). The protein is a well characterized transporter that can be heterologously expressed and actively reconstituted into liposomes (Taniguchi et al., 2002). Thus, we used it as a control for our following analysis. Both, ZmDCT2 and FbBASS4-1 proteins showed *in vitro* malate-dependent uptake activity in a homo-exchange manner (Fig. 2A). At the given malate concentration the activity of ZmDCT2 is higher than that of FbBASS4-1, as it has a higher initial velocity and reaches the plateau much earlier even though protein expression was much lower (Fig. 2A, B). However, expression of FbBASS4-1 was optimized for yeast, ZmDCT2 expression not and we cannot comment on the amount of actively expressed protein. Interestingly, FbBASS4-1 also catalyzed malate sym- or uniport, whereas ZmDCT2 does not (Fig. 2A). With our liposome system an antiporter like ZmDCT2 can only show uptake for an external substrate if the liposomes have been preloaded with a counter-exchange substrate. If the liposomes are not preloaded and consequently the counter-exchange substrate is lacking no uptake can be observed. FbBASS4-1 shows uptake activity without preloading of substrate indicating a possible uni- or symport activity of the protein. Since the protein belongs to a family of transporters that have shown to catalyze sodium-driven symport of their substrates (Alrefai and Gill, 2007; Furumoto et al., 2011), we hypothesize that the observed activity without preloading is due to a sodium-dependent symport activity of FbBASS4-1.

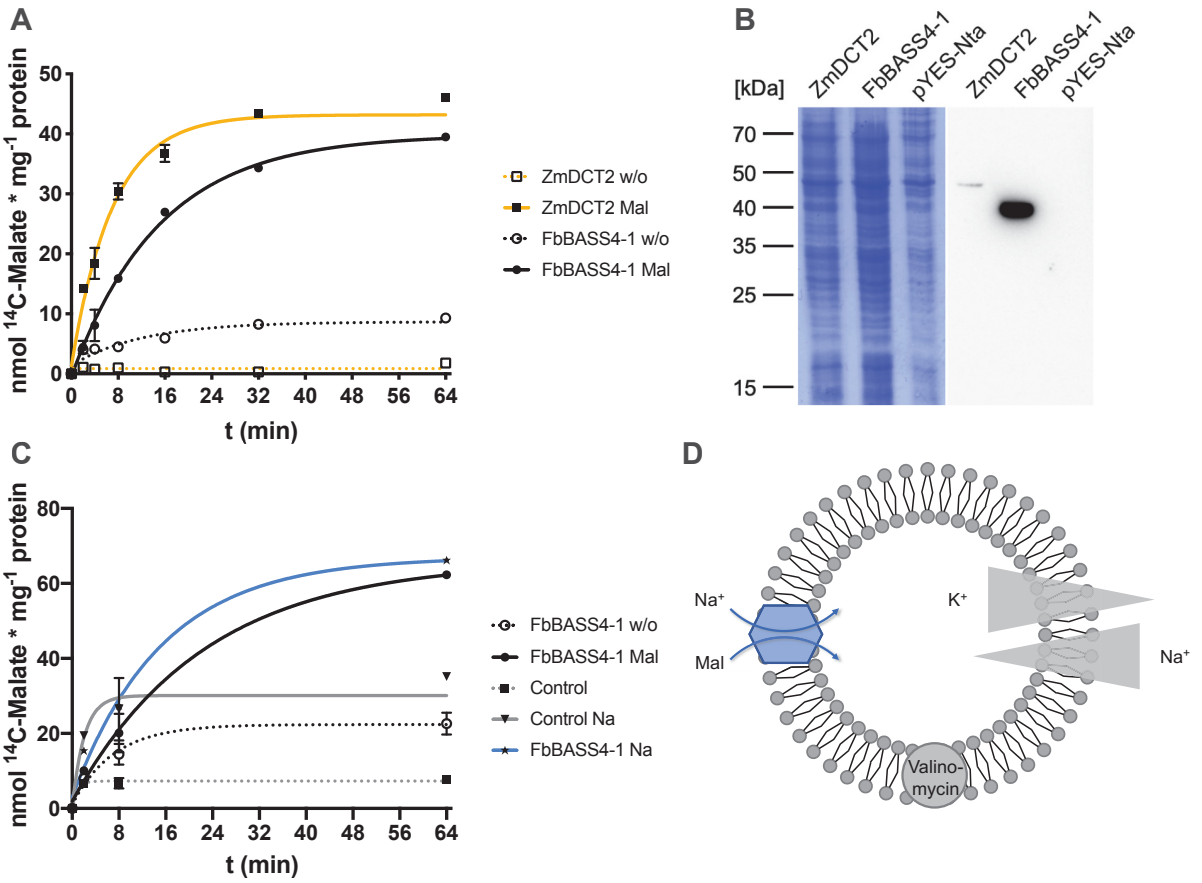

Figure 2: Analysis of the transport mechanism of FbBASS4-1. Representative picture of the malate homo-exchange activity of FbBASS4-1 (circles, black) and ZmDCT2 (squared symbols, yellow). (**A**). Proteins were heterologously expressed in yeast, reconstituted into liposomes with (filled symbols, solid line) or without (open symbols, dotted line) preloading of 20 mM malate, and transport was initiated by adding 0.2 mM malate/^{14}C-labeled malate to proteoliposomes. Samples were taken after 2, 4, 8, 16, 32 and 64 min and the radioactivity in the liposomes was measured by liquid scintillation counting. Values represent mean ± SD of technical triplicates. Isolated yeast membranes harboring the expressed proteins FbBASS4-1, ZmDCT2, and the empty vector control pYES-Nta (**B**). Yeast membranes were isolated as described in Materials and Methods. 20 µg each were separated on a 12% SDS-PAGE and transferred onto a nitrocellulose membrane. Membranes were probed with Anti-His antibody coupled to horse radish peroxidase. Proteins were visualized using a chemiluminescent detection system. Representative picture of sodium-driven malate symport activity of FbBASS4-1 (**C**). Samples of FbBASS4-1 without (open circles, dotted black line), with 20 mM malate preloading (filled circles, black line), and a control (filled squared symbols, grey dotted line) were reconstituted using the malate homo-exchange system. Samples of FbBASS4-1 (star symbols, blue line) and the control (triangle symbols, grey solid line) were reconstituted using the sodium-symport system as described in Materials and Methods. Transport was initiated by adding 0.2 mM malate/^{14}C-labeled malate and 3 nM valinomycin to proteoliposomes. Samples were taken after 2, 8, and 64 min and the radioactivity in the liposomes was measured by liquid scintillation counting. Values represent mean ± SD of technical triplicates. Schematic representation of the sodium system (**D**). Liposomes were created with an outward-facing potassium gradient that is balanced by an inward-facing sodium gradient. The reaction was initiated by adding radioactive-labeled malate and valinomycin, a potassium-selective ionophore, to proteoliposomes. Blue hexagon represents reconstituted transport protein.

To test whether FbBASS4-1 can catalyze sodium-driven malate symport we set up a liposome system which is capable of measuring malate uptake in a sodium-dependent manner. We created liposomes with an inward-facing sodium gradient that is balanced by an outward-facing potassium gradient. Transport was initiated by the addition of radioactive labeled malate and valinomycin. Valinomycin is a potassium selective ionophore that can integrate itself into biological membranes due to its hydrophobic nature (Pressman, 1976). It facilitates the transport of potassium ions down the electrochemical gradient, in our system out of the liposomes. This in turn will lead to an influx of sodium ions along the concentration gradient. If FbBASS4-1 is a sodium-dependent malate transporter, it should be able to use the generated sodium gradient to import the radioactive labeled malate to the same extent as in the homo-exchange system (Fig. 2D). As a control we used isolated yeast membranes from an empty vector control. FbBASS4-1 showed uptake activity for malate in our sodium-dependent system that was comparable with the malate uptake in the homo-exchange system (Fig. 2C). The control showed a higher uptake in the sodium-dependent system as well. However, the uptake of the control reached the plateau already within the first 8 min of the reaction (Fig. 2C). Most likely this is due to a higher rate of diffusion as we applied several gradients and created a membrane potential.
From our results, we conclude that FbBASS4-1 can catalyze sodium-driven malate symport in an *in vitro* system.

FbBASS4 knockdown lines are impaired in growth and show a carbon concentrating phenotype

To analyze the functional role of FbBASS4-1 *in vivo* we generated *FbBASS4* knockdown lines via RNA interference (RNAi) using the coding sequence of *F. trinerva* BASS4 as template. Plasmids were integrated into the pHannibal/pKannibal vector system and subsequently introduced into *Agrobacterium tumefaciens* (*Agrobacterium*; Lazo et al., 1991; Gleave, 1992). *F. bidentis* were transformed by co-cultivating *Agrobacteria* containing the RNAi construct with hypocotyls of the plants. Regenerated shoots were selected on *Agrobacterium*-free medium. The first transformation event resulted in four independent lines namely *FbBASS4 2-4*, *FbBASS4 4-5*, *FbBASS4 7-6*, and *FbBASS4 9-3*. They showed a strong reduction in *FbBASS4* transcript in the T1 generation (data not shown). Plants in the T1 generation showed a carbon concentrating phenotype as they required at least 0.08% (v/v) CO_2 under high light conditions (500 µmol m^{-2} s^{-1}). Furthermore, a preliminary analysis showed that they were characterized by a reduced CO_2 assimilation rate and an increased CO_2 compensation point (data not shown). The values were similar to that of C_3 *Flaveria* indicating that BASS4 plays a role in the carbon concentrating pathway. The selected transgenic lines that showed a carbon concentrating phenotype (*FbBASS4 2-4*, *FbBASS4 4-5*, *FbBASS4 7-6*, and *FbBASS4 9-3*) were grown to seed. Transgenic lines of

the T2 generation were delayed in germination and strongly reduced in growth (Fig. 3A, B). They required elevated CO_2 (0.08% [v/v] CO_2) under high light conditions (500 µmol m^{-2} s^{-1}) but were able to grow at ambient CO_2 (0.038% [v/v] CO_2) under low light (150 µmol m^{-2} s^{-1}). More individuals are currently propagated by shoot cuttings to repeat experiments on CO_2 assimilation rate, CO_2 compensation point and transcript abundance in the mutants compared to wildtype.

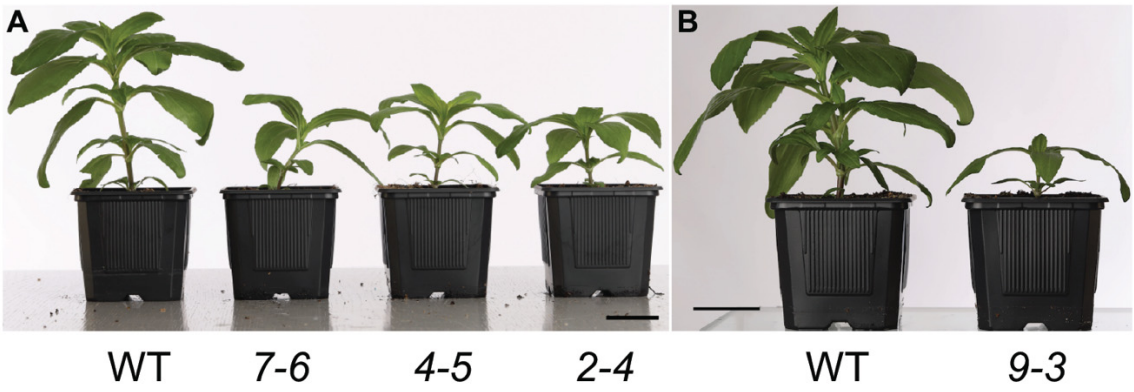

Figure 3: Growth phenotype of *F. bidentis* wildtype (WT) and *BASS4* knockdown lines. Approximately 10 week old *F. bidentis* WT and *BASS4* RNAi lines *7-6*, *4-5*, and *2-4* grown in elevated CO_2 conditions (0.3% [v/v] CO_2; **A**). Scale bar = 4 cm. Approximately 10 week old *F. bidentis* WT and *BASS4 9-3* knockdown plants grown in elevated CO_2 conditions (0.3% [v/v] CO_2; **B**). Scale bar = 4 cm.

Effect of *BASS4* knockdown on metabolite levels and enzyme activities

To assess the physiological role of FbBASS4-1 on the C_4 metabolism in *F. bidentis* we selected the transgenic line *BASS4 9-3* for an initial metabolomics experiment. WT and *BASS4 9-3* plants were grown in elevated CO_2 conditions (0.3% [v/v] CO_2) for approximately 10 weeks until they had a fully developed fourth leaf pair as previous analyses showed that expression of *BASS4* coincides with transcript abundance of the photosynthetic genes *NADP-ME* and *PPDK* and is strongest in fully developed leaves (Billakurthi et al., 2018). The fully developed fourth leaf pair was harvested at the end of the light period in elevated CO_2 conditions (0.3% [v/v] CO_2; HC EOD) and 12 h (AC + 12h), 15 h (AC + 15h), and 39 h (AC + 39h) after shift to ambient CO_2 conditions (0.038% [v/v] CO_2). Plants with reduced *BASS4* expression showed only minor changes in the core C_4 metabolites (Fig. 4A). Malate tended to be reduced at all time points whereas pyruvate tended to be increased (Supplemental Fig. S4). Aspartate and alanine tended to be increased at the first two time points, their levels reverted back to WT levels 15 h after shift to ambient CO_2 and were reduced 39 h after the shift. However, except for the reduction in malate in *BASS4 9-3* at elevated CO_2, and 12 h and 39 h after shift to ambient CO_2 none of the changes were significant (Supplemental Fig. S4).

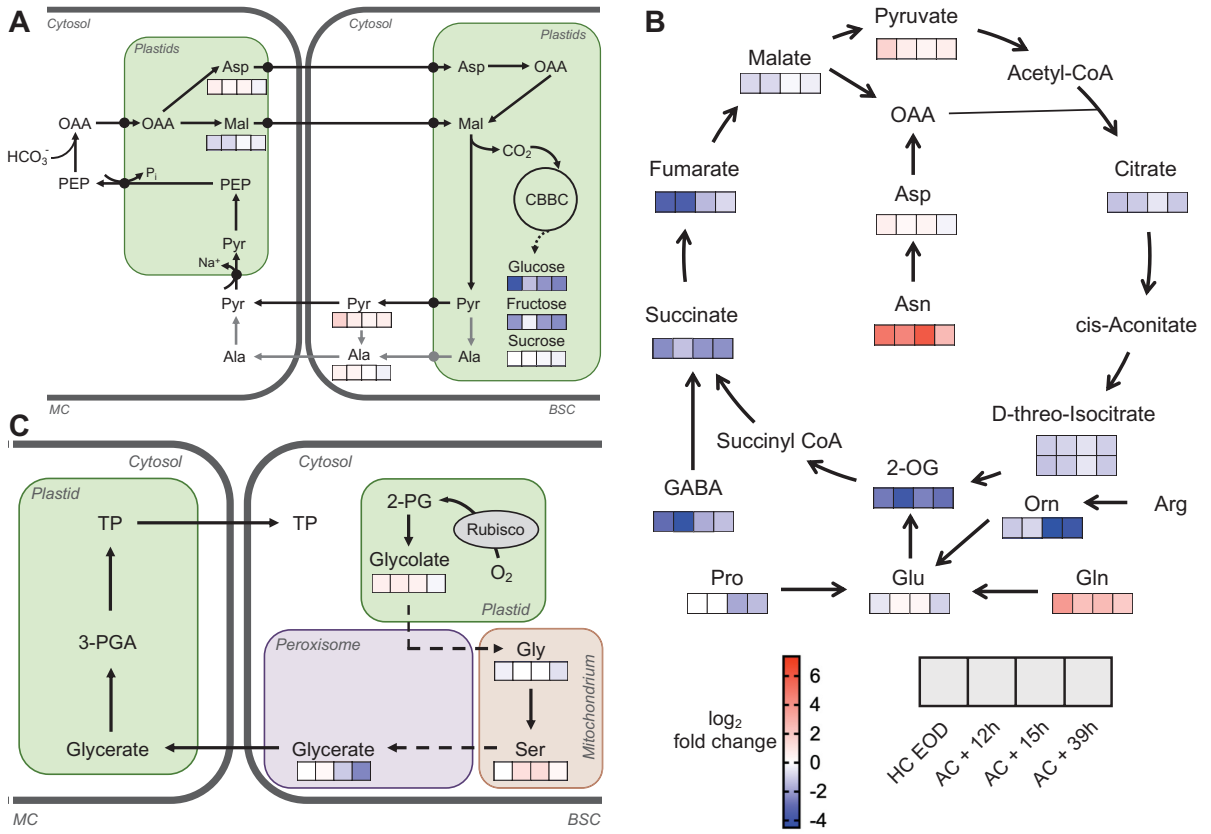

Figure 4: Selected changes in metabolites in WT and *BASS4 9-3* leaves. Schematic depiction of the carbon concentrating mechanism in the NADP-ME type species *F. bidentis* (**A**). Black circles represent transport steps. Grey lines and circles indicate reactions for which more detailed information is needed. Schematic depiction of the TCA cycle including pyruvate with selected anaplerotic reactions (**B**). Distribution of photorespiration between MC and BSC in C_4 plants (**C**). Dashed lines indicate reaction with several transformation steps. Changes are displayed as $\log_2$ fold change from reduced in *BASS4 9-3* blue to increased in red. Samples were taken at the end of the light period after approximately 10 weeks growth in elevated CO_2 conditions (0.3% [v/v] CO_2; HC EOD), and 12 h (AC + 12h), 15 h (AC + 15h), and 39 h (AC + 39h) after shift to ambient CO_2 conditions (0.038% [v/v] CO_2). Two panels are shown for isocitrate due to an overlap in the retention time with citrate. Abbreviations: CBBC, Calvin-Benson-Bassham cycle BSC, Bundle sheath cell; GABA, *gamma*-Aminobutyric acid; MC, Mesophyll cell; OAA, Oxaloacetate; 2-OG, 2-oxoglutarate; Orn, Ornithine; PEP, Phosphoenolpyruvate; 2-PG, 2-Phosphoglycolate; 3-PGA, 3-Phosphoglycerate; Pyr, Pyruvate; TP, Triose phosphate.

In addition to the changes in C_4 metabolites we could observe a significant reduction of glucose, fructose, maltose and sucrose levels 39 h after shift to ambient CO_2 conditions (Fig. 4A; Supplemental Fig. S4). Surprisingly, we found that metabolites of the TCA cycle are strongly reduced in the mutant as well as additional metabolites that could feed into the cycle via different anaplerotic pathways (e.g. GABA shunt, proline degradation, urea cycle). This indicates that the redox state of the plant especially the mitochondria is impaired. Interestingly, levels of glutamine and arginine were increased in the mutant indicating an imbalance in nitrogen metabolism (Fig. 4B, Supplemental Fig. S4). In addition to the accumulation of glutamine and asparagine, we also saw accumulation of the amino acids

methionine, phenylalanine, tryptophan, and lysine which could indicate that carbon is redirected into the biosynthesis of amino acids in the mutant (Supplemental Fig. S4). The photorespiratory intermediates glycolate and serine were increased in the mutant whereas glycerate was reduced. Glycolate was increased in the first three time points but reverted back to WT level 39 h after shift to ambient CO_2 conditions. Glycerate was not changed in plants grown at elevated CO_2 and 12 h after shift to ambient CO_2. However, it was reduced 15 h after shift. The effect was even more pronounced 39 h after shift. The serine content was not changed in samples taken from elevated CO_2 conditions. It was increased 12 h and 15 h after shift and reverted back to WT levels 39 h after shift (Fig. 4C; Supplemental Fig. 4). In C_4 plants serine is likely converted into glycerate in peroxisomes of BSC and then shuttled towards chloroplasts of MC where it gets converted into 3-phosphoglycerate (Weber and von Caemmerer, 2010; Levey et al., 2019). Conversion of serine into glycerate in BSC peroxisomes is dependent on redox power generated by malate. With reduced malate availability in BSC these steps might be impaired leading to accumulation of serine and reduction in glycerate content in the mutant.

In addition, the knockdown of *BASS4* resulted in altered activities of selected enzymes (Fig. 5A-F). With reduced malate availability we expected changes in the activities of the core C_4 enzymes NADP-MDH in chloroplasts of MC and NADP-ME in chloroplasts of BSC. However, the activity of both was not affected in the mutant under any of the applied conditions (Fig. 5A, B). NADP-ME activity was significantly increased after 39 h after shift to ambient CO_2 conditions (Fig. 5B). If the plants cannot efficiently shuttle malate due to reduction of *BASS4* expression but are able to maintain decarboxylation activity in the BSC, we expected more carbon shuttled in form of aspartate. Indeed, we saw not only increased levels of aspartate in the mutant but also significantly increased AspAT under all conditions (Fig. 5C). If more aspartate is shuttle towards the BSC due to reduced malate availability, we would expect that increased levels of alanine are shuttled back towards MC, to maintain nitrogen balance between the two cell types. Consequently, with this hypothesis we observed increased levels of alanine in the mutant and significantly increased alanine aminotransferase (AlaAT) activities (Fig. 5D). However, we cannot comment on the actual flux of carbon as this requires a detailed $^{13}CO_2$ labelling experiment.

Interestingly, we found in our metabolite analysis that intermediates of the TCA cycle are strongly reduced whereas glutamine and asparagine are increased (Fig. 4B) indicating a possible impairment of the redox state of the mitochondria and an imbalance of nitrogen metabolism. Therefore, we assayed NAD-dependent MDH (NAD-MDH) and glutamate dehydrogenase (GluDH) activity. Both enzyme activities are significantly increased in the mutant grown at elevated CO_2 conditions and 12 h after shift to ambient CO_2 (Fig. 5E, F).

Levels of NAD-MDH reverted back to WT levels 15 h after the shift and were significantly reduced 39 h after shift to ambient CO_2 (Fig. 5E). GluDH was significantly increased in the mutant 15 h after shift to ambient CO_2 and reverted back to WT levels 39 h after the shift (Fig. 5F). In line with the metabolite dataset this could indicate an impairment in mitochondrial metabolism. However, all enzyme activities were assayed in total leaf extracts. Therefore, we cannot comment on the individual activities of the different isoforms. Consequently, it is not clear which isoform(s) is (are) affected in the mutant. Additionally, we assayed isocitrate dehydrogenase activity but could not detect any activity in total leaf samples (data not shown). This likely requires enrichment of mitochondria.

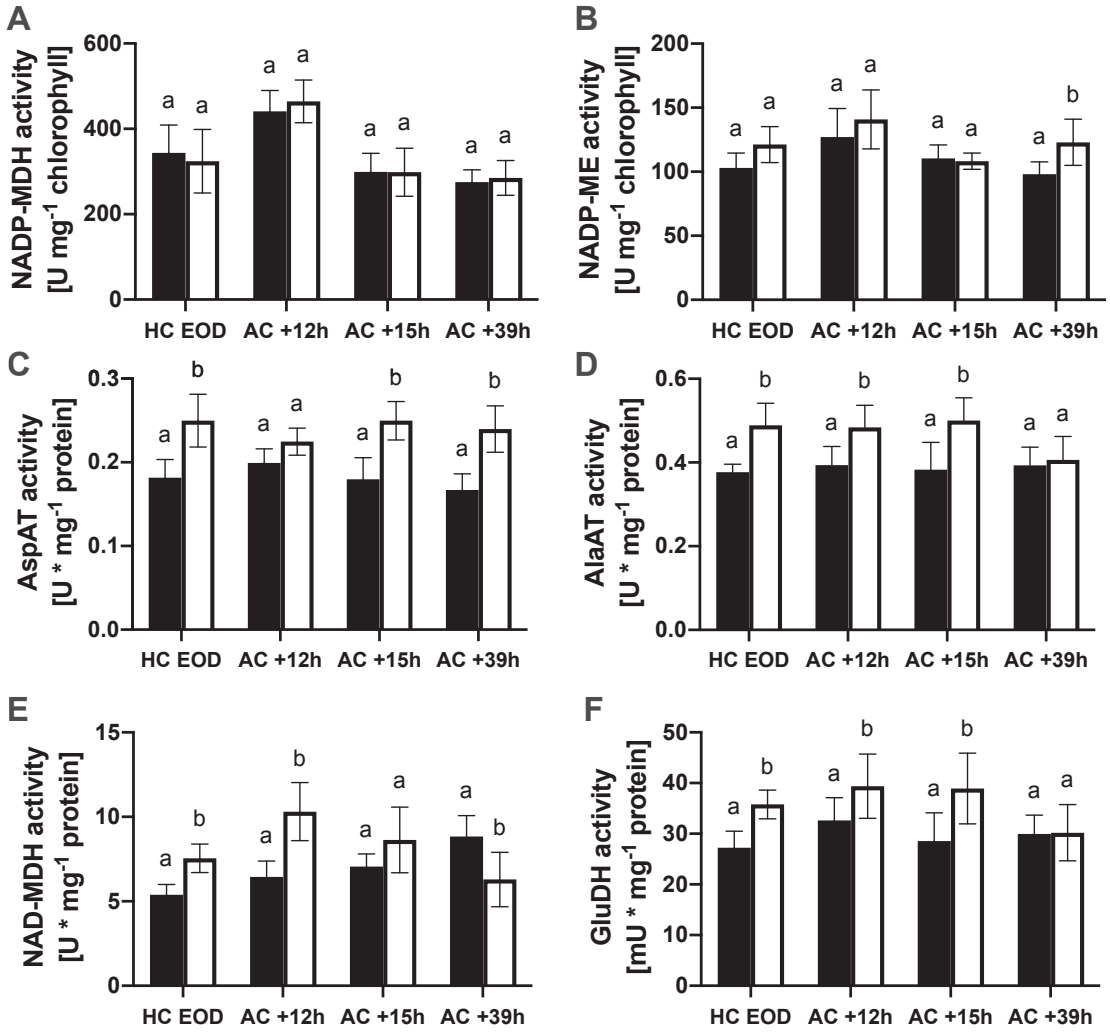

Figure 5: Enzyme activities of *F. bidentis* WT (black boxes) and *BASS4 9-3* (white boxes). The fully developed fourth leaf pair was sampled after approximately 10 weeks growth in elevated CO_2 conditions (0.3% [v/v] CO2; HC EOD) and 12 h (AC + 12h), 15 h (AC + 15h), and 29 h (AC + 39h) after shift to ambient CO_2 conditions (0.038% [v/v] CO_2). Activities of NADP-dependent malate dehydrogenase (NADP-MDH; **A**), NADP-dependent malic enzyme (NADP-ME; **B**) aspartate aminotransferase (AspAT; **C**), alanine aminotransferase (AlaAT; **D**), NAD-dependent malate dehydrogenase (NAD-MDH; **E**) and glutamate dehydrogenase (GluDH; **F**) were measured as described in Materials and Methods. Values represent means ± SD of three biological replicates. Letters indicate statistical significant differences between means ($P < 0.05$; one-way ANOVA).

DISCUSSION

BASS4 was previously identified by comparative transcriptomic analyses between C_3 and C_4 *Flaveria* species. It was suggested as a candidate for a BSC-specific malate importer because (1) its transcript is highly abundant in C_4 compared to C_3 *Flaveria*, (2) its expression coincide with the expression of the C_4 genes *NADP-ME* and *PPDK*, and (3) it has a predicted plastid transit peptide (Furumoto et al., 2011; Billakurthi et al., 2018). Genes encoding for BASS4 proteins are highly conserved among different C_4 species with homologs in Cleome, Sorghum and *Z. mays* (Furumoto et al., 2011). Previous results showed that *BASS4* is not highly expressed in Cleome which coincides with the fact that Cleome is categorized as NAD-ME type species which decarboxylate malate in mitochondria of BSC (Furumoto et al., 2011). In *Z. mays BASS4* is only weakly expressed as well (Pick et al., 2011; Wang et al., 2014a; Ding et al., 2015; Denton et al., 2017). Like *Flaveria* it belongs to the NADP-ME subtype in which mainly malate is decarboxylated in chloroplasts of BSC indicating the presence of different malate transport mechanisms within this C_4 subtype. Here, we describe the plastidic BASS4 protein as an integral part of the carbon concentrating mechanism in the C_4 plant *F. bidentis*.

Transport characteristic of FbBASS4-1 and FbBASS4-2

We analyzed the transport characteristics of FbBASS4-1 and FbBASS4-2 by using heterologously expressed protein in an artificial liposome system (Supplemental Fig. S2). FbBASS4-1 showed uptake activity for malate and OAA whereas FbBASS4-2 showed no uptake activity under any of the tested conditions (Fig. 1). Both, FbBASS4-1 and FbBASS4-2, share 69% sequence identity, are integral membrane proteins with an N-terminal plastid target peptide and could be successfully expressed in our heterologous yeast system (Supplemental Figs. S1, S2). As they are closely related proteins of the same transport family we are convinced that both can be actively expressed in the same system. However, it could be possible that the transport substrate of FbBASS4-2 was not among the tested. Alternatively, activators or auxiliary factors are needed that were not present in our system. Additionally, we cannot exclude that the gene encodes for a membrane protein without transport function or is a pseudogene that has no function anymore.

Interestingly, FbBASS4-1 has a very defined substrate spectrum. It showed activity exclusively for malate and OAA but not alanine, aspartate, glutamate, 2-OG, and pyruvate. Our data on the substrate specificity was supported by inhibitor studies with substrate analogs of malate (Fig. 1). All inhibitors were supplied in sufficient concentrations indicating that cysteine residues could play an important role in the transport mechanism as malate uptake was inhibited by NEM which irreversibly binds to cysteine residues (Smyth et al., 1964). Another possibility could be that disulfide bonds are important for the structure and

thus the functionality of the transport protein suggesting a possible redox regulation of the protein. The reversible binding of cysteine residues by pHMB and MER showed a much lower percentage of inhibition likely due to sufficient concentrations of malate (Fig. 1). We found that FbBASS4-1 catalyzes sodium-driven malate symport *in vitro* (Fig. 2). Therefore, we set up a liposome system with an inward-facing sodium gradient which is balanced by an outward-facing potassium gradient. We could not use the gluconate system for our measurements as the uptake of externally added malate without the simultaneous export of a charged counter-exchange substrate will lead to the formation of a membrane potential which in turn will inhibit the uptake activity. We performed the experiment with the gradients five times independently. Out of those, three times the uptake in our sodium-system was as high as the malate uptake in the homo-exchange system. Two times it was lower but still higher compared to the negative control. The liposomes for our uptake experiments were prepared by sonication, and membrane proteins reconstituted via the freeze-thaw procedure. Generally this leads to the production of small not very uniformly vesicles (Lasic, 1988). Therefore, different reconstitution events lead to differently sized proteoliposomes. They strongly differ in their internal volume and thus the amount of reconstituted ions which led to varying results. To obtain constant uptake results with our sodium-system proteins should be reconstituted via the detergent removal method as this leads to the production of larger uniform vesicles (Lasic, 1988). We understand that the use of ion gradients in a liposome system is a challenging approach as this can lead to rupture and leakiness of the vesicles, and generally a higher rate of diffusion. However, we carefully designed and optimized the system with two ion gradients that balance each other to reduce the possibility of rupture of the liposomes due to osmotic pressure (Supplemental Fig. S3). We are currently considering additional control experiments to strengthen our results. Malate uptake should be in the range of the control when the gradients are reversed or lithium ions are used instead of sodium. To date we have not analyzed whether FbBASS4-1 might be able to catalyze proton-driven malate symport. In terms of pyruvate uptake, *Flaveria* has shown to be a sodium-dependent species in contrast to *Z. mays* which relies on a proton gradient (Ohnishi and Kanai, 1987; Ohnishi and Kanai, 1990; Furumoto et al., 2011). From our results we cannot exclude that malate transport is coupled to protons. However, setting-up a reproducible system to measure proton-coupled transport is challenging. Previously, it has been shown, that light-driven proton pumps like bacteriorhodopsin can be purified and actively reconstituted into liposome systems. They create proton gradients upon light illumination (Verchère et al., 2012; Lee et al., 2013; Veshaguri et al., 2016). To set up a stable proton-coupled transport system it should be considered to use a pump for the creation of a proton gradient rather than artificially diluting the proteoliposomes in a buffer with reduced pH.

Physiological role of BASS4 in *F. bidentis*

To assess the physiological role of BASS4 in *F. bidentis* we created transgenic lines with reduced *BASS4* expression via RNAi. The lines were delayed in germination, strongly impaired in growth, showed an increased CO_2 compensation point, and a reduced CO_2 fixation rate (Fig. 3). Interestingly, the values of the CO_2 compensation point and the CO_2 fixation rate were much more similar towards a C_3 *Flaveria* species than a C_4 indicating that the mutant is not able to efficiently concentrate CO_2 around Rubisco. However, the analysis was performed with T1 transformants and has to be repeated with the T2 generation and more replicates. Our preliminary metabolite analysis supports this hypothesis as mutant plants displayed reduction in sugars and TCA cycle intermediates likely due to a reduced availability of carbon because of a reduced rate of photosynthesis (Fig. 4; Supplemental Fig. 4). Interestingly, we found reduced levels of malate (Fig. 4; Supplemental Fig. 4). Generally this was not expected as the photosynthetic active malate pool accounts only for a small portion of the total malate pool in leaves (Hatch, 1979). Furthermore, we found increased levels of serine and a reduction of glycerate indicating a reduced availability of malate which is necessary for regeneration of NAD^+ during photorespiration in BSC peroxisomes (Fig. 4; Supplemental Fig. 4). Together with our data on enzyme activities, our data suggest that mutant plants are able to maintain decarboxylation rates by shuttling more carbon in form of aspartate (Figs. 4, 5; Supplemental Fig. 4). However, this in contrast to the significant reduction in sugar levels. Previous results suggested a correlation of increased AspAT activities in BSC chloroplasts as a result of carbon shuttled in form of aspartate with an increase in PSII activity as conversion of OAA into malate in BSC chloroplasts requires reducing equivalents (Meister et al., 1996). If the *BASS4* mutant is able to maintain decarboxylation activity in BSC by shuttling more carbon in form of aspartate it requires a higher amount of reducing equivalents in BSC chloroplasts. This might be achieved by an increase of PSII activity in BSC chloroplasts or by taking out NADPH from the CBBC. The latter would lead to a reduced CBBC activity and likely explain the observed reduction in sugar levels in the *BASS4* mutant. However, we are currently working on propagating more individuals from all transgenic lines to create full phenotype and metabolite data sets. Because it is impossible to understand carbon flux in the mutant lines with a steady state metabolite data set, we are considering labelling experiments with $^{13}CO_2$. With those experiments we will be able to decipher whether carbon is indeed mainly shuttled in form of aspartate and alanine in the mutant. Moreover, those data will help to understand whether the mutant extracts carbon from the TCA cycle to direct it into biosynthesis of sugars and amino acids or whether the mutant is not able to feed into the TCA cycle because of reduced carbon availability. For a better evaluation of our measured enzyme activities isolation of intact organelles should be considered as many of the enzymes we assayed have isoforms

in different cell compartments. Moreover, it would be advantageous to have isolated chloroplasts from both BSC and MC separately to not only measure enzyme activities of AspAT, NADP-MDH and NADP-ME but also to use them for determination of malate uptake rates. Generally, uptake with intact organelles has proven to be rather difficult because of the overlapping activities of different transport proteins within the membranes. However, if BASS4 is the main malate import protein in chloroplasts of BSC we would expect a strong difference in the malate transport capacity between wildtype and the mutant.

The BSC-specific localization of FbBASS4-1 is still under debate. From our results we cannot conclude that the protein is localized to chloroplasts of BSC. However, because of our current results on plant growth, metabolites levels, and enzyme activities we hypothesize that the protein plays a crucial role within the C_4 carbon concentrating mechanism. In the MC, OAA formed by the primary fixation reaction is imported into chloroplasts and converted into malate or aspartate. Both, malate and aspartate, need to be exported from chloroplasts of MC and diffuse towards the BSC (Hatch, 1987). Transport of malate and OAA across the inner envelope of MC chloroplasts is likely catalyzed by the 2-oxoglutarate/malate translocator (OMT1) which is enriched in MC of C_4 species (Taniguchi et al., 2002; Taniguchi et al., 2004; Bräutigam et al., 2008; Majeran et al., 2008; Majeran et al., 2010). *Z. mays* OMT1 shows high activity for malate and OAA and has been hypothesized to import OAA into chloroplasts of MC in exchange for malate (Taniguchi et al., 2004; Tausta et al., 2014). In *F. bidentis OMT1* is highly abundant and expressed in a C_4-like manner indicating it might have the same function as its *Z. mays* orthologue (Billakurthi et al., 2018). In *Z. mays*, malate is likely imported into chloroplasts of BSC by DCT2 (Weissmann et al., 2016). DCT2 is enriched in chloroplasts of BSC compared to MC in *Z. mays* and plants with reduced *DCT2* expression show reduced NADP-ME activity and pyruvate formation rates in isolated BSC chloroplasts indicating a crucial role of DCT2 in the C_4 pathway (Majeran et al., 2010; Weissmann et al., 2016). In *F. bidentis DCT2* is neither highly nor differentially expressed and shows higher activity for succinate and fumarate than malate indicating it has a different physiological role than its *Z. mays* orthologue (Renné et al., 2003; Billakurthi et al., 2018). Consistent with those observations and our current metabolite results, we hypothesize that FbBASS4-1 is a BSC-specific malate translocator. The production of a specific antibody directed against FbBASS4 is currently in progress to confirm the localization of the protein *in vivo*. Additionally, the localization could be assessed by southern blotting, ribosome profiling or promotor analyses. As indicated above, it would be advantageous to perform isolations and purifications of chloroplasts of MC and BSC not only for physiological experiments but also for proteomics. On the one hand proteomic analyses would prove our localization hypothesis; on the other hand we might be able to identify additional transport systems. In *Flaveria*, aspartate accounts for 35–40% of the total carbon being assimilated in BSC

chloroplasts (Meister et al., 1996). Therefore, an aspartate transporter in the inner envelope of BSC chloroplasts is required. However, BASS4 does not show uptake activity for aspartate (Fig. 1). Proteomic analyses on isolated MC and BSC chloroplasts might be a key factor in identifying potential candidates mediating the aspartate transport across the inner envelope of BSC chloroplasts (Majeran et al., 2005; Bräutigam et al., 2008; Majeran et al., 2008). In *Z. mays*, the presence of an aspartate transporter in the inner envelope of BSC has been suggested as well (Weissmann et al., 2016). If the protein has been identified in *Z. mays* its orthologue in *Flaveria* might be a potential candidate as well.

We conclude from our results that FbBASS4-1 is a BSC-specific malate translocator that mediates sodium-driven malate uptake into chloroplasts of BSC. This differs from the proposed malate uptake into BSC chloroplasts in the NADP-ME type species *Z. mays* and *S. bicolor* and might be a result of the independent evolution of C_4 photosynthesis within the plant lineage (Sage et al., 2011; Weissmann et al., 2016; Weissmann et al., 2019).

MATERIALS AND METHODS

Construction of expression constructs

The coding sequence of *Flaveria bidentis* (*F. bidentis*) *BASS4-1* (FbBASS4-1) and *BASS4-2* (FbBASS4-2) were synthesized codon-optimized for expression in *Saccharomyces cerevisiae* (*S. cerevisiae*) from ThermoFisher Scientific. The cDNA of codon-optimized *FbBASS4-1* and codon-optimized *FbBASS4-2* was amplified with a proofreading polymerase omitting the first 66 (FbBASS4-1) or the first 39 amino acids (FbBASS4-2), respectively, and integrated into pYES2-Nt a (pYES-Nta) vector, containing a hexa histidine-tag, via restriction-based cloning.

Heterologous expression of FbBASS4-1 and FbBASS4-2 in *S. cerevisiae*

The constructed plasmids pYES-FbBASS4-1, pYES-FbBASS4-2 and the empty vector pYES-Nta were used to transform *S. cerevisiae* INVScI strain with the lithium acetate method. Transgenic yeast cells were selected on uracil-free YNB medium (0.67% [w/v] yeast nitrogen base without amino acids) supplemented with 2% (w/v) glucose and drop-out mix (0.01% [w/v] adenine, 0.01% [w/v] arginine, 0.01% [w/v] cysteine, 0.01% [w/v] leucine, 0.01% [w/v] lysine, 0.01% [w/v] threonine, 0.01% [w/v] tryptophan, 0.005% [w/v] aspartate, 0.005% [w/v] histidine, 0.005% [w/v] serine, 0.005% [w/v] isoleucine, 0.005% [w/v] phenyl-alanine, 0.005% [w/v] methionine, 0.005% [w/v] proline, 0.005% [w/v] tyrosine, 0.005% [w/v] valine). Single colonies were inoculated in uracil-free YNB medium supplemented with 2% (w/v) raffinose and drop-out mix and grown over night at 30°C with moderate shaking (200 rpm). Cells were inoculated in 50 ml uracil-free YNB medium supplemented with 2% (w/v) galactose and drop-out mix to an OD_{600} of 0.4. The cell suspension was incubated at 30°C and moderate shaking (200 rpm) for 6 h. Cells were harvested by centrifugation and the membranes isolated as described previously (Roell et al., 2017).

Reconstitution of isolated yeast membranes and measurement of transport activities

Isolated yeast membranes harboring the recombinant proteins FbBASS4-1 and FbBASS4-2 or the control vector (pYES-Nta) were reconstituted into liposomes via the freeze-thaw procedure. In brief, 50 µl isolated yeast membranes were rapidly mixed with 3% (w/v) sonicated lipid (L-α-phosphatidylcholine from egg yolk, Sigma Aldrich) in reconstitution buffer with (100 mM Tricine-KOH [pH 7.6], 30 mM K-gluconate, 20 mM substrate) or without (100 mM Tricine-KOH [pH 7.6], 50 mM K-gluconate) preloading of substrate and frozen in liquid nitrogen. Proteoliposomes were thawed at 24°C and external substrate was removed by size-exclusion chromatography using Sephadex G-75 columns (GE-Healthcare) pre-equilibrated with PD-10 buffer (10 mM Tricine-KOH, [pH 7.6], 100 mM Na-gluconate, 40 mM K-gluconate). Transport was initiated by adding ^{14}C-labeled substrate and 0.2 mM non-

labeled substrate to proteoliposomes with or without preloading of substrate. Uptake of external L-[14C]-malate or L-[14C]-aspartate or L-[14C]-glutamate or [14C]-2-OG or L-[14C]-alanine (all from Hartmann Analytics) was measured at 30°C. If not stated otherwise, transport was stopped by adding 140 µl of the mixture to pre-equilibrated size-exclusion or anion exchange columns. Liposomes were separated from external radioactivity by passing through AG1-X8 resin columns (Bio-Rad Laboratories, Hercules, California, USA; malate, aspartate, 2-OG) with 150 mM sodium acetate (pH 7.6) or Sephadex G-75 medium columns (Sigma Aldrich; glutamate, alanine) with PD-10 buffer. The radioactivity inside the liposomes was determined by liquid scintillation counting (LS 6000, Beckmann).

For inhibition experiments the following inhibitors (all Sigma Aldrich) were used: mersalyl (MER; final concentration: 0.1 mM), phenylsuccinic acid (PHS; final concentration: 5 mM), butylmalonic acid (BMA; final concentration: 5 mM), *p*-hydroxymercuribenzoic acid (pHMB; final concentration: 0.1 mM), α-cyano-4-hydroxycinnamic acid (CCN; final concentration: 1 mM) and N-ethylmaleimide (NEM; final concentration: 1 mM). Inhibitors were added 2 min before the labeled substrate. Activities were calculated from initial velocities.

For the determination of the apparent K_m value for malate reaction was terminated with the inhibitor-stop method using BMA as inhibitor of malate uptake. Activities were calculated from initial velocities. Apparent K_m constant for malate was determined from Michaelis-Menten plot.

Measurement of sodium-coupled malate symport of heterologously expressed FbBASS4-1

Isolated yeast membranes harboring the recombinant proteins FbBASS4-1 and ZmDCT2 or the control vector (pYES-Nta) were reconstituted into liposomes via the freeze-thaw procedure as described above. Liposomes were preloaded with sodium-symport buffer (10 mM Tricine-KOH [pH 7.6], 10 mM KCl, 0.1 mM NaCl). External sodium and potassium ions were removed by size-exclusion chromatography using Sephadex G-75 columns (GE-Healthcare) pre-equilibrated with 10 mM Tricine-KOH (pH 7.6). Transport was initiated by adding 1 mM NaCl, 0.1 mM KCl, L-[14C]-malate, 0.2 mM malate and 3 nM valinomycin (Sigma Aldrich) to proteoliposomes. Uptake of external L-[14C]-malate was measured at 30°C. Transport was stopped and the radioactivity inside the liposomes was measured as described above.

Plant growth conditions

F. bidentis plants were grown on multiplication substrate (Floraton, Floragard) in a 12 h light/12 h dark environment (22°C/18°C) under 150 µmol m^{-2} s^{-1} light intensity in a CO_2-enriched atmosphere (0.3% [v/v] CO_2) if not stated otherwise. If necessary plants were propagated vegetatively from shoot cuttings and grown in perlite under 16 h light/8 h dark

with 300–600 µmol m^{-2} s^{-1} light intensity for the first two weeks. Afterwards, they were transferred in the above described conditions.

Construction of transgenic *Flaveria* lines

A 300 bp region of the 5' terminus of the *BASS4* coding sequence (NCBI Accession AB522103) was amplified with a proofreading polymerase containing *Xho*I and *Eco*RI, and *Xba*I and *Hind*III restriction sites and subsequently inserted into the multiple cloning site of pART7 vector via restriction-based cloning (Gleave, 1992). From 5' to 3' end the total DNA fragment containing the 35S promoter of cauliflower mosaic virus, the *BASS4* 300 bp fragment, the 1st intron of PPDK, the *BASS4* 300 bp antisense fragment, and the Cos Terminator was introduced into pART27 vector via restriction-based cloning using *Not*I restriction sites (Gleave, 1992). The construct was introduced into *Agrobacterium tumefaciens* strain AGL1 (Lazo et al., 1991). The agrobacterium was co-cultivated with hypocotyls of *F. bidentis* plants, and regenerated shoots were selected on plates containing 150 mg l^{-1} kanamycin (Chitty et al., 1994). The reduction of *BASS4* transcript level was analyzed by qRT-PCR. Transgenic lines with reduced transcripts were selected for further analysis. Oligonucleotides used for generation of transgenic *F. bidentis* plants and qRT-PCR are listed in Supplemental Table S1.

Metabolite analysis

Approximately 10 week-old *F. bidentis* WT and *BASS4 9-3* RNAi plants with a fully developed 4th leaf pair (8-10 cm; Billakurthi et al., 2018) were used for metabolite analyses. The 4th leaf pair was cut at the base and immediately frozen in liquid nitrogen. Samples were taken end of night (EON) in high CO_2 (0.3% [v/v] CO_2) and 12 h, 15 h and 39 h after shift to ambient CO_2 conditions (0.038% [v/v] CO_2). Metabolites were analyzed by gas chromatography-mass spectrometry (Fiehn, 2007). Metabolites were extracted from 40-70 mg fresh weight of ground leaf material using 1.5 ml pre-cooled (-20°C) $CHCl_3$:CH_3OH:H_2O (1:2.5:1; v/v) mixture containing 5 µM of each ribitol and dimethylphenylalanine as internal standard, incubated for 10 min on an end-over-end rotator (30 rpm) and subsequently centrifuged at 20,000 x *g* for 2 min. The supernatant was transferred into a new tube, dried in a vacuum concentrator and derivatized in two steps via an MPS-Dual-head autosampler (Gerstel): (1) with 10 µl methoxyamine hydrochloride [Acros organics; freshly prepared at 20 mg ml^{-1} in pure pyridine (Sigma-Aldrich)] and shaking at 37°C for 90 min, and (2) addition of 90 µl *N*-Methyl-*N*-(trimethylsilyl)trifluoroacetamide (MSTFA; Macherey-Nagel) and shaking at 37°C for 30 min.

After incubation for 2 h at room temperature, 1 µl of derivatized compounds was injected with an automatic liner exchange system in conjunction with a cold injection system (Gerstel) in

splitless mode (ramping from 50°C to 250°C at 12°C s^{-1}) into the GC with a helium flow of 1 ml min^{-1}. Chromatography was performed using a 7890B GC system (Agilent Technologies) with a HP-5MS column with 5% phenyl methyl siloxane film (Agilent 19091S-433, 30 m length, 0.25 mm internal diameter, 0.25 µM film). The oven temperature was held constant at 70°C for 2 min and then ramped at 12.5°C min^{-1} to 320°C at which it was held constant for 5 min; resulting in a total run time of 27 min. Metabolites were ionized with an electron impact source at 70 V and 200°C source temperature and recorded in a mass range of m/z 60 to m/z 800 at 20 scans per second with a 7200 GC-QTOF (Agilent Technologies).

Metabolites were identified via MassHunter Qualitative (v b08.00, Agilent Technologies) by comparison of spectra to the NIST14 Mass Spectral Library (https://www.nist.gov/srd/nist-standard-reference-database-1a-v14). A standard mixture containing all target compounds at a concentration of 50 µM was processed in parallel to the samples as a response check and retention time reference. Peaks were integrated using MassHunter Quantitative (v b08.00, Agilent Technologies). For relative quantification, all metabolite peak areas were normalized to the corresponding fresh weight used for extraction and the peak area of the internal standard ribitol or dimethylphenylalanine (Sigma-Aldrich).

Enzyme assays

Enzymatic activities of AlaAT, AspAT, GluDH, NAD-MDH, NADP-MDH and NADP-ME were measured in a plate-reader spectrophotometer by following the absorbance at 340 nm. Therefore, 50 mg of ground and frozen leaf material was extracted in 1 ml ice-cold extraction buffer (50 mM HEPES-KOH [pH 8.0], 10 mM DTT, 1 mM EDTA, 0.1% [v/v] Triton X-114), incubated for 5 min at 4°C on an end-over-end rotator (30 rpm) and subsequently centrifuged for 5 min at 13,000 x *g* (4°C). The supernatant containing the extracted enzymes was used for enzyme assays. Activities of AlaAT, AspAT, NADP-MDH and NADP-ME were measured as previously described by Ashton et al. (1990). For NADP-MDH activity measurements extracts were pre-incubated with 100 mM DTT for 1 h at room temperature to fully reduce the enzyme (Ashton et al., 1990). GluDH activity was assayed in the amination direction as described previously (Turano et al., 1996). NAD-MDH activity was assayed by following the oxidation of NADH to NAD^+ as described previously (Tomaz et al., 2010).

Determination of protein and chlorophyll content

Protein concentration of isolated yeast membranes and extracted leaf samples was determined using the Pierce™ BCA Protein Assay Kit (ThermoFisher Scientific) according to the manufacturer's instructions with BSA as standard.

Total chlorophyll content was calculated as previously described with 100% Ethanol as solvent (Ritchie, 2008).

SDS-PAGE and immunoblot analysis

20 µg of isolated yeast membranes were analyzed by SDS-PAGE and immunoblot analysis with Anti-His-horse-radish peroxidase antibody (Miltenyi Biotec) using standard protocols. To prevent aggregation of membrane proteins, isolated yeast membranes were incubated for 30 min at 30°C in SDS-loading buffer prior to the analysis (Laemmli, 1970).

20 µg of total leaf protein was analyzed by SDS-PAGE using standard protocols (Laemmli, 1970).

SUPPLEMENTAL DATA

Supplemental Figure S1. Bioinformatic analysis of the amino acid sequence of FbBASS4-1 and FbBASS4-2.

Supplemental Figure S2. Heterologous expression of FbBASS4-1 and FbASS4-2 in *S. cerevisiae* and reconstitution into proteoliposomes.

Supplemental Figure S3. Schematic representation of the vector used for transformation of *Agrobacterium tumefaciens* strain AGL1 and subsequent transformation of *F. bidentis*.

Supplemental Figure S4. Results of all quantified metabolites.

Supplemental Figure S5. SDS-PAGE pictures of isolated protein samples used for enzyme activities.

Supplemental Table S1. Oligonucleotides used in this study.

REFERENCES

Alrefai WA, Gill RK (2007) Bile Acid Transporters: Structure, Function, Regulation and Pathophysiological Implications. Pharm Res **24**: 1803–1823

Ashton AR, Burnell JN, Furbank RT, Jenkins CLD, Hatch MD (1990) Enzymes of C4 Photosynthesis. Enzym Prim Metab **3**: 39–72

Billakurthi K, Wrobel TJ, Bräutigam A, Weber APM, Westhoff P, Gowik U (2018) Transcriptome dynamics in developing leaves from C3 and C4 Flaveria species reveal determinants of Kranz anatomy. bioRxiv. doi: 10.1101/473181

Bräutigam A, Hoffmann-Benning S, Weber APM (2008) Comparative Proteomics of Chloroplast Envelopes from C3 and C4 Plants Reveals Specific Adaptations of the Plastid Envelope to C4 Photosynthesis and Candidate Proteins Required for Maintaining C4 Metabolite Fluxes. Plant Physiol **148**: 568–579

von Caemmerer S, Furbank RT (2003) The C(4) pathway: an efficient CO(2) pump. Photosynth Res **77**: 191–207

Chapman KSR, Hatch MD (1981) Regulation of C4 photosynthesis: Mechanism of activation and inactivation of extracted pyruvate, inorganic phosphate dikinase in relation to dark/light regulation. Arch Biochem Biophys **210**: 82–89

Chitty JA, Furbank RT, Marshall JS, Chen Z, Taylor WC (1994) Genetic transformation of the C4 plant, Flaveria bidentis. Plant J **6**: 949–956

Claro da Silva T, Polli JE, Swaan PW (2013) The solute carrier family 10 (SLC10): Beyond bile acid transport. Mol Aspects Med **34**: 252–269

Denton AK, Maß J, Külahoglu C, Lercher MJ, Bräutigam A, Weber APM (2017) Freeze-quenched maize mesophyll and bundle sheath separation uncovers bias in previous tissue-specific RNA-Seq data. J Exp Bot **68**: 147–160

Ding Z, Weissmann S, Wang M, Du B, Huang L, Wang L, Tu X, Zhong S, Myers C, Brutnell TP, et al (2015) Identification of Photosynthesis-Associated C4 Candidate Genes through Comparative Leaf Gradient Transcriptome in Multiple Lineages of C3 and C4 Species. PLoS One **10**: e0140629

Fiehn O (2007) Validated High Quality Automated Metabolome Analysis of Arabidopsis Thaliana Leaf Disks. *In* BJ Nikolau, ES Wurtele, eds, Concepts in Plant Metabolomics. Springer Netherlands, Dordrecht, pp 1–18

Furbank RT (2011) Evolution of the C4 photosynthetic mechanism: are there really three C4 acid decarboxylation types? J Exp Bot **62**: 3103–3108

Furumoto T, Yamaguchi T, Ohshima-Ichie Y, Nakamura M, Tsuchida-Iwata Y, Shimamura M, Ohnishi J, Hata S, Gowik U, Westhoff P, et al (2011) A plastidial sodium-dependent pyruvate transporter. Nature **476**: 472–475

Gigolashvili T, Yatusevich R, Rollwitz I, Humphry M, Gershenzon J, Flügge U-I (2009) The Plastidic Bile Acid Transporter 5 Is Required for the Biosynthesis of Methionine-Derived Glucosinolates in Arabidopsis thaliana. Plant Cell **21**: 1813–1829

Gleave AP (1992) A versatile binary vector system with a T-DNA organisational structure conducive to efficient integration of cloned DNA into the plant genome. Plant Mol Biol **20**: 1203–1207

Gowik U, Bräutigam A, Weber KL, Weber APM, Westhoff P (2011) Evolution of C4 Photosynthesis in the Genus Flaveria : How Many and Which Genes Does It Take to Make C4? Plant Cell **23**: 2087–2105

Halestrap AP, Scott RD, Thomas AP (1980) Mitochondrial pyruvate transport and its hormonal regulation. Int J Biochem **11**: 97–105

Hatch MD (1979) Mechanism of C4 photosynthesis in Chloris gayana: Pool sizes and kinetics of 14CO2 incorporation into 4-carbon and 3-carbon intermediates. Arch Biochem Biophys **194**: 117–127

Hatch MD (1987) C4 photosynthesis: a unique blend of modified biochemistry, anatomy and ultrastructure. Biochim Biophys Acta - Rev Bioenerg **895**: 81–106

Hatch MD, Kagawa T, Craig S (1975) Subdivision of C_4-Pathway Species Based on Differing C_4 Acid Decarboxylating Systems and Ultrastructural Features. Funct Plant Biol **2**: 111–128

Hatch MD, Slack C (1966) Photosynthesis by sugar-cane leaves. A new carboxylation reaction and the pathway of sugar formation. Biochem J **101**: 103–111

Huang L, Pyc M, Alseekh S, McCarty DR, de Crécy-Lagard V, Gregory JF, Henry CS, Fernie AR, Mullen RT,

Hanson AD (2018) A plastidial pantoate transporter with a potential role in pantothenate synthesis. Biochem J **475**: 813–825

Krogh A, Larsson B, von Heijne G, Sonnhammer EL (2001) Predicting transmembrane protein topology with a hidden markov model: application to complete genomes. J Mol Biol **305**: 567–580

Ku MSB, Monson RK, Littlejohn RO, Nakamoto H, Fisher DB, Edwards GE (1983) Photosynthetic Characteristics of C3 -C4 Intermediate Flaveria Species. Plant Physiol **71**: 944–948

Laemmli UK (1970) Cleavage of Structural Proteins during the Assembly of the Head of Bacteriophage T4. Nature **227**: 680–685

Lasic DD (1988) The mechanism of vesicle formation. Biochem J **256**: 1–11

Lazo GR, Stein PA, Ludwig RA (1991) A DNA Transformation–Competent Arabidopsis Genomic Library in Agrobacterium. Bio/Technology **9**: 963–967

Lee C, Kang HJ, von Ballmoos C, Newstead S, Uzdavinys P, Dotson DL, Iwata S, Beckstein O, Cameron AD, Drew D (2013) A two-domain elevator mechanism for sodium/proton antiport. Nature **501**: 573–577

Levey M, Timm S, Mettler-Altmann T, Luca Borghi G, Koczor M, Arrivault S, Weber APM, Bauwe H, Gowik U, Westhoff P (2019) Efficient 2-phosphoglycolate degradation is required to maintain carbon assimilation and allocation in the C4 plant Flaveria bidentis. J Exp Bot **70**: 575–587

Madeira F, Park YM, Lee J, Buso N, Gur T, Madhusoodanan N, Basutkar P, Tivey ARN, Potter SC, Finn RD, et al (2019) The EMBL-EBI search and sequence analysis tools APIs in 2019. Nucleic Acids Res **47**: W636–W641

Majeran W, Cai Y, Sun Q, van Wijk KJ (2005) Functional Differentiation of Bundle Sheath and Mesophyll Maize Chloroplasts Determined by Comparative Proteomics. Plant Cell **17**: 3111–3140

Majeran W, Friso G, Ponnala L, Connolly B, Huang M, Reidel E, Zhang C, Asakura Y, Bhuiyan NH, Sun Q, et al (2010) Structural and Metabolic Transitions of C4 Leaf Development and Differentiation Defined by Microscopy and Quantitative Proteomics in Maize. Plant Cell **22**: 3509–3542

Majeran W, Zybailov B, Ytterberg AJ, Dunsmore J, Sun Q, van Wijk KJ (2008) Consequences of C 4 Differentiation for Chloroplast Membrane Proteomes in Maize Mesophyll and Bundle Sheath Cells. Mol Cell Proteomics **7**: 1609–1638

McKown AD, Moncalvo J-M, Dengler NG (2005) Phylogeny of Flaveria (Asteraceae) and inference of C4 photosynthesis evolution. Am J Bot **92**: 1911–1928

Meister M, Agostino A, Hatch M (1996) The roles of malate and aspartate in C4 photosynthetic metabolism of Flaveria bidentis (L.). Planta **199**: 262–269

Ohnishi J, Kanai R (1990) Pyruvate uptake induced by a pH jump in mesophyll chloroplasts of maize and sorghum, NADP-malic enzyme type C4 species. FEBS Lett **269**: 122–124

Ohnishi J, Kanai R (1987) Na + -induced uptake of pyruvate into mesophyll chloroplasts of a C4 plant, Panicum miliaceum. FEBS Lett **219**: 347–350

Palmieri F, Passarella S, Stipani I, Quagliariello E (1974) Mechanism of inhibition of the dicarboxylate carrier of mitochondria by thiol reagents. Biochim Biophys Acta - Bioenerg **333**: 195–208

Pick TR, Bräutigam A, Schlüter U, Denton AK, Colmsee C, Scholz U, Fahnenstich H, Pieruschka R, Rascher U, Sonnewald U, et al (2011) Systems Analysis of a Maize Leaf Developmental Gradient Redefines the Current C4 Model and Provides Candidates for Regulation. Plant Cell **23**: 4208–4220

Pressman BC (1976) Biological Applications of Ionophores. Annu Rev Biochem **45**: 501–530

Renné P, Dreßen U, Hebbeker U, Hille D, Flügge U-I, Westhoff P, Weber APM (2003) The Arabidopsis mutant dct is deficient in the plastidic glutamate/malate translocator DiT2. Plant J **35**: 316–331

Ritchie RJ (2008) Universal chlorophyll equations for estimating chlorophylls a, b, c, and d and total chlorophylls in natural assemblages of photosynthetic organisms using acetone, methanol, or ethanol solvents. Photosynthetica **46**: 115–126

Roell M-S, Kuhnert F, Zamani-Nour S, Weber APM (2017) In Vitro Analysis of Metabolite Transport Proteins. Methods Mol Biol **1653**: 83–96

Sage RF, Christin P-A, Edwards EJ (2011) The C4 plant lineages of planet Earth. J Exp Bot **62**: 3155–3169

Smyth D, Blumenfeld O, Konigsberg W (1964) Reactions of N-ethylmaleimide with peptides and amino acids. Biochem J **91**: 589–595

Sonnhammer ELL, von Heijne G, Krogh A (1998) A hidden Markov model for predicting transmembrane

helices in protein sequences. Proceedings Int Conf Intell Syst Mol Biol **6**: 175–82

South PF, Walker BJ, Cavanagh AP, Rolland V, Badger M, Ort DR (2017) Bile Acid Sodium Symporter BASS6 Can Transport Glycolate and Is Involved in Photorespiratory Metabolism in Arabidopsis thaliana. Plant Cell **29**: 808–823

Taniguchi M, Taniguchi Y, Kawasaki M, Takeda S, Kato T, Sato S, Tabata S, Miyake H, Sugiyama T (2002) Identifying and Characterizing Plastidic 2-Oxoglutarate/Malate and Dicarboxylate Transporters in Arabidopsis thaliana. Plant Cell Physiol **43**: 706–717

Taniguchi Y, Nagasaki J, Kawasaki M, Miyake H, Sugiyama T, Taniguchi M (2004) Differentiation of Dicarboxylate Transporters in Mesophyll and Bundle Sheath Chloroplasts of Maize. Plant Cell Physiol **45**: 187–200

Tausta SL, Li P, Si Y, Gandotra N, Liu P, Sun Q, Brutnell TP, Nelson T (2014) Developmental dynamics of Kranz cell transcriptional specificity in maize leaf reveals early onset of C4-related processes. J Exp Bot **65**: 3543–3555

Tomaz T, Bagard M, Pracharoenwattana I, Lindén P, Lee CP, Carroll AJ, Ströher E, Smith SM, Gardeström P, Millar AH (2010) Mitochondrial Malate Dehydrogenase Lowers Leaf Respiration and Alters Photorespiration and Plant Growth in Arabidopsis. Plant Physiol **154**: 1143–1157

Turano FJ, Dashner R, Upadhyaya A, Caldwell CR (1996) Purification of Mitochondrial Glutamate Dehydrogenase from Dark-Grown Soybean Seedlings. Plant Physiol **112**: 1357–1364

Verchère A, Broutin I, Picard M (2012) Photo-induced proton gradients for the in vitro investigation of bacterial efflux pumps. Sci Rep **2**: 306

Veshaguri S, Christensen SM, Kemmer GC, Ghale G, Moller MP, Lohr C, Christensen AL, Justesen BH, Jorgensen IL, Schiller J, et al (2016) Direct observation of proton pumping by a eukaryotic P-type ATPase. Science (80-) **351**: 1469–1473

Wang L, Czedik-Eysenberg A, Mertz RA, Si Y, Tohge T, Nunes-Nesi A, Arrivault S, Dedow LK, Bryant DW, Zhou W, et al (2014a) Comparative analyses of C4 and C3 photosynthesis in developing leaves of maize and rice. Nat Biotechnol **32**: 1158–1165

Wang Y, Bräutigam A, Weber APM, Zhu X-G (2014b) Three distinct biochemical subtypes of C4 photosynthesis? A modelling analysis. J Exp Bot **65**: 3567–3578

Weber AP, von Caemmerer S (2010) Plastid transport and metabolism of C3 and C4 plants—comparative analysis and possible biotechnological exploitation. Curr Opin Plant Biol **13**: 256–264

Weber APM, Menzlaff E, Arbinger B, Gutensohn M, Eckerskorn C, Fluegge U-I (1995) The 2-oxoglutarate/malate translocator of chloroplast envelope membranes: molecular cloning of a transporter containing a 12-helix motif and expression of the functional protein in yeast cells. Biochemistry **34**: 2621–2627

Weissmann S, Huang P, Furuyama K, Wiechert MA, Taniguchi M, Schnable JC, Brutnell TP, Mockler TC (2019) DCT4 - a new member of the dicarboxylate transporter family in C4 grasses. bioRxiv. doi: 10.1101/762724

Weissmann S, Ma F, Furuyama K, Gierse J, Berg H, Shao Y, Taniguchi M, Allen DK, Brutnell TP (2016) Interactions of C4 Subtype Metabolic Activities and Transport in Maize Are Revealed through the Characterization of DCT2 Mutants. Plant Cell **28**: 466–484

SUPPLEMENTS

Supplemental Figure S1

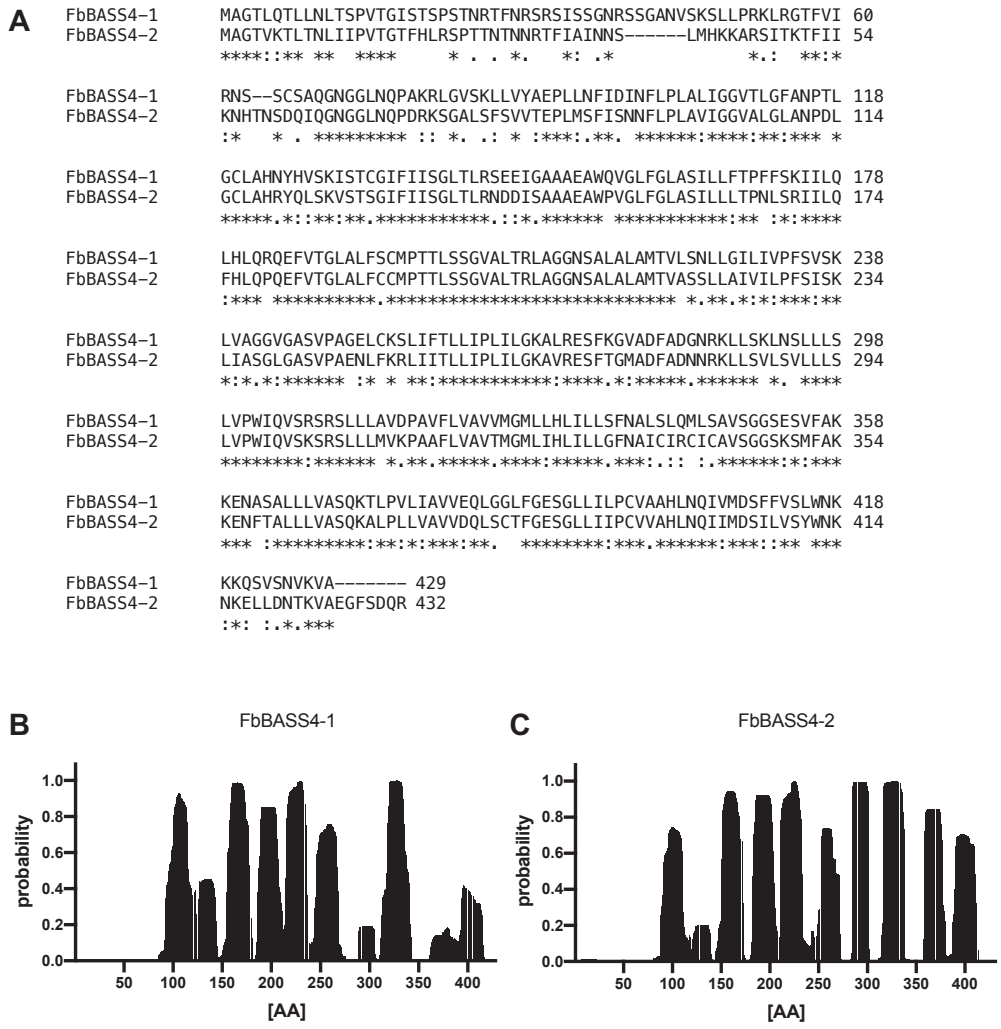

Supplemental Figure S1: Bioinformatic analysis of the amino acid sequence of FbBASS4-1 and FbBASS4-2. Amino acid sequences of FbBASS4-1 and FbBASS4-2 were aligned using Clustal Omega 1.2.2 (**A**; Madeira et al., 2019). Transmembrane helices in FbBASS4-1 (**B**) and FbBASS4-2 (**C**) were predicted using the TMHMM Server 2.0 (Sonnhammer et al., 1998; Krogh et al., 2001).

Supplemental Figure S2

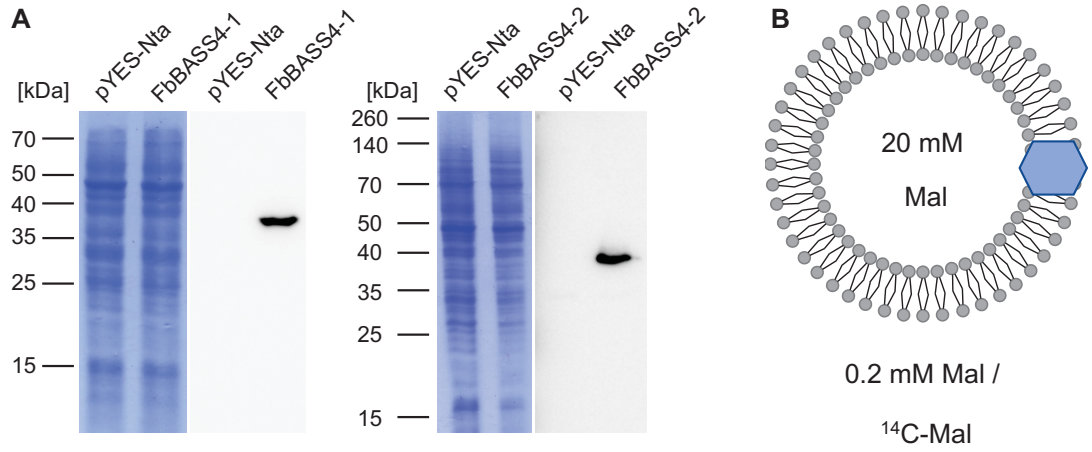

Supplemental Figure S2: Heterologous expression of FbBASS4-1 and FbASS4-2 in *S. cerevisiae* and reconstitution into proteoliposomes. Isolated yeast membranes harboring the expressed proteins FbBASS4-1, FbBASS4-2, and the empty vector control pYES-Nta (**A**). Yeast membranes were isolated as described in Materials and Methods. 20 µg each were separated on a 12% SDS-PAGE and transferred onto a nitrocellulose membrane. Membrane were probed with Anti-His antibody coupled to horse radish peroxidase. Proteins were visualized using a chemiluminescent detection system. Schematic representation of proteoliposomes used for malate homo-exchange uptake experiments (**B**). Blue hexagon represents reconstituted transport protein.

Supplemental Figure S3

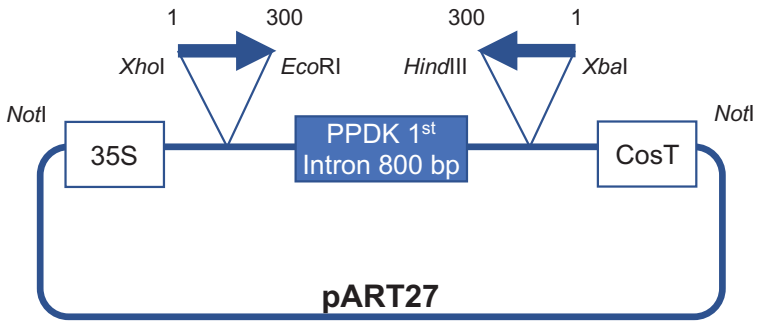

Supplemental Figure S3: Schematic representation of the vector used for transformation of *Agrobacterium tumefaciens* strain AGL1 and subsequent transformation of *F. bidentis*. The multiple cloning site of pART27 vector was constructed from 5' to 3' end of the 35S promoter of cauliflower mosaic virus, the *BASS4* 300 bp fragment, the 1st intron of pyruvate phosphate dikinase (PPDK), the *BASS4* 300 bp antisense fragment, and the Cos Terminator (CosT; Gleave, 1992; Chitty et al., 1994).

Supplemental Figure S4

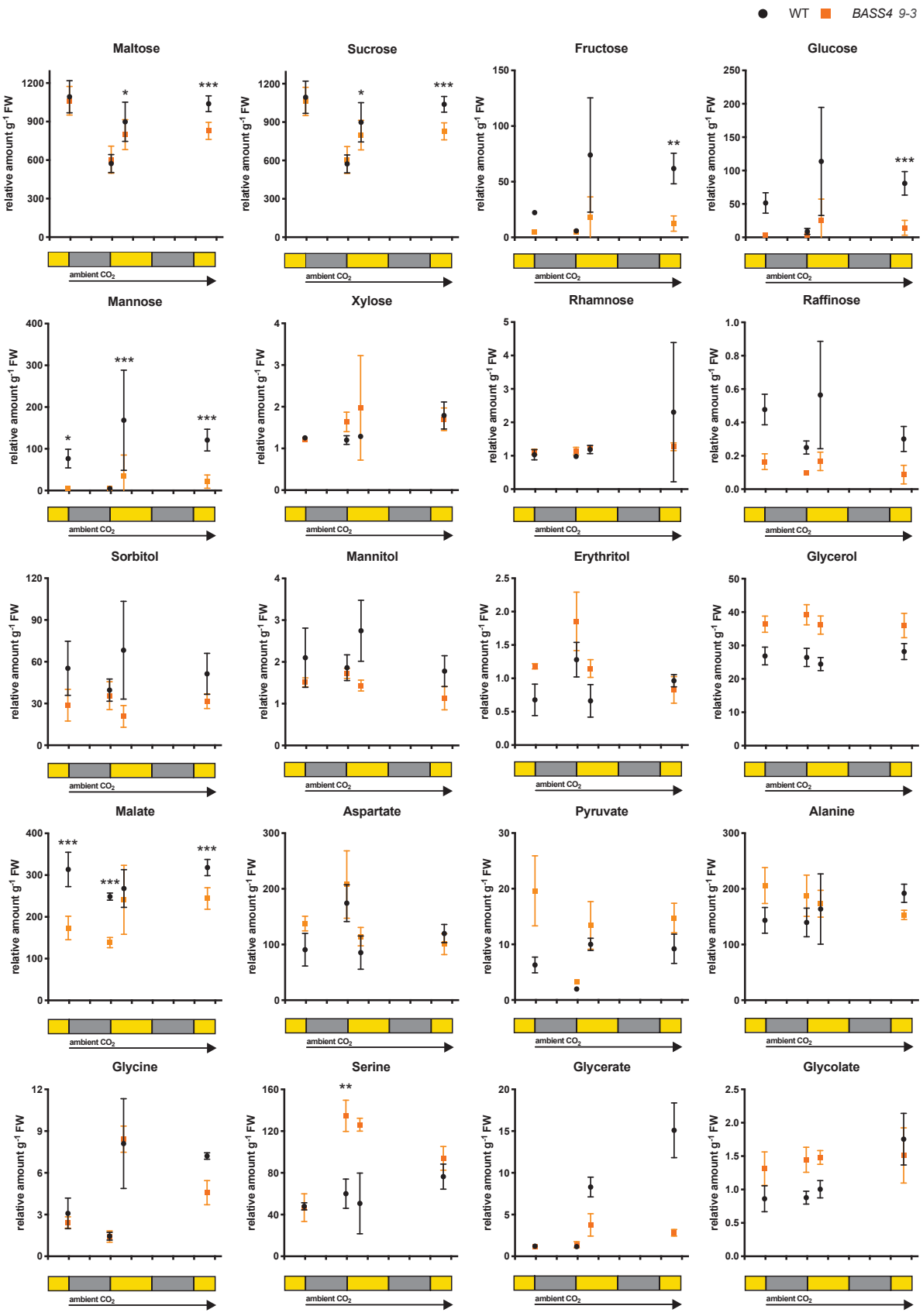

Supplemental Figure S4 continued

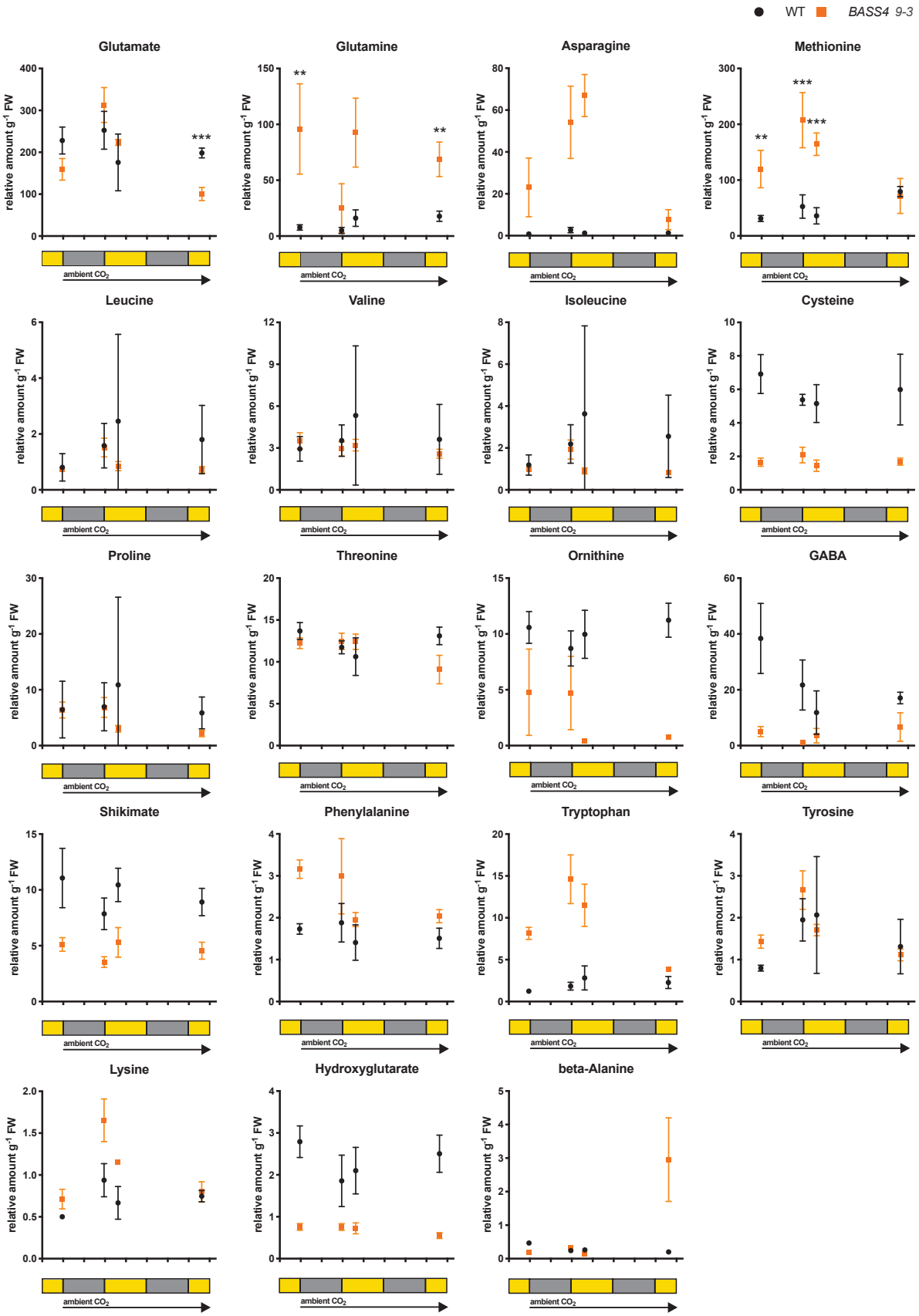

Supplemental Figure S4 continued

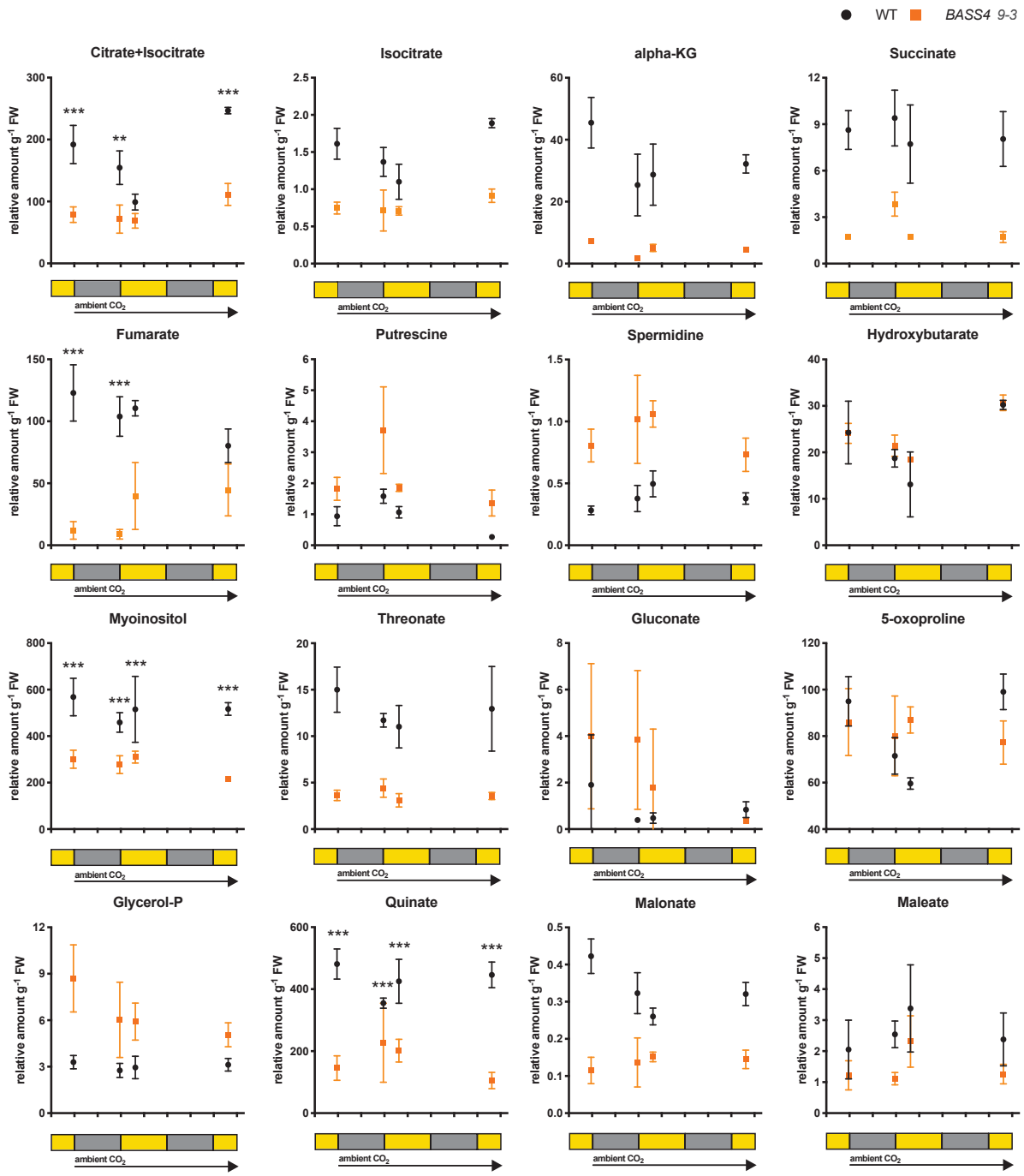

Supplemental Figure S4 continued

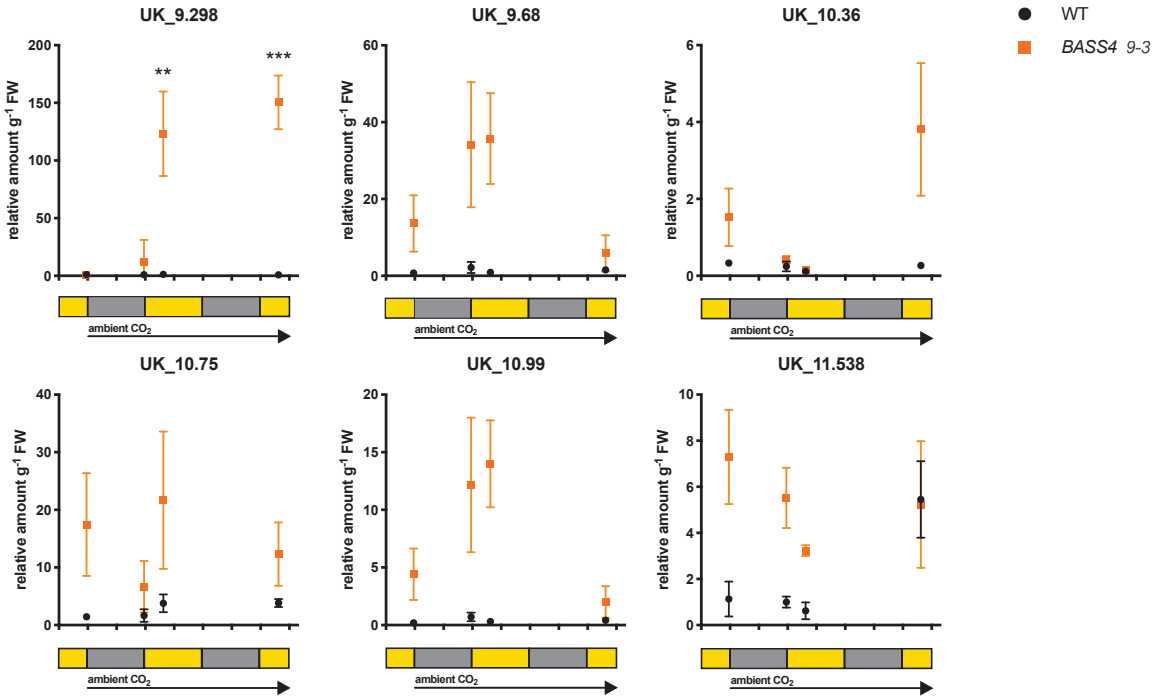

Supplemental Figure S4: Results of all quantified metabolites. Samples of *F. bidentis* WT (black circles) and *BASS4 9-3* (orange squares) were harvested and metabolites extracted as described in Materials and Methods. Timeline is indicated below each diagram in yellow (day) and grey (night). The start of the arrow below each diagram marks the time point at which plants were shifted to ambient CO_2 (0.038% [v/v] CO_2) conditions. Asterisks indicate statistical differences between means (*, $P < 0.05$; **, $P < 0.01$; ***, $P < 0.001$; one-way ANOVA with Bonferroni's multiple comparisons test). UK, unknown component; WT, wildtype.

Supplemental Figure S5

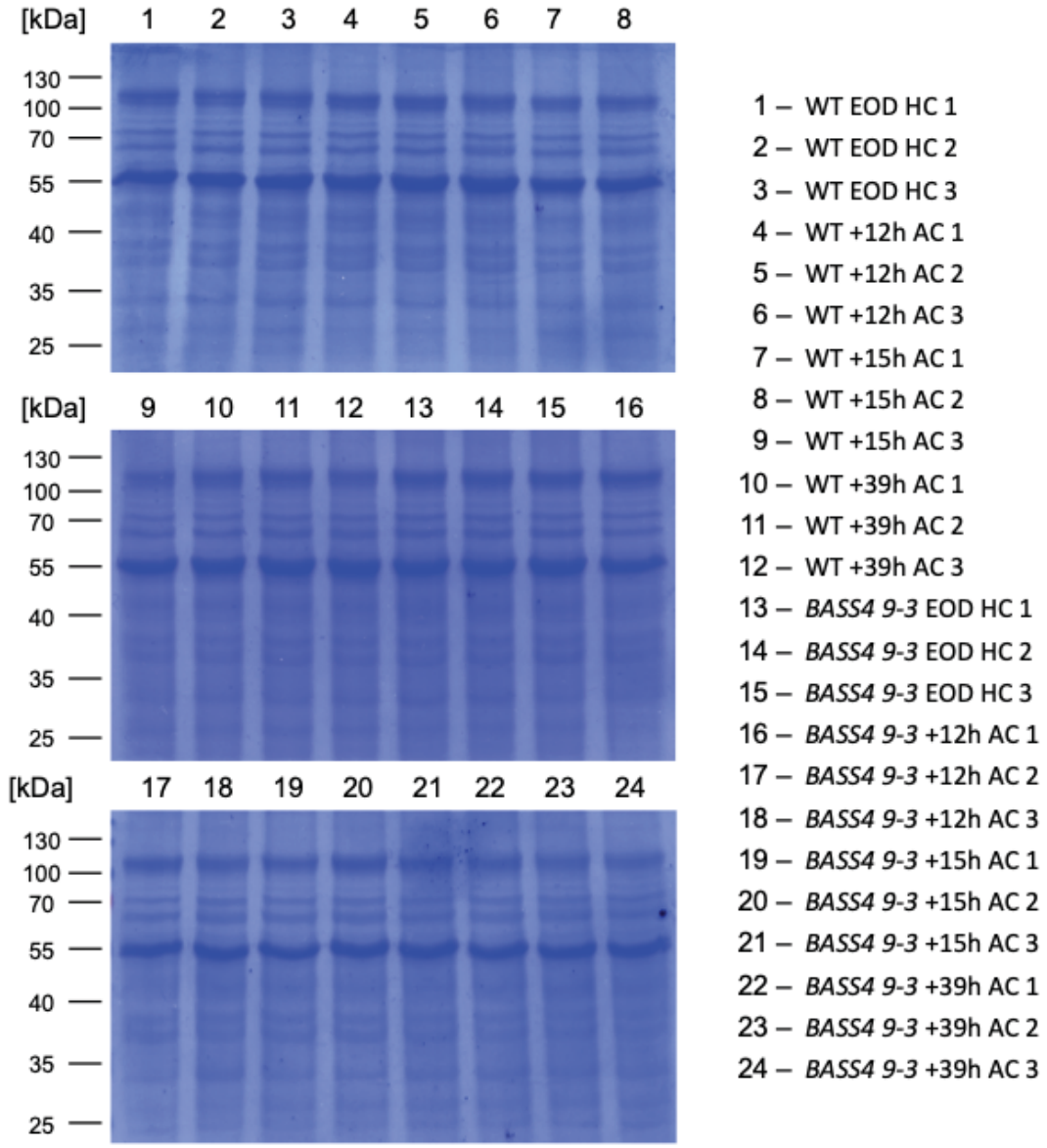

Supplemental Figure S5: SDS-PAGE pictures of isolated protein samples used for enzyme activities. Samples were isolated and processed as described in Material and Methods. Samples were separated on 12% separating gels.

Supplemental Table S1

Supplemental Table S1: Oligonucleotides used in this study. Sequence that is identical to BASS4 sequence is depicted in capital letters, restriction sites are shown in italics.

Name	5'-3' sequence	Application
XhPy2f1	ta*ctcgag*TGCGGTGTGAGCCTGAGGAG	Generation of *BASS4* 300 bp fragment
EcPy2r1	tt*gaattg*GTTTCGAAACTCCCAACCGC	
XbPy2f2	ta*tctaga*TGCGGTGTGAGCCTGAGGAG	Generation of *BASS4* 300 bp antisense fragment
HiPy2r2	tt*aagctt*GTTTCGAAACTCCCAACCGC	
qRT-fwd	TTCTTCCGTGTGTTGCAGCA	qRT-PCR oligonucleotides
qRT-rev	CGTTAAAAGTATTGTGGACTTT	

Acknowledgments

First of all I want to thank **Prof. Dr. Andreas Weber** for his guidance and supervision since my Master's degree, for interesting projects and the opportunity to attend many conferences throughout my PhD.

My thank goes to my mentor **Prof. Dr. Peter Westhoff** and my committee member **Prof. Dr. Petra Bauer** for fruitful discussions and their time during my annual committee meetings.

I want to thank our collaboration partners from the UKD Düsseldorf (**Dr. Leonie Drews** and **Prof. Dr. Andreas Reichert**), the Ghent University (**Dr. Simon Strobbe**, **Prof. Dr. Dominique Van Der Straeten**, **Jana Verstraete**, and **Prof. Dr. Christoph Stove**), and the University of Geneva (**Dr. Maite Colinas**, **Dr. Michael Moulin**, and **Prof. Dr. Teresa Fitzpatrick**) for their excellent collaboration on various stages of our Mito-tagging and BOU project as well as our collaboration partners from the Ryukoku University of Japan (**Prof. Dr. Tsuyoshi Furumoto** and his colleagues) for teaming up with us on very interesting C_4 research on the BASS4 project.

I am grateful to **Dr. Philipp Westhoff** for his profound knowledge on metabolite analyses and showing me that nothing is 'unmeasurable', for running and analyzing our *Flaveria* samples, for our ongoing effort in measuring metabolites in isolated mitochondria, for lots of interesting discussions, and for many more analyses to come. I also want to acknowledge **Katrin Weber**, **Elisabeth Klemp** and **Maria Graf** for their excellent technical assistance.

I want to express my gratitude towards **PD Dr. Marion Eisenhut** for introducing me into plant work and the BOU project, and for proofreading the BOU manuscript.

I would like to offer my special thanks to **Anastasija Plett**, **Marc-Sven Röll**, **Lennart Charton**, **Dr. Björn Hielscher** and **Thomas Wrobel** for various stages of proofreading, for good scientific discussions, for your everyday help in the lab, for afternoon coffee breaks and cooking sessions, for many funny Thursday evenings and all the after work beers.

I want to thank all my colleagues from the **Weberlab** for their everyday help and support, for nice lunch breaks and social field trips, for many BBQs and lots of fun in the lab.

I wish to thank the Bachelor and Master students I could supervise throughout the years, former colleagues of which many have become dear friends in the last years as well as the girls in our office (**Eva Maleckova** and **Meng-Ying Lin**) for creating an excellent working atmosphere.

I am grateful to **Dr. Petra Fackendahl** coordinator of the iGRAD Plant program as well as all the current and former **iGRAD Plant students** for nice discussions during our annual retreats.

I am indebted to our former secretary **Anja Nöcker** for her constant support in solving all of my bureaucratic issues.

I thank the **Gardeners** of the Heinrich-Heine University for solving all the problems with my research and some of my non-research plants.

I am entirely grateful to my **Family** for supporting me during this entire time, and to **Jan** and **Phine**, for their love and support, for all the fun we had and all the tears we shed, for always being there for me, simply for everything since Potsdam.